Bulletin

of

The Geological Society of America

VOLUME 70 May 1959 NUMBER 5

CONTENTS

	Pages
Optical properties of potassic feldspars. By C. G. Hewlett	511–538
Overthrust Ordovician and the Nannie's Peak intrusive, Lone Mountain, Elko County, Nevada. By Donald W. Lovejoy	539–564
The tangue, a "nonconforming" sediment. By Jacques Bourcart and Roger H. Charlier	565–568
Effect of grain size on strength of mixtures of clay, sand, and water. By Parker D. Trask	569–580
Eocene stratigraphy and paleontology, Orocopia Mountains, southeastern California. By John C. Crowell and Takeo Susuki	581–592
Chemical composition of argillites of the Cobalt series (Precambrian) and the problem of soda-rich sediments. By F. J. Pettijohn and Harry Bastron	593–600
Re-evaluation of the salt chronology of several Great Basin lakes. By Wallace S. Broecker and Alan F. Walton	601–618
Geology of the Buffalo Mountain-Cherokee Mountain area, northeastern Tennessee. By Richard J. Ordway	619–636
Short Notes	
Re-evaluation of the salt chronology of several Great Basin lakes: a discussion. By J. H. Feth	637–640
Rock compass: a new aid for collecting oriented specimens. By D. E. T. Bidgood and W. B. Harland	641–644
Upper Ordovician (?) and Upper Silurian formations of the northern Klamath Mountains, California. By Francis G. Wells, George W. Walker, and Charles W. Merriam	645–650
Preliminary study of stochastic terms used in geology. By Bahngrell W. Brown	651–654
Experimental study of chromatographic-type accumulation of organic compounds in sediments: an introductory statement. By Bartholomew Nagy and John P. Wourms, Jr.	655–660
Froth veins, formed by immiscible hydrothermal fluids, in mercury deposits, California. By Edgar H. Bailey	661–664
Terminology of post-Valders time:	
A discussion. By J. Terasmae	665–666
A reply. By William S. Cooper	666
Tensional concept of rifting. By Robert R. Wheeler	667–668

Subscription $15.00 per year.

Printing Office: Mt. Royal & Guilford Aves., Baltimore 2, Md.

Communications for publications should be addressed to The Geological Society of America, Dr. H. R. Aldrich, Secretary, 419 West 117 Street, New York, N. Y.

Please give notice of change of address 4 weeks in advance. Claims for nonreceipt of the Bulletin of a given month must be sent to the Secretary of the Society before the end of the second succeeding month.

Second-class Postage paid at Baltimore, Md.
Accepted for mailing at special rate of postage provided for in Section 1103
Act of October 3, 1917, authorized on July 8, 1918.

PAPERS IN PRESS FOR FORTHCOMING ISSUES

Ion Exchange in Clays and Other Minerals. By Dorothy Carroll

Granite Emplacement with Special Reference to North America. By A. F. Buddington

Geologic Significance of Accumulator Plants in Rock Weathering. By T. S. Lovering

Contact Metamorphism, Crestmore, California. By C. Wayne Burnham

Origin of the Ultramafic Complex at Union Bay, Southeastern Alaska. By John C. Ruckmick and James A. Noble

Granitization, Migmatization, and Fusion in the Northern Entiat Mountains, Washington. By Dwight F. Crowder

BULLETIN OF THE GEOLOGICAL SOCIETY OF AMERICA
VOL. 70, PP. 511-538, 5 FIGS. MAY 1959

OPTICAL PROPERTIES OF POTASSIC FELDSPARS

BY C. G. HEWLETT*

ABSTRACT

Optical and X-ray studies of 15 chemically analyzed feldspars show that the optical properties of potassic feldspars may vary because of (1) compositional differences, such as degree of substitution of Fe^{3+} for Al and of Na, Ca, Ba, Sr, and Rb for K in the feldspar structure, with corresponding substitution of Al for Si where necessary to balance electrostatic charges, (2) presence on a submicroscopic scale of twinning or intergrowths of materials of different refractivities, such as unmixing of a plagioclase from a potassic host or partial inversion of orthoclase to microcline, and (3) degree of order in the distribution of Si and Al within the tetrahedral sites of the feldspar structure. The α refractive index of homogeneous feldspars provides a measure of composition because it does not vary appreciably with Si/Al ordering. The substitution of Na for K, however, causes such a small index increase in the range $Or_{100}Ab_0$ to $Or_{60}Ab_{40}$ that its effects normally are masked by the larger increases due to substitution of minor amounts of Ca, Sr, Ba, and Fe. As a consequence refractive indices of alkali feldspars are not useful for determining chemical composition. The decrease in the α index when cryptoperthites are homogenized at 850° C. is a measure of the degree of unmixing. The optic angle 2V and the birefringence "b" $-$ α provide a measure of the degree of Si/Al ordering, provided composition is known. In this paper "b" is defined as the refractive index of the ray vibrating parallel or nearly parallel to the b crystallographic direction. Most existing diagrams relating optical properties to composition of alkali feldspars are constructed for groups of feldspars with the same state of Si/Al ordering and do not emphasize the importance of degree of unmixing in determining refractive indices. These diagrams are valid only if the state of order varies sympathetically with the degree of unmixing. Zoning in some sanidines is attributed to variations in the concentration of divalent alkali ions or, possibly, of Fe^{3+}, and in other sanidines to variations in the degree of Si/Al ordering.

CONTENTS

TEXT

	Page
Introduction	512
Acknowledgments	512
Experimental investigation	512
Chemical analysis	512
X-ray diffraction	514
Optical data	515
Methods	515
Indices of refraction	515
Optic angle	515
Extinction angles	516
Variations in optical properties	518
Introduction	518
Variations with chemical composition	520
Indices of refraction	520
Optic angle	523
Extinction angles	524
Variations caused by submicroscopic intergrowths	525
Variations due to distribution of Si/Al	530
Discussion	532
Optical classification of alkali feldspars	534
References cited	537

ILLUSTRATIONS

Figure	Page
1. The K_2O and Na_2O values for samples 1–15	516
2. Refractive-index curves for homogeneous and unmixed K/Na feldspars	522
3. Range in optic angle for samples 1–15	523
4. Extinction angles on (010)	524
5. Diagrams indicating degree of order-disorder of Si/Al for samples 1–15	531

* Doctor Hewlett's death in the course of field work in August 1956 terminated early the productive life of a most promising young scientist. The original paper from which the present paper was somewhat condensed was awarded the Peacock Memorial Prize of the Walker Mineralogical Club for 1955. S. W. Bailey and R. C. Emmons were responsible for revision of the paper and for final checking and proofreading.

TABLES

Table		Page
1.	Description of samples	513
2.	Chemical analyses of samples 1–10	514
3.	Spectrographic and flame-photometer analyses of samples 1–15	515
4.	Chemical analyses calculated to weight per cent feldspar	517
5.	Samples 11–15 calculated to weight per cent feldspar	518
6.	Optical data	519
7.	Correlation between refractive-index decrease due to homogenization and degree of unmixing as determined by b-axis oscillation method	526
8.	Comparison of composition from chemical analysis and from d(201) graph	527
9.	Lattice spacings d(001) and d(010) for samples 1–15	529
10.	Changes in optic angle caused by heating to 850° C. for 2 hours	530
11.	Analyses of microclines found unsuitable for accurate optical measurements	536

Introduction

This paper is based on an optical and X-ray-diffraction study of 15 chemically analyzed potassic feldspars and on published data of other workers. Its purpose is to explain variations in optical properties in terms of compositional and structural factors and to determine the extent to which the optical properties are diagnostic of these factors.

The samples listed in Table 1 include 10 sanidines and 1 anorthoclase from volcanic rocks, 3 microclines from granitic rocks, and 1 adularia from a fissure vein. The samples are optically homogeneous and were selected on the basis of purity from an original collection of 108 potassic feldspars. Many specimens were rejected because of alteration, inclusions, complex twinning, extreme perthitic texture, or insufficient quantity. No attempt was made to select unzoned feldspars, because all the volcanic specimens were found to be zoned.

Acknowledgments

R. C. Emmons suggested the study and, with S. W. Bailey, supervised the course of research. The work was supported in part by a grant from the Wisconsin Alumni Research Foundation. The writer is indebted to The Geological Society of America for a grant to cover the cost of the chemical analyses, gravimetric and spectrographic, and to Dr. S. S. Goldich of the University of Minnesota and Dr. Oiva Joensuu of the University of Chicago for directing these analyses. Thanks are also due Dr. J. A. S. Adams, now of Rice Institute, for arranging and supervising flame-photometer analyses and assisting in the evaluation of chemical data. R. M. Crump, C. D. Reynolds, and R. A. Bell aided in the selection of specimens and preliminary separations. D. L. Morgridge performed all X-ray-diffractometer analyses.

Experimental Investigation

Chemical Analysis

The samples were prepared for chemical analysis by crushing and sizing to 100–140 mesh, then purifying by a series of magnetic and heavy-liquid separations. Only 10 purified samples were obtained in sufficient quantity for standard silicate analysis. These were submitted to the Rock Analysis Laboratory of the University of Minnesota. Gravimetric analyses were performed by E. H. Oslund under the direction of S. S. Goldich. Spectrographic analyses of these same samples plus 5 additional samples, which were available in smaller quantities, were performed by O. Joensuu of the Department of Geology, University of Chicago. Flame-photometer analyses of K_2O and Na_2O for 12 of the 15 samples were performed by W. J. Maeck under the direction of J. A. S. Adams in the Department of Chemistry, University of Wisconsin.

The results of the gravimetric analyses for samples 1–10 are listed in Table 2; results of the spectrographic and flame-photometer analyses for samples 1–15 are listed in Table 3. The values obtained by the three methods for the two most abundant large cations, Na and K, are shown graphically in Figure 1, broken for convenience into three sections. The diagonal line in the diagram is between 11.824 per cent Na_2O and 16.926 per cent K_2O and represents the stoichiometric requirements for pure potassium-sodium feldspars. Since natural alkali feldspars also may contain Ca, Ba, Sr, and Rb they should plot below this stoichiometric line. Inclusions that do not contain K or Na also cause natural feldspars to fall below the stoichiometric line. Figure 1 shows that Na_2O plus K_2O reported spectrographically are consistently higher than when examined by other methods and in some samples

exceed the stoichiometric requirements for alkali feldspars. Many flame-photometer values are low for pure feldspar. The gravimetric data for Na_2O and K_2O are generally intermediate between the spectrographic and flame-photometer values and have been used where possible (samples 1–10) for calculating per cent feldspar. The discrepancy between the three methods is primarily in the K_2O determination.

Values differ for CaO and BaO determined gravimetrically and spectrographically for samples 1–10. Values for CaO are consistently higher by spectrographic analysis, and some values for BaO are appreciably higher by the gravimetric method, although some agree well. Values for SrO and Rb_2O determined by the two methods generally agree well.

Table 4 shows the gravimetric analyses of samples 1–10 calculated to weight per cent feldspar, both uncorrected and corrected to total 100 per cent feldspar. Calculated excess SiO_2 and Al_2O_3 on the latter basis could indicate (1) quartz and layer silicates as impurities, (2) a deficiency of large cations in the feldspar structure, or (3) a small bias in the chemical analyses. Since all samples except 7 and 8 appear to be free from sericite, the calculated excess of Al_2O_3 seems best explained as a slight cation deficiency that may be real or due to a bias in the analyses. By calculating the excess Al_2O_3 to feldspar and allocating the

TABLE 1.—DESCRIPTION OF SAMPLES

New number	Old number	Source	Locality	Description	Per cent* impurity	Inclusions seen microscopically
1	0-30	Wards	Viterbo, Italy	Sanidine phenocrysts 15 mm long in felsic matrix	0.18	Few opaque inclusions
2	0-38	Wards	White Pine County, Nevada	Sanidine phenocrysts 3 mm diameter in rhyolite	0.11	Very clean, some opaque inclusions
3	0-40	Wards	Fort Bayard, New Mexico	One large sanidine phenocryst from porphyry	0.12	Gas inclusions and a few opaque inclusions
4	0-32	Wards	Drachenfels, Rhenish Prussia	Sanidine phenocrysts 20 mm long in felsic matrix	0.32	Gas inclusions and a few opaque inclusions
5	0-43	Wards	Mineral Hill, Cripple Creek, Colorado	Sanidine phenocrysts 20 mm long in trachyte	0.26	Alteration products along cracks, some opaque inclusions
6	0-39	Wards	St. Gotthard, Switzerland	Prismatic crystals of adularia	0.05	Very clean, many fluid inclusions
7	0-42	R. M. Gates, collector	Bethlehem, Connecticut	Microcline from Woodbury granite gneiss	0.08	Some quartz and sericite, very minor perthite
8	0-41	R. M. Gates, collector	Bethlehem, Connecticut	Microcline from Woodbury granite	0.06	Some perthite and sericitized perthite, no quartz
9	0-14	Johnston Granite Co.	Lithonia, Georgia	Microcline from Lithonia granite	0.12	Some quartz and fine perthite, no sericite
10	0-48	R. M. Gates, collector	Devil's Tower, Wyoming	Anorthoclase phenocrysts 5 mm long in phonolite porphyry	0.37	Alteration products along cracks, few opaque inclusions
11	0-45	Wards	Ariccia, Italy	Sanidine phenocrysts 4 mm long in leucite-rich lava	0.09	Small inclusions of analcite (?) and colored minerals
12	0-86	Univ. Wisconsin A-40-13	Peau Castaquaio, Auvergne, France	Sanidine phenocrysts 15 mm long in trachyte	0.03	Very clean, mostly gas inclusions
13	0-83	Univ. Wisconsin Museum specimen 4505	Mt. Somma, Italy	Sanidine crystals under 5 mm diameter in drusy cavities with nepheline	0.04	Very clean
14	0-85	Univ. Wisconsin Museum specimen 20709	Arendal, Norway	Single large crystal of sanidine	0.04	Many small opaque inclusions
15	0-87	Univ. Wisconsin A-39-1	Drachenfels, Siebengebirge, Germany	Sanidine phenocrysts 25 mm long in felsic matrix	0.16	Some opaque inclusions and gas inclusions

* Per cent impurities on basis of total $Fe_2O_3 + FeO + MgO + TiO_2$ determined gravimetrically for samples 1–10 and as FeO determined spectrographically for samples 11–15

necessary SiO_2 to correspond, much of the apparent SiO_2 excess is consumed. Similar excesses of SiO_2 were found in the plagioclase analyses of Emmons (1953, p. 15, 17, 20; 1955, p. 1061). Both Emmons' analyses and those of this paper can be allocated to satisfactory structural formulas, however, without invoking excess of either SiO_2 or Al_2O_3 (S. W. Bailey, personal communication). This suggests the reality of alkali deficiency and raises the question of the validity, in precise work, of the procedure of calculating percentages of end-member feldspars from the molecular proportions of the alkalies present.

Samples 11–15 calculated to weight per cent feldspar are listed in Table 5. For these samples spectrographic data were used to calculate Ca, Ba, Sr, and Rb feldspars. Sodic feldspar was determined by taking the mean value reported spectrographically and by flame-photometer. The values listed for potassic feldspar were obtained by summing the calculated percentages of Na, Ca, Ba, Sr, and Rb feldspar and assigning sufficient potassic feldspar to total 100 per cent. This procedure was adopted because of the large difference between spectrographic and flame-photometer values for K_2O in some samples. The procedure assumes that all inaccuracies are in the K_2O determination and that each sample is pure feldspar. Although neither of these assumptions is strictly valid, impurities are small for each sample, and the poorest agreement for the various methods is in the K_2O determination (Fig. 1). Since samples 11–15 are all K_2O-rich, the effect of these assumptions is to give percentages that are equivalent to the percentages of samples 1–10 after correcting to 100 per cent feldspar. For purposes of uniformity the corrected percentages, which differ by less than 2 per cent from the uncorrected values, are used throughout this paper.

TABLE 2.—CHEMICAL ANALYSES OF SAMPLES 1–10

(In weight per cent)

	1	2	3	4	5	6	7	8	9	10
SiO_2	64.57	65.65	64.46	65.13	63.49	64.76	64.60	64.90	64.89	66.28
Al_2O_3	18.95	18.61	19.03	19.18	19.72	18.57	18.55	18.65	18.44	19.42
TiO_2	0.04	0.02	0.02	0.04	0.03	0.02	0.02	0.02	0.02	0.03
Fe_2O_3	0.11	0.06	0.08	0.24	0.14	0.01	0.05	0.03	0.04	0.26
FeO	0.02	0.02	0.02	0.04	0.02	0.02	0.01	0.01	0.04	0.04
MgO	0.01	0.01	0.00	0.03	0.07	0.00	0.00	0.00	0.02	0.04
MnO	...	...	...	...	0.00	....	....	....	....	0.00
SrO	0.14	0.02	0.09	0.10	0.82	0.04	0.04	0.02	0.01	0.36
CaO	0.31	0.17	0.03	0.41	0.36	0.02	0.02	0.02	0.00	0.29
Na_2O	2.16	2.76	2.98	4.33	2.97	1.08	0.73	0.87	0.93	7.94
K_2O	12.98	12.50	11.64	9.73	11.37	15.11	15.44	15.20	15.41	4.85
Rb_2O	0.04	0.03	0.01	0.03	0.03	0.04	0.03	0.07	0.08	0.004
BaO	0.48	0.05	1.51	0.61	0.72	0.29	0.36	0.04	0.06	0.26
H_2O-	0.01	0.00	0.00	0.04	0.03	0.01	0.01	0.00	0.03	0.00
H_2O+	0.09	0.09	0.05	0.07	0.10	0.10	0.05	0.18	0.09	0.04
	99.91	99.99	99.92	99.98	99.87	100.07	99.91	100.01	100.06	99.81

X-Ray Diffraction

Both single-crystal and powder techniques of X-ray diffraction were used in this study. A series of b-axis oscillation photographs was taken for each sample with a Unicam single-crystal goniometer, using filtered Cu X radiation. These pictures were taken to detect the unmixed plagioclase component of cryptoperthites and to determine the twinning and mutual orientation of the two components. Zero-level precession photographs using Mo X radiation also were taken for some of the crystals. The results of the single-crystal studies are listed in Table 7.

The lattice spacings of the 002, 060, and $\bar{2}01$ reflections were measured with a Norelco diffractometer using approximately 200 mg of powdered sample. Peak positions for these

reflections were determined by plotting fixed-count times at intervals of 0.01° 2θ after calibration with a silicon standard. The results are listed in Tables 8 and 9. All diffractometer measurements were made by D. L. Morgridge.

8, and 9, which are microclines from medium-grained granitic rocks, showed a much smaller range in refractive indices than sanidines from volcanic rocks. In the sanidines zoning may be seen in thin sections.

TABLE 3.—SPECTROGRAPHIC AND FLAME-PHOTOMETER ANALYSES OF SAMPLES 1–15

(S = spectrographic; FP = flame photometer)

		1	2	3	4	5	6	7	8	9	10	11	12	13	14	15
		(In weight per cent)														
K_2O	S	12.7	13.5	12.0	9.5	11.7	15.0	16.5	16.3	16.0	4.8	14.2	14.0	11.2	10.3	10.3
	FP	12.2	11.50	....	....	10.40	....	14.55	14.45	14.35	4.80	12.6	12.35	11.50	10.38	9.04
Na_2O	S	1.95	2.8	2.85	4.3	2.9	1.1	0.55	0.80	0.90	7.7	1.40	1.9	3.5	4.35	4.9
	FP	2.34	3.08	....	....	3.45	....	0.73	0.78	0.93	8.64	2.01	2.03	3.61	4.22	4.74
CaO	S	0.40	0.30	0.10	0.60	0.60	<0.05	<0.05	0.15	0.07	0.57	0.35	0.45	0.35	0.13	0.65
BaO	S	0.28	0.08	0.75	0.43	0.39	0.22	0.30	0.047	0.17	0.24	0.65	0.35	<0.05	0.06	0.70
SrO	S	0.14	0.021	<0.1	0.11	0.37	0.055	0.034	0.026	0.012	0.28	0.88	0.089	0.015	0.025	0.095
FeO	S	0.11	0.035	<0.03	0.19	0.17	0.18	0.06	0.07	0.045	<0.03	0.09	<0.03	0.04	0.04	0.16
		(In parts per million)														
Rb_2O	S	820	440	200	260	310	810	480	900	1260	60	1500	1100	1200	1500	650
Li_2O	S	78	27	12	39	15	36	12	100	33	55	30	25	60	35	30
Cs_2O	S	7	2	2	2	2	2	3	19	2	2	2	<2	<2	<2	<2
Tl_2O	S	2.5	2	0.6	0.6	1.2	3.5	5.5	2.0	4.2	0.6	2	7	5	5	2
PbO	S	100	44	20	14	20	110	30	190	50	9	100	120	110	70	55

Optical Data

Methods.—Refractive-index determinations were made by the double-variation method and were plotted on Hartmann nets to obtain the benefit of averaging. Reproducibility is within ±.0002. Orientation was done with the universal stage at first, but later this was abandoned for orientations in which the grain rests on (010). Such grains are easily obtained and may be checked reliably with an interference figure. The universal stage was used when it was needed.

Indices of refraction.—The refractive indices are given in Table 6 for samples 1–15. In most samples the range of values obtained required 4–15 measurements for each sample, depending on the spread of values from successively used grains. In general more measurements were made of α than were made of β and γ. The birefringence values, $\gamma - \alpha$ and $\beta - \alpha$, were found to be fairly constant on the Hartmann net plots of the refractive indices of the grains of a given sample, though the individual index values showed a range. Therefore the following procedure was adopted for arriving at averaged values: a simple average was calculated for α, and to this was added the fairly constant values $\beta - \alpha$ to obtain β, and $\gamma - \alpha$ to obtain γ. Samples 7,

The refractive indices of two samples described by Spencer (1937, p. 482) as "Si" and "Ha" were measured here and are included in Table 6. These samples were obtained from S. W. Bailey who is indebted to Dr. Edmondson Spencer for a few fragments of the original sample. Sample "Si" with a composition of $Or_{62}Ab_{35}An_3$ is from Siebengebirge, Germany, and sample "Ha" with a composition of $Or_{59}Ab_{35}An_6$ is from Haddington, Scotland. The chemical analyses are listed in Spencer's paper (1937, p. 482).

Optic angle.—Because of the wide range in the optic angle found in most samples (Table 6) no attempt has been made to give a mean value. The range, determined by examining a large number of grains from the gravity fraction used for chemical analysis, in most cases may be measured in a thin section of a single zoned crystal. This range in 2V is believed to result from two factors; in some samples the range in divalent cation content is apparently dominant, and in others the variable degree of Si/Al ordering is dominant.

The letters N and P are used in Table 6 to indicate the position of the optic plane as normal or parallel to the symmetry plane (010). In samples 1, 2, and 12 the optic plane is normal to (010) for some crystals and parallel to (010) for others. In large zoned crystals

from samples 1 and 12 some zones have the optic plane normal and others parallel to (010). A zone where 2V is zero occurs between these zones.

curves—the ray that has a vibration direction closest to crystallographic c has the steeper slope. The formula changes from v > r to r > v when β and γ change places.

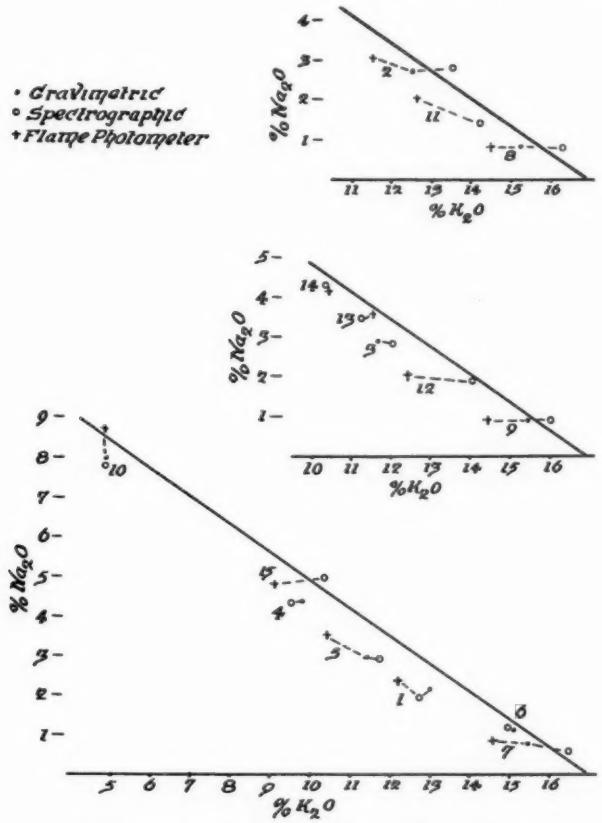

FIGURE 1.—K_2O AND Na_2O VALUES FOR SAMPLES 1–15

The inclined line represents the stoichiometric requirements for pure K/Na feldspar. The diagram has been broken into three sections to avoid overlapping of points.

All the sanidines show a pronounced dispersion in interference figures that serves to locate (010). The dispersion of the bisectrices is inclined if the optic plane is parallel to (010) and is horizontal if it is normal to (010). As was pointed out by Spencer (1937, p. 477) this is more evident when 2V is small. All the sanidines show dispersion of the optic axes: v > r if the optic plane is parallel to (010), and r > v if the optic plane is normal to (010). The basis for the dispersion may be seen in the Hartmann net plot of the refractive-index

Extinction angles.—The extinction angles as measured are given in Table 6; the range in general is ±1°. The extinction angle on (001) is essentially 0° except for samples 7, 8, 9, and 10. In the microclines (7, 8, and 9) a larger range up to 3° was obtained. In the anorthoclase (10) the extinction value is about 1½°, somewhat obscured by exceedingly fine twinning. The mean values on (010) are given in Table 6.

Spencer's sample "Si" (1937) gave an extinction angle on (010) between 5° and 7°, and

TABLE 4.—CHEMICAL ANALYSES CALCULATED TO WEIGHT PER CENT FELDSPAR

Column *A* uncorrected; column *B* corrected to total 100 per cent feldspar

Feldspar	Sample																			
	1		2		3		4		5		6		7		8		9		10	
	A	B	A	B	A	B	A	B	A	B	A	B	A	B	A	B	A	B	A	B
$KAlSi_3O_8$	76.69	78.05	73.85	75.12	68.77	70.08	57.49	58.64	67.17	68.18	89.27	89.74	91.22	92.51	89.80	91.95	91.04	91.62	28.65	28.93
$NaAlSi_3O_8$	18.27	18.59	23.34	23.74	25.20	25.68	36.62	37.35	25.12	25.50	9.13	9.18	6.17	6.26	7.36	7.54	7.87	7.92	67.15	67.81
$CaAl_2Si_2O_8$	1.54	1.57	0.84	0.85	0.15	0.15	2.03	2.07	1.79	1.82	0.10	0.10	0.10	0.10	0.10	0.10	0.00	0.00	1.44	1.45
$BaAl_2Si_2O_8$	1.18	1.19	0.12	0.12	3.70	3.77	1.49	1.52	1.76	1.79	0.71	0.71	0.88	0.89	0.10	0.10	0.15	0.15	0.64	0.65
$SrAl_2Si_2O_8$	0.44	0.45	0.06	0.06	0.28	0.28	0.31	0.32	2.58	2.62	0.13	0.13	0.13	0.13	0.06	0.06	0.03	0.03	1.13	1.14
$RbAlSi_3O_8$	0.14	0.14	0.10	0.10	0.03	0.03	0.10	0.10	0.10	0.10	0.14	0.14	0.10	0.10	0.24	0.25	0.28	0.28	0.01	0.01
Total	98.26	99.99	98.31	99.99	98.13	99.99	98.04	100.00	98.52	100.01	99.48	100.00	98.60	99.99	97.66	100.00	99.37	100.00	99.02	99.99
Calculated excess SiO_2		1.08		1.31		1.25		1.21		0.40		0.28		0.87		1.49		0.33		0.38
Calculated excess Al_2O_3		0.31		0.16		0.38		0.27		0.58		0.16		0.30		0.65		0.14		0.07

his sample "Ha" gave a fairly constant 7° on (010). His 2V values are 33° for "Si" and 34° for "Ha".

or in unmixing of phases of different Si:Al ratios. The extent and scale of unmixing is influenced by original composition.

TABLE 5.—SAMPLES 11—15 CALCULATED TO WEIGHT PER CENT FELDSPAR

		K_2O	Na_2O	CaO	BaO	SrO	Rb_2O
11	Spectrograph	14.2	1.40	0.35	0.65	0.88	0.15
	Flame photometer	12.6	2.01				
	Value used	13.38	1.70	0.35	0.65	0.88	0.15
	Per cent feldspar	79.02	14.38	1.74	1.59	2.75	0.52
12	Spectrograph	14.0	1.9	0.45	0.35	0.089	0.11
	Flame photometer	12.35	2.03				
	Value used	13.48	1.96	0.45	0.35	0.089	0.11
	Per cent feldspar	79.67	16.58	2.23	0.86	0.28	0.38
13	Spectrograph	11.2	3.5	0.35	<0.05	0.015	0.12
	Flame photometer	11.5	3.61				
	Value used	11.47	3.55	0.35	0.00	0.015	0.12
	Per cent feldspar	67.77	30.02	1.74	0.00	0.05	0.42
14	Spectrograph	10.3	4.35	0.13	0.06	0.025	0.15
	Flame photometer	10.38	4.22				
	Value used	10.56	4.28	0.13	0.06	0.025	0.15
	Per cent feldspar	62.41	36.20	0.64	0.15	0.08	0.52
15	Spectrograph	10.3	4.9	0.65	0.70	0.095	0.065
	Flame photometer	9.04	4.74				
	Value used	9.10	4.82	0.65	0.70	0.095	0.065
	Per cent feldspar	53.78	40.76	3.22	1.71	0.30	0.23

VARIATIONS IN OPTICAL PROPERTIES

Introduction

Three factors account for most, if not all, of the variations in optical properties of potassic feldspars: (1) compositional differences, such as degree of substitution of Fe^{3+} for Al and of Na, Ca, Ba, Sr, and Rb for K in the feldspar structure, with corresponding substitution of Al for Si where necessary to balance electrostatic charges, (2) presence on a submicroscopic scale of twinning or intergrowths of materials of different refractivities, such as unmixing of a plagioclase from a potassic host or partial inversion of orthoclase to microcline, and (3) degree of order in the distribution of Al and Si within the tetrahedral sites of the feldspar structure. These factors overlap to a certain extent. For example, the degree of order of Al and Si may be reflected in partial nversion of a "high" phase to a "low" phase

Variations of optical properties with composition between K feldspar and Na feldspar and between K feldspar and Ba feldspar are probably best known from the diagrams of Winchell (1925). Spencer (1937) and Tuttle (1952) provided more up-to-date data for the K-Na series. Oftedahl (1948) constructed a triangular diagram to represent some optical properties of K-Na-Ca feldspars, but no one has constructed diagrams for Sr-bearing or Rb-bearing feldspars. Coombs (1954) presented optical data for ferriferous orthoclases.

The optical properties of crystals that are intergrowths of two or more phases on a submicroscopic scale are weighted averages of those of the component phases. Raman *et al.* (1950) have shown that such intergrowths may show schiller caused by diffusion of light, if the components have sufficiently different refractivities and form noncoplanar domains about the size of the wave length of light. A difference in optical properties between homo-

geneous and submicroscopically unmixed alkali feldspar of the same bulk composition was first indicated by Kozu and Suzuki (1925) who showed that homogenization of moonstone by heating caused a small change in optic angle. Spencer (1930; 1937), in the most comprehensive optical studies of unmixed potassic feldspars undertaken to date, showed that the average refractive indices of orthoclase microperthites and sanidine cryptoperthites are substantially higher than for the same feldspars after homogenization and that the optic angle is only slightly different. Tuttle and Keith (1954, p. 69–70) and MacKenzie and Smith (1955, p. 729) have found that specimens with both high and low albite present submicroscopically have optic axial angles intermediate between those expected from orthoclase microperthites and sanidine cryptoperthites. Specimens with both orthoclase and microcline present submicroscopically have optic axial angles intermediate between the orthoclase and microcline microperthite curves (MacKenzie and Smith, 1955, p. 729, Fig. 6). Laves (1950, p. 548–553) has shown by X-ray study that some optically monoclinic potassic feldspars are composed of triclinic elements or domains twinned submicroscopically according to the albite and/or pericline laws. On the basis of these observations Goldsmith and Laves (1954b, p. 111–112) proposed that in many orthoclase specimens the twinned domains are so small that the material appears monoclinic to X-ray study also, even though the domains themselves may be as ordered with respect to Si and Al as in microcline.

Taylor's work on the crystal structure of sanidine (1933) led Barth (1934) to suggest that the difference between various modifications of $KAlSi_3O_8$ is the result of difference in the distribution of Si and Al in the feldspar. This has been well established by more recent structural work (Cole, Sorum, and Kennard, 1949; Bailey and Taylor, 1955; Ferguson, Traill, and Taylor, 1958), so that variations in the distribution of aluminum in the feldspar structure can be considered a third cause of optical variations. The optical changes that occur when homogenous alkali feldspars are heated for prolonged periods above 1000° C. (sanidinized) reflect a change in the arrangement of Si and Al from an ordered or partly ordered to a disordered distribution in the structure.

To study any one of the above factors independently is difficult, because few natural feldspars have identical compositions, are unmixed to exactly the same degree, or have

TABLE 6.—OPTICAL DATA

The letters *N* and *P* indicate that the optic plane is normal or parallel to (010)

Sample	Range of values for α	Mean values			Range of values for optic angle 2V	Extinction angle (±1°)	
		α	β	γ		on(010)	on (001)
1	1.5198–1.5222	1.5206	1.5248	1.5248	24½P–25N	6	0
2	1.5185–1.5195	1.5191	1.5237	1.5237	18P–19½N	5½	0
3	1.5205–1.5214	1.5211	1.5253	1.5258	31N–40½N	5	0
4	1.5223–1.5227	1.5226	1.5269	1.5275	37½N–46N	7	0
5	1.5231–1.5241	1.5235	1.5277	1.5283	38N–47N	5½	0
6	1.5192–1.5195	1.5193	1.5231	1.5246	60N–72N	ND	0
7	1.5186–1.5190	1.5188	...	1.5256	75N ± 5°	ND	17–20
8	1.5180–1.5182	1.5181	...	1.5253	82N ± 5°	ND	15–17
9	1.5177–1.5185	1.5182	...	1.5253	86N ± 5°	ND	17–19½
10	1.5253–1.5260	1.5258	1.5313	1.5328	54½N–56½N	9	1½
11	1.5219–1.5236	1.5228	1.5269	1.5270	20N–36N	6	0
12	1.5190–1.5210	1.5199	1.5241	1.5241	30½P–10N	6	0
13	1.5190–1.5197	1.5194	1.5239	1.5240	18½N–25N	6½	0
14	1.5198–1.5200	1.5200	1.5247	1.5250	29N–31½N	7½	0
15	1.5220–1.5227	1.5223	1.5269	1.5274	38½N–44N	7	0
"Si"	1.5218–1.5227	1.5223	1.5270	1.5274	ND	ND	ND
"Ha"	1.5226–1.5232	1.5229	1.5275	1.5280	ND	ND	ND

identical states of Si/Al distribution. Heating submicroscopically unmixed natural K/Na feldspars to about 800° C. for a few hours will usually homogenize them completely, thereby eliminating the complications introduced by unmixing. The writer believes that little or no disordering of aluminum takes place with this heat treatment.

Not all feldspars can be homogenized so readily: Perthites with visible, coarse albitic lamellae, perhaps as a consequence of replacement rather than unmixing, may be difficult to homogenize. Dittler and Köhler (1925, p. 257–258), Spencer (1930, p. 318–319), and Heald (1950, p. 79–80) have described specimens of this type. Feldspars in which the two (or more) phases differ either in the nature of the distribution of Si and Al, for example "high" versus "low" phases, or in the actual ratio of Si to Al require sanidinization treatments to effect complete homogeneity. If it is assumed that maximum microcline and low albite have the same degree of order of Si and Al, then orthoclase microperthites in which the plagioclase component is close to low albite fall in this category. Several of Spencer's (1930; 1937) specimens are of this type. Potassic feldspars are also known in which both high albite and low albite coexist within the potassic host (Tuttle and Keith, 1954, p. 70) and in which both monoclinic and triclinic potassic phases coexist with an albitic phase (MacKenzie and Smith, 1955, p. 722–726; Muir and Smith, 1956, p. 186, 192). Peristerites (Laves, 1954, p. 409) and certain calcic microperthites (Laves, 1952, p. 572; MacKenzie and Smith, 1955, p. 726–727) contain phases that differ in their Si:Al ratios and homogenize only at temperatures that will cause diffusion of Si and Al. These exceptions point out the need for checking homogenization by X-ray techniques. In the present study heat treatments are confined to high-temperature submicroscopic intergrowths, for which X-ray studies confirm complete homogenization after 2 hours at 850° C.

To study the optical variations with composition the factor of aluminum distribution must be held constant. This probably could be accomplished by sanidinizing all samples, thus bringing them to the same state of complete aluminum disorder. Another possibility would be to fuse all samples to glasses and to relate the refractive index of feldspar glass to composition (Foster, 1955). Neither of these procedures seems necessary because the refractive index α of potassic feldspars appears to be independent of the distribution of Si and Al. The data of Spencer (1937, p. 464–469) show that upon sanidinization of homogeneous alkali feldspars α remains essentially constant. The large change in 2V that occurs during sanidinization reflects changes in the β and γ indices.

The procedure followed in this investigation is to homogenize samples by heating them to 850° C. for 2 hours (verifying homogeneity by single-crystal X-ray studies), to measure α of the homogenized feldspars, and to correlate this index with chemical composition. No attempt is made to correlate β and γ with composition because these indices vary with sanidinization and, therefore, with the distribution of Si and Al.

Variations with Chemical Composition

Indices of refraction.—The correlation of the complete analyses of very pure alkali feldspars and their optical properties shows the extreme importance of Ca, Ba, and Sr in determining the refractive indices of alkali feldspar. In most alkali feldspar Rb is present in small amounts, but it seems to have no measurable effect on the optical properties. Ferric iron, even in small amounts, may be very important, but its presence may not be suspected since iron-bearing mineral inclusions occur in most feldspar samples. By measuring and estimating the influence of these other cations an attempt is made to determine the relationship between Na substitution for K in homogeneous alkali feldspars and their refractive indices (Fig. 2).

Emphasis is placed on the refractive index α of homogeneous feldspars (either naturally homogeneous or homogenized) on the assumption that α is independent of the Si/Al distribution. Common alkali feldspars contain, in addition to K and Na, minor amounts of the four large cations Ca, Ba, Sr, and Rb. The refractive indices of pure Ca, Ba, and Sr feldspars are known. If a straight-line variation is assumed between pure K feldspar (α = 1.518) and pure Ca feldspar, an increase of 0.0006 per 1 per cent (mol) anorthite should occur. If pure Ba feldspar is compared similarly, the increase is about 0.0007 per 1 per cent (mol) of celsian. Eskola (1922) prepared artificial Sr feldspar and determined the indices of refraction to be almost identical with those of anorthite. Thus, Sr would cause an increase

of 0.0006 per 1 per cent (mol) of Sr feldspar. Little information could be found on refractive indices of Rb-bearing feldspar except for one sample of a white microcline from Varutrask for which $\alpha = 1.5179$ and $\gamma = 1.5247$. It contains 6.42 per cent Rb feldspar and no Ca feldspar. On the basis of this one sample, it is concluded that Rb causes a very slight decrease in the refractive index. Thus, Na would be expected to cause 0.0001 increase per 1 per cent (mol) of albite.

In Figure 2*a*, a graph of the α refractive indices of samples 1–9 and 11–15, a curve (1) is deduced to represent the increase in α caused by the presence of Na. Three points are plotted for each sample: the highest is the mean value for α of the natural feldspar (Table 6), the intermediate point is the mean value for α after homogenization (heating to 850° C. for 2 hours) (Table 7), and the lowest point is the value obtained by subtracting the corrections for Ca, Ba, and Sr, as outlined above, from α of the homogeneous feldspar. The curve showing the influence of Na on K feldspar is drawn through these lowest points and is much lower than the straight line (2) between K feldspar and Na feldspar, which would give an increase of 0.0001 per 1 per cent Na feldspar. The deduced curve may be too flat because the factors for Ca, Ba, and Sr may have been chosen incorrectly or because of bias in the chemical data for these minor elements, but the curve may not be raised above the values for samples 2, 13, and 14 after homogenization. Spencer's data (1937), plotted in Figure 2*b* by the same method, yield a similarly flat curve. He had Ba determined for only 2 samples and Sr for none, so that the corrected values may be expected to be high. The curve determined up to $Or_{60}Ab_{40}$ in Figure 2*a* is extrapolated below the corrected values to $Or_{45}Ab_{55}$ in Figure 2*b*. The curve has been defined both by the α index after correction for minor-element content and by the index decrease due to homogenization. If the straight line (2) represents the average α index for completely unmixed K/Na cryptoperthites, the lower curve must lie below the straight line by an amount equal to, or (because of incomplete unmixing) greater than, the index decrease upon homogenization.

The proposed curve for homogeneous K/Na feldspar emphasizes the negligible effect of Na on the refractive index up to about 30 per cent albite and the major effect of small amounts of divalent Ca, Sr, and Ba. For example, samples 1, 11, and 12, all apparently homogeneous crystals, have a range of values for α ranging between 0.0017 and 0.0024. If this range were attributed to compositional differences in K/Na alone it would be as great as the entire range of the proposed curve from $Or_{100}Ab_0$ to $Or_{40}Ab_{60}$. It is more probable that the range is a consequence of much smaller fluctuations in the content of the minor elements Ca, Sr, Ba, and perhaps Fe. No experimental refractive-index curve is available for homogeneous K/Na feldspars free of these minor elements, although one could be determined from suitable synthetic materials, to test the validity of the proposed curve. The curve might be questioned on the ground that linear variations between K feldspar and the Ca, Sr, and Ba end members were assumed to show that the K/Na variation is nonlinear. The fact that 5 of the 15 samples have uncorrected indices well below the straight line between K and Na feldspars proves the nonlinearity of this series, but nonlinearity of any or all of the other series is also possible. Greater deviation from linearity would be expected in the K/Na series, however, because of the greater size differential of the cations.

Gravimetric analyses were used in the construction of Figure 2*a* for samples 1–9, and a combination of spectrographic and flame-photometer values for samples 11–15. For samples 1–10 (Tables 3, 4) Ca determined spectrographically is consistently higher than Ca determined by gravimetric methods. This may explain why the corrected values for samples 12, 13, 14, and 15 fall below the proposed curve based on gravimetric analyses. Some of the scatter may also be due to the generally poor agreement between gravimetric and spectrographic Ba determinations. Corrected values for samples 11 and 5 fall well above the curve. These are the only samples containing appreciable Sr, which suggests that the correcting factor should be about .0009 per 1 per cent (mol) Sr feldspar rather than .0006. Additional Sr-rich feldspars must be studied before this factor is known. For samples containing zoned feldspars much of the scatter of Figure 2*a* may reflect insufficient optical determinations to obtain an average for the sample.

Microcline samples 7, 8, and 9 fall close to the proposed curve after the appropriate factors for Ca, Ba, and Sr have been applied.

The importance of Ba in determining the index of sample 7 is obvious from Figure 2*a*.

The high refractive index of sample 6 (Figure 2*a*) and of Spencer "B" (Fig. 2*b*) cannot be explained in terms of chemical composition. These are both adularias from St. Gotthard, Switzerland. Other unusual properties of adularia include its highly rotated position of the optic plane in some samples described by Chaisson (1950, p. 542–546) and its well-known resistance to sanidinization. These factors may reflect an important structural difference between adularia and orthoclase.

Faust (1936) recognized the existence of an iron feldspar end member and concluded that it may be present in any feldspar in small amount. He made no estimate of the effect on the refractive indices except to anticipate a slight increase. Coombs (1954) in a detailed study of Madagascar orthoclase also recognized that the iron feldspar molecule raises the index, and he cites Gaubert's (1926) figure for synthetic iron orthoclase: $\alpha = 1.601$. This figure and Coombs' values suggest an increase of .0008 in α for 1 per cent (mol) in K feldspar. The presence of Fe^{3+} has not been considered an important factor in determining

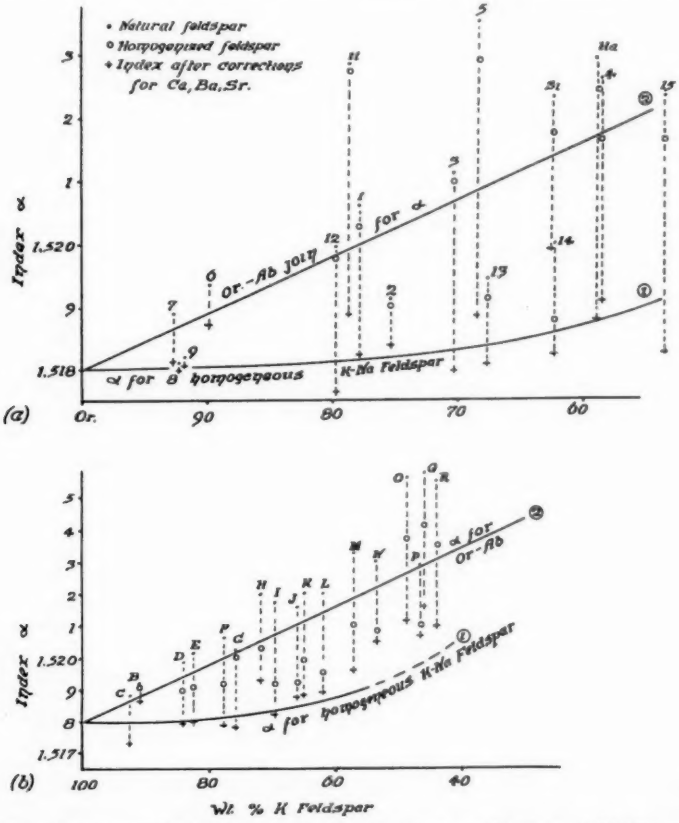

FIGURE 2.—REFRACTIVE-INDEX CURVES FOR HOMOGENEOUS AND UNMIXED K/Na FELDSPARS

(a) The α refractive index for samples 1–9, 11–15, and "Ha" and "Si" plotted against weight per cent K feldspar. Curve (1) represents α index for homogeneous K/Na feldspar, derived by homogenization and correction for divalent alkali-ion content. Line (2) is linear between α indices of K feldspar and Na feldspar and represents theoretical locus of average α index of completely unmixed K/Na cryptoperthites. (b) Same procedure applied to samples of Spencer (1937), recalculated to 100 per cent feldspar

the refractive indices of samples 1–15, since it is thought to occur as inclusions in the feldspar. The largest value for Fe_2O_3 is 0.26 per cent, which is equivalent to 1 per cent (mol) $KFeSi_3O_8$, and could raise α by .0008. The amount of iron reported as FeO is extremely small.

The indices of refraction for Spencer's samples "Si" and "Ha" as determined here are included in Figure 2*a*. Since BaO and SrO are not reported in the analysis the only correction factor that could be applied is for 3 per cent Ca feldspar in "Si" and 6 per cent Ca feldspar in "Ha"; "Ha" falls close to the curve, whereas "Si" is considerably above, probably indicating the presence of Ba or Sr in "Si". Samples 4 and 15, like "Si", come from Siebengebirge and have 1.5 and 1.7 per cent Ba feldspar respectively.

Optic angle.—The optic angle varies with both composition and the status of aluminum distribution. Spencer (1937) determined the optic angles of sanidinized feldspars that were believed to be near equilibrium at 1075° C. and proposed the curve reproduced in Figure 3*a*. From this diagram substitution of Na for K in sanidinized potassium feldspar appears to cause a large increase in 2V when the optic plane is normal to (010) and a large decrease in 2V when the optic plane is parallel to (010). In terms of the refractive indices the substitution of Na for K increases the index of the ray that vibrates parallel to the b crystallographic direction (γ for most natural feldspars) more than the index of the ray that vibrates closest to the c crystallographic direction (β for most natural feldspars) and increases both β and γ more than α. Coombs (1954) studied the in-

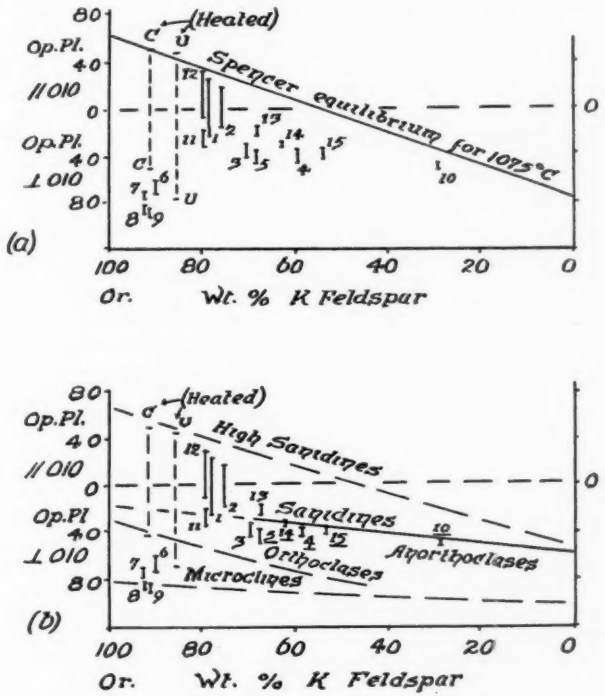

FIGURE 3.—RANGE IN OPTIC ANGLE FOR SAMPLES 1–15

(a) Range in 2V values graphed in relation to curve of Spencer (1937, Fig. 2, p. 458) for crystals sanidinized at 1075° C. Spencer's natural and sanidinized samples *C* and *U*, the structures of which have been determined accurately, are included for comparison after recalculation to 100 per cent feldspar. (b) Range in 2V values graphed in relation to four series of alkali feldspars defined by Tuttle (1952, Fig. 1, p. 557). Numbers of unmixed samples are underlined. Figure modified after MacKenzie and Smith (1956, Fig. 1, p. 406)

fluence of ferric iron on 2V and notes that feldspars with apparent iron substitution show considerable irregularity in the optic angle.

In Figure 3*b* the same ranges of 2V are plotted in relation to the four series of alkali

Several specimens in this study that show considerable range in value of the α index, shown to be nearly independent of Si/Al order, also show considerable range in 2V. This suggests that small variations in content

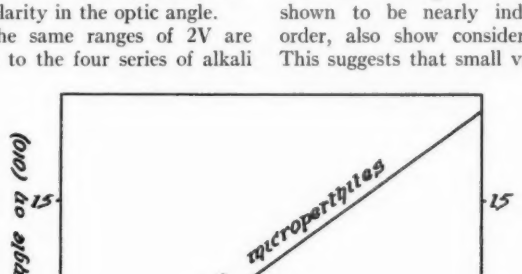

FIGURE 4.—EXTINCTION ANGLES ON (010)
Curves taken from Tuttle (1952, Fig. 3, p. 563). Points of unmixed samples are circled.

feldspars recognized by Tuttle (1952). Tuttle (1952) and MacKenzie and Smith (1955; 1956) have shown that many natural alkali feldspars fall on or close to these curves of 2V versus composition. Certain specimens with optic angles between the sanidine and orthoclase curves consist of potassic feldspar plus an albitic phase partly inverted from a high-temperature form to a low-temperature form, suggesting a genetic significance to the curves (Tuttle and Keith, 1954, p. 69–70; MacKenzie and Smith, 1955, p. 729–730). Most specimens of this paper, however, have optic angles that fall either between the high sanidine-sanidine curves or between the sanidine-orthoclase curves. For the latter specimens no indication was found by X-ray study of partial inversion of the albitic phase to a low-temperature form. Sample 14, which does lie on the sanidine curve, is the only specimen in which low albite was identified.

Tuttle's curves form a useful basis for classification of alkali feldspars of known composition, especially since the optic angle is not affected greatly by degree of unmixing. Specimens with optic angles that fall between the curves do not necessarily contain partly inverted phases of different refractivities, however, although they may be intermediate in degree of Si/Al order.

of the minor elements must also be considered as a possible source of variation of optic angle. The substitution of Na for K increases the refractive indices β and γ more than it does α for the K-rich end of the series. This substitution affects 2V. Although data are not available on the influence of Ca, Ba, and Sr, calculations from the refractive indices suggest that the role of these divalent ions is even more effective in modifying 2V. These observations do not cancel the effect of Si/Al order-disorder on 2V but do place the emphasis on the presence or absence of divalent ions in bringing about the observed differences in 2V, as reflected especially in the zoning.

Extinction angles.—Spencer's data (1937) show that the extinction angle on (010) for homogeneous feldspars is 3°–4° greater for the composition $Or_{50}Ab_{50}$ than for pure potassic feldspar. For completely unmixed cryptoperthites this extinction angle is about 7° greater for composition $Or_{50}Ab_{50}$ than for pure potassic feldspar. The extinction angles recorded in Table 6 of this paper are expressed graphically in Figure 4. They fit the sanidine-anorthoclase cryptoperthite curve of Tuttle (1952) quite closely, although with some scatter.

A correlation between composition and extinction angle on (001) for microcline has

not been established. Barth (1931) attributed a decrease in extinction angle of a microcline to diffusion of Na into the structure during heat treatment at 1000° C. It seems much more probable that the changes were the result of partial sanidinization (disordering of Si/Al). The optic angle of the microcline was reduced from 80° to 50°, and albite by the same treatment was apparently converted to high albite. MacKenzie (1954, p. 363–366) proposed that the lattice geometry of microcline, and hence extinction angle on (001), is a function of the amount of Na in solid solution. When most triclinic, it would contain less than approximately 8 per cent dissolved Na feldspar. Bailey (1954, Ph.D. dissertation, Univ. Cambridge) stated that the primary cause for change of geometry is degree of order of Si/Al, although the same environmental conditions that favor ordering of Si/Al would also favor unmixing of dissolved Na feldspar. Bailey showed exceptions to MacKenzie's compositional limits. Goldsmith and Laves (1954a, p. 3) also proposed that the triclinicity of microcline is a function of degree of order and showed (1954b, p. 115) that the amount of dissolved Na is not critical in determining lattice geometry.

Variations Caused by Submicroscopic Intergrowths

Submicroscopic intergrowths of feldspars are easily detected by single-crystal X-ray-diffraction methods and were first so studied by Kozu and Endo (1921) using the Laue method. Spencer's (1937) suite of microperthites and cryptoperthites was extensively described by Chao, Smare, and Taylor (1939), Chao and Taylor (1940), and MacKenzie and Smith (1955) utilizing the oscillation method. Other cryptoperthites were studied by Ito (1938; 1950), Ito and Sadanaga (1952), and MacKenzie and Smith (1956) using powder, Sauter, Weissenberg, and oscillation methods. These X-ray investigations proved that cryptoperthites are intergrowths of two feldspars and can be homogenized by heat treatment.

Oscillation X-ray photographs were taken of all the writer's samples, except 7 and 9, and of Spencer's samples "Si" and "Ha" to determine whether they are cryptoperthites. All these samples are optically homogeneous. A summary description of the X-ray patterns obtained is given in Table 7. The patterns can be divided into three groups, those showing only one set of reflections, those showing two sets of reflections, and an intermediate group showing a single set but with diffuse streaks associated with some of the reflections.

Those patterns showing only one set of sharply defined reflections represent homogeneous crystals free from imperfections that cause diffuseness. Those showing two sets of reflections are from intergrowths of two feldspars, one monoclinic and the other triclinic and invariably twinned. Twinning on the pericline law causes doubling of reflections parallel to the layer lines of b-axis oscillation photographs, and twinning according to the albite law causes doubling of reflections almost perpendicular to the layer lines (Chao and Taylor, 1940; Smith and MacKenzie, 1955). Samples of this group show some diffuseness between the two sets of reflections but reveal both sets clearly. The group showing a single set of reflections but with some diffuseness includes many of the samples described in Table 7. Except for sample 6, adularia, and sample 8, microcline, which show a diffuseness perpendicular to b-axis oscillation layer lines, the diffuseness is parallel to the layer lines. This diffuseness is rarely symmetrical about the main reflection. In most of these samples the diffuse streak is at a greater value of 2θ than the main reflection itself. These streaks can be attributed to very small regions of unmixed high-temperature Na feldspar that are not of great enough extent to produce discrete spots by X-ray diffraction. Since Na feldspar has a shorter a-axis length than K feldspar it will give hkl reflections (h large) at higher 2θ values. Samples 3, "Si", and "Ha" show slight diffuse streaks at smaller 2θ values than the main reflections. The interpretation of these streaks is uncertain. They could be due to very small regions of K feldspar having less Na in solid solution than the bulk of the sample or to imperfections in the K-feldspar structure, such as small triclinic areas twinned by the pericline law.

All sanidine samples more sodium-rich than Or_{68} were found to be unmixed by single-crystal X-ray study; the more potassium-rich samples were homogeneous. In the region of Or_{68} samples 13 and 3 with compositions $Or_{67.8}$ and $Or_{70.1}$ are homogeneous, whereas sample 5 of composition $Or_{68.2}$ is unmixed. This unmixing limit is slightly more potassic than the Or_{60} value set by MacKenzie and

Smith (1956, p. 410) for their sanidine specimens.

The straight line (2) drawn between the α indices of K feldspar and Na feldspar in Figure 2 is proposed as the locus of average indices for submicroscopic intergrowths of K/Na feldspars that are completely unmixed. The increase of α-index values due to small amounts of divalent alkali ions is so great, however, that the measured values do not fit the curve. The points lying between curves (1) and (2) include homogeneous feldspars, samples 2 and 13, whose indices fall above curve (1) because of the minor-element content and a cryptoperithite, sample 14, falling below curve (2) because of incomplete unmixing.

A decrease in refractive indices occurs when those feldspars which have been shown to be intergrowths on a submicroscopic scale are homogenized by heating at 850° C. for 2 hours. The three refractive indices α, β, and γ were found to decrease by about the same amount, giving only a small change in 2V. These results are in general agreement with the findings of Spencer (1937, p. 463–473). The decrease in the α index for each sample is listed in Table 7.

The amount of index decrease is proportional to the intensity of the X-ray reflections from the unmixed plagioclase component of the natural feldspar. Table 7 shows that sample 14 has the densest and most clearly defined Na-feldspar reflections and shows the largest drop in refractive index (0.0012). Samples 4 and 15 have very diffuse and poorly resolved Na-feldspar reflections. They decrease in index by 0.0010 and 0.0007 respectively. Samples 5 and "Si" have only diffuse streaks from the main reflections, and both have index drops of 0.0006 (the particular crystal of "Si" that was X-rayed has an index drop of 0.0006). The other samples show very slight diffuseness or none at all and were found to decrease in index between 0.0005 and 0.0001. The correlation between decrease in refractive index and the intensity of Na-feldspar reflections is therefore good. All crystals show an index decrease after heating, even if X-ray study indicates no unmixing. This may mean that very small amounts of unmixed feldspar cannot be detected by the X-ray method or that heating causes a small permanent volume increase even for homogeneous crystals. The writer does not believe that

TABLE 7.—CORRELATION BETWEEN REFRACTIVE-INDEX DECREASE DUE TO HOMOGENIZATION AND DEGREE OF UNMIXING AS DETERMINED BY b-AXIS OSCILLATION METHOD

Sample	Decrease in α	Description of b-axis oscillation photographs
1	0.0003	One set of reflections, no diffuseness
2	0.0001	One set of reflections, no diffuseness
3	0.0001	One set of reflections, very slight diffuseness at smaller 2θ
4	0.0010	One set of reflections with much diffuseness at greater 2θ; second set of reflections scarcely resolved
5	0.0006	One set of reflections with some diffuseness; more diffuse at greater 2θ than smaller 2θ
6	ND	One set of reflections with diffuseness perpendicular to layer lines
8	ND	One set of reflections with diffuseness perpendicular to layer lines
10	ND	Four sets of reflections of equal intensity, no diffuseness
11	0.0001	One set of reflections, no diffuseness
12	0.0002	One set of reflections, no diffuseness
13	0.0003	One set of reflections, no diffuseness
14	0.0012	Two sets of reflections with some diffuseness between sets, albite twin superstructure in plagioclase of most crystals, pericline law in others
15	0.0007	One set of reflections with much diffuseness at greater 2θ; second set of reflections scarcely resolved
"Si"	0.0004 to 0.0009	One set of reflections with some diffuseness, more diffuse at smaller 2θ than greater 2θ
"Ha"	0.0005	One set of reflections with very slight diffuseness, more diffuse at smaller 2θ than greater 2θ

disordering of Si/Al is the explanation, since only the α index, relatively insensitive to order-disorder variations, is considered here.

TABLE 8.—COMPARISON OF COMPOSITION FROM CHEMICAL ANALYSIS AND FROM d($\bar{2}$01) GRAPH

Values for d($\bar{2}$01) were determined by diffractometer method, except for sample 14 which was calculated from cell dimensions determined by the precession method on single crystals.

Sample	Composition by chemical analysis		Composition by d($\bar{2}$01)		Per cent total feldspar unmixed as $NaAlSi_3O_8$
	Per cent Na feldspar	Per cent Na+Ca feldspar	d($\bar{2}$01) in Å	Per cent Na feldspar	"y"
1	18.59	20.16	4.1952	18	0.7
			4.1996	16 heated	
2	23.74	24.59	4.1829	23.5	0.3
			4.1917	19 heated	
3	25.68	25.83	4.1824	24	2.2
			4.1880	21.5 heated	
4	37.35	39.42	4.1590	36	2.1
			4.1532	39 heated	
5	25.50	27.32	4.1746	28	
			4.1765	27 heated	
6	9.18	9.28	4.2223	4	5.4
			4.2237	3.5 heated	
7	6.26	6.36	4.2195	6	0.3
8	7.54	7.64	4.2169	7.5	0.0
9	7.92	7.92	4.2207	5	3.1
10	67.81	69.26	4.0923	69	
			4.0916	69.5 heated	
11	14.38	16.12	4.2073	12.5	2.1
			4.2059	13 heated	
12	16.58	18.81	4.1998	15.5	1.3
			4.2021	14.5 heated	
13	30.02	31.76	4.1804	25	6.7
			4.1884	21 heated	
14	36.20	36.84		17	21.0
15	40.76	43.98	4.1563	38	4.5
			4.1578	37 heated	

A quantitative attempt was made to relate the percentage of unmixed Na feldspar to the observed decrease in refractive index. Two methods were used, both involving Bowen and Tuttle's (1950) curve relating the lattice spacing d($\bar{2}$01) to the Or/Ab ratio for synthetic alkali feldspars. It was assumed that the composition of the potassic component (major part) of a given cryptoperthite could be determined from its d($\bar{2}$01) spacing, thereby determining the percentage of Na feldspar in solid solution in the K feldspar. In the first method the percentage of unmixed Na feldspar was calculated by comparison with the total Na feldspar by chemical analysis. If "y" is the per cent of total feldspar unmixed, then

$$y = \text{total Na feldspar from analysis} - \frac{\%\ \text{Na feldspar in solid sol. (or } 100 - y)}{100}.$$

Values calculated for "y" are listed in Table 8. Comparison with Table 7 shows that there is poor correlation for a few samples between values for "y" and the degree of unmixing

indicated by oscillation photographs. For example, oscillation photographs show that sample 4 is unmixed appreciably, yet its "y" value is only 2.1 per cent unmixed albite. Sample 13 appears homogeneous from oscillation photographs, but its calculated "y" value indicates that 6.7 per cent of the total feldspar is unmixed as albite. The index drop on homogenization for these two samples supports the evidence given by the oscillation photographs rather than that given by d($\bar{2}$01).

Samples 1, 2, 3, 11, 12, and 13, which are essentially homogeneous feldspars as indicated by oscillation photographs and by the index drop on homogenization, provide a useful comparison between the composition determined by chemical analysis and by d($\bar{2}$01). For all these samples except 13 the per cent Na feldspar by d($\bar{2}$01) agrees fairly well with the composition by chemical analysis or is at least within the limits of the values obtained by gravimetric, spectrographic, and flame-photometer analyses. Although the curve for d($\bar{2}$01) against composition was determined for the pure K-Na system, the ionic radius of Ca (1.06) is such that it would be expected to act like Na (0.98), whereas Sr (1.27), Ba (1.43), and Rb (1.49) would act like K (1.33) in determining the spacing d($\bar{2}$01). The comparison should therefore be made between total Na + Ca feldspar by chemical analysis and the per cent Na feldspar as determined from the d($\bar{2}$01) graph. Composition by d($\bar{2}$01) for the naturally homogeneous feldspars is consistently lower than by chemical analysis in this case, but for samples 1, 2, 3, 11, and 12 the difference amounts to 3.6 per cent at most. For sample 13 Na + Ca feldspar by chemical analysis (31.76 per cent) is significantly higher than the d($\bar{2}$01) composition (25.0 per cent).

The second method used was to compare the spacing d($\bar{2}$01) for natural samples with d($\bar{2}$01) for samples homogenized at 850° C. It was postulated that this spacing should decrease when unmixed Na + Ca feldspar was taken back into solid solution in the host structure, and that the decrease could be interpreted in terms of per cent unmixed feldspar in the natural sample. The results of these heating experiments are listed in Table 8 and, except for samples 4, 10, and 11, indicate the opposite of what was anticipated. Instead of homogenization causing a decrease in d($\bar{2}$01), it caused an increase. Sample 15 is an example of the observed facts. From b-axis oscillation photographs this sample is known to be unmixed; the Na feldspar component is twinned on the pericline law. Precession photographs of this sample also show faint but distinct reflections for the Na feldspar component. After heating the crystal at 850° C. for 2 hours only one set of sharp reflections was obtained on oscillation photographs. A refractive-index drop of 0.0007 was obtained on three different crystals from this sample. The d($\bar{2}$01) spacing increased very slightly upon homogenization, however, indicating 1 per cent less Na feldspar in solid solution than before. Samples 2 and 3, which are homogeneous according to oscillation and precession pictures and have an index drop of only 0.0001 on heating, exhibit an even greater increase in d($\bar{2}$01). Sample 2 showed a decrease of 4.5 per cent and sample 3 of 2.5 per cent Na feldspar in solid solution. Samples cooled in air and those quenched in water gave the same anomalous results. The increase in d($\bar{2}$01) cannot be explained on the basis of partial sanidinization due to further disordering of Si and Al. Cole *et al.* (1949, p. 287) and Bailey and Taylor (1955, p. 632) have shown that in all samples so far investigated the effect of sanidinization is a decrease in the c-axial length, an increase in b, and essentially no change in a. These changes cancel one another in the calculation of the d($\bar{2}$01) spacing for most compositions. The heating may have caused a metastable expansion of the entire lattice. This view is supported by the observation that in all samples except 4, 11, and 12 heating at 850° C. for 2 hours also caused an increase in both d(001) and d(010) (Table 9). The small decrease in the α refractive index of homogeneous feldspars is a consequence of this expansion.

The d($\bar{2}$01) curve seems to apply to many naturally homogeneous sanidines and was found to apply also to the three microclines and the anorthoclase of this paper, samples 7–10. Laves (1952, p. 562), Coombs (1954, p. 424), and MacKenzie and Smith (1955, p. 722) also noted inconsistencies in compositions determined from lattice spacings, so that independent checks of composition are desirable until the reasons for the deviations are established.

Small changes in optic angle accompany homogenization of most cryptoperthites. The change was first described by Kozu and Suzuki (1925) who found that moonstones from Ceylon and Korea showed increases of 4° and 8° respectively. The increase began at

about 550° C. and was completed between 650° and 750° C. In this same temperature range schiller disappeared, and the extra set of reflections on Laue X-ray photographs disappeared. Thus a correlation between homogenization and change in optic angle seems to have been well established by this early work. Spencer (1937, p. 471) noted a similar increase of optic angle between 600° and 800° C. for several microperthites and cryptoperthites. He related the increase to re-solution of unmixed Na feldspar. The increase was noted only in feldspars with 30 per cent or more Na feldspar. His sample *G* (Eifel sanidine) with 21 per cent Na feldspar shows a 2-degree decrease in optic angle after heating to 850° C. MacKenzie and Smith (1956, p. 419–421) heated a number of high-temperature K/Na feldspars at 900° C. for 24 hours. They found a slight decrease in 2V for specimens more potassic than Or_{60}, a progressive increase in 2V with increasing sodium for specimens ranging from Or_{60} to Or_{40}, and either no change or a slight increase in 2V for triclinic anorthoclases more sodic than Or_{40}. No explanation is given for the differing reactions of these three groups to heat.

All the sanidines and sanidine cryptoperthites of this paper with the optic plane normal to (010) have a slight decrease of 2V after heating at 850° C. for 2 hours and a slight increase of 2V for specimens with the optic plane parallel to (010). The values are listed in Table 10. For all these samples the angular change is the result of a greater decrease in the refractive index of the ray vibrating parallel to crystallographic b than in the critical index of the ray vibrating nearest to crystallographic c upon homogenization. No change was detected in samples 6 and 14, but a slight increase in 2V was observed for sample 10, an anorthoclase. Since both homogeneous and unmixed sanidines show a decrease in 2V the effect cannot be related entirely to homogenization. Slight sanidinization or a metastable expansion of the structure not due to disordering may be involved.

A marked difference of extinction angle on (010) between sanidines and orthoclase microperthites of the same composition has been noted by Spencer (1930; 1937), Oftedahl (1948), and Tuttle (1952). The writer believes that the heating experiments of Spencer (1930, p. 316–319) indicate that most of the difference is caused by the degree of submicroscopic unmixing, although some of the difference could be related to differences in Si/Al distribution. By heating white moonstone of

TABLE 9.—LATTICE SPACINGS d(001) AND d(010) FOR SAMPLES 1–15

Spacings determined by diffractometer, except for three values (*) determined on single crystals by precession method.

Sample	d(001) in Å		d(010) in Å	
	Natural	Heated	Natural	Heated
1	ND	6.450	13.024	13.034
2	6.438	6.445	13.013	13.016
3	6.447	6.454	13.016	13.021
4	6.440	6.433	13.004	13.004
5	6.442	6.449	12.99*	ND
6	6.470	6.480	12.977	12.977
7	6.490	ND	12.965	ND
8	6.485	ND	12.960	ND
9	6.488	ND	12.955	ND
10	6.407	6.412	12.923	12.935
11	6.461	6.451	13.034	13.025
12	6.448	6.446	13.036	13.031
13	6.446	6.451	13.010	13.020
14	6.44*	ND	12.98*	ND
15	6.431	6.441	13.006	13.008

composition $Or_{60}Ab_{40}$ Spencer reduced the extinction angle from 10.5° to 7.5° and at the same time reduced the optic angle by only 3°–4°. Thus sanidinization had scarcely begun and probably had little effect on the extinction angle. The change seems best related to disappearance of the white schiller.

Heating experiments were made on samples 4, 14, and 15, which are somewhat unmixed, to determine whether homogenization caused a decrease in extinction angle. A decrease of not more than 1° was determined for several grains from each of these samples. Such a small decrease would be expected from feldspars that are only slightly unmixed.

TABLE 10.—CHANGES IN OPTIC ANGLE CAUSED BY HEATING TO 850° C. FOR 2 HOURS

The letters *N* and *P* denote the position of the optic plane as either normal or parallel to (010). The measurements listed were made on carefully oriented thin slices, so that the same part of each crystal was measured before and after heat treatment.

Sample	Change in optic angle
1	23°P up to 24°P
2	18°P up to 20°P
3	39°N down to 37°N
4	36°N down to 33°N
5	46°N down to 43°N
6	no change detected
10	55°N up to 56½°N
11	ND
12	28°P up to 29°P
13	23°N down to 18°N
14	no change detected
15	38½°N down to 36°N

Variations Due to Distribution of Si/Al

A direct correlation of optical properties with Si/Al distribution is not possible because too few structural analyses have been done with sufficient accuracy to determine the distribution in feldspars. However, the optical changes that occur when orthoclase and microcline are sanidinized provide a measure of the effects of disordering the tetrahedral cations. All alkali feldspars change their optical properties in the same general way when they are heated for prolonged periods above 1000° C. The refractive index of the ray vibrating parallel to the b crystallographic axis decreases, the index of the ray vibrating in the optic direction closest to the c crystallographic axis increases, and α remains essentially unchanged. These index changes cause the optic angle to change also. With heating it becomes progressively smaller and may pass through zero and become progressively larger in the plane parallel to (010). The optic angle is a very sensitive indicator of small changes in the β and γ indices, particularly when the optic angle is small.

If the α, β, and γ indices changed by the same amount with variations in composition, a measure of 2V or birefringence $\gamma - \alpha$ or $\beta - \alpha$ would provide an estimate of the state of aluminum disorder independent of composition. The substitution of Na for K increases γ more than β when the optic plane is normal to (010) and increases both γ and β more than α. This causes an increase in 2V as the Ab/Or ratio increases. The effect of Ca, Ba, and Sr on 2V of potassic feldspars has not been determined experimentally, but the refractive-index increases suggest that 2V must increase appreciably also. If the small amounts of Ca, Ba, and Sr are neglected the optic angle and birefringence can be used as a measure of aluminum disorder for feldspars of a given Ab/Or ratio. The problem remains to determine the variation of 2V with Ab/Or ratio for feldspars with constant degree of aluminum disorder. Fortunately Spencer (1937, p. 458) determined the variation of 2V with Ab/Or ratio for some completely sanidinized

feldspars (those which reached equilibrium at 1075° C.). His curve shown in Figure 3*a* is the best available for completely disordered feldspars. None exists for partly or completely ordered feldspars.

The range of optic angles obtained for samples 1–15 is plotted in Figure 3*a*. In Figure 5*a* the same samples are plotted according to birefringence "b" $-$ α instead of 2V. This diagram emphasizes the importance of the "b" index in differentiating sanidine and microcline. The "b" index denotes the refractive index of the ray that vibrates most nearly parallel to the b crystallographic axis. This will be the index γ for feldspars having the optic plane normal to (010) and β for feldspars having the optic plane parallel to (010). For microcline, "b" refers to γ even though γ is not quite coincident with the b crystallographic axis. The refractive index "b" is chosen because it changes most during sanidinization and is therefore the most sensitive index to changes in aluminum distribution. The index α varies with composition but is independent of changes in aluminum distribution. The effect of subtracting the α index from the "b" index, therefore, is to cancel part of the contribution that composition makes to the "b" index without affecting its sensitivity to Si/Al disorder. The birefringence "b" $-$ α has the added advantage of being easily determined on (001) cleavage flakes. The curve in Figure 5*a* represents the birefringence of sanidinized samples believed to be at equilibrium at 1075° C., as calculated from Spencer's data (1937, Table 2). No information is available

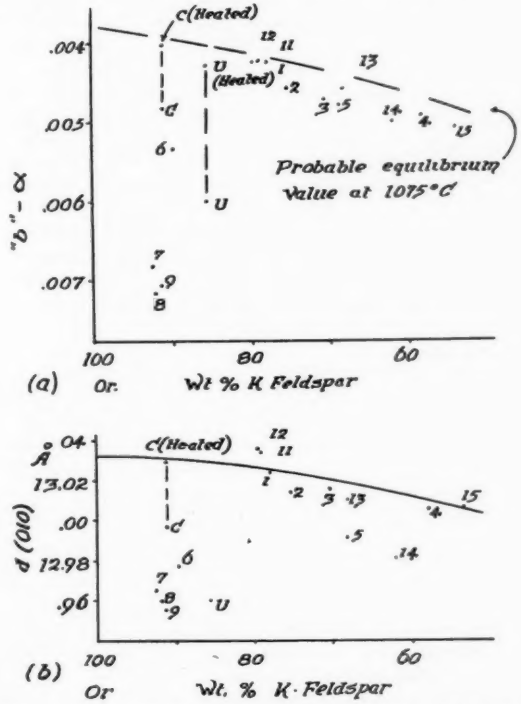

FIGURE 5.—DIAGRAMS INDICATING DEGREE OF ORDER-DISORDER OF Si/Al FOR SAMPLES 1–15

(a) Birefringence "b" $-$ α graphed in relation to bulk composition; "b" denotes refractive index of the ray vibrating most nearly parallel to crystallographic *b* (either β or γ). Dashed line calculated from data of Spencer (1937, Table 2) for crystals sanidinized at 1075° C. Spencer's samples *C* and *U*, recalculated to 100 per cent feldspar, are included for comparison. Sanidinized *C* has complete disorder of Si/Al (Cole *et al.*, 1949), whereas natural *C* and *U* have a partial ordering (Chao *et al.*, 1940; Bailey and Taylor, 1955). (b) Lattice spacing d(010) graphed in relation to bulk composition. Curve adapted from Donnay and Donnay (1952, Fig. 6, p. 127) for synthetic alkali feldspars.

to determine the shape of this curve for completely ordered microclines or for partly ordered feldspars.

If the birefringence "b" $-\alpha$ can be used as a measure of the state of Si/Al distribution, the 10 sanidines are all highly disordered and close to the curve for completely disordered sanidine. Three microclines from granitic rocks, samples 7, 8, and 9, are the most highly ordered, and adularia, sample 6, occupies an intermediate position. Detailed structures have been determined for sanidinized sample *C* and for the intermediate microcline, sample *U* of Spencer (1937). Cole *et al.* (1949) found that sanidine *C* was completely disordered, and Bailey and Taylor (1955) found a partial ordering of Si/Al in microcline *U*. In a less detailed structure determination Chao *et al.* (1940) found that orthoclase *C* possessed a state of order intermediate between those of sanidine *C* and microcline *U*. The birefringence "b" $-\alpha$ appears to be a good measure of Si/Al distribution for these three samples. Figure 5*a* emphasizes the difference between microcline, adularia, and orthoclase, but the sanidines are grouped together more closely than in Figure 3.

Interesting correlations can be made between the lattice spacing d(010) and the refractive index of the ray that vibrates nearly normal to (010) (the "b" index) and between the spacing d(001) and the refractive index of the ray that vibrates approximately normal to (001). For Spencer's sample *C* the decrease in the "b" refractive index caused by sanidinization is accompanied by an increase in the d(010) spacing (Cole *et al.*, 1949, p. 282), and the increase in the critical refractive index closest to crystallographic c is accompanied by a decrease in the d(001) spacing. The spacing d(010) is larger for sanidines than for microclines, whereas the spacing d(001) is smaller for sanidines than for microclines. Upon sanidinization the largest change occurs in the spacing d(010), just as the largest change occurs in the "b" index. If the changes in d(010) and d(001) bear a linear relation to the degree of aluminum disorder, they provide a rapid method of estimating the distribution of Si/Al.

Lattice spacings d(001) and d(010) for samples 1–15 are listed in Table 9, and the d(010) spacings for samples 1–15 are graphed in Figure 5*b*. The curve in the diagram has been plotted from the data of Donnay and Donnay (1952) for synthetic alkali feldspars. It shows the influence of composition (Or/Ab) on the spacing d(010) and presumably applies to completely disordered feldspars. The shape of the curve for completely ordered feldspars is not known, nor is the influence of Ca, Ba, Sr, or Fe substitutions. Samples plotted in Figure 5*b* have the same general distribution as those in Figure 5*a*, but in detail the correlation is poor. The values plotted in Figure 5*b* are for natural feldspars, some of which are definitely unmixed; however, the lattice spacings for homogenized samples (heated to 850° C.) when plotted show about the same amount of scatter.

A quantitative relation between order-disorder of Si/Al in microcline and the deviation from monoclinic symmetry has been suggested recently by Goldsmith and Laves (1954a, p. 3–5). They employ the difference between d(131) and d($1\bar{3}1$) as a measure of "triclinicity" and suggest that the difference for completely ordered microcline is close to 0.08Å. Values obtained by the writer for samples 7–9 are all about 0.07Å, indicating a highly ordered state by this criterion. Reciprocal lattice angles were also measured on an untwinned single crystal from sample 8 by the precession method. These were determined as $\alpha^* = 90°26'$, $\beta^* = 64°01'$, and $\gamma^* = 92°15'$, all $\pm 05'$. These values compare favorably with the most triclinic microcline described by Laves (1950, p. 551; 1951, p. 510).

Discussion

Variations in chemical composition, degree of unmixing, and state of order-disorder of Si/Al in potassic feldspars are reflected as variations in the optical properties. Optical properties can therefore be used to obtain information about the composition and structure of potassic feldspars. An important conclusion of this work is that the refractive indices of alkali feldspars are not useful for determining chemical composition. Although the α index of homogeneous or homogenized alkali feldspars provides a measure of the amount of Na, Ca, Ba, Sr, and Rb substituting for K and of Fe substituting for Al in the structure, it gives no information about the relative amounts of each. The substitution of Na for K causes such a small index increase in the range $Or_{100}Ab_0$ to $Or_{60}Ab_{40}$ that its effects normally are masked by the larger increases due to substitution of minor amounts of Ca, Sr, Ba, and Fe.

The β and γ indices are not useful indicators of chemical composition because they vary with the nature of the distribution of Si/Al within the structure. The index of the ray vibrating most nearly parallel to crystallographic b (either β or γ) varies most with changes in Si/Al order-disorder and therefore provides the best measure of the distribution of Si/Al; 2V is sensitive to very small changes in both β and γ and therefore can be correlated with the state of order-disorder. The chemical composition, however, must be known before the significance of 2V or the "b" index can be properly evaluated. The birefringence "b" $-$ α seems to be sensitive to Si/Al order-disorder and relatively insensitive to composition.

The amount of sodic feldspar unmixed as submicroscopic perthite can be estimated by the decrease in refractive indices resulting from heat treatment at 850° C. For feldspars that differ only as to the localization of the alkali ions within the structure less than 2 hours of heating at 850° C. is required for complete homogenization, but for feldspars that also differ in the distribution or ratio of Si/Al long heating periods at 1000° C. or higher are necessary. Since α is not significantly changed by sanidinization, temperatures above 850° C. can be used to obtain the index drop caused by homogenization. The optic angle is not appreciably affected by unmixing, but the extinction angle measured on (010) may be a useful measure of degree of unmixing provided composition is known. For completely unmixed cryptoperthites, this extinction angle gives a measure of chemical composition (Oftedahl, 1948). The extinction angle on (001) of microclines is a useful measure of the departure from monoclinic symmetry and probably a measure of the degree of order of Si/Al beyond the stage represented by orthoclase.

The conclusions presented above can be used to explain a number of apparently conflicting statements in the literature. The work of Heald (1950) is representative of experimental observations that appear to conflict with other data, including some in this paper, and has been chosen to illustrate some of the principles of this paper. The writer accepts Heald's data as correct but believes they can be interpreted to resolve the apparent conflict.

Heald (1950, p. 85–87) proposed that a decrease in refractive indices upon heating is not related solely to solution of sodic feldspar lamellae. He described three microperthites that were still visibly perthitic after the index drop was completed and a moonstone that retained its schiller and perthitic structure to a temperature well above 800° C., the temperature at which the drop in index ceased. Heald demonstrated that no index drop occurred in the moonstone when final solution of the perthite was obtained at higher temperatures. Therefore he concluded (p. 87) ". . . it is doubtful whether the decrease in indices on heating is related only to solution of the lamellae."

Heald's observations can be explained in the light of Figure 2*a*. The straight line drawn from pure K feldspar to pure Na feldspar is the average index obtained from submicroscopic mixtures of K feldspar and Na feldspar and applies to completely unmixed cryptoperthites, assuming negligible content of the minor elements. The lower curve of Figure 2*a* shows the effect on the α refractive index of Na substitution for K in homogeneous K feldspar. The process of homogenization should reduce the α refractive index of a cryptoperthite from the upper straight line to the lower curve, although incomplete unmixing and presence of other alkali ions cause appreciable scatter in α for most natural specimens. The process of homogenization is one of changing Na and K ions from an orderly arrangement in two distinct minerals to a disordered arrangement within a common structure. A homogeneous alkali feldspar has a more expanded structure and therefore a lower specific gravity and refractive index than an unmixed feldspar of the same bulk composition.

The preceding discussion of an index drop when perthitic feldspar is homogenized applies only when the perthitic intergrowth is on a submicroscopic scale. Thus for cryptoperthites the monoclinic K feldspar and the Na feldspar, which is pseudomonoclinic by virtue of submicroscopic twinning, give rise in the immersion technique to one Becke line that is an average of both components. When the perthite is large enough to be resolved by the petrographic microscope two Becke lines are obtained, one for the K-rich feldspar and one for the Na-rich feldspar. When this visible perthite is homogenized a slight index increase should occur in the K-feldspar component because of the added Na ions.

The writer offers the following interpretation of Heald's data. A decrease in the α index

in Heald's samples 1–7 indicates homogenization of submicroscopic perthite only. Visible Na feldspar lamellae in these samples are not appreciably affected because they are large and require a much longer heat treatment to complete diffusion. The change in indices of the K component after homogenization of the visible perthite should be very small, as observed, increasing with added Na by an amount indicated by the lower curve of Figure 2*a*. Heald's data on microperthites, therefore, should not be directly compared with heating data on optically homogeneous cryptoperthites. Heald used the immersion method to determine refractive indices, whereas Spencer (1937, p. 456) used total reflection from oriented polished mineral sections on an Abbe refractometer. In the latter method average indices can be obtained even for many microperthites.

Heald also noted (p. 79–80, 83–84) that temperatures higher than 1000° C. were required to homogenize his low-sodium microperthites, in contrast to Spencer's data, and suggested structural differences in the specimens. The writer believes, as Laves (1952, p. 567) has suggested, that in the high-optic-angle microperthites the potassic and sodic components may not have the same degree of order of Si/Al. Regions of different refractivity will exist within the crystal even after disordering of alkali ions is completed. Schiller, if present, will persist until true homogenization is attained by disordering Si/Al to the same degree in both components. In view of the significant levels of divalent Ca, Sr, and Ba found in the samples of this paper it is also possible that the two components differ enough in their Si/Al ratios to impede homogenization still further.

Optical Classification of Alkali Feldspars

Alkali feldspars have been classified by various authors on many bases including the refractive indices, the extinction angles, and the optic angles. Any classification is rendered difficult by multiple variations such as the occurrence of intergrowths that may be submicroscopic, the possible gradations from high-temperature to low-temperature forms, and the acceptance of sodium, calcium, barium, strontium, and rubidium into the potassic feldspar structure. Charts relating the optical properties to composition for these feldspars have been prepared by Winchell (1925), Alling (1926), Spencer (1937), Larsen *et al.* (1938), Oftedahl (1948), and most recently by Tuttle (1952). The charts of Winchell and Alling have been outdated by recent optical and X-ray data; the others are undoubtedly useful, though each has limitations. Most of Spencer's charts refer to his "orthoclase-microperthite series" comprising potassium-sodium feldspars, the majority of which have large optic angles and are intergrowths. The curve of Larsen *et al.* (1938) is drawn for sanidines with small optic angles, some of which exhibit a blue schiller and are thus cryptoperthites. Oftedahl (1948) combines feldspars from Spencer (1937), Larsen *et al.* (1938), Wolff (1938), and Seto (1922) with some from Norway into a determinative chart based on refractive indices and extinction angle. This diagram emphasizes the importance of calcium in determining refractive index and seems to apply to cryptoperthites but not to the more homogeneous feldspars which have lower refractive indices and smaller extinction angles. Tuttle (1952) provides a chart (Fig. 3*b*, this paper) for a more detailed optical classification by grouping alkali feldspars into four series on the basis of optic angles. The series are named: (1) high sanidine-high albite (cryptoperthite?), (2) sanidine-anorthoclase cryptoperthite, (3) orthoclase cryptoperthite, and (4) microcline cryptoperthite. Although the series as defined are useful, examples can be found which are intermediate between all four series, at least at the potassium-rich end. Unmixing may affect the optic angle slightly and the other optic properties more measureably but receives little emphasis in the commonly used charts.

Indices of refraction have been used mainly to determine the composition of alkali feldspars with most emphasis on determining the Or/Ab ratio. Most published diagrams for determining composition apply to feldspars with a constant degree of unmixing and are misleading for feldspars that have a different degree of unmixing. Thus the diagrams of Spencer (1937) and Oftedahl (1948) apply only to completely unmixed cryptoperthites. In Spencer's orthoclase-microperthite series two samples (*G* and *P*) have indices that are well below his proposed curve. These are both sanidines; *G* is homogeneous, and *P* is partly unmixed. All feldspars with small optic angles may be rejected from Spencer's curves because most natural alkali feldspars that are

completely unmixed also have a highly ordered aluminum distribution and thus a large optic angle. All the diagrams cited relating composition to refractive indices published for natural alkali feldspars are valid only in so far as the size of optic angle varies sympathetically with the degree of unmixing. These are not dependent variables, however, because for a given composition the optic angle depends on the state of ordering of aluminum, whereas the index of refraction α depends on the degree of unmixing and is independent of the state of aluminum distribution. The diagram of Larsen *et al.* (1938) for determining the composition of sanidines must be used with caution because it includes sanidines with various degrees of unmixing. This curve is based on apparently homogeneous sanidines and those with blue schiller even though all samples have a small optic angle. Larsen's diagram is further complicated by use of the index γ which varies most in determining the optic angle of feldspars with the optic plane normal to (010).

Oftedahl (1948) makes use of a combination of extinction angles and refractive indices to determine composition for feldspars that are completely unmixed. His diagram does not apply to feldspars that are partly unmixed because they have smaller extinction angles and refractive indices than completely unmixed cryptoperthites. The diagram does provide probably the best method for determining the Or/Ab/An ratio of completely unmixed cryptoperthites. The refractive index used in Oftedahl's diagram is $\frac{1}{2}(\alpha + \gamma)$; β was left out because it was believed to vary with the optic angle. Actually it is γ that varies most in the determination of 2V for alkali feldspars when the optic plane is normal to (010). When the optic plane is parallel to (010) β varies most.

The diagrams of Tuttle (1952) also depend upon the sympathetic variation of the degree of unmixing and the degree of aluminum ordering. Four series of alkali feldspars are defined on the basis of increasing optic angle, which is a function of increasing Al/Si ordering. This order is also the order of increasing degree of unmixing. The "high sanidine-high albite series" has the optic plane parallel to (010) for potassium-rich compositions and comprises essentially homogeneous alkali feldspars. With Na substitution up to $Or_{50}Ab_{50}$, α shows practically no increase, as would be expected from Figure 2 of this paper. Members of the "sanidine-anorthoclase cryptoperthite series" have small optic angles in a plane normal to (010) and are slightly unmixed. Therefore α is slightly greater than it is in the previous series. For the "orthoclase cryptoperthite series" and the "microcline cryptoperthite series" α is still higher because of the almost complete unmixing of the sodium feldspar component. The γ refractive index shows an even greater relative difference between the high- and low-temperature forms than for α because of the increase due to ordering of aluminum as well as the accompanying unmixing. For all four series β is almost the same, because the decrease in β due to ordering of aluminum approximately equals the increase due to unmixing.

The fact that diagrams like those by Tuttle (1952) can be applied to natural feldspars attests to the sympathetic character of the relation between 2V and the degree of unmixing. The points that do not fall on the proposed curves (Fig. 3*b*), however, merely emphasize that the relationship is not wholly fixed. Since the degree of Si/Al order and the degree of unmixing (K/Na segregation) both depend on cooling history it is conceivable that all gradations from complete Si/Al order of homogeneous feldspar to complete unmixing of feldspars with disordered aluminum could be obtained. In general, however, a cooling history that permits the ordering of aluminum should also permit unmixing. A metamorphic environment could be postulated in which perthitic feldspar would be homogenized at a temperature not capable of disordering aluminum. This situation has not been reported, but homogeneous microclines that have at least 10 per cent albite in solid solution are known.

The influence of small amounts of Ca, Ba, and Sr on α, β, and γ complicates all interpretations based on refractive indices. For instance, Spencer's (1937) curves for indices of the "orthoclase microperthite series" are based on feldspars with about 1–2 per cent Ca feldspar. Three of his samples (O, Q, and R) that have indices higher than the curves contain more than 4 per cent Ca feldspar. The substitution of ferric iron for aluminum is also a complicating factor because it increases the refractive indices. Small amounts of Rb substituting for K seem to cause a slight decrease in refractive indices.

The analyses of sanidines listed in this paper illustrate the amount of Ca, Ba, Sr, and

Rb found in samples from several localities. There seems to be no constant ratio of these elements, although Rb is small in all samples.

quantity to increase measurably the refractive indices of some samples. Sample 20 is a green microcline with most, but not all, of the Na

TABLE 11.—ANALYSES OF MICROCLINES FOUND UNSUITABLE FOR ACCURATE OPTICAL MEASUREMENTS

(*G = gravimetric: S = spectrographic*)

		16	17	18	19	20
		(In weight per cent)				
SiO_2	G	64.79	64.70			
Al_2O_3	G	18.68	18.58			
TiO_2	G	0.02	0.02			
Fe_2O_3	G	0.04	0.04			
FeO	S	<0.03	<0.03	0.07	<0.03	0.04
MgO	G	0.00	0.00			
K_2O	G	15.55	15.61			
	S	16.2	16.3	15.0	16.0	15.2
Na_2O	G	0.80	0.69			
	S	0.62	0.57	1.2	0.95	0.95
CaO	G	0.06	0.00			
	S	0.07	<0.05	0.18	0.09	<0.05
BaO	G	0.02	0.35			
	S	0.05	0.35	0.26	0.30	<0.05
SrO	G	0.01	0.02			
	S	0.035	0.020	0.040	0.042	0.020
Rb_2O	G	0.06	0.03			
	S	0.06	0.06	0.14	0.16	0.26
H_2O-	G	0.00	0.00			
H_2O+	G	0.06	0.02			
		(In parts per million)				
Li_2O	S	20	<20	<20	<20	<20
Cs_2O	S	3	<2	<2	<2	6
Tl_2O	S	8	6	6	7	30
PbO	S	220	250	110	120	600

16. Microcline 0–56 from granite at Mt. Rushmore, South Dakota, coll. by R. M. Gates
17. Microcline 0–57 from granite at Peekskill, New York, supplied by Wards
18. Microcline 0–17 from granite at Elberton, Georgia, supplied by Harmony Blue Granite Co.
19. Microcline 0–19 from granite at Elberton, Georgia, supplied by American Granite Co.
20. Green microcline 0–77 from pegmatite, Calvin County, Ontario, supplied by Wards

The relative abundance of the elements Ca, Ba, and Sr bears no fixed relation to the Or/Ab ratio of the sample.

Analyses of five microclines from granitic rocks are listed in Table 11. These samples were unsuitable for accurate optical measurements and were not included in Tables 2 and 3 with the other microclines 7, 8, and 9. The analyses show that the amounts of Na, Ca, Ba, and Sr are generally much lower than those in the sanidines, although Ba occurs in sufficient

feldspar perthitic component removed by heavy-liquid separation. This feldspar has the highest Rb_2O content (2600 ppm) of the analyzed samples and by far the highest Tl_2O content (30 ppm) and PbO content (600 ppm) of all samples studied. The association of green microcline with high Rb and Tl is discussed by Goldschmidt (1954), but the element responsible for the color seems to be in doubt.

The important correlation between 2V and the degree of unmixing in the relationship of

refractive indices to composition has already been discussed. The importance of interpreting 2V correctly in terms of aluminum disorder and the Or/Ab ratio was also mentioned earlier. In some recent papers describing optic-angle variations in granitic rocks, these variations are said to be petrogenically significant. Tuttle and Keith (1954) describe variations as large as 20° in one specimen of the Beinn an Dubhaich granite of the Island of Skye. This variation is attributed to partial transformation from sanidine to orthoclase cryptoperthite. Tuttle and Keith state that refractive-index data indicate that little if any of the variation is due to compositional variations. Harker (1954) describes similar variations for microclines in granitic rocks. An excellent correlation is shown between the size of optic angle and the extinction angle on (001). If the extinction angle on (001) is a measure of deviation from monoclinic symmetry and thus a measure of aluminum disorder, the optic-angle variation seems to reflect variation in the degree of aluminum disorder.

Large variations in the optic angle of some of the samples of the present study (1–5, 10–15) may be caused by compositional variations or by variations in the state of aluminum distribution. Thick sections were prepared to study the zoned crystals by the interference-figure method on the universal stage. Zoning was seen most clearly on acute bisectrix sections as zones of different interference colors attributable to differences in 2V. Sample 3 shows oscillatory zoning as well as a progressive zoning from 2V = 37° at the core to 30° at the rim. The optic plane is normal to (010) in this sample. A crystal from sample 12 measuring 2 mm in width ranges progressively from 2V = 8° at the core to 2V = 30° at the rim. The optic plane here is parallel to (010). A crystal from sample 1 has the optic plane parallel to (010) at the core, where 2V = 17°, and the optic plane normal to (010) at the rim, where 2V = 25°; 2V passes through 0° at an intermediate zone. This zoning, like changes in the optic angle, may be attributed to the nature of the Si/Al distribution or may be explained more easily as a variation in the content of divalent cations substituting for K in the structure The latter explanation is favored because of the variation in the α index shown by these same samples. The data in Table 6 indicate that the feldspars having the greatest range in 2V and in visible zoning also have the greatest range for the α index. As a further check on this statistical correlation a few grains from one of the crushed zoned sanidines were examined in detail. In these individual grains 2V increased in a ratio roughly proportional to the increase in the α index. Since the α index is relatively insensitive both to degree of Si/Al ordering and to the K/Na ratio this variation must be due to the content of divalent alkali ions or, possibly, to Fe^{3+}. Under this proposal different zones have different concentrations of the divalent cations, an explanation reminiscent of the familiar color banding in other minerals. This type of variation, of course, may be superimposed upon variation in the state of order-disorder of Si/Al.

References Cited

Alling, H. L., 1926, The potash-soda feldspars: Jour. Geology, v. 34, p. 591–611

Bailey, S. W., and Taylor, W. H., 1955, The structure of a triclinic potassium felspar: Acta Crystallographica, v. 8, p. 621–632

Barth, T. F. W., 1931, Permanent changes in the optical orientation of feldspars exposed to heat: Norsk Geol. Tidsskr., v. 12, p. 57–72

—— 1934, Polymorphic phenomena and crystal structure: Am. Jour. Sci., v. 27, p. 273–286

Bowen, N. L., and Tuttle, O. F., 1950, The system $NaAlSi_3O_8$-$KAlSi_3O_8$-H_2O: Jour. Geology, v. 58, p. 484–511

Chaisson, U., 1950, The optics of triclinic adularia: Jour. Geology, v. 58, p. 537–547

Chao, S. H., Hargreaves, A., and Taylor, W. H., 1940, The structure of orthoclase: Mineralog. Mag., v. 25, p. 498–512

Chao, S. H., Smare, D. L., and Taylor, W. H., 1939, An X-ray examination of some potash-soda felspars: Mineralog. Mag., v. 25, p. 338–350

Chao, S. H., and Taylor, W. H., 1940, The lamellar structure of potash-soda felspars: Royal Soc. London Proc. A, v. 174, p. 57–72

Cole, W. F., Sorum, H., and Kennard, O., 1949, The crystal structure of orthoclase and sanidinized orthoclase: Acta Crystallographica, v. 2, p. 280–287

Coombs, D. S., 1954, Ferriferous orthoclase from Madagascar: Mineralog. Mag., v. 30, p. 409–427

Dittler, E., and Köhler, A., 1925, Zur Frage der Entmischbarkeit der Kali-Natronfeldspäte und über das Verhalten des Mikroklins bei hohen Temperaturen: Tscherm. Min. Petr. Mitt., v. 38, p. 229–261

Donnay, G., and Donnay, J. D. H., 1952, The symmetry change in the high-temperature alkali-feldspar series: Am. Jour. Sci., Bowen Volume, p. 115–132

Emmons, R. C., *Editor*, 1953, Selected petrogenic relationships of plagioclase: Geol. Soc. America Mem. 52, 142 p.

—— 1955, Plagioclase silica: Geol. Soc. America Bull., v. 66, p. 1061

Eskola, P., 1922, The silicates of strontium and barium: Am. Jour. Sci., 5th ser., v. 4, p. 331–375

Faust, G. T., 1936, The fusion relations of iron-orthoclase: Am. Mineralogist, v. 21, p. 735–763

Ferguson, R. B., Traill, R. J., and Taylor, W. H., 1958, The crystal structures of low-temperature and high-temperature albites: Acta Crystallographica, v. 11, p. 331–348

Foster, W. R., 1955, Simple method for the determination of the plagioclase feldspars: Am. Mineralogist, v. 40, p. 179–185

Gaubert, P., 1926, Sur les propriétés optiques de quelques minéraux artificiels: Comptes rendus Cong. Soc. Savantes, p. 402–408

Goldschmidt, V. M., 1954, Geochemistry: Oxford, Clarendon Press, 730 p.

Goldsmith, J. R., and Laves, F., 1954a, The microcline-sanidine stability relations: Geochim. et Cosmochim. Acta, v. 5, p. 1–19

—— 1954b, Potassium feldspars structurally intermediate between microcline and sanidine: Geochim. et Cosmochim. Acta, v. 6, p. 100–118

Harker, R. I., 1954, The occurrence of orthoclase and microcline in the granitic gneisses of the Car Chuinneag-Inchbae Complex, E. Rossshire: Geol. Mag., v. 91, p. 129–137

Heald, M. T., 1950, Thermal study of potash-soda feldspars: Am. Mineralogist, v. 35, p. 77–89

Ito, T., 1938, The existence of monoclinic soda feldspar: Zeitschr. f. Krist., v. 100, p. 297–310

—— 1950, Moonstone, p. 122–131 *in* Ito, T., *Editor:* X-ray studies on polymorphism: Tokyo, Maruzen Co., Ltd., 231 p.

Ito, T., and Sadanaga, R., 1952, The lamellar structure of certain microcline and anorthoclase: Acta Crystallographica, v. 5, p. 441–449

Kozu, S., and Endo, Y., 1921, X-ray analysis of adularia and moonstone and the influence of temperature on the atomic arrangement of these minerals: Tohoku Imp. Univ. Sci. Repts., v. 1, p. 1–17

Kozu, S., and Suzuki, M., 1925, The influence of temperature on the optic axial angle of adularia, yellow orthoclase and moonstone: Tohoku Imp. Univ. Sci. Repts., v. 2, p. 187–201

Larsen, E. S., Irving, J., Gonyer, F. A., and Larsen, E. S., 3rd, 1938, Petrologic results of a study of the minerals from the Tertiary volcanic rocks of the San Juan region, Colorado: 8, Orthoclase: Am. Mineralogist, v. 23, p. 417–425

Laves, F., 1950, The lattice and twinning of microcline and other potash feldspars: Jour. Geology, v. 58, p. 548–571

—— 1951, A revised orientation of microcline and its geometrical relation to albite and cryptoperthites: Jour. Geology, v. 59, p. 510–511

—— 1952, Phase relations of the alkali feldspars: Jour. Geology, v. 60, p. 436–450, 549–574

—— 1954, The coexistence of two plagioclases in the oligoclase compositional range: Jour. Geology, v. 62, p. 409–411

MacKenzie, W. S., 1954, The orthoclase-microcline inversion: Mineralog. Mag., v. 30, p. 354–366

MacKenzie, W. S., and Smith, J. V., 1955, The alkali feldspars: I. Orthoclase microperthites: Am. Mineralogist, v. 40, p. 707–732

—— 1956, The alkali feldspars: III. An optical and X-ray study of high-temperature feldspars: Am. Mineralogist, v. 41, p. 405–427

Muir, I. D., and Smith, J. V., 1956, Crystallization of feldspars in larvikites: Zeitschr. f. Krist., v. 107, p. 182–195

Oftedahl, C., 1948, Studies on the igneous rock complex of the Oslo region, IX. The feldspars: Norske vidensk.-acad. Oslo Skr. 1 Math.-natur. Kl., no. 3, p. 1–77

Raman, C. V., Jayaraman, A., and Srinivasan, T. K., 1950, The structure and optical behavior of the Ceylon moonstones: Indian Acad. Sci., v. 32, p. 123–140

Seto, K., 1922, Studies of feldspars. 2: Geol. Soc. Tokyo Jour., v. 29

Smith, J. V., and MacKenzie, W. S., 1955, The alkali feldspars: II. A simple X-ray technique for the study of alkali feldspars: Am. Mineralogist, v. 40, p. 733–747

Spencer, E., 1930, A contribution to the study of moonstone from Ceylon and other areas and of the stability-relations of the alkali-feldspars: Mineralog. Mag., v. 22, p. 291–367

—— 1937, The potash-soda feldspars. 1. Thermal stability: Mineralog. Mag., v. 24, p. 453–494

Taylor, W. H., 1933, The structure of sanidine and other felspars: Zeitschr. f. Krist., v. 85, p. 425–442

Tuttle, O. F., 1952, Optical studies on alkali feldspars: Am. Jour. Sci., Bowen Volume, p. 553–567

Tuttle, O. F., and Keith, M. L., 1954, The granite problem: Evidence from the quartz and feldspar of a Tertiary granite: Geol. Mag., v. 91, p. 61–73

Winchell, A. N., 1925, Studies in the feldspar group: Jour. Geology, v. 33, p. 714–727

Wolff, I. E., 1938, Igneous rocks of the Crazy Mountains, Montana: Geol. Soc. America Bull., v. 49, p. 1569–1626

Department of Geology, University of Wisconsin, Madison 6, Wis. (Bailey and Emmons)

Manuscript Received by the Secretary of the Society, March 26, 1956

BULLETIN OF THE GEOLOGICAL SOCIETY OF AMERICA
VOL 70., PP. 539-564, 3 FIGS., 1 PL. MAY 1959

OVERTHRUST ORDOVICIAN AND THE NANNIE'S PEAK INTRUSIVE, LONE MOUNTAIN, ELKO COUNTY, NEVADA

BY DONALD W. LOVEJOY

ABSTRACT

The Lower Paleozoic rocks of the Great Basin consist of an eastern facies, composed of carbonate rocks, in eastern Nevada and western Utah, and a western facies, composed of clastic rocks, cherts, and volcanic rocks, in central and western Nevada. Major thrust faults have moved the rocks of the western facies eastward over the rocks of the eastern facies.

The trace of one such thrust fault is exposed on the flanks of Lone Mountain in Elko County, Nevada. The rocks of the eastern facies lie beneath the thrust fault and are subdivided into the autochthonous McClellan Creek sequence and the allochthonous Coal Creek sequence. The McClellan Creek sequence is composed of Devonian? limestones; it is successively overthrust by the Devonian fractured limestone of the lower plate of the Coal Creek sequence and by the Upper Devonian limestones, shales, and calcareous siltstones of the upper plate of the Coal Creek sequence.

The rocks of the western facies lie above the thrust fault in a series of thrust slices. The name Basco formation is proposed for mappable lithic units in one of the thrust slices. The Basco formation is Ordovician and contains four members: (1) basal calcareous siltstone with a sandstone bed and lenses of altered peridotite, (2) lower chert, (3) shale, and (4) upper chert. About 1750 feet of the Basco formation is exposed within the thrust slice. The calcareous siltstone member of the Basco formation contains Early Ordovician graptolites, and the shale member contains Middle Ordovician graptolites. The Basco formation is overlain by Silurian siltstone.

The thrust fault at Lone Mountain is domed up by intrusive rocks of probable Miocene age. The most striking of these is the Nannie's Peak intrusive, which forms the crest of Lone Mountain; the intrusive is arcuate in map view, and it is interpreted to be a dike. Related stocks and dikes crop out on the east flank of the mountain.

North, west, and south of Lone Mountain, the Paleozoic rocks are overlain by Cenozoic conglomerate that grades upward into welded tuffs. Normal faulting may bound Lone Mountain along its eastern margin, and the desert valley to the east is floored with vitric tuffs and with younger alluvium. The vitric tuffs are probably of late Miocene age, and they seem to grade laterally into the welded tuffs that lie north, west, and south of Lone Mountain.

CONTENTS

TEXT

	Page
Introduction	540
Acknowledgments	540
Previous work	541
Two Paleozoic facies	542
Eastern facies	542
General statement	542
McClellan Creek sequence	542
Coal Creek sequence	544
Western facies	545
General statement	545
Basco formation	545
Silurian	551
Cenozoic rocks	552
General statement	552
Nannie's Peak intrusive	552
Stocks and dikes	553
Conglomerate	555
Welded tuffs	555
Vitric tuffs and alluvium	556
Structural geology	558
General statement	558
Thrust faults	558
Intrusive rocks	560
Normal faults	560
References cited	561
Appendix. Fossil localities	563

ILLUSTRATIONS

Figure — Page
1. Lone Mountain viewed from the northeast ... 540
2. Index map of Nevada ... 541
3. Columnar section of Basco formation along Basco Creek ... 546

Plate — Facing page
1. Geologic map and cross sections, Lone Mountain ... 564

TABLES

Table — Page
1. Fossils of the McClellan Creek sequence ... 543
2. Fossils of the Coal Creek sequence (upper plate) ... 545
3. Fossils of the calcareous siltstone member of the Basco formation ... 550
4. Fossils of the shale member of the Basco formation ... 550

Introduction

Recent geologic investigations in Nevada indicate that major thrust faults have moved Lower Paleozoic clastic rocks, cherts, and volcanic rocks eastward over carbonate rocks of the same age. The trace of one such thrust fault was found exposed on the flanks of Lone Mountain in Elko County, Nevada.

Lone Mountain is an isolated mountain that trends north within the Independence Range of northeastern Nevada. Its summit has an elevation of 8780 feet, and the adjoining desert valleys are about 6000 feet above sea level, so that the mountain has a maximum relief of about 2800 feet (Fig. 1). In the reports of the Fortieth Parallel Survey, the mountain was called Nannie's Peak, and this name is retained for the highest peak of Lone Mountain in order to avoid confusion with other peaks called Lone Mountain in the geologic literature of Nevada. The geographic co-ordinates of Nannie's Peak are lat. 41° 07′ 35″ and long. 115° 58′ 31″.

Lone Mountain lies about 22 miles northwest of Elko (Fig. 2). It is most accessible from the east: 16.1 miles north of the junction of U. S. Highway 40 and State Highway 11, a dirt road leads west from State Highway 11 to the south end of the mountain; 24.3 miles north of the same junction, a dirt road leads west from State Highway 11 to the north end of the mountain.

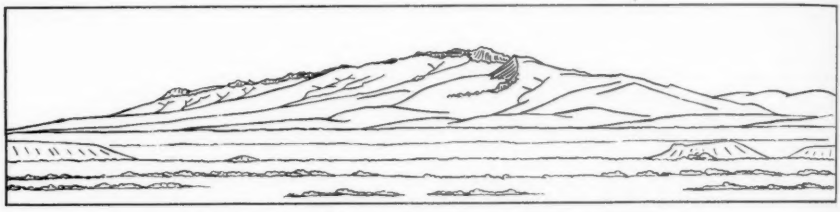

FIGURE 1.—LONE MOUNTAIN VIEWED FROM THE NORTHEAST

Elevation of summit is 8780 feet; elevation of foreground is about 6000 feet. Nannie's Peak intrusive extends from prominent knob on left to highest peak and then swings down mountain toward the observer as a jagged ridge curving to the left. Limestones of the McClellan Creek sequence dip northward (to the right) at the north end of the mountain and southward (to the left) at the south end of the mountain. Hills in middle distance are outcrops of upper Miocene vitric tuff at the Lone Mountain fossil locality.

Geology, drainage, and culture were plotted on air photographs of the Jack Ammann Surveys on the scale of 1:20,000, and the geologic map (Pl. 1) was constructed by the radial-line method based on plane-table control. All fossil identifications were made by the writer unless otherwise stated; vertebrate faunules were donated to the American Museum of Natural History, and invertebrate faunules are deposited in the Columbia University stratigraphic collections.

Acknowledgments

Marshall Kay gave helpful advice and criticism throughout the investigation. The writer benefited particularly from conversations with M. P. Billings, R. W. Fairbridge, John Imbrie, Arie Poldervaart, J. L. Rosenfeld, P. K. Hamilton, and his fellow students, J. P. Crawford, H. E. Kellogg, and Jerome Regnier. R. R. Coats, James Gilluly, Marshall Kay, C. W. Merriam, Arie Poldervaart, and

R. J. Roberts criticized the manuscript and made numerous suggestions for its improvement. Important fossil identifications were made by G. A. Cooper, C. H. Falkenbach, and E. C. Stumm; L. E. Long made a geochemical age analysis. L. L. Brannick, T. B. Lovejoy, H. G. Vore, Jr., and R. H. Washburn assisted in mapping. Research was made possible by assistantships in geology at Columbia University, grants from the Kemp Memorial Fund of Columbia University, and the generosity of the writer's parents.

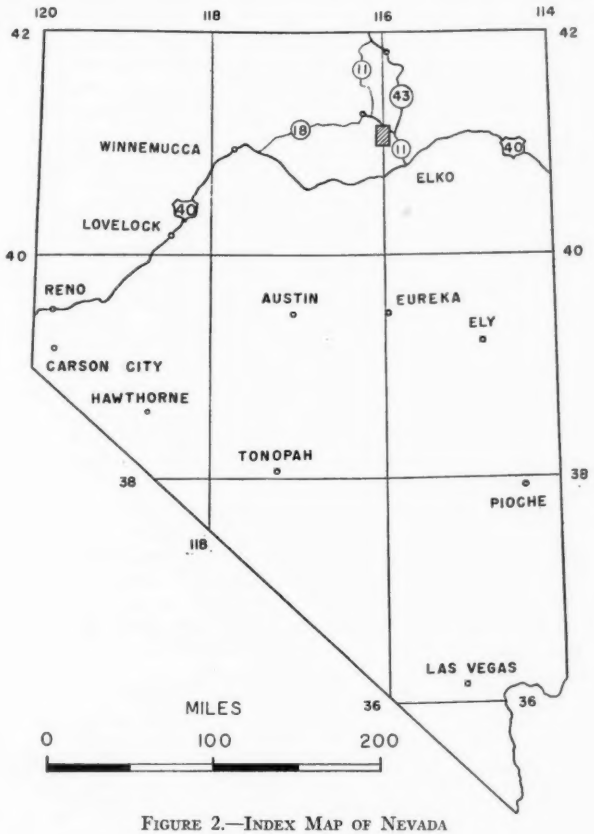

FIGURE 2.—INDEX MAP OF NEVADA
Area of Plate 1 ruled

PREVIOUS WORK

The earliest published references to Lone Mountain discuss the Lone Mountain mining district (Raymond, 1871, p. 219–220; Wheeler, 1871, p. 35; White, 1871, p. 58; Raymond, 1872, p. 158; Whitehill, 1877, p. 25). The Fortieth Parallel Survey made the first comprehensive study of the geology of Lone Mountain (King, 1876, geol. map iv; Zirkel, 1876, p. 47, 61–62, 102, 150, 192; Hague and Emmons, 1877, p. 602–608; King, 1878, p. 74–75, 107–109, 211–213, 595–596, 618–619, 740). Subsequent references to Lone Mountain are largely concerned with the mining district (Emmons, 1910, p. 24–29, 84–86; Lincoln, 1923, p. 51; Smith and Trengove, 1949; T. S. Lovering and W. M. Stoll, Preliminary report on the Rip Van Winkle mine, Elko County, Nevada, U. S. Geol. Survey open-file report, 9 p.; Granger, Bell, Simmons, and Lee, 1957, p. 106–112; Minerals Yearbooks for 1921, 1930, 1937–1951, 1954, 1956). Dott (1955, p. 2233)

discussed the rocks at Lone Mountain, and reconnaissance geologic maps of Lone Mountain were made by Granger, Bell, Simmons, and Lee (1957, Pl. 1) and Roberts, Hotz, Gilluly, and Ferguson (1958, Fig. 4).

Two Paleozoic Facies

Ordovician clastic rocks, cherts, and volcanic rocks are found at many places in central and western Nevada (J. P. Crawford, 1958, Ph.D. thesis, Columbia Univ., Fig. 1); dominantly carbonate rocks of the same age are found in eastern Nevada and western Utah. These two Ordovician facies were called the western facies and the eastern facies respectively by Merriam and Anderson (1942, p. 1699). Roberts and Lehner (1955, p. 1661) stated that both the western and the eastern facies contain rocks of Cambrian to Mississippian age; they suggested that the rocks of the western and the eastern facies were deposited in a single geosynclinal basin and that the thicker clastic facies accumulated in the western part and the thinner shelf sediments in the eastern part. The rocks of the western facies are now separated from the rocks of the eastern facies by thrust faults; Kay (1956, p. 67) stated that thrust faulting has moved the rocks of the western facies eastward 100 km or more over the rocks of the eastern facies and that the thrust faulting probably took place in the early Carboniferous.

Eastern Facies

General Statement

Limestones, shales, and calcareous siltstones that belong to the eastern facies crop out on the flanks of Lone Mountain and are subdivided into the autochthonous McClellan Creek sequence and the allochthonous Coal Creek sequence. These sequences are structural units and have been superimposed by thrust faulting.

McClellan Creek Sequence

NAME: The name McClellan Creek sequence is proposed for the autochthonous limestones exposed on the flanks of Lone Mountain. The name is taken from McClellan Creek, which drains the north flank of Lone Mountain.

DISTRIBUTION: The limestones of the McClellan Creek sequence are well exposed on the north, west, and south flanks of Lone Mountain and can be traced along the east flank of Lone Mountain as a screen of country rock between the Nannie's Peak intrusive and the stocks that crop out on the east flank of the mountain. North of Lone Mountain, erosion has locally removed the overthrust Ordovician-Silurian cherts and shales to expose in a fenster limestone that is thought to belong to the McClellan Creek sequence.

LITHOLOGY: The limestones of the McClellan Creek sequence are fine- to medium-grained and are gray. They are thin-bedded to massive, and locally they contain silt-sized or sand-sized grains of quartz. Because of their resistance to weathering, the limestones form prominent cuestas on the north and south flanks of Lone Mountain. An excellent example of penecontemporaneous deformation is seen in the portal of the drift at the head of the road that winds up the north flank of Lone Mountain: the beds are bowed up and down around a central lump, within which they are highly contorted, although underlying and overlying beds are essentially undisturbed. On the south flank of Lone Mountain, and near the foot of the northward-facing scarp of a cuesta that dips 25° S., an intraformational conglomerate contains rounded fragments of limestone as much as 9 inches in length.

On the north, west, and south flanks of Lone Mountain, the limestones of the McClellan Creek sequence are intruded by small dikes and stocks that are not shown in Plate 1. These dikes and stocks are related to the Nannie's Peak intrusive and to the stocks and dikes that crop out on the east flank of the mountain. On the east flank of Lone Mountain the limestones of the McClellan Creek sequence are intruded by unmapped dikes of biotite-hornblende-quartz latite and of quartz monzonite porphyry.

Silicification of the limestones of the McClellan Creek sequence is secondary and structurally controlled. The silicified limestones range from red through brown to black and are laminated to massive; lenses of chert of one color in chert of another color may indicate two periods of silicification. Veins of chert extend from silicified areas into unaltered limestone. The limestones are commonly silicified where they are in contact with the Nannie's Peak intrusive and with the stocks and dikes that crop out on the east flank of the mountain. On the north flank of Lone Mountain they are silicified where erosion has exposed the footwall of the major

thrust fault below the Ordovician-Silurian cherts and shales, and on the south flank of Lone Mountain they are silicified where erosion has exposed the footwall of the minor thrust fault below the fractured limestone of the lower plate of the Coal Creek sequence. Silicified limestone breccia half a mile north of the Lone Wolf mine on the northeast flank of the mountain may be related to the normal fault that is thought to bound Lone Mountain along its eastern margin; silicified limestone fragments from this locality have Liesegang color bands parallel to the edges of weathered fragments.

The limestones of the McClellan Creek sequence are cut by white calcite veins in many places and are recrystallized to coarse-grained white marble near the Nannie's Peak intrusive and the stocks and dikes that crop out on the east flank of the mountain. In the screen of limestone country rock on the east flank of the mountain, coarse-grained white marble is common, and the limestones are replaced locally by garnet, magnetite, and actinolite.

THICKNESS: Because the limestones of the McClellan Creek sequence have undergone deformation, their thickness cannot be measured accurately. On the basis of exposures on the north and south flanks of Lone Mountain, the limestones of the McClellan Creek sequence are estimated to be about 1000 feet thick.

STRATIGRAPHIC RELATIONS: Neither the base nor the top of the limestones of the McClellan Creek sequence is exposed at Lone Mountain. The limestones are intruded by the Nannie's Peak intrusive and by the stocks and dikes that crop out on the east flank of the mountain. On the north and west flanks of Lone Mountain they are overthrust by Ordovician-Silurian cherts and shales, and on the south flank of Lone Mountain they are overthrust by the limestones, shales, and calcareous siltstones of the Coal Creek sequence.

FAUNA: The limestones of the McClellan Creek sequence contain many thin beds that are rich in crinoid columnals or in broken fragments of fossils that include crinoid columnals and articulate brachiopod valves (Pl. 1, fossil localities 4, 6, 8, 10–13, 15). On the north flank of Lone Mountain a biostrome about 1 foot thick is characterized by *Favosites* (Pl. 1, fossil locality 9). *Microspongia?* is common on the south flank of Lone Mountain (Pl. 1, fossil locality 14). All the fossils that are found in the limestones of the McClellan Creek sequence are marine invertebrates (Table 1), but they do not allow assignment of a definite age to the rocks. G. A. Cooper studied the valve of an articulate brachiopod from fossil locality 7 (Pl. 1), but he did not date it. He stated (Personal communication) that the valve looked like "a brachial valve of the genus *Rhysostrophia*, which would suggest that it came from high Pogonip rocks", but he concluded that "in view of the fossils you list as associated with this one, the identification seems to be grossly in error".

TABLE 1.—FOSSILS OF THE MCCLELLAN CREEK SEQUENCE

Porifera:
Microspongia?
Coelenterata:
Solitary rugose corals (unidentified)
Favosites
Coenites
Brachiopoda:
Articulate brachiopods (unidentified)
Cephalopoda:
Straight nautiloid
Echinodermata:
Crinoid columnals

AGE AND CORRELATION: The limestones of the McClellan Creek sequence are overlain on the south flank of Lone Mountain by the rocks of the Coal Creek sequence, which are Upper Devonian in part. The two sequences are separated by an inferred minor thrust fault that is thought to represent little more than movement along the bedding planes; if this be the case, then the Coal Creek sequence overlies the McClellan Creek sequence stratigraphically as well as structurally, and the McClellan Creek sequence must be Devonian or older Paleozoic. On the basis of their postulated stratigraphic position below the Coal Creek sequence, the fossil evidence, and the lithic similarity to the Devonian limestones in the Toquima Range (pointed out by Marshall Kay), the limestones of the McClellan Creek sequence are tentatively assigned to the Devonian. The limestones of the McClellan Creek sequence belong to the eastern facies but they cannot be correlated with other Devonian sections for eastern Nevada and Utah.

Coal Creek Sequence

NAME: The name Coal Creek sequence is proposed for the allochthonous limestones, shales, and calcareous siltstones that are exposed on the south flank of Lone Mountain. The name is taken from Coal Creek, which drains the south flank of Lone Mountain. The rocks of the Coal Creek sequence are subdivided into a lower plate composed of fractured limestone and an upper plate composed of limestone, shale, and calcareous siltstone; the upper plate has been thrust eastward over the lower plate, and a remnant of the upper plate, which has been isolated by erosion, lies on the lower plate as a klippe.

DISTRIBUTION: The rocks of the Coal Creek sequence crop out on the south flank of Lone Mountain north of Coal Creek and appear south of Coal Creek as a long wedge within the brecciated Ordovician-Silurian cherts and shales.

LITHOLOGY OF LOWER PLATE: The lower plate of the Coal Creek sequence consists of fractured gray limestone that weathers buff to gray. The limestone is commonly laminated, and undulating laminae suggest that the rock has flowed plastically. Veins of white calcite are characteristic. The fractured limestone is less resistant to weathering than the limestones of the McClellan Creek sequence and forms low hills and ridges. Small unmapped lenses of altered gabbro are present at many places within the lower plate of the Coal Creek sequence. Saussuritized plagioclase and subhedral crystals of augite are major constituents of the altered gabbro. Biotite and green and brown hornblende are minor constituents, and opaque iron ore is an accessory mineral.

LITHOLOGY OF UPPER PLATE: The upper plate of the Coal Creek sequence consists of limestone, shale, and beds of calcareous siltstone and limestone; poor exposure and the deformation that these rocks have undergone made unravelling of the stratigraphic sequence impossible. The ledge-forming beds of calcareous siltstone and limestone are characteristic; they are as much as 30 feet thick and are composed of layers 1 inch to 1 foot thick of gray- to buff- to dark-brown-weathering calcareous siltstone and of thin-bedded to massive light-gray-weathering dark-gray limestone. North of Coal Creek the beds are composed predominantly of calcareous siltstone layers, but south of Coal Creek only limestone layers appear.

The calcareous siltstone layers are composed of rounded silt-sized grains of quartz in a calcareous matrix. Most of the layers are laminated, and some contain rounded sand-sized quartz grains as much as 1 mm in diameter. Where a calcareous siltstone layer dipping 60° S. crops out in the road cut along Coal Creek, an intraformational conglomerate contains rounded fragments of calcareous siltstone and of limestone as much as 6 inches in diameter.

The ledge-forming beds of calcareous siltstone and limestone are separated by limestone and shale. The limestone is fine-grained, dark gray, and weathers light gray to buff; it is in layers as much as 1 inch thick and is laminated in many places. The shale is buff to gray, weathers buff, and has partings as much as 0.25 inch thick.

The rocks of the upper plate of the Coal Creek sequence are more resistant to weathering than the fractured limestone of the lower plate and form high hills and ridges.

THICKNESS: Because the lower and the upper plates of the Coal Creek sequence have undergone deformation, the thickness of the rocks cannot be measured accurately; on the basis of exposures on the south flank of Lone Mountain north of Coal Creek, the rocks in the lower and upper plates of the Coal Creek sequence are estimated to be about 500 feet thick.

STRATIGRAPHIC RELATIONS: The bases and tops of the rocks in the lower and upper plates of the Coal Creek sequence are not exposed at Lone Mountain. The rocks of the lower plate are separated from the rocks of the upper plate by an inferred minor thrust fault that is thought to represent little more than movement along the bedding planes; if this be the case, then the upper plate overlies the lower plate stratigraphically as well as structurally.

The rocks of the Coal Creek sequence are thrust over the limestones of the McClellan Creek sequence on the south flank of Lone Mountain north of Coal Creek, and they are overthrust by brecciated Ordovician-Silurian cherts and shales along Coal Creek.

FAUNA AND AGE: No fossils were found in the fractured limestone of the lower plate of the Coal Creek sequence. Because the lower plate is thought to underlie the upper plate stratigraphically as well as structurally, and because the rocks of the upper plate contain Upper Devonian corals, the rocks of the lower plate are tentatively assigned to the Devonian.

Fossils are rare in the rocks of the upper plate of the Coal Creek sequence. A biostrome about 1 foot thick crops out at the top of a hill (Pl. 1, fossil locality 17); it is characterized by a compound tetracoral that E. C. Stumm (Personal communication) stated "appears to be conspecific with or very close to the species *Hexagonaria minuta* described by me from the Upper Devonian Martin limestone" (Stumm, 1948, p. 43). On the north side of the same hill conglomerate layers as much as 2 inches thick contain rounded rock fragments, crinoid columnals, and fragments of articulate brachiopods. At the foot of the hill (Pl. 1, fossil locality 16) the float contains fragments of a coquina composed of poorly preserved articulate brachiopods. All the fossils that are found in the rocks of the upper plate of the Coal Creek sequence are marine invertebrates (Table 2), and they indicate that the rocks of the upper plate are Upper Devonian, at least in part.

TABLE 2.—FOSSILS OF THE COAL CREEK SEQUENCE (UPPER PLATE)

Coelenterata:
Actinostroma
Solitary rugose corals (unidentified)
Hexagonaria minuta Stumm?
Pachyphyllum
Coenites
Brachiopoda:
Articulate brachiopods (unidentified)
Echinodermata:
Crinoid columnals

CORRELATION: The rocks of the Coal Creek sequence belong to the eastern facies; those of the upper plate seem to be correlative, at least in part, with the Devils Gate limestone of central Nevada (Merriam, 1940, p. 16–17) and with the Martin limestone of Arizona (Ransome, 1904, p. 33–42).

WESTERN FACIES

General Statement

Clastic rocks, cherts, and volcanic rocks that belong to the western facies crop out north, west, and south of Lone Mountain and contain Ordovician and Silurian graptolites. Where structural complication or poor exposure make subdivision of these rocks impossible they are mapped as undifferentiated Ordovician-Silurian cherts and shales. Southwest of Lone Mountain the rocks of the western facies are in a westward-dipping homoclinal succession. Several mappable lithic units are present north and south of Basco Creek and can be traced along the strike for about 2½ miles. The name Basco formation is proposed for these lithic units.

Basco Formation

NAME: The name Basco formation is proposed for the mappable units of calcareous siltstone, sandstone, altered peridotite, chert, and shale exposed southwest of Lone Mountain on both sides of Basco Creek. The formation contains four members: (1) a basal calcareous siltstone member that includes a sandstone bed and lenses of altered peridotite, (2) a lower chert, (3) a shale, and (4) an upper chert (Fig. 3). The name is taken from Basco Creek, which drains the southwest flank of Lone Mountain. The type locality for the Basco formation is the valley slopes north and south of Basco Creek.

DISTRIBUTION: The Basco formation crops out in a thrust slice southwest of Lone Mountain. The belt of outcrop trends northwest; it is about half a mile wide and about 2½ miles long. Where Basco Creek crosses the northern end of the belt of outcrop, the outcrop patterns of the members of the Basco formation form V's that point downstream. The thrust slice in which the Basco formation crops out is one of at least five thrust slices that compose the westward-dipping homoclinal succession southwest of Lone Mountain. The shale member of the Basco formation is present in four other thrust slices; it crops out in two northwest-trending belts to the east of, and stratigraphically below, the thrust slice in which the entire Basco formation crops out, and in two northwest-trending belts to the west of, and stratigraphically above, the thrust slice in which the entire Basco formation crops out. Northwest of Lone Mountain, the shale member of the Basco formation crops out in a northwest-trending belt within undifferentiated Ordovician-Silurian cherts and shales. This belt probably lies in a thrust slice similar to the thrust slices that compose the homoclinal succession southwest of Lone Mountain.

LITHOLOGY OF CALCAREOUS SILTSTONE MEMBER: The calcareous siltstone member of the Basco formation consists of layers 0.5 inch to 1 foot thick of calcareous siltstone with inter-

beds as much as 1 foot thick of black shale and of chert. The calcareous siltstone member contains a sandstone bed and lenses of altered peridotite.

The black shale that is interbedded with the calcareous siltstone layers weathers gray and has partings as much as 0.25 inch thick; graptolites and inarticulate brachiopods, which

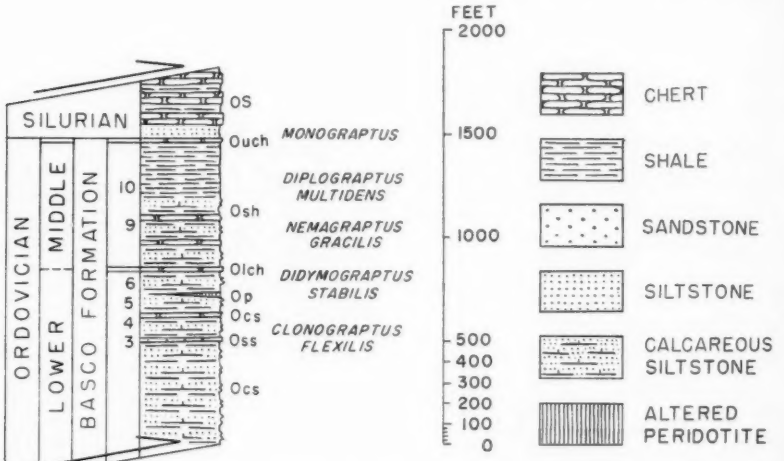

FIGURE 3.—COLUMNAR SECTION OF BASCO FORMATION ALONG BASCO CREEK

Numbers refer to British graptolite zones. OS = Ordovician-Silurian chert and shale. Ouch = upper chert member. Osh = shale member. Olch = lower chert member. Ocs = calcareous siltstone member. Op = altered peridotite lens. Oss = sandstone bed.

The layers of calcareous siltstone form small ledges; the rock is gray to black, weathers gray to buff, and is laminated in part. The calcareous siltstone is composed of rounded to well-rounded silt-sized grains of quartz in a calcareous matrix; in some places the rock is a calcareous spiculite composed of siliceous monaxon sponge spicules less than 2 mm long in a calcareous matrix. Pyrite nodules are present in the calcareous siltstone layers, and disseminated microscopic pyrite is common. The laminae in the calcareous siltstone layers are 0.1–1 mm thick and are formed by light-colored layers composed of silt-sized grains of quartz that alternate with dark layers composed of clay-sized particles. Objects on bedding planes of the calcareous siltstone layers include well-rounded frosted sand-sized grains of quartz as much as 1 mm in diameter, well-rounded chert pebbles as much as 1 cm in diameter, siliceous monaxon and triaxon sponge spicules, fragments of articulate brachiopods, a coiled archeogastropod, and echinoderm columnals; these objects may have been introduced from outside the area of sedimentation by density currents.

are preserved as carbonaceous films, are present on the bedding planes in many places. The chert interbedded with the calcareous siltstone layers is gray to black and is mottled in many places.

LITHOLOGY OF SANDSTONE BED: A ledge-forming bed of sandstone crops out discontinuously in the calcareous siltstone member of the Basco formation. The stratigraphic position of the sandstone bed is variable. The sandstone is massive and dark gray; the weathered surface is tan to limonite-stained. In thin section the sandstone is seen to be composed of fairly well-sorted subrounded to rounded grains of quartz. The grains are as much as 1 mm in diameter and show trails of minute rounded cavities. The grains are in a matrix of silt-sized quartz grains and of opaque grains probably of an iron mineral. A polished surface of the sandstone reveals undulating gray and black bands suggestive of penecontemporaneous deformation.

On the valley slope north of Basco Creek the sandstone bed contains blocks of calcareous siltstone and of chert up to several feet in diameter. The massiveness of the

sandstone, the undulating gray and black bands seen on a polished surface, and the blocks of calcareous siltstone and of chert all suggest that the sandstone bed was emplaced by a submarine landslide.

PETROGRAPHY OF ALTERED PERIDOTITE LENSES: Lenses of a rock that was identified by J. L. Rosenfeld as an altered peridotite are present above and below the sandstone bed in the calcareous siltstone member of the Basco formation. The altered peridotite is dark gray and weathers dark green to buff. A thin section of the lens of altered peridotite exposed in the road cut along Basco Creek reveals that the major constituents of the rock are brown hornblende and what appear to be anhedral to euhedral carbonate pseudomorphs after pyroxene and possibly after olivine and/or melilite. Biotite is a minor constituent, and the accessory minerals are apatite, spinel or perovskite, and a mineral that is opaque in transmitted light and white in reflected light, which may be leucoxene. Weathered surfaces of the rock are large serpentinized. The lenses of altered peridotite are interpreted as intrusive.

LITHOLOGY OF LOWER CHERT MEMBER: The calcareous siltstone member of the Basco formation is overlain by the lower chert member, which forms a prominent ledge and is composed of layers 0.5 inch to 1 foot thick of chert with a few interbeds 1–2 inches thick of light-brown calcareous siltstone. The chert is light gray to black, and the weathered surface is limonite-stained. The chert contains flecks of black organic material and is laminated in part. The chert layers pinch and swell, and many lense out. In the field, the top of the lower chert member is marked in many places by a coarse cellular gossan. The gossan is orange to dark brown and has iridescent blue and green stains. The cells of the gossan are angular, and most contain powdery limonite.

LITHOLOGY OF SHALE MEMBER: The lower chert member of the Basco formation is overlain by the shale member, which is composed of a lower part, which consists of black shale with interbeds of calcareous siltstone and of chert, and an upper part, which consists of black shale.

The lower part of the shale member is well exposed only north of Basco Creek in the vicinity of fossil locality 39 (Pl. 1). The black shale weathers bluish gray and has partings as much as 0.25 inch thick. Graptolites and inarticulate brachiopods, which are preserved as carbonaceous films, are present on the bedding planes in many places. The layers of calcareous siltstone that are interbedded with the black shale are as much as 1.5 feet thick. The calcareous siltstone is laminated, gray, and weathers buff. The calcareous siltstone layers contain disseminated pyrite, and siliceous monaxon sponge spicules are present on the bedding planes in many places. The chert layers that are interbedded with the black shale are as much as 7 inches thick. The chert is gray to black and weathers buff to black; it is silty and is laminated or mottled.

The upper part of the shale member consists entirely of black shale, which weathers buff to light gray and has partings as much as 0.25 inch thick. Graptolites and inarticulate brachiopods, which are preserved as carbonaceous films or in slight relief, are present on the bedding planes in many places.

The upper part of the shale member of the Basco formation is present in five thrust slices southwest of Lone Mountain and in a probable thrust slice northwest of Lone Mountain. At the south end of the thrust slice that lies immediately southwest of the thrust slice in which the entire Basco formation crops out, the lower part of the shale member seems to be present, at least in part, because the buff- to light-gray-weathering black shales, which are characteristic of the upper part of the shale member, are underlain by bluish-gray-weathering black shales, which are characteristic of the lower part of the shale member; the interbeds of calcareous siltstone and of chert are not present, however. In the first thrust slice that lies above the major thrust fault separating the rocks of the eastern and the western facies southwest of Lone Mountain, the buff- to light-gray-weathering black shales of the upper part of the shale member are underlain at three places by gray limestone that is laminated to massive (Pl. 1, *ls*); inasmuch as limestone is not present in the shale member of the Basco formation at the type locality, the rocks in the first thrust slice may represent a facies slightly different from that of the other thrust slices.

LITHOLOGY OF UPPER CHERT MEMBER: The shale member of the Basco formation is overlain by the upper chert member, which forms a prominent ledge and upholds the highest ridge in the westward-dipping homoclinal succession southwest of Lone Mountain. The upper chert member is composed of layers 0.5–8 inches thick of chert with a few inter-

beds as much as 1 inch thick of black shale. The chert is light gray to black, and the weathered surface is limonite-stained. The chert is in part laminated or mottled, and lenses and irregular patches of chert of one color are present in chert of another color. The pinching and swelling of the chert layers, which commonly lense out, suggest intrastratal flow after deposition. In the field, the upper chert member is characterized by the presence on the bedding planes of knobs, which average 1.5 inches in diameter. The bedding planes are commonly pitted by weathering. Microscopic flakes of a gold-colored mineral and radiating aggregates as much as 1 inch in diameter of a hydrous iron oxide, which is probably goethite, are present on the bedding planes in some places. At a few places the chert is riddled with minute cavities that are less than 1 mm in diameter. At one place the chert contains spherical nodules of chert, as much as 6 mm in diameter, which either bow the laminae up and down or transect them. Much of the chert contains white quartz veinlets, fractures, slickensides, and breccia, and some contains megascopic pyrite crystals. A surface etched in hydrofluoric acid commonly shows microscopic pyrite crystals or flecks of black organic material. In a few places clear round areas can be detected with a hand lens on a polished surface; in thin section these prove to be clear aggregates or spherulites of chalcedony similar to those described by Merriam and Anderson (1942, p. 1696) from the upper Vinini cherts of the Roberts Mountains and interpreted by them as recrystallized radiolaria.

DEPOSITIONAL ENVIRONMENT: The undisturbed graptolite rhabdosomes and the absence of markings of organic origin on the bedding planes suggest that scavengers were not present on the depositional surface when the Basco formation was deposited. With the exception of the larger sponge spicules, which may have been contributed by benthonic sponges, and the fragments of articulate brachiopods, the coiled archeogastropod, and the echinoderm columnals, all of which are thought to have been introduced from outside the area of sedimentation by density currents, the fossils found in the Basco formation are kinds that have been assigned by Ruedemann (1934, p. 25–42) to the plankton. John Imbrie (Personal communication) suggested that the inarticulate brachiopods were bottom-dwellers, but the fact that they are found as flattened films on the same bedding planes as the graptolites, in contrast with the articulate brachiopods, which are found as broken fragments on the same bedding planes as sand grains and small pebbles, supports the suggestion of Ruedemann (1934, p. 33) that the Paleozoic inarticulate brachiopods were epiplankton attached to floating objects. The restricted bottom life is perhaps best explained by bottom waters that were low in oxygen and poisoned with hydrogen sulfide; this interpretation is strengthened by the presence of organic material and pyrite throughout the Basco formation.

The ubiquitous well-sorted terrigenous material indicates that the Basco formation was deposited in the vicinity of land. The fineness of the particles indicates either that the land was of low topographic relief or that deposition took place a considerable distance offshore. The evidence for density currents and for a submarine landslide suggests that the Basco formation was deposited near or at the foot of a surface sloping down from the source area. Precise determination of the depth of water in which the Basco formation was deposited is impossible, but the undisturbed graptolite rhabdosomes and the absence on the bedding planes of primary structures, such as ripple marks and mud cracks, indicate that the Basco formation was deposited below the zone of wave action and suggest that the water was of moderate depth; nowhere in the Basco formation is there any evidence that the depositional surface was subjected to wave action or exposed to subaerial erosion.

THICKNESS: The thickness of the calcareous siltstone member of the Basco formation was determined graphically from average dips and the width of outcrop, corrected for terrain. The thicknesses of the sandstone bed, the lenses of altered peridotite, and the other members of the Basco formation were measured with a steel tape.

The total thickness of the calcareous siltstone member is not known because the lower beds are cut off by a thrust fault, but at least 1100 feet is present. At the type locality of the Basco formation along Basco Creek, the calcareous siltstone member is about 800 feet thick, and the sandstone bed crops out about 300 feet below the top of the member; 1 mile to the southeast, however, the calcareous siltstone member is about 1100 feet thick, and the sandstone bed crops out about 700 feet below the top of the member. The thickness of

the rocks of the calcareous siltstone member above the sandstone bed decreases northwestward along the strike; this may be due to original thinning, removal of beds by erosion along an unrecognized unconformity at the top of the calcareous siltstone member, omission of beds during thrusting, or the presence of two sandstone beds, one stratigraphically higher than the other. The final possibility arises because the sandstone bed cannot be walked through from one locality to the other because of thrust faulting.

The calcareous siltstone member contains a sandstone bed, which has a fairly constant thickness of about 15 feet, and lenses of altered peridotite. The thickest lens of altered peridotite observed in the course of mapping was 20 feet.

The lower chert member of the Basco formation has a fairly constant thickness of about 25 feet. South of Basco Creek the outcrop pattern of the lower chert member widens enormously on the dip slope of a cuesta. The shale member of the Basco formation is about 600 feet thick on the valley slope south of Basco Creek. It was not possible to measure the thickness of the lower and upper parts of the shale member, but each is inferred to be about 300 feet thick. The thickness of the shale member remains fairly constant both within the thrust slice in which the entire Basco formation crops out as well as within the other thrust slices southwest and northwest of Lone Mountain. The upper chert member of the Basco formation has a fairly constant thickness of about 20 feet; the outcrop pattern of the upper chert member widens considerably on dip slopes.

About 1750 feet of the Basco formation is exposed in the thrust slice southwest of Lone Mountain. At the type locality of the Basco formation along Basco Creek, the guide fossil for zone 3 of the Ordovician appears for the first time just below the sandstone bed. About 1000 feet higher in the stratigraphic sequence, the upper chert member of the Basco formation is overlain with apparent conformity by Silurian siltstone. If we can assume continuous deposition and no unrecognized structural complications, then the post-Tremadocian Ordovician (graptolite zones 3–15) is only about 1000 feet thick at the type locality of the Basco formation along Basco Creek. An even thinner section of Ordovician rocks of the same facies is present at Moffat, in the south of Scotland, where the Caradocian and Ashgillian (graptolite zones 9–15) are represented by black shales and cherts not more than 200 feet thick (Pringle, 1948, p. 14–15).

STRATIGRAPHIC RELATIONS: The base of the calcareous siltstone member of the Basco formation is not exposed because the lower beds are cut off by a thrust fault. Within the calcareous siltstone member the contacts of the lenses of altered peridotite are not exposed; the contacts of the sandstone bed are exposed only on the valley slope north of Basco Creek, and the sandstone bed seems to be essentially conformable, although the beds are so disturbed that this is uncertain. The contact between the calcareous siltstone member of the Basco formation and the overlying lower chert member is not well exposed; on the valley slope south of Basco Creek, the calcareous siltstone member seems to grade conformably into the overlying lower chert member through a transitional zone of interbedded calcareous siltstone and chert. The contact between the lower chert member of the Basco formation and the overlying shale member is nowhere exposed, but the parallelism of structure within the two members suggests that they are conformable. The contact between the shale member of the Basco formation and the overlying upper chert member is poorly exposed; on the valley slope north of Basco Creek, the shale member seems to grade conformably into the overlying upper chert member through a transitional zone of interbedded shale, calcareous siltstone, and chert. The contact between the upper chert member of the Basco formation and the overlying Silurian siltstone is nowhere exposed, but the parallelism of structure within the upper chert member and the overlying siltstone suggests that they are conformable.

FAUNA AND AGE: The only members of the Basco formation in which fossils were found are the calcareous siltstone member (Table 3) and the shale member (Table 4); within the calcareous siltstone member, the sandstone bed and the lenses of altered peridotite proved unfossiliferous. In Tables 3 and 4, fossils that appeared less than 10 times among 1000 fossiliferous specimens are rare, those that appeared 10–100 times among 1000 specimens are common, and those that appeared more than 100 times among 1000 fossiliferous specimens are abundant. All the fossils that are found in the calcareous siltstone member and the shale member of the Basco formation are marine invertebrates. The graptolites were

the most helpful guides to time, and the Basco formation was zoned on the basis of the characteristic assemblages of the graptolite zones in the British Isles that were described by Elles (1925, p. 337–347).

TABLE 3.—FOSSILS OF THE CALCAREOUS SILTSTONE MEMBER OF THE BASCO FORMATION

A—abundant; C—common; R—rare

Porifera:	
Siliceous monaxon spicules	C
Siliceous triaxon spicules	R
Brachiopoda:	
Lingulella	R
Obolus	R
Paterula	R
Articulate brachiopods	R
Mollusca:	
Coiled archeogastropod	R
Crustacea:	
Caryocaris	R
Echinodermata:	
Echinoderm columnals	R
Graptolithina:	
Dendrograptus	R
Clonograptus flexilis (Hall)	R
Tetragraptus harti (Hall)	R
Tetragraptus similis (Hall)	R
Horizontal to pendent didymograptids	C
Didymograptus stabilis Elles and Wood	R
Azygograptus	R
Isograptus	A

The calcareous siltstone member of the Basco formation contains Early Ordovician graptolites (Table 3); the oldest graptolite zone present is zone 3, which is represented by *Clonograptus flexilis* (Hall), and the youngest graptolite zone present is zone 6, which is represented by *Didymograptus stabilis* Elles and Wood. In the field, the calcareous siltstone member is characterized by *Isograptus*, horizontal to pendent didymograptids, and *Tetragraptus*. The calcareous siltstone member of the Basco formation is thought to be entirely of Early Ordovician age, although along Basco Creek the calcareous siltstone member contains almost 500 feet of unfossiliferous rocks stratigraphically below the first appearance of *Clonograptus flexilis* (Hall). The lower chert member of the Basco formation contains no fossils; inasmuch as it is underlain with apparent conformity by rocks belonging to graptolite zone 6 of the Ordovician and overlain with probable conformity by rocks belonging to graptolite zone 9 of the Ordovician, the lower chert member was probably deposited during the interval of time

TABLE 4.—FOSSILS OF THE SHALE MEMBER OF THE BASCO FORMATION

Porifera:	
Siliceous monaxon spicules	R
Brachiopoda:	
Acrotreta	R
Lingulella	R
Obolus	R
Paterula	R
Crustacea:	
Caryocaris	R
Graptolithina:	
Reclined didymograptids	R
Glossograptus	R
Nemagraptus gracilis (Hall) var. surcularis (Hall)	R
Dicellograptus	R
Dicranograptus	C
Climacograptus	A
Climacograptus bicornis (Hall)	R
Diplograptus multidens Elles and Wood var. compactus Lapworth	C
Unspined orthograptids	C
Spinose orthograptids	R

when rocks belonging to graptolite zones 7 and 8 were deposited in the British Isles. If this be the case, then the lower chert member is in part of Early Ordovician age and in part Middle Ordovician. The shale member of the Basco formation contains Middle Ordovician graptolites (Table 4). The lower part of the shale member roughly corresponds with graptolite zone 9, which is represented by *Nemagraptus gracilis* (Hall) var. surcularis (Hall); in the field, the lower part is characterized by *Dicellograptus*. The upper part roughly corresponds with graptolite zone 10, which is represented by *Diplograptus multidens* Elles and Wood var. compactus Lapworth; in the field, the upper part is characterized by *Climacograptus, Dicranograptus, Diplograptus multidens* Elles and Wood var. compactus Lapworth, and unspined orthograptids, all preserved in slight relief. The shale member of the Basco formation is Middle Ordovician. The upper chert member of the Basco formation contains no fossils; inasmuch as it overlies Middle

Ordovician rocks with apparent conformity and is overlain with probable conformity by Silurian siltstone, the upper chert member may well have been deposited during Late Ordovician time and is tentatively dated as Late Ordovician. The Basco formation, therefore, is Ordovician; Lower and Middle Ordovician rocks are present, and Upper Ordovician rocks may be present as well.

CORRELATION: The Ordovician rocks of the western facies that are exposed in central and western Nevada have been assigned to formations of local extent such as the Palmetto formation of the Silver Peak Range (Turner, 1902, p. 265–266), the Toquima formation in the Manhattan district (Ferguson, 1924, p. 22–25), the Vinini formation of the Roberts Mountains (Merriam and Anderson, 1942, p. 1693–1698), and the Comus and Valmy formations of north-central Nevada (Roberts, 1951).

The rocks of the Basco formation belong to the western facies and are correlative, at least in part, with the above-mentioned formations. In reviewing this paper as a critic, James Gilluly was opposed to coining a new formation name for rocks of such a small area of outcrop and "so similar both in lithology and stratigraphy to the Vinini formation that they appear difficult, if not impossible, to distinguish in mapping". He stated that "A new name therefore not only seems unnecessary and a cluttering of the literature; it seems an impractical refinement from the standpoint of stratigraphic discrimination. Although the Vinini in the Roberts Mountains, according to published descriptions, contains only fossils of Lower and Middle Ordovician ages, fossils of Upper Ordovician age have since been found there. Accordingly, there is not even an age difference between the rocks in the Lone Mountain area and those of the type Vinini; cartographic discrimination would appear quite impractical." He suggested therefore that the rocks of the Basco formation should be called Vinini if any formation name was to be used.

Reconnaissance in the Independence Range indicates the presence of clastic rocks and cherts of the western facies north and south of Lone Mountain; future workers may recognize within these rocks members of the Basco formation and thus increase the area over which the Basco formation crops out. The use of the name Vinini for the rocks of the Basco formation does not seem to be justified at this time because of differences in lithology and in stratigraphic sequence. Until the other Ordovician formations of the western facies in Nevada have been described in sufficient detail to allow recognition within them of the stratigraphic sequence exposed at Lone Mountain, the use of a local formation name for the Ordovician rocks of the western facies exposed at Lone Mountain seems to be warranted.

Silurian

DISTRIBUTION: A Silurian siltstone that contains *Monograptus* overlies the upper chert member of the Basco formation. The siltstone is present above the upper chert member southwest of Lone Mountain in the thrust slice in which the entire Basco formation crops out, and open triangles indicate those localities where *Monograptus* was collected (Pl. 1). The siltstone is poorly exposed and is overlain by a poorly exposed sequence of cherts with some shales; the cherts and shales are unfossiliferous but are probably partly Silurian. On the geologic map (Pl. 1) the Silurian siltstone is not differentiated from the overlying cherts and shales but is mapped with them as undifferentiated Ordovician-Silurian cherts and shales. The structure of the undifferentiated Ordovician-Silurian cherts and shales is not known, and unrecognized thrust faults may be present within them. In the thrust slice that lies immediately southwest of the thrust slice in which the entire Basco formation crops out, isolated patches of siltstone that contains *Monograptus* crop out at three places (Pl. 1, localities 62, 63, 64).

LITHOLOGY: The Silurian siltstone is composed of silt-sized grains of quartz and ranges from greenish gray through buff to purple. The siltstone has partings about 0.25 inch thick and is commonly laminated. Where the siltstone is limonite-stained or has Liesegang rings, it generally contains disseminated black metallic grains as much as 0.1 mm in diameter that are probably of an iron mineral. The cherts and shales that overlie the siltstone are probably Silurian in part and resemble the cherts and shales in the Basco formation.

THICKNESS: The upper limit of the Silurian siltstone is not clearly marked, and the thickness of the siltstone varies along the strike; not more than a few tens of feet of siltstone appear to be present, however. The structure of the cherts and shales overlying the siltstone is not known, and thicknesses were not measured.

STRATIGRAPHIC RELATIONS: The contact between the Silurian siltstone and the underlying upper chert member of the Basco formation is nowhere exposed, but the parallelism of struc-

ture within the siltstone and the underlying upper chert member suggests that they are conformable. The contact between the siltstone and the overlying cherts and shales is nowhere exposed, and its nature could not be ascertained.

FAUNA AND AGE: *Monograptus* is the only fossil present in the siltstone and characterizes it in the field; the best preserved specimens of *Monograptus* are found at fossil locality 62 (Pl. 1). The presence of *Monograptus* indicates that the siltstone is Silurian. The overlying cherts and shales are unfossiliferous and are tentatively considered to be Ordovician-Silurian.

Cenozoic Rocks

General Statement

The limestones of the McClellan Creek sequence are intruded by the Nannie's Peak intrusive, which is an arcuate body of quartz monzonite prophyry that forms the crest of Lone Mountain, and by stocks and dikes that crop out on the east flank of Lone Mountain. The Ordovician and Silurian rocks of the western facies are overlain by lenses of conglomerate; the conglomerate grades upward into the welded tuffs that mantle the foothills north, west, and south of Lone Mountain. The desert valley east of Lone Mountain is floored with vitric tuffs and with younger alluvium; the vitric tuffs seem to grade laterally into the welded tuffs that lie north, west, and south of Lone Mountain.

Nannie's Peak Intrusive

NAME: The name Nannie's Peak intrusive is proposed for the arcuate body of quartz monzonite porphyry that crops out along the crest of Lone Mountain. The name is taken from Nannie's Peak, which is the highest peak of Lone Mountain.

DISTRIBUTION: The Nannie's Peak intrusive crops out for 4 miles along the crest of Lone Mountain. In map view the intrusive is arcuate; the south end is blunt, but the north end tapers to a point and is strongly recurved. The intrusive encompasses 110° of the possible 360°, and the maximum radius measured from the outer margin of the intrusive to its center of curvature is 2 miles. The contacts of the intrusive are not regular in map view, and small dikes project outward radially at several places. The intrusive is resistant to weathering and crops out boldly; it forms steep slopes, which become precipitous cliffs locally, and rocky knobs that rise like cockscombs along the crest of the mountain (Fig. 1).

PETROGRAPHY: The Nannie's Peak intrusive is composed of quartz monzonite porphyry. At the south end of the intrusive, the rock is white and has a fine- to coarse-grained hypidiomorphic-porphyritic texture. The rock contains subhedral to euhedral phenocrysts of andesine that are as much as 7 mm in length and show distinct zoning under the microscope. Anhedral quartz and potassium feldspar are major constituents of the rock, and the minor constituents include augite, biotite, and green and brown hornblende; the accessory minerals are apatite, zircon, sphene, and opaque iron ore. Arie Poldervaart (Personal communication) pointed out that the fringes of augite around the biotites indicate a reversal of Bowen's reaction series and suggest that the rock has been reheated. At the north end of the Nannie's Peak intrusive, the rock is pink and identical with the rock at the south end except that the biotites have no fringes of augite. The absence of fringes of augite around the biotites at the north end of the intrusive indicates that the north end of the intrusive has not been reheated as much as the south end of the intrusive, if it has been reheated at all.

The Nannie's Peak intrusive is cut by aplite dikes as much as several inches in width. Xenoliths as much as 2 feet in diameter of metamorphosed granite porphyry are present along the inner contact of the Nannie's Peak intrusive south of Nannie's Peak and along the outer contact of the intrusive at the Lone Wolf mine. The metamorphosed granite porphyry is dark gray. The rock is composed of anhedral phenocrysts as much as 7 mm in diameter of quartz and potassium feldspar. The phenocrysts have a relic blastoporphyritic texture inherited from the original granite porphyry and are riddled with subhedral to euhedral green and brown hornblende crystals produced during metamorphism. Subhedral to euhedral plagioclase is also a major constituent of the rock. Biotite and what appears to be cummingtonite are minor constituents of the rock, and apatite, zircon, and opaque iron ore are accessory minerals. Xenoliths of metamorphosed limestone are also present in the Nannie's Peak intrusive; the drift at the Lone Wolf mine that is driven westward through the intrusive passes through a xenolith of recrystallized limestone that is 14 feet in diameter.

THICKNESS: The Nannie's Peak intrusive has a maximum thickness of 1800 feet south of Nannie's Peak. The intrusive becomes gradu-

ally thinner northward, and it is only 170 feet thick in the drift that is driven westward through it at the Lone Wolf mine.

RELATIONS: The Nannie's Peak intrusive intrudes the limestones of the McClellan Creek sequence; the south end of the intrusive abruptly cuts off a ridge of silicified limestone that dips 35° E., and discordant relations are well exposed in workings along the outer contact of the intrusive at the head of the road that winds up the north flank of Lone Mountain. As the intrusive is approached, the limestones become increasingly deformed and may be cut by small stocks and dikes. In many places the limestones are silicified, cut by white calcite veins, or recrystallized to coarse-grained white marble; undulating bedding and aligned recrystallized fossils suggest that the rock flowed plastically. The outer contact of the Nannie's Peak intrusive dips 70° NW. in a shaft at the head of the road that winds up the north flank of Lone Mountain, and the inner contact of the intrusive dips 70° W. in the drift at the Lone Wolf mine that is driven westward through the intrusive.

NATURE OF THE INTRUSIVE: The arcuate shape of the Nannie's Peak intrusive and its discordant relations with the older limestones at first suggested that the intrusive was a ring dike. In reviewing this paper as a critic, however, R. R. Coats pointed out that "the tectonics involved must differ from those we have come to expect with ring dikes. The plastic flow of the limestones near the intrusive strongly suggests forcible intrusion, rather than the passive filling of a semi-cylindrical or cylindroconical fracture". He suggested, therefore, that the Nannie's Peak intrusive is actually "a peripheral sill, partly transgressive of bedding". The writer agrees that the term ring dike has genetic implications which may not be justified for the Nannie's Peak intrusive, but he remains of the opinion that the intrusive should be interpreted as a dike, rather than as a sill, in view of its discordant relations and the hook at its north end.

AGE: L. E. Long, of the Lamont Geological Observatory, made a geochemical age analysis by the potassium-argon method on a piece of quartz monzonite porphyry from the north end of the Nannie's Peak intrusive at the Lone Wolf mine, and he concluded (Personal communication) that "the age should be interpreted as 12 m.y. ± 20 m.y." The Nannie's Peak intrusive is therefore assigned to the Cenozoic and is probably of Miocene age.

Stocks and Dikes

GENERAL STATEMENT: The oldest Cenozoic intrusive rocks exposed at Lone Mountain are a biotite-quartz latite stock that crops out on the east flank of the mountain and biotite-hornblende-quartz latite dikes that intrude the screen of limestone country rock between the Nannie's Peak intrusive and the stocks on the east flank of the mountain. A stock composed of altered diorite was subsequently intruded; it crops out on the east flank of Lone Mountain and contains large masses of biotite-quartz latite. Intrusion of the stock of altered diorite was followed by intrusion of the Nannie's Peak intrusive, which in turn was followed by intrusion of the quartz monzonite stock that crops out on the southeast flank of Lone Mountain. The youngest intrusive rocks exposed at Lone Mountain are the altered quartz porphyry dikes that trend north along the east flank of the mountain.

BIOTITE-QUARTZ LATITE STOCK: Biotite-quartz latite crops out on the east flank of Lone Mountain over an area 1.5 miles long north-south and 0.5 mile wide. The rock is light gray and has subhedral to euhedral phenocrysts as much as 2 mm in diameter of quartz, plagioclase, and potassium feldspar. In thin section the quartz phenocrysts are seen to be corroded by partial resorption. Shreds of biotite, which enclose opaque iron ore, account for about 1 per cent of the rock, and the groundmass is microcrystalline. The biotite-quartz latite is inferred to form a stock, although the relations with the limestones of the McClellan Creek sequence and with the surrounding igneous rocks are not exposed. Dikes of altered diorite cut the biotite-quartz latite stock and indicate that the biotite-quartz latite stock is older than the altered diorite stock. The biotite-quartz latite stock is cut by a dike of altered quartz porphyry, and Cenozoic vitric tuffs and alluvium unconformably overlie the biotite-quartz latite stock on the east. The biotite-quartz latite stock is probably Miocene because it belongs to the same cycle of igneous activity as the Nannie's Peak intrusive.

BIOTITE-HORNBLENDE-QUARTZ LATITE DIKES: Unmapped dikes of biotite-hornblende-quartz latite intrude the screen of limestone country rock that lies between the Nannie's Peak intrusive and the stocks on the east flank of Lone Mountain. The dikes trend roughly parallel to the Nannie's Peak intrusive. The biotite-hornblende-quartz latite is light gray; it contains subhedral to euhedral andesine phenocrysts,

which are as much as 7 mm in length, and subhedral to euhedral phenocrysts of quartz and biotite as much as 2 mm in diameter. In thin section the quartz phenocrysts are seen to be corroded by partial resorption, and the biotite phenocrysts are seen to be partly altered to chlorite. Minor amounts of green and brown hornblende are present, and the accessory minerals are apatite, zircon, sphene, and opaque iron ore. The groundmass is microcrystalline. The biotite-hornblende-quartz latite dikes are as much as a few tens of feet thick. They intrude the limestones of the McClellan Creek sequence. The relations of the dikes with the altered diorite stock are obscure, but xenoliths of biotite-hornblende-quartz latite in the altered diorite stock indicate that the biotite-hornblende-quartz latite dikes are older than the altered diorite stock. The dikes are probably of about the same age as the biotite-quartz latite stock and are tentatively assigned to the Miocene because they belong to the same cycle of igneous activty as the Nannie's Peak intrusive.

ALTERED DIORITE STOCK: A stock of altered diorite crops out on the east flank of Lone Mountain over an area about 2 miles long north-south and about 1 mile wide. The rock is dark gray and has eudedral andesine phenocrysts as much as 2 mm in length. Pyroxene is present, but most of it is altered to chlorite. Muscovite is a minor constituent of the rock, and opaque iron ore is an important accessory mineral. The groundmass is microcrystalline. The altered diorite stock intrudes the limestones of the McClellan Creek sequence. Along the contact with the stock, the limestones are deformed, silicified, recrystallized to coarse-grained white marble, or replaced by garnet, magnetite, and actinolite. Along the contact with the limestones, the altered diorite contains xenoliths of limestone, which are silicified in many places, and xenoliths of biotite-hornblende-quartz latite. Large masses of biotite-quartz latite that are present within the altered diorite stock may represent unassimilated xenoliths or roof pendants. The altered diorite stock is younger than the biotite-quartz latite stock and the biotite-hornblende-quartz latite dikes. Relations with the quartz monzonite stock are not exposed. The altered diorite stock is cut by dikes of a quartz monzonite porphyry that is identical with the quartz monzonite porphyry of the Nannie's Peak intrusive, and the altered diorite stock is assumed to be older than the Nannie's Peak intrusive. The altered diorite stock is also cut by a dike of altered quartz porphyry. The altered diorite stock is tentatively assigned to the Miocene because it belongs to the same cycle of igneous activity as the Nannie's Peak intrusive; the stock was intruded after the intrusion of the biotite-quartz latite stock and the biotite-hornblende-quartz latite dikes and before the intrusion of the Nannie's Peak intrusive.

QUARTZ MONZONITE STOCK: A stock of quartz monzonite crops out on the southeast flank of Lone Mountain. The stock is more or less circular in map view, and it has a maximum diameter of 1.7 miles. It is not resistant to weathering, and it forms a conspicuous topographic basin. The rock is pink and has a fine- to medium-grained hypidiomorphic-granular texture. The main constituents of the rock are subhedral andesine and anhedral potassium-feldspar and quartz. The minor constituents in clude subhedral to euhedral crystals of biotite, which have fringes of stilpnomelane, and brown hornblende. The accessory minerals are apatite, zircon, and opaque iron ore. Arie Poldervaart (Personal communication) pointed out that the fringes of stilpnomelane around the biotite crystals indicate adherence to Bowen's reaction series and suggest that the rock has not been reheated. He was of the opinion that the quartz monzonite porphyry of the Nannie's Peak intrusive and the quartz monzonite of the stock have the same chemical composition, that the differences in color and in resistance to weathering are due to subsequent reheating of the quartz monzonite porphyry, and that the quartz monzonite contains a greater percentage of biotite than the quartz monzonite porphyry because much of the biotite in the quartz monzonite porphyry was used up in the formation of augite. The quartz monzonite stock intrudes the limestones of the McClellan Creek sequence. Along the contact with the stock, the limestones are deformed, silicified, recrystallized to coarse-grained white marble, or replaced by magnetite. The relations of the quartz monzonite stock with the biotite-quartz latite stock and with the altered diorite stock are not exposed. The quartz monzonite stock is inferred to be younger than the Nannie's Peak intrusive because the quartz monzonite porphyry of the Nannie's Peak intrusive has been reheated and the quartz monzonite of the stock has not. The fact that the quartz monzonite porphyry of the Nannie's Peak intrusive has been reheated more at the south end of the intrusive than at the north end suggests that it was reheated by the

intrusion of the quartz monzonite stock near the south end of the intrusive. The stock is cut by altered quartz porphyry dikes, and Cenozoic vitric tuffs and alluvium unconformably overlie it on the east. It is tentatively assumed to be Miocene because it belongs to the same cycle of igneous activity as the Nannie's Peak intrusive.

ALTERED QUARTZ PORPHYRY DIKES: Dikes of altered quartz prophyry trend north along the east flank of Lone Mountain. The longest dike is a little more than 1 mile in length. The altered quartz porphyry is yellowish brown and deeply weathered. Fragments of the rock have Liesegang rings parallel to joint planes and broken edges. In thin section the rock is seen to be composed of subhedral to euhedral quartz phenocrysts, which are as much as 4 mm in diameter, and of muscovite. The feldspars are altered to sericite. The thickest altered quartz porphyry dike observed in the course of mapping was about 1000 feet. The altered quartz porphyry dikes intrude the quartz monzonite stock, the altered diorite stock, and the biotite-quartz latite stock. Cenozoic vitric tuffs and alluvium unconformably overlie the altered quartz porphyry dikes on the east. The altered quartz porphyry dikes are assigned to the Miocene or later Cenozoic because they were intruded after the Nannie's Peak intrusive.

Conglomerate

DISTRIBUTION: Lenses of conglomerate crop out north, west, and south of Lone Mountain along the contact between the Ordovician and Silurian rocks of the western facies and the overlying welded tuffs.

LITHOLOGY: The lenses are composed primarily of conglomerate, but locally the conglomerate may grade upward into breccia. The conglomerate is massive and is commonly limonite-stained. It is composed of fragments of chert in a matrix that is either siliceous or tuffaceous. The fragments of chert are poorly sorted and range from angular to well rounded; they are as much as 1 foot in diameter and are green, red, brown, gray, or black. Where the matrix is siliceous, the rock may be so tenacious that it splits through the chert fragments; where the matrix is tuffaceous, it commonly contains glass shards. The conglomerate is interbedded with welded tuff immediately west of the south end of the outcrop of the upper chert member and is interbedded with stratified vitric tuff immediately north of a road leading west at the southwest end of the area mapped.

THICKNESS: The thicknesses of the lenses of conglomerate cannot be measured with confidence because of the absence of bedding, but the thickest lens is estimated to be a few hundreds of feet.

STRATIGRAPHIC RELATIONS: The lenses of conglomerate unconformably overlie the Ordovician and Silurian rocks of the western facies. The conglomerate grades upward into welded tuffs. Gradational relations are well exposed at the extreme southeast end of the area mapped; conglomerate with a tuffaceous matrix grades upward into breccia with a tuffaceous matrix and then into welded tuff.

AGE AND CORRELATION: No fossils were found in the conglomerate. Dott (1955, p. 2233) compared the conglomerate at Lone Mountain with the Mississippian-Pennsylvanian Tonka formation in the Elko Range region, but a Cenozoic age for the conglomerate at Lone Mountain seems more probable. The conglomerate must belong to the same period of deposition as the welded tuffs and the vitric tuffs because of (1) the distribution of the conglomerate in lenses along the contact between the Paleozoic rocks and the welded tuffs, (2) the tuffaceous matrix of the conglomerate, (3) the interbeds of welded tuff and of vitric tuff, and (4) the upward gradation of the conglomerate into welded tuff. Van Houten (1956, p. 2814–2819) described a vitric tuff unit of late Miocene to middle Pliocene age that is extensively exposed in Nevada. His vitric tuff unit includes vitric tuff, reworked ash, interbedded sedimentary rocks, and welded tuffs derived from local sources. He stated (p. 2815) that the vitric tuff unit overlaps extensively on Paleozoic rocks, and that in the areas of overlap a red-stained basal conglomerate is commonly present. The vitric tuffs on the east side of Lone Mountain are of late Miocene age, at least in part, and are correlative with the vitric tuffs of Van Houten's vitric tuff unit. The welded tuffs north, west, and south of Lone Mountain seem to grade laterally into the vitric tuffs east of the mountain and are probably correlative with the locally derived welded tuffs in Van Houten's vitric tuff unit. The conglomerate that gradationally underlies the welded tuffs at Lone Mountain would then seem to be correlative with the conglomerate that is commonly present at the base of Van Houten's vitric tuff unit.

Welded Tuffs

DISTRIBUTION AND PETROGRAPHY: Welded tuffs mantle the foothills north, west, and south

of Lone Mountain. An eastward-dipping sequence of acidic and basaltic welded tuffs with interbedded volcanic breccias crops out north of Coon Creek in the northwestern part of the area mapped. Parting planes that dip 25° E. in the middle of the sequence are interpreted as compaction structures. Farther west, parting planes of diverse orientation in the basal part of the sequence are interpreted as contorted flow banding and suggest the presence within the sequence of a semiviscous surface flow.

A light-colored welded tuff is well exposed northwest of the Rip Van Winkle mine on the west flank of Lone Mountain. It has parting planes dipping 35° W. that are interpreted as compaction structures. It is composed of subhedral to euhedral phenocrysts of biotite, which are as much as 3 mm in diameter, and of subhedral phenocrysts of quartz, which are as much as 3 mm in diameter. The phenocrysts of quartz are corroded by partial resorption. The matrix is cryptocrystalline quartz and has spherulitic structures.

One mile south of the Rip Van Winkle mine, a horizontal dark band is exposed on the face of a cliff just east of the road. The cliff is composed of light-colored welded tuff. In thin section the rock is seen to be composed of phenocrysts of quartz, pumice fragments, and angular fragments of chert in a matrix of glass shards that are somewhat deformed. The phenocrysts of quartz are subhedral to euhedral, as much as 2 mm in diameter, and corroded by partial resorption The horizontal dark band is 3 feet thick. It is composed of a breccia of angular fragments of chert, which are as much as 1 inch in diameter, subhedral to euhedral phenocrysts of quartz, and pumice fragments in a matrix of cryptocrystalline quartz. The origin of the band of breccia can only be inferred; the absence of graded bedding suggests that it is not a layer of explosion breccia between two welded tuffs. The sharp, planar upper and lower contacts of the band of breccia and the presence of a parallel fracture in the underlying welded tuff suggest that the band of breccia is a clastic dike or sill.

Patches of silicified tuff crop out in the southwestern part of the area mapped. In thin section the silicified tuff is seen to be a cryptocrystalline aggregate of quartz that contains relic glass shards.

THICKNESS: The welded tuffs were not mapped in detail, and thicknesses were not measured. Locally the welded tuffs must be a few thousand feet thick.

STRATIGRAPHIC RELATIONS: The welded tuffs either unconformably overlie the Ordovician and Silurian rocks of the western facies or gradationally overlie the lenses of conglomerate. Eastward the welded tuffs seem to grade laterally into the vitric tuffs, and the welded tuffs are unconformably overlain by alluvium.

AGE AND CORRELATION: The only fossils found in the welded tuffs were pieces of silicified wood, which are locally abundant (Pl. 1). The welded tuffs are tentatively assigned to the late Miocene because they seem to grade laterally into the vitric tuffs, which are of late Miocene age, at least in part. As stated in an earlier paragraph, the welded tuffs are probably correlative with the locally derived welded tuffs in Van Houten's vitric tuff unit.

Vitric Tuffs and Alluvium

DISTRIBUTION AND PETROGRAPHY: Vitric tuffs and alluvium floor the desert valley on the east side of Lone Mountain. The vitric tuffs are largely concealed by alluvium and are well exposed only north and south of Coal Creek in the southeastern part of the area mapped. North of Coal Creek massive buff vitric tuff dips 20°–30° E. and contains interbeds of white vitric tuff. The buff vitric tuff is composed of glass shards, crystals as much as 1 mm in diameter, and pumice fragments as much as 5 mm in diameter. The crystals are of quartz, potassium feldspar, plagioclase, green and brown hornblende, pyroxene, and opaque iron ore. The interbeds of white vitric tuff are as much as 5 feet thick. The white vitric tuff is composed of glass shards and of crystals as much as 2 mm in diameter of quartz, potassium feldspar, brown hornblende, pyroxene, and opaque iron ore. The interbeds of white vitric tuff must have been deposited in water because (1) they are laminated, (2) they contain intraformational conglomerates with rounded fragments of buff vitric tuff that are as much as 1 foot in diameter, and (3) ripple marks with a wave length of 2 mm are locally present. At the extreme northwest end of the outcrop, an interbed of white vitric tuff contains borings normal to the bedding that are filled with white or buff vitric tuff; the borings are about 1 inch in diameter and about 1 foot in length.

South of Coal Creek a sequence of vitric tuffs dips 10° NE. Massive buff vitric tuff is overlain by a bed of dark-green vitric tuff 2 feet thick, which in turn is overlain by massive light-gray vitric tuff. The massive buff vitric tuff is composed of glass shards and of crystals as much as

1 mm in diameter of quartz, potassium feldspar, plagioclase, green and brown hornblende, pyroxene, and opaque iron ore. The dark-green vitric tuff is composed of glass shards, crystals as much as 1 mm in diameter, and pumice fragments as much as 4 mm in diameter. The crystals are of quartz, potassium feldspar, plagioclase, brown hornblende, pyroxene, and opaque iron ore. The massive light-gray vitric tuff is composed of glass shards and of crystals as much as 3 mm in diameter of quartz, potassium feldspar, plagioclase, brown hornblende, pyroxene, and opaque iron ore. The light-gray vitric tuff contains an intraformational conglomerate with rounded fragments of buff vitric tuff as much as 6 inches in diameter and must have been deposited in water.

The alluvium present east of Lone Mountain includes gravels, which floor the stream valleys, and detritus, which mantles the low terrane east of the mountain. The stream gravels consist of poorly sorted angular to rounded rock fragments of local derivation, and the detritus that mantles the terrane east of the mountain. The stream gravels consist of poorly sorted angular to rounded rock fragments of local derivation, and the detritus that mantles the terrane east of the mountain consists of angular to rounded cobbles and boulders intermingled with finer-grained sediments.

THICKNESS: The vitric tuffs and alluvium were not mapped in detail, and thicknesses were not measured. Locally the vitric tuffs at Lone Mountain must be a few hundreds of feet thick.

STRATIGRAPHIC RELATIONS: The vitric tuffs and alluvium unconformably overlie the Paleozoic sedimentary rocks and the Cenozoic stocks and dikes. The vitric tuffs seem to grade laterally into the welded tuffs westward and are unconformably overlain by the alluvium.

CAMP CREEK FAUNA: The vitric tuffs exposed north and south of Coal Creek are unfossiliferous, and a reconnaissance was made southward along the east flank of the Independence Range. At the foot of Swails Mountain, the remains of vertebrates were found along Camp Creek in a bed of massive gray vitric tuff; the bed is about 30 feet thick and dips 15° W. The gray vitric tuff is composed of glass shards and glassy material, crystals as much as 2 mm in diameter, pumice fragments as much as 5 mm in diameter, and rounded rock fragments. The crystals are of quartz, plagioclase, green and brown hornblende, pyroxene, and opaque iron ore. Pseudomorphs of hydrous iron oxide, probably goethite after pyrite, are found loose on the outcrops. The pseudomorphs are as much as 2 inches in diameter and are stream-rounded; octahedron faces are common, but cube faces are rare.

Unaware that the Camp Creek locality had been previously described by Sharp (1939, p. 151–152), the writer collected the remains of vertebrates north of Camp Creek at a point about 1 mile west of the junction with Susie Creek. The fossils were donated to the American Museum of Natural History. Jerome Regnier (1958, Ph.D. thesis, Columbia Univ., p. 36) stated that the catalogue numbers of the fossils are AM-45823 to AM-45827 and that the fossils include "*Merychippus* sp., resembling forms in the lower Snake Creek of Nebraska (identification by M. F. Skinner); camelids of late Miocene age (identification by C. H. Falkenbach); turtle (not identified)". The earlier collections from Camp Creek were never described, and Van Houten (1956, Figs. 1, 2) assigned them to the late Miocene or early Pliocene.

LONE MOUNTAIN FAUNA: After the Camp Creek locality had been studied, a bed of massive light-gray vitric tuff was discovered at Lone Mountain just northeast of the area mapped. The light-gray vitric tuff is composed of glass shards and glassy material, crystals as much as 1 mm in diameter, and pumice fragments as much as 2 mm in diameter. The crystals are of quartz, plagioclase, brown hornblende, pyroxene, and opaque iron ore. The massive light-gray vitric tuff so closely resembled the massive gray vitric tuff at Camp Creek that a careful search for the remains of vertebrates was made. North of State Highway 11 and about 3.2 miles west of the junction with State Highway 43, the partial jaw of an oreodont was found loose on an outcrop. The jaw was donated to the American Museum of Natural History (catalogue number AM-55598). C. H. Falkenbach believed the jaw to be of the genus *Brachycrus*; he stated that the jaw is equivalent in age to the Sheep Creek, which includes the Sheep Creek and the lower Snake Creek, and he assigned it to the upper Miocene. Jerome Regnier subsequently collected additional remains of vertebrates along the outcrop of the light-gray vitric tuff south of State Highway 11 (Fig. 1). The fossils are kept at the American Museum of Natural History, and Jerome Regnier informed the writer that they include *Brachycrus* (AM-45820), oreodont (AM-45821), and three

molars of equid (AM–45822). The similarity in lithology and in age of the massive gray vitric tuff exposed along Camp Creek and the massive light-gray vitric tuff exposed northeast of Lone Mountain suggests that the two vitric tuffs are correlative.

AGE AND CORRELATION: Although no fossils were found in the vitric tuffs north and south of Coal Creek in the area mapped, the vitric tuffs are tentatively assigned to the upper Miocene because of their similarity to the upper Miocene vitric tuff just northeast of the area mapped and to the upper Miocene vitric tuff along Camp Creek. The alluvium that unconformably overlies the vitric tuffs at Lone Mountain is clearly late of Miocene or later Cenozoic age. As stated in an earlier paragraph, the vitric tuffs are probably correlative with the vitric tuffs of Van Houten's vitric tuff unit.

Structural Geology

General Statement

The structural features of the rocks at Lone Mountain were formed during three major periods of deformation: (1) Thrust faulting took place after the deposition of the Upper Devonian rocks and before the Cenozoic igneous activity began. During this period the rocks of the western facies were thrust-faulted eastward over the rocks of the eastern facies. (2) Igneous activity probably took place in the Miocene. During this period the Nannie's Peak intrusive, the stocks on the east flank of Lone Mountain, and many of the dikes were intruded; the welded tuffs were probably extruded at this time as well. (3) Normal faulting took place in the Cenozoic after the period of igneous activity had come to an end. A normal fault is now exposed at the surface as well as in the subsurface at the Rip Van Winkle mine, and a major normal fault probably bounds Lone Mountain along its eastern margin.

Thrust Faults

MAJOR THRUST FAULT: A major thrust fault can be traced along McClellan Creek north of Lone Mountain and along Coal Creek south of Lone Mountain; it probably continues beneath the welded tuffs on the west flank of the mountain (Pl. 1). The thrust fault carries the Ordovician and Silurian rocks of the western facies eastward over the rocks of the eastern facies.

The fault plane of the thrust fault is nowhere exposed, but the evidence for the existence of the thrust fault is overwhelming:

(1) Rocks that contain Ordovician and Silurian graptolites stratigraphically overlie rocks that contain Devonian fossils.

(2) Detailed mapping south of Lone Mountain brings out the lack of accordance of the structures of the rocks of the western facies to the structures of the underlying rocks of the eastern facies.

(3) The thrust fault is marked by a thick zone of breccia. The breccia is composed of angular to rounded fragments of limestone, of limestone and chert, or of chert, in a calcareous matrix or in a matrix of finely ground chert and shale. The breccia is less resistant to weathering than the rocks above and below the thrust fault, and as a result subsequent streams have eroded their valleys along the belt of outcrop of the breccia zone. The thickness of the breccia zone depends on the nature of the overlying rock. On the north flank of Lone Mountain, the breccia zone is overlain by chert and is only a few tens of feet thick. South of Lone Mountain, it grades upward into fractured shale, in which all trace of bedding and of fossils has been destroyed, and the breccia zone is several hundreds of feet thick. The best exposures of the breccia zone are along the road that follows McClellan Creek up the northeast flank of Lone Mountain. Finely divided chert and shale, which weather to platy fragments less than 0.25 inch in diameter, are exposed in the gravel pits along the road. The finely divided chert and shale contain bands and lenses of fractured chert. Where the thrust fault crosses the road a few hundred feet west of the gravel pits, a limestone breccia is exposed; it consists of fragments of limestone and of chert in a buff calcareous matrix. The breccia zone is also exposed on the south flank of Lone Mountain where the road that leads up Coal Creek to the Lone Mountain mine forms two hairpin turns. Here the breccia is deeply weathered, and bands of buff earthy material alternate with bands of thin-bedded black chert.

(4) Although the bedding in the rocks above and below the thrust fault is essentially parallel, the rocks are considerably deformed directly above and below the thrust fault. The chert and shale directly above the thrust fault are unmetamorphosed but are commonly folded, fractured, and slickensided. The limestone directly below the thrust fault is folded, fractured, slickensided, recrystallized to coarse-grained white marble, or cut by white calcite veins.

(5) Limestones that are thought to belong to the McClellan Creek sequence appear in the fenster north of Lone Mountain.

(6) During the summer of 1957 a diamond-drill hole was begun in the Ordovician-Silurian cherts and shales that crop out at the northernmost workings of the Monarch mine, which lies on the northwest flank of Lone Mountain. The hole was abandoned at a depth of 235 feet after it had passed into limestone that probably belonged to the McClellan Creek sequence.

Because the fault plane of the thrust fault is nowhere exposed, the dip of the thrust fault cannot be measured directly. The fact that the trace of the thrust fault is semicircular in map view indicates that the fault plane has been domed up. The doming is probably related to the period of igneous activity rather than to the period of thrust faulting. The fault plane seems to be parallel to the bedding in the underlying limestones, and if this be the case, the thrust fault is a bedding thrust.

The most reliable evidence for the direction of movement of the hanging wall with respect to the footwall is the westward inclination of the axial planes in small overturned folds within the rocks of the western facies. The rocks of the western facies moved eastward relative to the rocks of the eastern facies, but the amount of displacement along the thrust fault cannot be inferred.

The youngest rocks exposed below the thrust fault are of Late Devonian age, and the thrust faulting came later than the deposition of these rocks. The doming of the fault plane of the thrust fault is probably related to the period of igneous activity, so that the thrust faulting probably took place before the igneous activity began in Cenozoic time.

The major thrust fault at Lone Mountain is correlative with the thrust faults which separate the rocks of the western facies from the rocks of the eastern facies elsewhere in Nevada. The best known of these thrust faults is the Roberts Mountains thrust fault, which was described by Merriam and Anderson (1942, p. 1701–1706) from the Roberts Mountains of central Nevada.

HANGING-WALL STRUCTURES: The hanging wall of the major thrust fault includes schuppen structure, a transverse fault, and imbrication of the rocks of the western and the eastern facies, all of which were formed at the same time as the major thrust fault, and a fenster, which was formed by subsequent erosion.

Within the westward-dipping homoclinal succession southwest of Lone Mountain, the upper part of the shale member of the Basco formation crops out in five belts, each stratigraphically higher than the last. The most reasonable interpretation of the field relations is that the hanging wall of the major thrust fault is composed of a series of westward-dipping thrust slices that have been thrust over one another in a schuppen structure (Pl. 1, sec. C-C′). An inferred minor thrust fault was drawn at the base of the upper part of the shale member of the Basco formation wherever the underlying part of the formation did not appear below it; fault breccias were found at many places along the traces of the inferred minor thrust faults.

North of Basco Creek, the thrust slice in which the entire Basco formation crops out is cut by a transverse fault. The transverse fault strikes perpendicular to the strike of the regional structure and represents a lateral break that allowed the southern part of the thrust slice to move eastward relative to the northern part. The lower part of the shale member of the Basco formation is not present above the lower chert member in the vicinity of fossil locality 38 (Pl. 1) and may have been eliminated during faulting; such an elimination of beds would have been most readily accomplished if the transverse fault appeared during the period of thrust faulting.

The rocks of the western facies are imbricated with the rocks of the eastern facies at the south end of Lone Mountain where the rocks of the Coal Creek sequence extend south of Coal Creek as a long wedge within the brecciated Ordovician-Silurian cherts and shales. The wedge is composed of a ledge-forming bed of light-gray-weathering dark-gray limestone that is overlain by buff shale, and the wedge is interpreted as a partially detached thrust slice.

A small patch of limestone crops out north of Lone Mountain and is surrounded by Ordovician-Silurian cherts and shales. In reviewing this paper as a critic, James Gilluly suggested that the patch of limestone was probably a fenster through the major thrust fault. The limestone is gray, fine- to medium-grained, and thin-bedded to massive; it contains no fossils but is assigned to the McClellan Creek sequence because of its similar lithology. The limestone is considerably deformed and dips northwestward, as do the limestones of the McClellan Creek sequence to the south. The fault plane of the thrust fault is not exposed.

FOOTWALL STRUCTURES: The footwall of the major thrust fault includes schuppen structure and folds, which were formed at the same time

as the major thrust fault, and a klippe, which was formed by subsequent erosion.

On the south flank of Lone Mountain the limestones of the McClellan Creek sequence are overlain by fractured limestone that is assigned to the lower plate of the Coal Creek sequence and is characterized by veins of white calcite and by undulating laminae. The limestones of the McClellan Creek sequence are silicified immediately below the fractured limestone, and the contact between the limestones of the McClellan Creek sequence and the fractured limestone is striking on air photographs or in the field. It is inferred to be a minor thrust fault that may represent little more than movement along the bedding planes, and the lower plate of the Coal Creek sequence is inferred to have moved eastward relative to the underlying limestones of the McClellan Creek sequence. The fractured limestone is overlain by the limestones, shales, and calcareous siltstones of the upper plate of the Coal Creek sequence, which are cut off abruptly at the contact. The contact is probably a minor thrust fault that represents little more than movement along the bedding planes, and the upper plate of the Coal Creek sequence is inferred to have moved eastward relative to the lower plate. The autochthonous limestones of the McClellan Creek sequence are thus overthrust by the lower and the upper plates of the Coal Creek sequence in a schuppen structure (Pl. 1, sec. C-C′).

The beds of calcareous siltstone and limestone in the upper plate of the Coal Creek sequence dip steeply north and south or stand vertically. A large synclinal fan fold, in which both limbs are overturned, can be traced along the strike for more than a mile. The axial plane strikes northwest and dips south; the fold plunges gently east. The north limb of the fold stands vertically and is overturned at the eastern end of the fold. The south limb is overturned and dips 30°–50° SW. If the folding was contemporaneous with the thrust faulting, then the upper plate of the Coal Creek sequence differs from the other thrust slices at Lone Mountain in that the resistant beds responded to the stresses that were set up during thrust faulting by folding rather than by shearing off.

A small klippe of the upper plate lies on the lower plate south of Lone Mountain. The klippe is composed of remnants of beds of calcareous siltstone and limestone that are separated by limestone and shale. The rocks are badly deformed, and the fault plane of the inferred minor thrust fault is not exposed.

Intrusive Rocks

GENERAL STATEMENT: During the period of igneous activity, the Nannie's Peak intrusive and the stocks and dikes that crop out on the east flank of Lone Mountain were intruded. The altered quartz porphyry dikes are the youngest intrusive rocks exposed on the east flank of the mountain and may be related to the period of normal faulting. The relation of the welded tuffs to the intrusive rocks is not clear, but if they grade laterally into upper Miocene vitric tuffs, they must be contemporaneous with the intrusive rocks, at least in part, because the Nannie's Peak intrusive is probably Miocene.

DOMING: Intrusion of the Nannie's Peak intrusive and of the stocks and dikes that crop out on the east flank of Lone Mountain domed up the central part of the mountain. The doming is indicated by the quaquaversal dips of the limestones of the McClellan Creek sequence. The semicircular trace of the major thrust fault indicates that the fault plane of the major thrust fault was domed up as well, and that the thrust faulting took place before the Cenozoic igneous activity began.

POSSIBLE TILTING: The only intrusive that has well-exposed contacts is the Nannie's Peak intrusive; both the inner and the outer contacts dip 70° W. (Pl. 1, sec. A-A′, B-B′). If the Nannie's Peak intrusive entered a vertical fracture, then the intrusive and the surrounding rocks have been tilted about 20° eastward.

JOINTING: The Nannie's Peak intrusive and the stocks and dikes that crop out on the east flank of Lone Mountain are conspicuously jointed. Three joint sets are well developed in the Nannie's Peak intrusive east of the Rip Van Winkle mine. One trends north and dips 45°–65° E; the second trends north and dips 50°–70° W.; the third trends east and is vertical, but it is locally replaced by vertical joint sets trending northeast and northwest. Two prominent joint sets are developed in the Nannie's Peak intrusive west of the Lone Wolf mine; one trends east and is vertical, and the other trends north and dips 60° E.

Normal Faults

RIP VAN WINKLE NORMAL FAULT: The only normal fault that is exposed at Lone Mountain passes through the Rip Van Winkle mine on the west flank of the mountain. It trends northwest and dips steeply west. Cenozoic welded tuffs on the west side of the fault are downthrown against Ordovician-Silurian cherts and shales

on the east side of the fault. The fault is exposed at the surface in a pit just north of the road at the southern workings of the Rip Van Winkle mine. T. S. Lovering and W. M. Stoll discovered the fault when they studied the mine in January 1943. In their report (T. S. Lovering and W. M. Stoll, Preliminary report on the Rip Van Winkle mine, Elko County, Nevada, U. S. Geol. Survey open-file report, 9 p.) they show the fault in cross section (Vertical sec. C-C'). They state (p. 5) that the main vein in the mine follows the fault and that "the drag of the shale along the vein suggests that the major part of the movement along it was of the normal fault type and that the western side is downthrown." The fault cuts the Cenozoic welded tuffs and must be Cenozoic.

PROBABLE NORMAL FAULT: Although physiographic evidence for a normal fault bounding Lone Mountain along its eastern margin is lacking, the presence of such a fault is considered probable for the following reasons:

(1) Slickensides and silicified limestone breccia are exposed on the northeast flank of Lone Mountain half a mile north of the Lone Wolf mine.

(2) A prominent joint set that trends north and dips 60°E. is developed in the Nannie's Peak intrusive west of the Lone Wolf mine.

(3) The altered quartz porphyry dikes that trend north along the east flank of Lone Mountain may have filled fractures that formed parallel to a normal fault on the east.

(4) Slickensides, breccias, quartz veins, and zones of hydrothermal alteration are present along the southeastern margin of the stock of quartz monzonite.

(5) The limestones of the McClellan Creek sequence are silicified on the southeast flank of Lone Mountain north of Coal Creek.

(6) Breccias are exposed south of Coal Creek along the contact of the brecciated Ordovician-Silurian cherts and shales with the overlying vitric tuffs and alluvium.

REFERENCES CITED

Dott, R. H., Jr., 1955, Pennsylvanian stratigraphy of Elko and northern Diamond Ranges, northeastern Nevada: Am. Assoc. Petroleum Geologists Bull., v. 39, p. 2211–2305

Elles, G. L., 1925, The characteristic assemblages of the graptolite zones of the British Isles: Geol. Mag., v. 62, p. 337–347

Emmons, W. H., 1910, A reconnaissance of some mining camps in Elko, Lander, and Eureka counties, Nevada: U. S. Geol. Survey Bull. 408, 130 p.

Ferguson, H. G., 1924, Geology and ore deposits of the Manhattan district, Nevada: U. S. Geol. Survey Bull 723, 163 p.

Granger, A. E., Bell, M. M., Simmons, G. C., and Lee, Florence, 1957, Geology and mineral resources of Elko County, Nevada: Nev. Bur. Mines Bull. 54, 190 p.

Hague, Arnold, and Emmons, S. F., 1877, Descriptive geology: U. S. Geol. Expl. 40th Parallel Rept., v. 2, 890 p.

Kay, Marshall, 1956, Paleozoic deformation and deposition in Nevada and Utah (Abstract): 20th Internat. Geol. Cong. (Mexico City) Resúmenes, p. 67.

King, Clarence, 1876, Geological and topographical atlas: U. S. Geol. Expl. 40th Parallel Rept., 12 pls.

—— 1878, Systematic geology: U. S. Geol. Expl. 40th Parallel Rept., v. 1, 803 p.

Lincoln, F. C., 1923, Mining districts and mineral resources of Nevada: Reno, Nev. Newsletter Publishing Co., 295 p.

Merriam, C. W., 1940, Devonian stratigraphy and paleontology of the Roberts Mountains region, Nevada: Geol. Soc. America Special Paper 25 114 p.

Merriam, C. W., and Anderson, C. A., 1942, Reconnaissance survey of the Roberts Mountains, Nevada: Geol. Soc. America Bull., v. 53, p. 1675–1728

Pringle, J., 1948, The south of Scotland, 2nd ed.: Geol. Survey and Mus., British regional geology, 87 p.

Ransome, F. L., 1904, The geology and ore deposits of the Bisbee quadrangle, Arizona: U. S. Geol. Survey Prof. Paper 21, 168 p.

Raymond, R. W., 1871 [1873], Report on the mineral resources of the states and territories west of the Rocky Mountains: Washington, D. C., Govt. Printing Office, 566 p.

—— 1872 [1874], Report on the mineral resources of the states and territories west of the Rocky Mountains: Washington, D. C., Govt. Printing Office, 550 p.

Roberts, R. J., 1951, Geologic map of the Antler Peak quadrangle, Nevada: U. S. Geol. Survey Geol. Quadrangle Map 10

Roberts, R. J., and Lehner, R. E., 1955, Additional data on the age and extent of the Roberts Mountain thrust fault, north-central Nevada (Abstract): Geol. Soc. America Bull., v. 66, p. 1661

Roberts, R. J., Hotz, P. E., Gilluly, James, and Ferguson, H. G., 1958, Paleozoic rocks of north-central Nevada: Am. Assoc. Petroleum Geologists Bull., v. 42, p. 2813–2857

Ruedemann, Rudolf, 1934, Paleozoic plankton of North America: Geol. Soc. America Mem. 2, 141 p.

Sharp, R. P., 1939, The Miocene Humboldt formation in northeastern Nevada: Jour. Geology, v. 47, p. 133–160

Smith, M. C., and Trengove, R. R., 1949, Investigation of the Rip Van Winkle lead-zinc-silver mine, Elko County, Nevada: U. S. Bur. Mines Rept. Inv. 4605, 13 p.

Stumm, E. C., 1948, Upper Devonian compound tetracorals from the Martin limestone: Jour. Paleontology, v. 22, p. 40–47

Turner, H. W., 1902, A sketch of the historical geology of Esmeralda County, Nevada: Am. Geologist, v. 29, p. 261–272

Van Houten, F. B., 1956, Reconnaissance of Cenozoic sedimentary rocks of Nevada: Am. Assoc. Petroleum Geologists Bull., v. 40, p. 2801–2825

Wheeler, G. M., 1871 [1872], Preliminary report concerning explorations and surveys principally in Nevada and Arizona: Washington, D. C., Govt. Printing Office, 96 p.

White, A. F., 1871, Report of the state mineralogist of Nevada for the years 1869 and 1870: Carson City, Nev., 128 p.

Whitehill, H. R., 1877, Biennial report of the state mineralogist of the state of Nevada for the years 1875 and 1876: Carson City, Nev., 226 p.

Zirkel, Ferdinand, 1876, Microscopical petrography: U. S. Geol. Expl. 40th Parallel Rept., v. 6, 297 p.

Burying Hill Road, Greenwich, Conn.

Manuscript Received by the Secretary of the Society, April 16, 1958

Appendix. Fossil Localities

1. *Climacograptus*
2. *Climacograptus bicornis* (Hall)
3. *Climacograptus*
4. Solitary rugose corals, articulate brachiopod fragments, crinoid columnals
5. *Coenites*
6. Solitary rugose corals, *Coenites?*, crinoid columnals
7. Articulate brachiopod valve studied by G. A. Cooper
8. Articulate brachiopod fragments, crinoid columnals
9. Solitary rugose corals, *Favosites*, articulate brachiopods, straight nautiloid
10. Articulate brachiopod fragments, crinoid columnals
11. Solitary rugose corals, crinoid columnals
12. Crinoid columnals
13. Solitary rugose corals, *Coenites?*, articulate brachiopod fragments, crinoid columnals
14. *Microspongia?*
15. Solitary rugose corals, *Favosites?*, *Coenites?*, articulate brachiopod fragments, crinoid columnals
16. Articulate brachiopods
17. *Actinostroma*, solitary rugose corals, *Hexagonaria minuta* Stumm?, *Pachyphyllum*, *Coenites*, articulate brachiopod fragments, crinoid columnals
18–20. *Climacograptus*
21. *Climacograptus bicornis* (Hall)
22. *Caryocaris*, *Glossograptus*, *Climacograptus*, *Climacograptus bicornis* (Hall)
23. *Climacograptus*
24. *Dicranograptus*, *Climacograptus*
25–26. *Climacograptus*
27. *Climacograptus*, spinose orthograptids
28–29. *Climacograptus*
30. Ordovician graptolites
31–32. *Climacograptus*
33–34. *Isograptus*
35. All fossils listed in Table 3 except *Didymograptus stabilis* Elles and Wood
36. Siliceous monaxon and triaxon spicules, *Linguella*, echinoderm columnals, all graptolites listed in Table 3 except *Azygograptus*
37. *Isograptus*
38. All fossils listed in Table 4 except siliceous monaxon spicules, *Caryocaris*, and *Glossograptus*
39. All fossils listed in Table 4 except *Paterula*, *Caryocaris*, *Glossograptus*, *Nemagraptus gracilis* (Hall) var. surcularis (Hall), and *Climacograptus bicornis* (Hall)
40. *Paterula*, *Climacograptus*
41. *Paterula*, *Dicranograptus*, *Climacograptus*, *Diplograptus multidens* Elles and Wood var. compactus Lapworth
42–43. *Climacograptus*
44–47. *Monograptus*
48–61. *Climacograptus*
62–64. *Monograptus*
65. Ordovician graptolites
66. *Dicranograptus*, *Climacograptus*
67. *Climacograptus*

BULLETIN OF THE GEOLOGICAL SOCIETY OF AMERICA
VOL. 70, PP. 565-568, 2 FIGS. MAY 1959

THE TANGUE, A "NONCONFORMING" SEDIMENT

BY JACQUES BOURCART AND ROGER H. CHARLIER

ABSTRACT

The tangue has been observed as a relatively shallow-water sediment along the French Atlantic coast, and especially in Brittany. It has a very high calcium carbonate content. The tangue was originally thought to be a recent deposit, but the discovery of considerable layers of old tangue made this original hypothesis untenable. Tangue beds are characterized by thin layers reminiscent of varves.

The tangue does not conform to the traditional deposit patterns inasmuch as, if one progresses seaward, the size distribution of grains is contrary to the distribution observed normally in other sediments.

CONTENTS

TEXT

Page
Introduction 565
Physical and dimensional properties 566
Traits of deposits 567
Conclusions 567
References cited 568

ILLUSTRATIONS

Figure Page
1. Bay of Mont Saint Michel showing distribution limits of the tangue 566
2. Tangue deposits between Grouin and Genets 566

INTRODUCTION

In a recent communication J. H. Hartshorn (1958) reported the existence of a new glacial sediment which he called flowtill. Because of its local character, flowtill was probably never considered a different sediment, and it had never been noticed by the layman. Such is not the case for the tangue, which has been used for many generations as a fertilizer along considerable parts of the French Atlantic coast and especially in Brittany. The tangue has been, thus, a well-known sediment, but from a geological point of view it has been studied only briefly (Bourcart and Francis-Boeuf, 1944a; 1944b; 1944c). The sediment was described by Claude Francis-Boeuf, J. Jacquet, J. Bourcart, P. Roa, and M. Auzel. The environment in which the tangue is commonly found, as well as references to its existence, are reported by L. and C. Berthois (1954; 1955), Cl. Francis-Boeuf (1947), and M. Philipponneau (1956).

In the vicinity of Mont Saint Michel and the estuary of the Rance River (Fig. 1), we have observed that the tangue is not exclusively a recent sediment. There is considerable old tangue below other deposits (Fig. 2). Contemporary tangue is essentially a very fine powder with a high concentration of calcium carbonate. The calcareous component of the sediment originates by the grinding of large banks of coquina—especially *Ostrea*—found in the bays we have investigated. The final grinding is facilitated by the destructive work done by mushrooms (*Lithopythium gangliiformis* and *Ostracobable implexa*) on the shells.

Spicules of sponges are also a calcareous component of the tangue; the remainder of the sediment is composed of a small fraction of fine sand, diatoms, and quartzose sand (median diameter 0.2–0.02 mm). The calcium-carbonate fraction may be as large as 80 per cent, although this is not a common occurrence.

Near Genets (Fig. 2) we observed the presence of both old and recent tangue. The recent tangue is brought to its depositional site by tidal movements: the water is extremely cloudy as it comes from the shore area. This is in striking contrast to the remarkably clear water observed some distance offshore. This tangue is then deposited at the limit of the beach or even at the foot of an occasional obstacle—*viz*, a seawall or a microcliff.

Other than in the shore area, deposits of tangue have been observed only in deltaic environment.

Physical and Dimensional Properties

The tangue is thus a littoral calcareous sediment (calcium carbonate 35–75 per cent). It is highly permeable but, in impressive contrast to sand, very coherent. Its origin is definitely organic; indeed, we observed the tangue in the Bay of Mont Saint Michel, near Veys, and in the creeks or indentations of the Brittany coast: yet this coast is not calcareous.

Two remarkable properties of tangue deposits are their color (the layers are silvery-pearly gray, different from sand, silts, and muds) and their stratification, if we may use the word. Indeed, the layers remind us somewhat of varves. The tangue deposits are made up of a succession of thin (about 2 mm) beds, separated by a surface covered by a "varnish", thin colloidal coating, corresponding to an interruption of sedimentation due to a temporary emergence. This determines a definitive foliation of the formation. The duration of this emergence usually extends over a more or less numerous series of low tides. As long as the tides are strong, little or no change will occur, but, when calmer seas occur, desiccation of the emerging material will take place; aeolian material, such as sand, will be added to the layers, and the interruption of the normal depositional process becomes visible. We have suggested for these interruptions the term of *hiatus*.

The tangue is a nonconforming sediment in

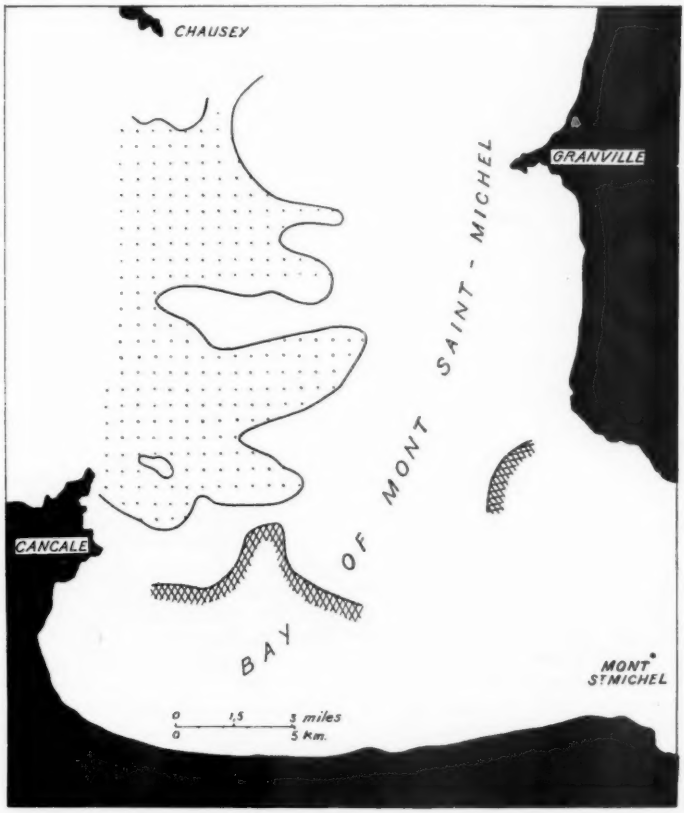

Figure 1.—Bay of Mont Saint Michel Showing Distribution Limits of the Tangue

Dotted area—sand and gravel deposits; blank area—sand and shell deposits; cross hatching indicates limit of tangue. Ginette Enard, draftswoman

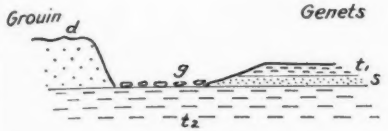

FIGURE 2.—TANGUE DEPOSITS BETWEEN GROUIN AND GENETS

d—dune; g—gravel; s—sand; t_1—recent tangue; t_2—old tangue

Ginette Enard, draftswoman

that it does not follow the traditional patterns of deposition. Indeed, the classical concept is that, as one progresses from the shore to the depths, the carrying strength of the transporting agent diminishes, and first the heavier materials are abandoned, then the smaller ones, ultimately the finest particles in suspension.

"The areas of largest energy dissipation occur along the barrier beach in the zone of large energy release by breaking waves. Areas of lesser energy application extend through the inlet and follow the tidal channels, diminishing in value further in the bay and along the side. Least mechanical energy is associated with the quiet water away from the tidal channel." (Krumbein, 1956, p. 190).

Since applied energy is used partly in transporting and sorting the sedimentary material, it may be expected that average particle size and other attributes of the sediments respond to the pattern of energy distribution.

In general, hence, the coarse detrital material remains near shore, and the fine material is gradually disseminated over the seaward part of the environment, accumulating as mud. Thus there is a more or less rapid decrease in the size of the deposited material.

Nothing of the sort occurs in the case of the tangue: the process is totally reversed. Average diameter sizes for the particles of the tangue are 2–0.002 mm, and the sizes decrease away from the ocean and toward the coast line. The reason for the grain size decreasing toward shore may be that the source of the material (the oyster banks) is offshore. The smallest diameters are observed in the great estuaries. Sizes also decrease from bottom to top in the deposit; at the surface of the sediment, dimensions are colloidal.

The ferro-humic colloidal role of the tangue is of little importance. Its color, however, varies with the dimensions of the particles; fine tangue will be dark, coarse tangue far lighter.

TRAITS OF DEPOSITS

Along the coast of Brittany, tangue deposits are much thicker than sand deposits on the beaches. This has been repeatedly proven by a variety of soundings (Bourcart *et al.*, 1944a; 1944b; 1944c). Deposits are most common upstream of estuaries. The sediment has an unusually good resistance to erosion, even aeolian; this is self-evident because of its coherence. It will persist, hence, where a granular deposit yields.

As in the case of varves, the presence of joints between successive layers of a deposit could permit an evaluation of the quantity of tangue deposited per year at each point, since each interruption corresponds to a more acute desiccation of the sediment during a long period of emergence in quiet water.

The tangue is commonly brought in by tidal currents, eroding in depth, arriving landward. It occasionally outcrops somewhat below the low-tide line.

In the southwestern part of the Mont Saint Michel Bay, we observed some accumulations of this fine powder; these deposits located under the upper layer are old tangue which outcrops here and there, in spots, under the sand deposit (Fig. 1). Today tangue forms more frequently deeper in the bay, toward the river delta, where currents have lost their strength and where the amount of suspended material is greater and deposits are more readily formed.

In places, tangue deposits are thick; soundings disclosed a thickness of 52.5 feet near Cancale and 55.8 feet at the mouth of the Rance River (Fig. 1). Here we found old tangue, a good fraction of which was made up of delta Mollusca. The calcium-carbonate fraction amounted to 40–60 per cent. There is consequently a difference in this calcium-carbonate concentration between old and recent tangue: contemporary tangue contains more calcareous material, and the old tangue contains spicules of calcareous and siliceous sponges.

CONCLUSIONS

This little-known sediment is thus remarkable because of its high calcium-carbonate concentration, its coherence with consequent resistance to erosion, and its reversal of traditional patterns of deposition.

From both mineralogical and geographical-distribution points of view, it offers an interesting field for further investigation.

References Cited

Berthois, L. and C., 1954, Etude de la sédimentation dans l'estuaire de la Rance: Bull. Labo. Dinard, v. 40, p. 4–15 (November).

——, 1955, Etude de la sédimentation dans l'estuaire de la Rance: Bull. Labo. Dinard, v. 41, p. 3–18 (July).

Bourcart, J., Jacquet, J., Francis-Boeuf, Cl., 1944a, Sur la nature du sédiment marin appelé tangue: Acad. des Sciences France, Comptes-Rendus, v. 218, p. 469

——, 1944b, La tangue de la Baie du Mont Saint Michel: Soc. de Biogéographie France, Comptes-Rendus Som., v. 180, p. 43

——, 1944c, Sur les propriétés physiques d'ensemble du sediment appelé tangue: Acad. des Sciences France, Comptes-Rendus, v. 219, p. 74

Francis-Boeuf, Cl., 1947, Recherches sur le milieu fluvio-marin et les dépôts d'estuaires: Ann. Inst. Océanographie, v. 23, p. 149–344

Hartshorn, J. H., 1958, Flowtill in southeastern Massachusetts: Geol. Soc. America Bull., v. 69, p. 477–482

Krumbein, W. C., and Sloss, L. L., 1956, Stratigraphy and sedimentation: San Francisco, W. H. Freeman, 497 p.

Philipponeau, M., 1956, La baie du Mont Saint-Michel, étude de morphologie littorale: Mém. Soc. Géol. et Minéral. de Bretagne, v. 9, p. 7–215

Dept. of Physical Geography, Marine Geology and Oceanography, Faculty of Sciences, a la Sorbonne, The University of Paris, France

Manuscript Received by the Secretary of the Society, July 3, 1958

BULLETIN OF THE GEOLOGICAL SOCIETY OF AMERICA
VOL 70, PP. 569-580, 9 FIGS. MAY 1959

EFFECT OF GRAIN SIZE ON STRENGTH OF MIXTURES OF CLAY, SAND, AND WATER

BY PARKER D. TRASK

ABSTRACT

Many factors affect the strength of what engineers call soil. This report deals primarily with the effect of the grain size of sand or silt particles mixed with the clay in the soil. In order to understand the effect of grain size, the influence of (1) water content, (2) type of clay mineral, and (3) ratio of clay to sand in the soil must be known. The effect of these four variables was investigated by measuring the strength of a series of synthetic soils in which the water content, clay type, clay-sand ratio, and grain size of admixed sand were changed from one experiment to another. For given water content, kaolin and illite are essentially equal in strength, and both are much weaker than montmorillonite. Ball clay—a kaolin containing organic matter—is intermediate in strength. For all clays the strength increases, for given water content and given grain size, as the ratio of clay to sand increases. For given water content and given clay-sand ratio, the strength increases as the grain size of the sand decreases below 135 microns. For coarser sand, grain size has little effect. The cause of the greater strength for increasing fineness of sand is ascribed to the well-known principle of greater surface area upon which forces can act.

CONTENTS

TEXT

Page
Introduction and acknowledgments 569
Settling-tank deposits 570
Sedimentary mixtures 573
Results of torque-vane studies 573
Atterberg blow-count studies 577
Conclusions 578
References cited 579

ILLUSTRATIONS

Figure Page
1. Vane-shear test apparatus 571
2. Relation of clay type and clay concentration to shear strength and water content. 573
3. Relation of bentonite concentration to shear strength and water content 574
4. Effect of varying content of illite and kaolin upon shear-strength water-content relationships of sand-clay mixtures 575
5. Relation of median diameter of sand component to shear strength and water content 575
6. Relation of bentonite concentration to Atterberg blow count and water content 576
7. Relation of illite concentration to Atterberg blow count and water content 576
8. Relation of grain size of admixed sand to Atterberg blow count and water content 577
9. Relation of clay type to clay concentration and liquid limit 578

TABLES

Table Page
1. Parameters of sediments used in strength studies 572
2. Shear strength of sediments deposited in cylindrical tank 572

INTRODUCTION AND ACKNOWLEDGMENTS

Four principal factors affecting strength of what the engineer calls soil are: water content, type of clay mineral, clay-sand ratio, and grain size of sand mixed with the clay. The influence of the first three factors has received considerable attention, notably by Bekker (1956), Casagrande (1932), Casagrande and Carillo (1953), Grim and his co-workers (1945; 1953), Knight and his associates (Knight and Rush, 1958), Pask and his associates (Langston and Pask, 1958), Rutledge (1940), Seed and his co-workers (1956), and Skempton (1953). With the object of studying the effect of the fourth factor—grain size—the authors investigated a series of natural and synthetic soils, in which each of the four principal variables in turn was allowed to vary while the other three were kept constant.

Three types of soils were studied: (1) prototype sediments as they occur in nature, (2) sedi-

ments artificially deposited in a settling tank, and (3) synthetic soils composed of water, clay, and sand or silt. Study of prototype sediments necessitates the examination of large numbers of samples in order to make a statistical analysis of the relative effects of the individual soil factors. Artificial deposition of sediment mixtures in a settling tank almost certainly results in more rapid deposition than occurs in nature. Disadvantages of the study of synthetic mixtures are artificiality of the resulting material and the disturbed character of the soil. Soil-mechanics engineers recognize that disturbed soils generally are weaker than fresh soils. Thus all three lines of approach lead to difficulties in interpretation, but in the 4 years during which these studies were carried on, each line of approach was used.

Two reports of these investigations have already been published: (1) the effect of clay content on the strength of natural sediments in the San Francisco Bay region (Langston, Trask, and Pask, 1958), and (2) the effect of clay content on strength of synthetic mixtures (Trask and Close, 1958). The first report showed that soils containing moderate or large amounts of montmorillonite are stronger, for given water content, than soils containing little or no montmorillonite. The second report indicates that montmorillonite soils for given water content are much stronger than soils composed of either kaolin or illite, and that the strength of soils increases as the ratio of clay to sand in the soil increases.

In connection with the present study of strength of sediments the authors have prepared a general review of the problem of strength of soils, together with an extended bibliography, for the forthcoming Second Review Volume on Engineering Geology, to be edited by George R. Kiersch.

People who assisted in the work of the present project are J. Peter Berge, Robert B. Langston, Harry MacMurray, Patrick O'Malley, Evelyn and William Quaide, Sigrid Snider, and Roger E. Skjei. Acknowledgment is also due J. W. Johnson and Robert L. Wiegel of the Waves Research Laboratory of the University of California where the work was done. James R. Kerrigan of the Sanitary Engineering Research Laboratory of the University of California at Berkeley made the analyses of carbon presented in Table 1. The work was carried on under the auspices of Contract No. DA-04-200-ORD-171 (9), of the Office of Ordnance Research, Ordnance Corps, U. S. Department of the Army.

Settling-Tank Deposits

In the settling-tank experiments, sedimentary materials are fed mechanically into a cylindrical tank 2 feet in diameter and 12 inches high. The water is circulated by a paddle 4 inches in diameter, rotating 39 revolutions a minute. The sediments are added to the tank at the rate of 10–15 grams per minute until a deposit 3 or 4 inches thick has accumulated, usually in 24–48 hours. At a distance of 10 inches from the center the water circulates at the rate of 1 revolution per minute, and at 3 inches from the center it circulates at 6 revolutions per minute. The water in the tank is buffered with sodium metasilicate and sodium hydroxide to keep the pH between 9.0 and 10.3, in order to inhibit flocculation. After the feeding apparatus is stopped, the strength of the sediment is determined by a shear vane and pulley device. Figure 1 shows how the instrument operates for sedimentary mixtures in a mortar bowl. A similar type of pulley device has been used for the synthetic-tank experiments. Water is poured into the container at the end of the pulley system until the weight of the water and consequent torque on the shaft of the embedded vane cause the sediment in the settling tank to fail and the vane to rotate. The results are reported both in terms of grams of water added and of the corresponding shear strength in pounds per square inch computed according to the formula of Capper and Cassie (1953, p. 112):

$$T = WR = C\pi\left(\frac{D^2H}{2} + \frac{D^3}{6}\right)$$

where T is the torque, W the weight of water required to cause failure, R the radius of the pulley wheel, C the shear strength, D the diameter of the circle of rotation of the shear vane, and H the height of the vane. In the present investigation the weight of water in the cup at time of failure of the sediment ranges from 100 to 1000 grams. As the height and diameter of the vane and the pulley radius of the torque wheel are the same for all tests, the weight in grams is directly proportional to the strength in pounds per square inch. The factor for converting weight of water in grams to shear strength of the sediment in pounds per square inch is 1.37×10^{-3}. The height of the vane is 0.764

inch, diameter of the circle of rotation 1.312 inches, and radius of pullley wheel 2.02 inches. The vane has four vertical blades of equal size placed at right angles to one other.

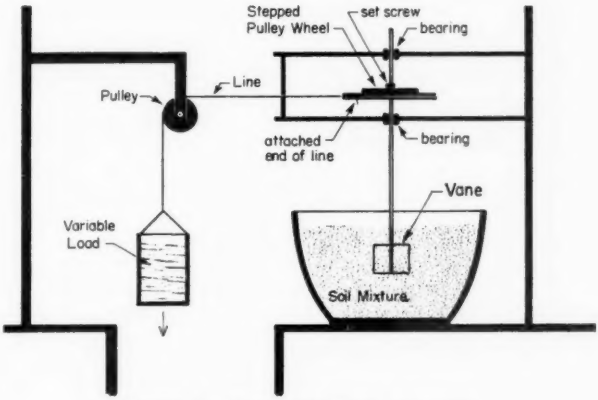

FIGURE 1.—VANE-SHEAR TEST APPARATUS

The parent materials in these experiments consist of a series of clays and ground or natural beach sand. The physical character of the clays is described by Langston, Trask, and Pask (1958, p. 222, 223). The clays are: Edgar china clay from Georgia, which is nearly pure kaolin midway in composition between a hydrogen and sodium clay; Illinois grundite which contains approximately 80 per cent illite, 1.2 per cent organic matter, and the rest clastic material, mainly quartz; Kentucky Old Mine No. 4 ball clay, a mixture estimated to contain 85 per cent kaolin, 14 per cent silica, and 2.4 per cent organic matter, called ball clay No. 1 in the present report; Kentucky Mine Special, a ball clay containing about 80 per cent kaolin, 5 per cent organic matter, and the rest quartz, called here ball clay No. 2; Wyoming bentonite—a clay estimated to contain 97 per cent sodium montmorillonite, and 3 per cent quartz and 0.1 per cent organic matter and volclay, a nearly pure bentonite. The median diameters of the clay grains range mainly between 1 and 2 microns. Sedimentary parameters of the clays are given in Table 1. Table 1 also contains data on the sands used in the present study.

The results of the strength measurements of the upper 1 inch of the deposits are presented in Table 2. Satisfactory duplicate measurements were obtained. The strength tends to increase slightly with depth in the deposits. Estimates of water content in Table 2 are taken from the sand-clay-mixture graphs (Fig. 2). As the slopes of the lines (Fig. 2) are constant, predictions can be made as to the strength for any given water content for the sedimentary types shown on the figure. Some of the data shown in column 4 of Table 2 are extrapolated considerably beyond the points of control for the curves. The reliability of such measurements therefore may not be great. The data in Table 2 show that the estimated water content of the sedimentary mixtures is similar to the actual water content of the settling-tank deposits for samples of equal strength. However, the sedimentary mixtures correspond to remolded soils, where as the settling-tank deposits simulate undisturbed sediments.

The water content of the synthetic sediments (Table 2) increases progressively from kaolin through illite to ball clay in essentially the same way as in the sedimentary-mixture experiments (Fig. 2), but the water content is considerably higher in the tank deposits than in the sedimentary mixtures. The ball and illite clays have a higher water content than kaolin and are considerably weaker than kaolin. The montmorillonite sediments flocculated and could not be studied.

The clastic sediments represented by the 16- and 1.2-micron silica deposits, and mixtures of these two, are considerably stronger than the clays. The silica deposits, being of a clastic nature, represent cohesionless sediments and are dilatant. Silica or clastic deposits show little

change in strength with increasing water content until they approach a state of liquefaction.

The data shown in Table 2 indicate that the strength decreases from 0.51 pound per square inch in 16-micron silica to 0.18 pound per square inch for a mixture of 80 per cent 16-micron silica and 20 per cent 1.2-micron silica. At the same time the water content increases from 32 to 45 per cent. Clastic deposits of clay size—that is. those that consist of 100 per cent 1.2-micron silica—form alternating hard and soft layers, possibly associated with the formation of colloidal sodium silicate caused by the addition of the sodium hydroxide used as a buffer. Both layers, however, are relatively weak. The hard layers have a strength of .035 pound per square inch and a water content of 48 per cent, whereas the soft layers have a strength of .004 pound per square inch and a water content of 72 per cent. The mixture of 80 per cent

TABLE 1.—PARAMETERS OF SEDIMENTS USED IN STRENGTH STUDIES

Sediment	First quartile	Median diameter	Third quartile	Sorting	Log_{10} Skewness	Carbon content (per cent)
	Microns					
Kaolin	0.58	1.24	3.25	2.37	+0.077	0.00
Ball clay No. 1	0.54	1.32	3.59	2.56	+0.024	1.86
Ball clay No. 2	0.82	2.30	8.20	3.16	+0.050	3.90
DMAF Silica	0.60	1.15	2.18	1.91	−0.002	0.10
16-micron silica	7.2	16.2	33.8	2.17	−0.008	0.00
Sands	41.5	55	73	1.33	+0.001	—
Sands	52	80	110	1.45	−0.048	—
Sands	87	136	175	1.42	−0.043	—
Sands	168	180	190	1.06	−0.003	—
Sands	295	350	425	1.20	+0.005	—
Sands	555	725	890	1.27	−0.016	—
Sands	700	945	1150	1.23	−0.023	—
Sands	1460	1680	1870	1.13	−0.007	—

Bentonite and illite flocculated; the median diameter presumably was about 1 micron. The carbon content of the bentonite is 0.10 per cent and of the illite 0.88 per cent. In this report organic matter has been estimated as 1.3 times the carbon content.

TABLE 2.—SHEAR STRENGTH OF SEDIMENTS DEPOSITED IN CYLINDRICAL TANK

The water content represents 100 W/S, where W is the weight of the water and S the weight of the solid constituents; p.s.i. is pounds per square inch.

Parent material	Shear strength p.s.i.	Water content	Extrapolated water content of sediment mixture of same strength
		(In per cent)	
Kaolin	.057	71	76
Illite	.015	92	82
Ball clay No. 1	.015	120	120
Ball clay No. 2	.013	116	100
80% 16-micron silica—20% ball clay No. 1	.09	41	37
100% 16-micron silica	.51	32	—
90% 16-micron silica—10% 1.2-micron silica	.24	39	—
80% 16-micron silica—20% 1.2-micron silica	.18	45	—
1.2-micron silica—hard layer	.035	48	—
1.2-micron silica—soft layer	.004	72	—

16-micron silica and 20 per cent ball clay No. 1 has a strength of 0.09 pound per square inch and a water content of 41 per cent; a mixture of 80 per cent 16-micron silica and 20 per cent 1.2-micron silica has a strength of 0.18 pound per square inch and a water content of 45 per cent. In experiments on sedimentary mixtures, described below, the addition of 1.2-micron clay in the place of 1.2-micron silica makes the sediment twice as strong, whereas in the above-mentioned experiments it makes them weaker, for comparable water content. The experiments described below, however, were made on cohesive sediments containing 20–100 per cent clay, whereas the experiments reported in Table 2 were made on more or less cohesionless material containing 0–20 per cent clay. In the cohesive soils, strength is affected to a considerable extent by plasticity, whereas in the cohesionless soils friction between grains is a major factor.

Sedimentary Mixtures

Results of Torque-Vane Studies

The main part of the present investigation is the study of artificial mixtures of clay and sand. Two measures of strength have been used: (1) the torque vane previously described, and (2) Atterberg limits (Casagrande, 1932). In the preparation of the sedimentary mixtures for torque-vane studies, the parent materials are combined with a quantity of water about equal to the liquid limit. The sediments are mixed in a 10-inch mortar bowl (Fig. 1). The strength is then determined by the shear-vane device used in the experiments on sediments deposited in a cylindrical tank. After the shear strength has been determined, a sample is removed for measurement of the water content. A small additional quantity of the parent sedimentary mixture is then added to the material in the mortar bowl, and the strength and water con-

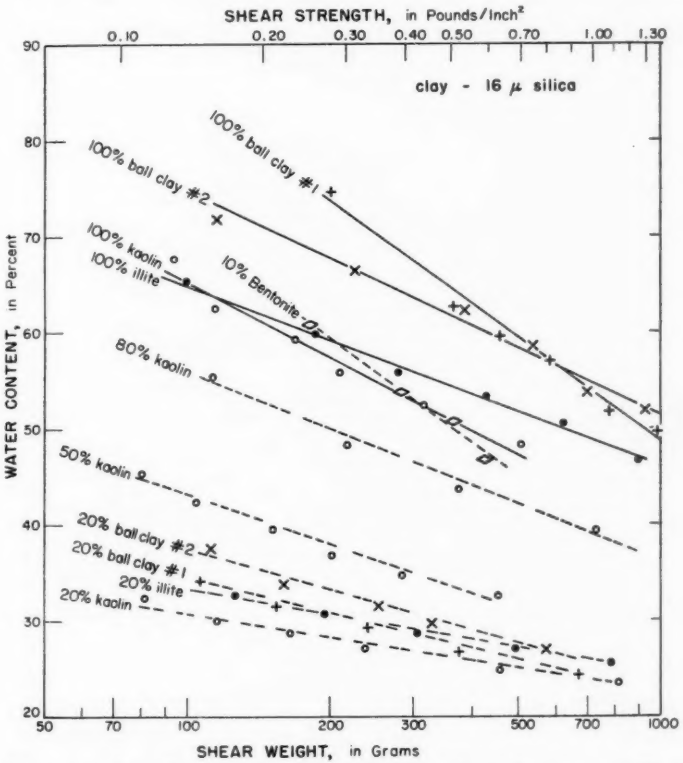

FIGURE 2.—RELATION OF CLAY TYPE AND CLAY CONCENTRATION TO SHEAR STRENGTH AND WATER CONTENT

tent of the resulting thicker mixture are measured. Increments of sediment are added until five or six mixtures with successively greater admixed clastic particles were measured. The strength-water relationships of the various mixtures of sand and clay are shown in Figures 2–5.

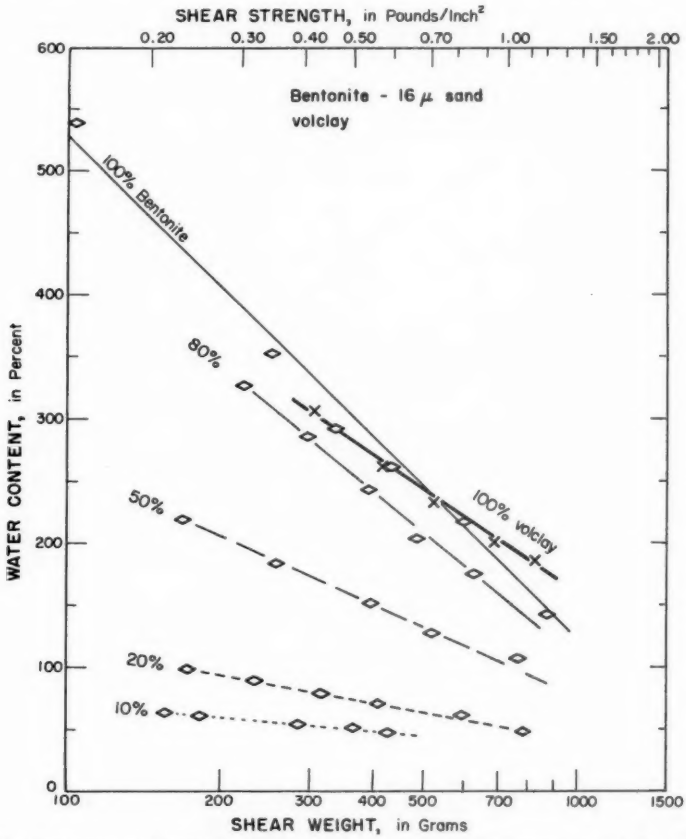

FIGURE 3.—RELATION OF BENTONITE CONCENTRATION TO SHEAR STRENGTH AND WATER CONTENT

proportions of solids have been tested. The results are then plotted on semilogarithmic paper (Fig. 2). Six types of clays—kaolin, illite, two ball clays, and two montmorillonites (Wyoming bentonite and volclay)—where studied. Sedimentary parameters of these parent materials are presented in Table 1.

The strength-water relationships for the parent clay materials were investigated first. Subsequently the strength-water relationships were determined for mixtures of these parent materials with different types of sand, in different proportions and of different grain size. In this way strength-water relationships for clay type, clay-sand proportion, and grain size of Figure 2 shows relationships for the pure clays, except bentonite, and for mixtures of all the clays with different proportions of sand. The sand in these tests had a median diameter of 16 microns. This 16-micron material more appropriately should be called silt, but it is convenient to refer to it as sand.

Figure 3 shows the results of tests on mixtures of bentonite and different proportions of 16-micron sand. For given water content the order of increasing strength in the pure clay types is kaolin, illite, ball clay, and bentonite. Bentonite is distinctly stronger than the other clays. Mixtures of kaolin and illite have essentially the same strength as either pure kaolin or pure

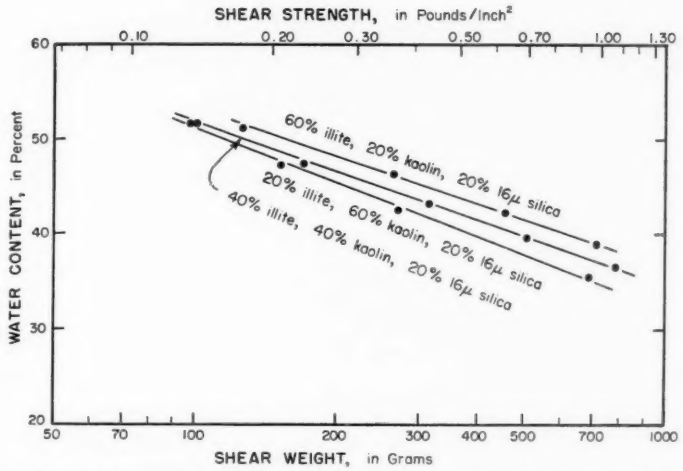

FIGURE 4.—EFFECT OF VARYING CONTENT OF ILLITE AND KAOLIN UPON SHEAR-STRENGTH WATER-CONTENT RELATIONSHIPS OF SAND-CLAY MIXTURES

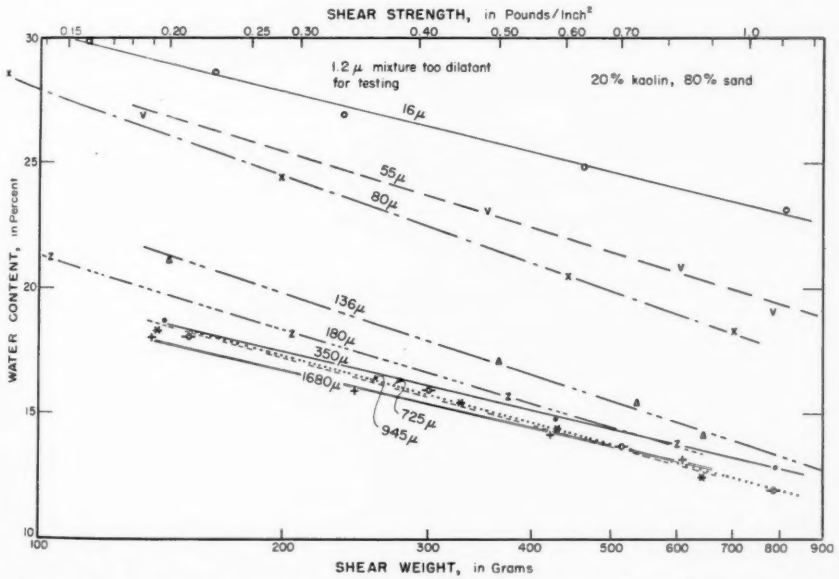

FIGURE 5.—RELATION OF MEDIAN DIAMETER OF SAND COMPONENT TO SHEAR STRENGTH AND WATER CONTENT

illite (Fig. 4). The relative strength for given water content is similar to the relative base-exchange capacity of the different clay types. Base-exchange capacity is relatively low in kaolin, moderate in illite, and high in montmorillonite (Grim, 1953).

When 16-micron sand is mixed with the clays, the strength progressively decreases, for given water content, as the proportion of sand increases. The slopes of the shear-strength water-content curves also decrease in a progressive order. A quantitative discussion of this

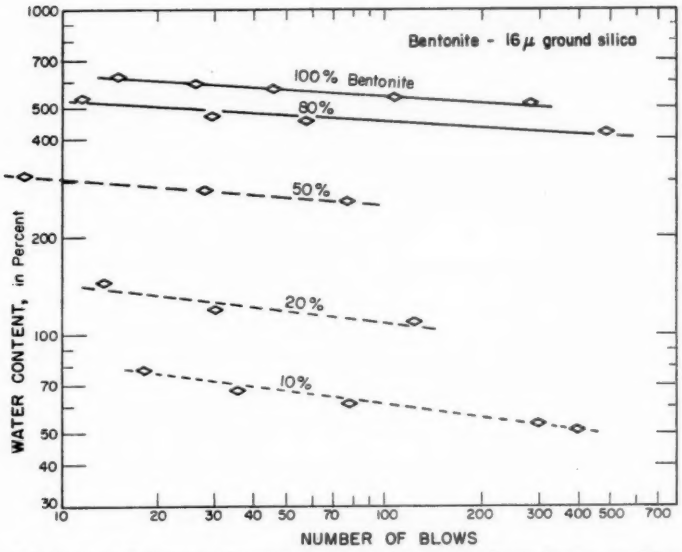

FIGURE 6.—RELATION OF BENTONITE CONCENTRATION TO ATTERBERG BLOW COUNT AND WATER CONTENT

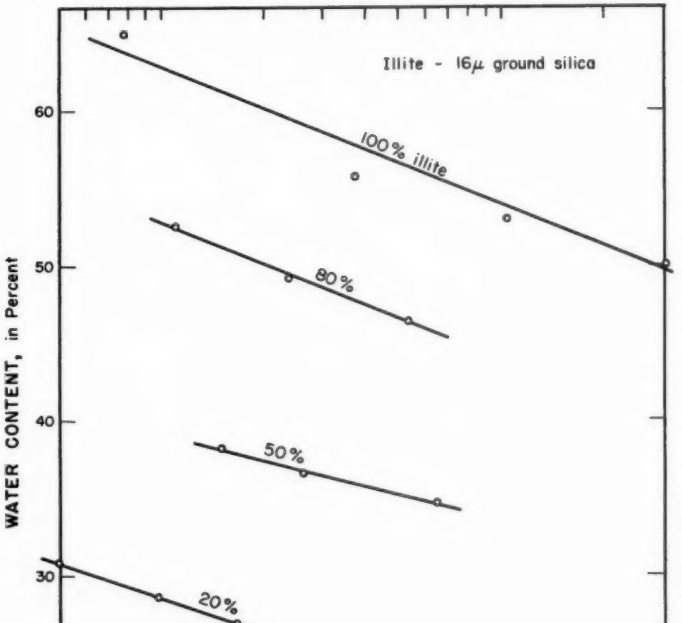

FIGURE 7.—RELATION OF ILLITE CONCENTRATION TO ATTERBERG BLOW COUNT AND WATER CONTENT

change in strength with change in clay-sand proportion is presented by Trask and Close (1958).

The effect of grain size of the admixed sand particles is shown in Figure 5. This figure shows

Atterberg Blow-Count Studies

Atterberg limits have been used for many years as a guide to the engineering properties of clay. In order to study the effect of the three

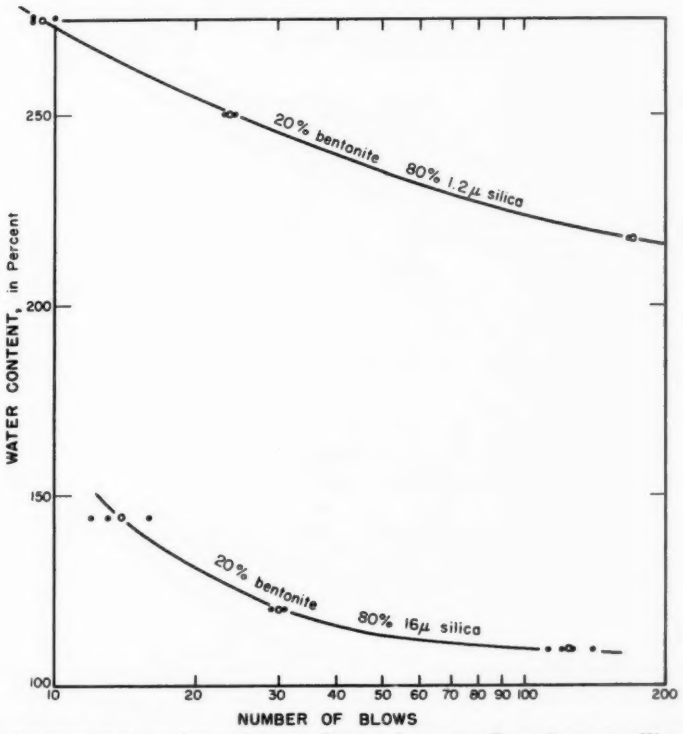

FIGURE 8.—RELATION OF GRAIN SIZE OF ADMIXED SAND TO ATTERBERG BLOW COUNT AND WATER CONTENT

strength-water relationships for different sizes of sand in a mixture of 80 per cent sand and 20 per cent kaolin. The strength for given water content increases as the grain size decreases. The rate of increase is greater below than above 135 microns. Similar increasing strength with increasing fineness of grain is noted for mixtures of other clays with differing proportions of sand. The 1.2-micron sand in a mixture of 80 per cent sand and 20 per cent kaolin was too dilatant for measuring strength-water relationships, but experiments made with bentonite, ball clay, and kaolin, with higher proportions of clay indicate that for given water content the resulting strength is considerably greater in the 1.2-micron sand mixture than in the 16-micron mixture.

variables—clay type, clay-sand proportion, and grain size of admixed particles—on the Atterberg limits, a series of clays and clay-sand mixtures were tested in the conventional Atterberg testing device. Measurements were made of the number of blows required to close the furrow used in the liquid-limit test, for varying water content of the different mixtures. The data for the tests of Wyoming bentonite (Fig. 6) show a straight-line logarithmic relationship for each mixture of clay and 16-micron silica. For a blow count of 25, which is the standard liquid-limit blow count, the water content ranges from 70 per cent for 10 per cent bentonite to 600 per cent for pure bentonite. Similar relationships, except for a much smaller range in water content, were observed for illite (Fig. 7) and kaolin

(Trask and Close, 1958). However, the relationships are more nearly semilogarithmic than logarithmic. The water content for a given blow count also increases as the fineness of grain increases (Fig. 8). The blow-count relationships for clay type, clay-sand proportion, and grain size of admixed particles thus are very similar to the strength-water relationships (Figs. 2–5).

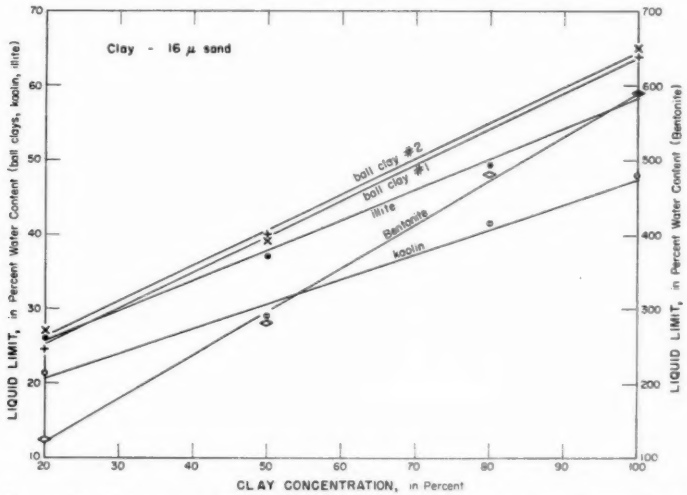

FIGURE 9.—RELATION OF CLAY TYPE TO CLAY CONCENTRATION AND LIQUID LIMIT

The relationships of clay-sand ratio to the liquid limit for different clays are shown in Figure 9. This figure indicates that the water content for given clay concentration progressively increases in the order of kaolin, illite, ball clay to bentonite. This relationship thus conforms with the standard relationships of different clay types shown in Figures 2 and 3. The clay-concentration curve for bentonite is much steeper than for the other clays, because the scale on the right side of the graph for bentonite is 10 times the scale for the other clays. The black diamond at 600 per cent water on the 100 per cent clay ordinate represents a duplication of position for data for the illite and montmorillonite curves.

CONCLUSIONS

Experimental work of the present investigators has been devoted primarily to determining the relative effect of three factors: (1) grain size of admixed particles, (2) clay type, and (3) clay-sand proportion. The effect of all three of these factors is subordinate to the effect of water on strength. The results show that for given water content the strength increases from kaolin through illite and ball clay to montmorillonite. Montmorillonite is relatively much stronger than the other three clays. This relative relationship is of essentially the same order of magnitude as the base-exchange capacity of the several clays. Evidently the strength relationships are intimately associated with clay chemistry. The sediments, as deposited in a settling tank, show essentially the same strength relationships for given water content as do the sediment mixtures, but as normally deposited they have a relatively high water content. This water content increases progressively from kaolin to illite and presumably to montmorillonite. The affinity of the sediments for water in a natural environment of deposition increases in the same order as does strength for given water content and as does base-exchange capacity. The relative change in water content of naturally deposited sediments may offer an explanation for the relative weakness of montmorillonite soil, which commonly is associated with landslides. Though montmorillonite soil is relatively strong for given water content, it has a large capacity to assimilate water and thus under certain conditions acquires so much water that it becomes relatively weak.

The increase in strength for given water content with increasing content of fine-grained

particles or increasing clay concentration seems to be related to the relative proportion of bound and unbound water in the soil, as numerous other people have shown. The surface area of the particles increases with increasing fineness of grain. Thus the relative content of bound water increases, and content of unbound water decreases. Consequently the strength increases. The greater strength of mixtures of clay particles of the same size as mixtures of clastic particles may be due to the greater affinity of clay particles for water than of sand particles for water.

The synthetic mixtures studied in the present experiments represent reworked sediments. As such they are weaker than normal sediments or engineering soils. The relative effects for changes in water content, clay type, clay-sand proportion, or grain size, however, should not change, even though the absolute effects may.

References Cited

Bekker, M. G., 1956, Theory of land locomotion: Ann Arbor, Mich., Univ. Michigan Press, 520 p.

Capper, P. L., and Cassie, W. F., 1953, The mechanisms of engineering soils: London, E. and F. N. Spon, 315 p.

Casagrande, A., 1932, Research on Atterberg limits of soils: Public Roads, v. 13, p. 121–130

Casagrande, A., and Carillo, N., 1953, Shear failure of anisotropic materials: Jour. Boston Soc. Civil Engineers, v. 31, p. 122–135

Grim, R. E., and Cuthbert, F. L., 1945, Some clay-water properties of certain clay minerals: Jour. Am. Ceramic Soc., v. 28, p. 90–95

Grim, R. E., 1953, Clay mineralogy: N. Y., McGraw-Hill Book Co., 384 p.

Knight, S. J., and Rush, E. S., 1958, A limited study of the factors that affect soil strength: U. S. Corps of Engineers, Waterways Expt. Sta. Misc. Paper 4–284, 34 p.

Langston, R. B., and Pask, J. A., 1958, Analysis of consistencies of kaolin-water systems below the plastic range: 5th Natl. Conf. on Clays and Clay Minerals Proc., p. 4–22

Langston, R. B., Trask, P. D., and Pask, J. A., 1958, Clay studies of bore-hole samples from brackish-water sediments in central California: Calif. Div. Mines Quart. Jour., v. 54, p. 215–238

Rutledge, P. C., 1940, Theories of failure of materials applied to the shearing resistance of soils: Purdue Conf. on Soil Mechanics Proc., p. 191–204

Seed, H. B., and McNeill, R. L., 1956, A comparative study of soil deformations and repeated loading tests: Highway Research Bull. 141, p. 44–53

Skempton, A. W., 1953, The colloidal "activity" of clays: 3d Internat. Conf. on Soil Mechanics and Found. Eng. Proc., v. 1, p. 57–61

Trask, P. D., and Close, J. E. H., 1958, Effect of clay content on strength of soils: Sixth Coastal Eng. Conf. Proc. (Coastal Engineering, v. 6), p. 827–843

Department of Engineering, University of California, Berkeley 4, California

Manuscript Received by the Secretary of the Society, March 11, 1958

DO NOT COPY

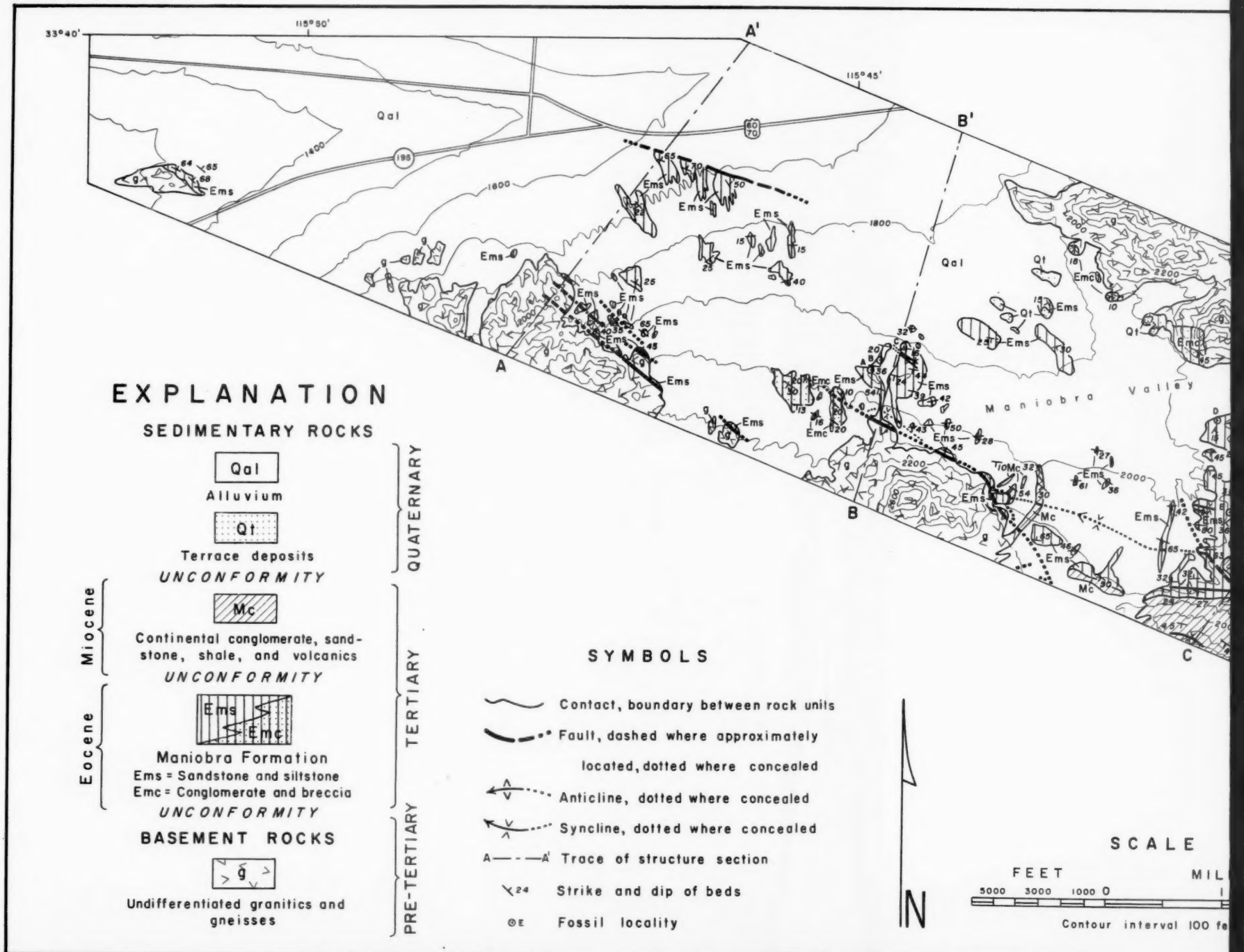

GEOLOGIC MAP OF NORTHERN OROCOPIA MOUNTAINS, RIVERSIDE COUNTY, SOUTH

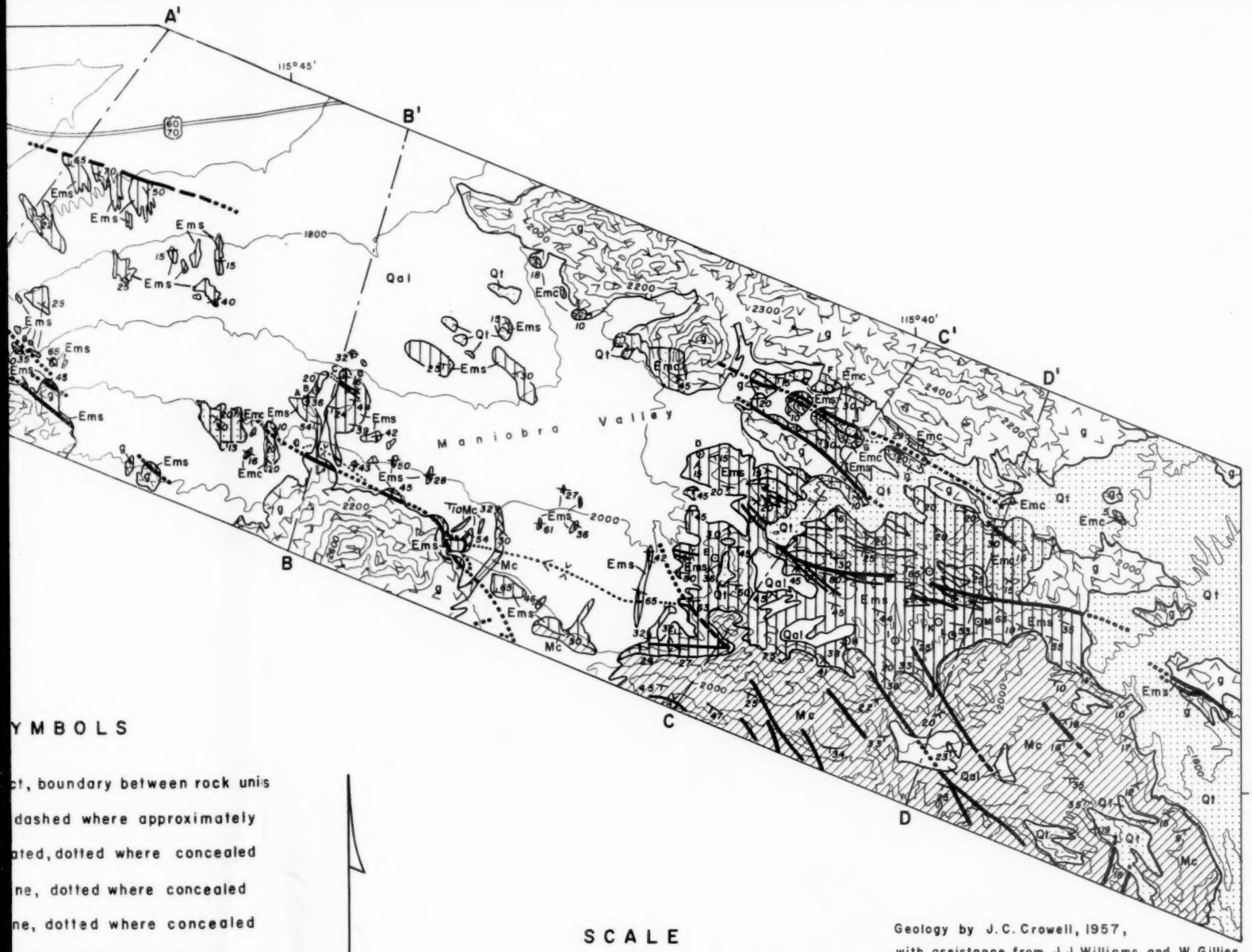

YMBOLS

ct, boundary between rock unis
dashed where approximately
ated, dotted where concealed
ne, dotted where concealed
ne, dotted where concealed
of structure section
and dip of beds
locality

RN OROCOPIA MOUNTAINS, RIVERSIDE COUNTY, SOUTHEASTERN CALIFORNIA

BULLETIN OF THE GEOLOGICAL SOCIETY OF AMERICA
VOL. 70, PP. 581-592, 4 FIGS., 3 PLS. MAY 1959

EOCENE STRATIGRAPHY AND PALEONTOLOGY, OROCOPIA MOUNTAINS, SOUTHEASTERN CALIFORNIA

BY JOHN C. CROWELL AND TAKEO SUSUKI

ABSTRACT

Marine Eocene strata underlie about 26 square miles in the northeastern Orocopia Mountains, Riverside County, California. The newly discovered section, which is about 4800 feet thick, lies in a structural trough within basement rocks and is overlain unconformably by about 5000 feet of undated nonmarine clastic and volcanic rocks.

The Eocene beds consist of interbedded siltstone, sandstone, conglomerate, and breccia with some sandy limestone and are here defined as constituting the Maniobra formation. On the east at the base of the section large granitic boulders up to 30 feet in diameter lie along the unconformity with basement granite. These give way upward to thick lenses of coarse granitic conglomerate and breccia with interbeds of buff siltstone and arkosic sandstone. The upper part of the section on the east consists of massive buff siltstone with sandstone and boulder beds. On the west the section consists largely of interbedded siltstone and sandstone with conspicuous isolated boulders of granite.

Mollusks and Foraminifera, including Orbitoids, occur at many localities throughout the section. Some characteristic forms are: *Turritella andersoni cf. lawsoni* Dickerson, *Turritella uwasana cf. applini* Hanna, *Clavilithes* sp., *Marginulina mexicana* (Cushman) var., *Pseudophragmina* (*Proporocyclina*) *clarki* (Cushman). This fauna indicates a lower and middle Eocene age, and the strata possibly correlate with similar rocks of the Coast Ranges.

CONTENTS

	Page
Introduction and acknowledgments	581
Stratigraphy	584
General features	584
Conglomerate and breccia	584
Siltstone and sandstone	586
Paleontology	588
Introduction	588
Mollusks	588
Foraminifera	589
Age and correlation	589
Origin	590
Summary	591
References cited	591
Appendix. Descriptions of Eocene fossil localities, Orocopia Mountains	592

ILLUSTRATIONS

Figure	Page
1. Location map showing geologic setting of Orocopia Mountains, southeastern California	582
2. Structure sections	583
3. Columnar section, Eocene strata, Orocopia Mountains, southeastern California	585
4. Field sketch showing emplacement of exotic blocks, Maniobra formation	586

Plate	Facing page
1. Geologic map	581
2. Characteristic species from the Eocene Maniobra formation	588
3. Maniobra formation	589

INTRODUCTION AND ACKNOWLEDGMENTS

Marine strata containing Lower and Middle Eocene fossils, unreported before 1955, are exposed in the northeastern Orocopia Mountains in the Colorado Desert of southern California (Fig. 1). These beds, defined as constituting the Maniobra formation, and some of their diagnostic fossils are described here for the first time. They extend significantly the known distribution of Eocene rocks in California.

The Eocene beds lie about 15 miles northeast of the San Andreas fault zone and are preserved in a broad east-west structural depression in the border zone between the Transverse Ranges and the Basin and Range Province (Fig. 1). On the north this depressed area is bounded by high-standing granitic terrain with associated gneisses of the Cottonwood Mountains and Eagle Mountains, which are part of the Joshua Tree National Monument. Included with these granitic rocks and gneisses is the prominent

northeastern ridge of the Orocopia Mountains south of Hayfield Reservoir named the Hayfield Mountains by Miller (1944, Pl. II). On the south the structurally depressed area is bordered by the Orocopia Mountains, which are underlain primarily by Orocopia schist (Miller, 1944) and deformed gabbro, diorite, anorthosite, gneiss, and other granitic rocks.

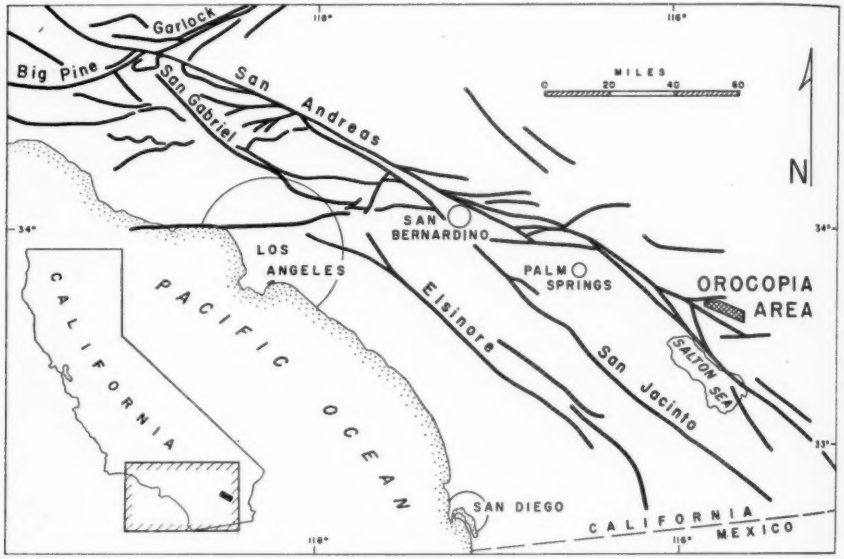

FIGURE 1.—LOCATION MAP SHOWING GEOLOGIC SETTING OF OROCOPIA MOUNTAINS, SOUTHEASTERN CALIFORNIA

Although a principal transcontinental highway (U. S. 60-70) skirts the area, fossils were not reported, and the Eocene age of the strata was not recognized until discovered by us in 1955. Early reconnaissance maps of the region show the area as underlain by undifferentiated granite, diorite, gabbro, and schist (Brown, 1923, Pl. XIII; Darton, 1933, Sheet 27). The State geologic map of California (Jenkins, 1938), scale 1:500,000, depicts an area of undivided nonmarine Miocene sedimentary rocks which corresponds roughly to the area of outcrop of both the Eocene strata and the younger nonmarine rocks. The western exposures of the Eocene, including strata along structure section B-B′ (Fig. 2; Pl. 1), are included by Miller in his extensive "Early pre-Cambrian" Chuckwalla complex of mixed metadiorite and granite (1944, Pl. II, scale 1:148,000).

Only Dibblee (1954, p. 24) suggested that marine Eocene rocks might occur in the region; he reported cobbles of sandstone with marine Eocene fossils in conglomerates of the Pliocene (?) Mecca formation northwest of Painted Canyon. These cobbles came from a point about 10 miles west of the Eocene outcrop area as now recognized.

The writers are grateful for help received in preparing this paper. Prof. W. Storrs Cole, Cornell University, kindly identified the orbitoids. Mr. Edwin C. Allison, Department of Paleontology, University of California, Berkeley, and Prof. V. Standish Mallory, Department of Geology, University of Washington, examined smaller Foraminifera. Profs. M. N. Bramlette, J. Wyatt Durham, Robert M. Kleinpell, W. P. Popenoe, E. L. Winterer, University of California, commented on aspects of the paleontology. The fossils were discovered on a field trip, led by the senior writer in early February 1955, which included several graduate students from the University of California, Los Angeles. The first fossil was picked up by Perry L. Ehlig. John C. Kirkpatrick, Warren Gillies, and James J. Williams undertook problems for Master's theses in the area, and their work has been particularly helpful. We are also indebted to W. P. Popenoe and E. L. Winterer for critical

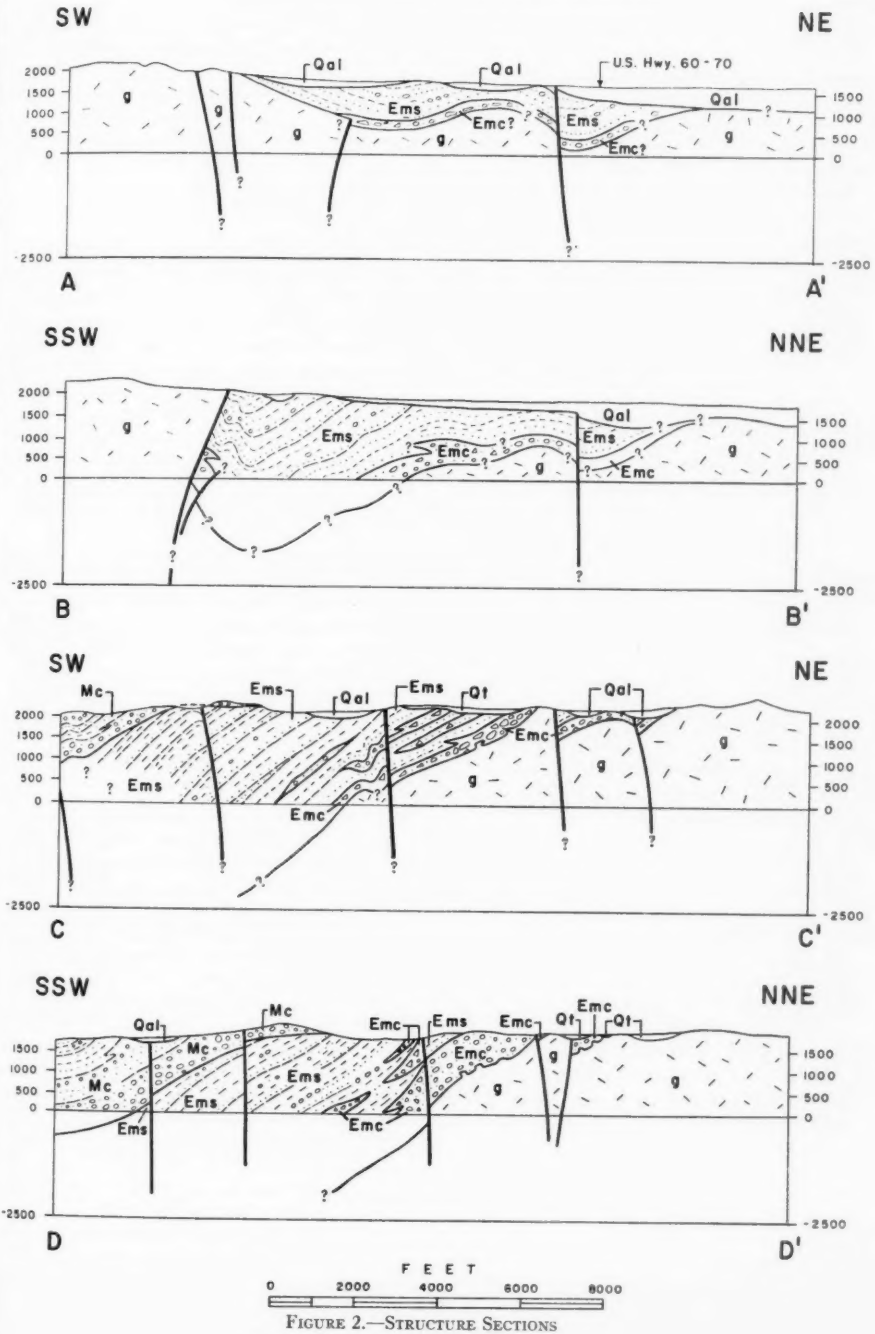

FIGURE 2.—STRUCTURE SECTIONS
See Plate 1 for location of sections.

reading of the manuscript and to Opal L. Kurtz and Betty Bruner Crowell for drafting. Crowell undertook the field work and stratigraphy, and Susuki the paleontology.

This paper is one of a series of proposed reports dealing with the distribution of rocks along the San Andreas fault zone in southern California. It is part of a project aimed at additional understanding of the tectonic significance of the San Andreas and associated faults. The work was supported in part by research grants from the Institute of Geophysics and the Committee on Research, University of California, Los Angeles.

Stratigraphy

General Features

The Maniobra formation, which is assigned to the Lower and Middle Eocene, consists of interbedded siltstone, sandstone, and breccia along with sandy limestone and conglomerate. These rocks total about 4800 feet in thickness; the thickest section is in the vicinity of structure sections C-C′ and D-D′ (Pl. 1). Here it is differentiated into two mappable units which intertongue. One unit, consisting of coarse sedimentary breccia and conglomerate (Pl. 1, Emc), in the main lies lower in the section. The other unit (Ems), composed of light-buff siltstone with conspicuous sandstone and grit layers, predominates high in the section but extends also as lenses and tongues to within a few feet of the base. With more detailed work on a larger scale the formation can be subdivided into additional members; this has been done in part by Williams (1956). Inasmuch as these units have not been traced throughout the area of Maniobra outcrop, and the map (Pl. 1) has a very small scale, only two units are differentiated here. Figure 3 is a diagrammatic and generalized columnar section.

The type section for the Maniobra formation is defined as comprising the strata exposed along the line of structure section C-C′ (Pl. 1). The type section lies between the granitic basement on the north and the basal conglomerate of the overlying nonmarine rocks on the south. In the absence of any suitable topographic name in the area after which to name the new formation, the valley just west of the type locality is here named Maniobra Valley. The valley was part of the maneuver area used during the early part of World War II by armored units from the Desert Training Center under the command of General George S. Patton, Jr. The region is scarred by tank tracks. Artillery shell casings and other remnants of training activities are scattered across the barren landscape. Since many of the topographic names in the region have come from Spanish, the writers have translated *maneuver* into the Spanish *maniobra*.

Conglomerate and Breccia

The Maniobra formation east of Maniobra Valley consists largely of beds of conglomerate and sedimentary breccia up to 100 feet thick. At places cliffs are composed of massive breccia containing blocks up to 20 feet in diameter set in very little matrix. Elsewhere the unit consists of subangular blocks, boulders, and cobbles in brown sandstone with thinner irregular lenses of conglomerate. At other places sandstone predominates, but breccia and conglomerate are conspicuous. All these intergrading rock types are grouped together as conglomerate and breccia (Pl. 1, Emc). Small lenses and tongues of the same lithology crop out throughout the Maniobra formation but have not been differentiated. Many sandstone layers contain streaks of angular fragments, and many include dispersed large blocks and boulders. Thick breccia beds cap some low hills and form steep cliffs. Interbedded conglomerate and sandstone, with minor siltstone, underlie swales and gentle slopes (Pl. 3).

At the base of the formation, near the north end of cross-section C-C′ (Fig. 2; Pl. 1), large granitic boulders lie along the contact. These immense clasts, which may reach 30 feet in diameter, are only slightly separated from the underlying basement. They are similar in size and shape to boulders lying on near-by granitic hills at present and probably also originated by differential weathering in place. These Eocene clasts can be distinguished from present-weathering boulders of granite in two ways: (1) cemented sandstone and siltstone of characteristic Maniobra lithology occur between Eocene blocks; (2) some adjacent Eocene boulders display slightly different textures, suggesting transportation of the giant clasts. Aplites and pegmatites cannot be followed from boulders to the underlying granite, as may generally be done on the granitic terrain of the Hayfield Mountains.

Above the base of the formation, thick units of sedimentary breccia lie on relatively undeformed siltstone and sandstone beds. At one place, 20 feet of massive breccia overlies 6 inches of laminated white siltstone, perhaps

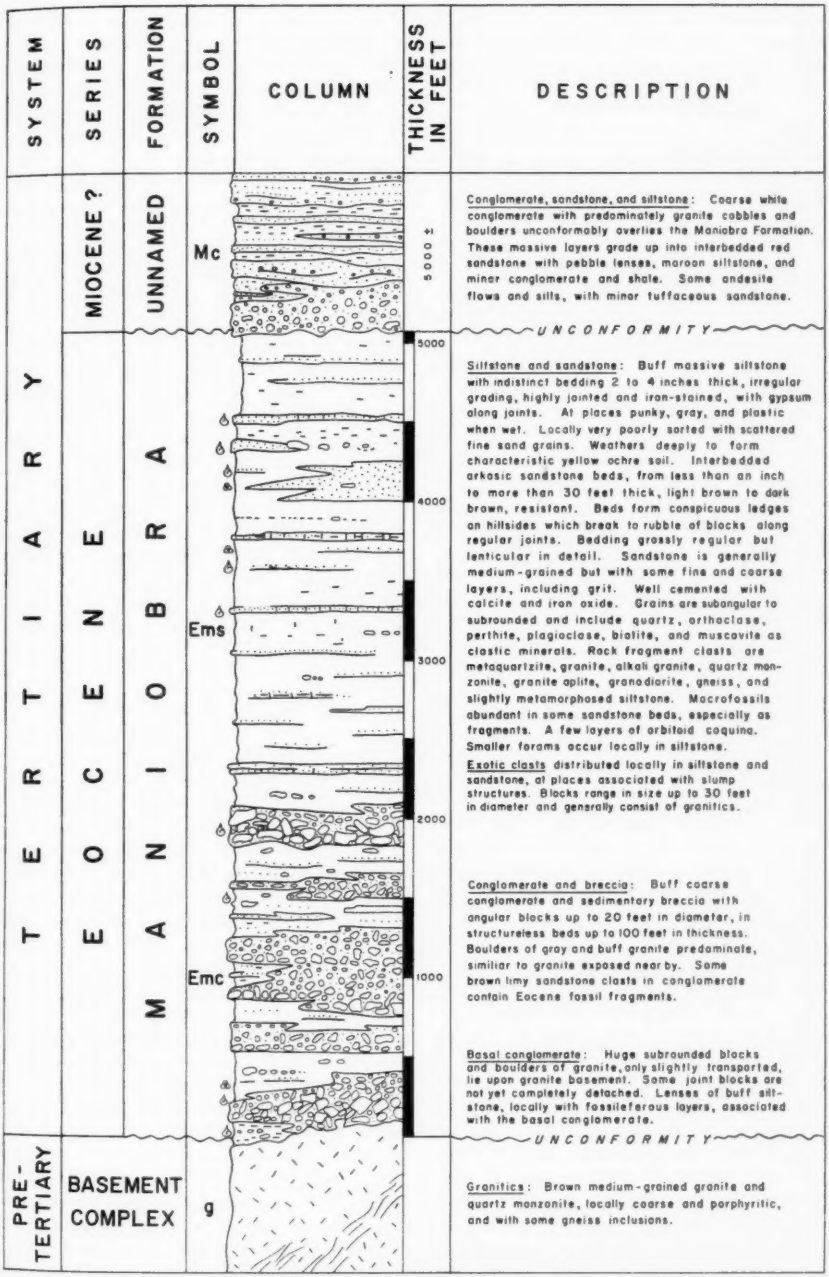
SYSTEM
SERIES
FORMATION
SYMBOL
COLUMN
THICKNESS IN FEET
DESCRIPTION
TERTIARY
MIOCENE?
UNNAMED
Mc
5000 ±
Conglomerate, sandstone, and siltstone: Coarse white conglomerate with predominately granite cobbles and boulders unconformably overlies the Maniobra Formation. These massive layers grade up into interbedded red sandstone with pebble lenses, maroon siltstone, and minor conglomerate and shale. Some andesite flows and sills, with minor tuffaceous sandstone.
UNCONFORMITY
EOCENE
MANIOBRA
Ems
Emc
5000
4000
3000
2000
1000
Siltstone and sandstone: Buff massive siltstone with indistinct bedding 2 to 4 inches thick, irregular grading, highly jointed and iron-stained, with gypsum along joints. At places punky, gray, and plastic when wet. Locally very poorly sorted with scattered fine sand grains. Weathers deeply to form characteristic yellow ochre soil. Interbedded arkosic sandstone beds, from less than an inch to more than 30 feet thick, light brown to dark brown, resistant. Beds form conspicuous ledges on hillsides which break to rubble of blocks along regular joints. Bedding grossly regular but lenticular in detail. Sandstone is generally medium-grained but with some fine and coarse layers, including grit. Well cemented with calcite and iron oxide. Grains are subangular to subrounded and include quartz, orthoclase, perthite, plagioclase, biotite, and muscovite as clastic minerals. Rock fragment clasts are metaquartzite, granite, alkali granite, quartz monzonite, granite aplite, granodiorite, gneiss, and slightly metamorphosed siltstone. Macrofossils abundant in some sandstone beds, especially as fragments. A few layers of orbitoid coquina. Smaller forams occur locally in siltstone.
Exotic clasts distributed locally in siltstone and sandstone, at places associated with slump structures. Blocks range in size up to 30 feet in diameter and gensrally consist of granitics.
Conglomerate and breccia: Buff coarse conglomerate and sedimentary breccia with angular blocks up to 20 feet in diameter, in structureless beds up to 100 feet in thickness. Boulders of gray and buff granite predominate, similiar to granite exposed near by. Some brown limy sandstone clasts in conglomerate contain Eocene fossil fragments.
Basal conglomerate: Huge subrounded blocks and boulders of granite, only slightly transported, lie upon granite basement. Some joint blocks are not yet completely detached. Lenses of buff siltstone, locally with fossiliferous layers, associated with the basal conglomerate.
UNCONFORMITY
PRE-TERTIARY
BASEMENT COMPLEX
g
Granitics: Brown medium-grained granite and quartz monzonite, locally coarse and porphyritic, and with some gneiss inclusions.

FIGURE 3.—COLUMNAR SECTION, EOCENE STRATA, OROCOPIA MOUNTAINS, SOUTHEASTERN CALIFORNIA

altered tuff, with almost no deformation of the lower beds. These relations seem to require that breccia was emplaced passively as a huge breccia flow which failed to plough into the

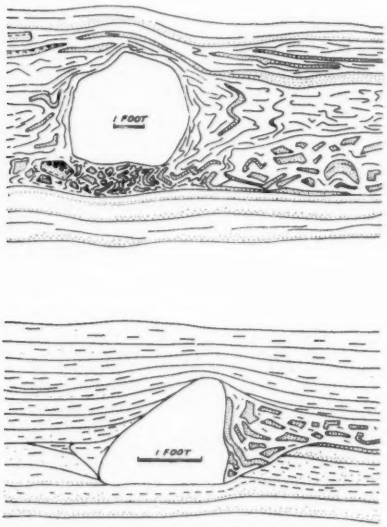

FIGURE 4.— FIELD SKETCH SHOWING EMPLACEMENT OF EXOTIC BLOCKS, MANIOBRA FORMATION

Sketch shows structural details and intraformational breccia in bedded siltstone resulting from the emplacement of larger granitic boulders, probably by slumping; exposed in cutbank of stream course 2800 feet west-southwest of fossil locality M.

underlying strata. Since marine fossils occur both above and below these lenses, emplacement took place in sea waters. A near-by rugged shore may have provided a source for the blocks, most of which consist of granite similar to that now exposed in the surrounding hills. This rock is mainly biotite granite with some quartz monzonite. It is generally gray and medium-grained with porphyritic masses characterized by conspicuous microcline phenocrysts. Locally perthite and mildly crushed but recrystallized textures are present.

Isolated boulders of granite occur in siltstone and sandstone beds throughout the Maniobra formation, but most exposures do not reveal much information on their manner of sedimentation. At one steep cliff, however, structural details in the soft rocks surrounding the boulders can be seen (Fig. 4). A 4-foot granite clast lies within a jumbled mixture of mudstone with twisted slabs and shreds of fine-grained sandstone. The boulder apparently arrived during slumping, which also churned and mixed newly deposited layers on the sea floor. An older slump breccia was partly consolidated and then ruptured again as a second slump arrived with the boulder. After slumping, sedimentation continued on an irregular surface, so that new units were patchy and lenticular. Some of these drape over the boulder, since it is less compactible than the slump mixture surrounding it.

Another boulder near by, about 2 feet across, lies isolated within a sequence of faintly bedded sandy siltstone and sandstone (Fig. 4). It appears to have skidded into place, accompanied by slumping, because some thin sandstone layers are tipped and broken in front of it. These relations, the direction of thinning of near-by breccia lenses, and the direction to exposures of similar granite all indicate that the clast came from the north.

These two large boulders lie in a zone with others that weather out conspicuously and mark the strike line across the hills. Where granite clasts are especially abundant and exposures poor, small hillocks seem to be made of basement. Here it is only after careful mapping that the boulders are recognizable as clasts.

Siltstone and Sandstone

Most of the Maniobra formation consists of interbedded siltstone and sandstone. The siltstone, which predominates, is generally light buff or ochre with very indistinct bedding. It is friable and poorly sorted and generally contains dispersed sand grains and vague clayey patches. At some exposures crude bedding is revealed in units 2–4 inches thick with irregular and incomplete grading, but at most places practically no internal structure is discernible. Jointing is more conspicuous than bedding and at places forms a boxwork outlined by iron staining, emphasized by gypsum plates. Blocks between joints are blue gray when freshly broken and turn white on drying. Many steep cut banks of Maniobra siltstone are covered with dried mud that flowed down in small rivulets during infrequent rains and congealed to form minute stalactites, droplets, and leveed lobes. Good exposures of the siltstone are rare, owing to its weak resistance, but its presence between sandstone ledges is revealed by gray and yellow chips in the soil and by flakes of gypsum. In proportion to the sandstone, the

siltstone is somewhat more abundant to the east.

Interbedded sandstone layers of the Maniobra formation stand out on hillsides as low ledges and form dry waterfalls in gullies. The beds range in thickness from less than an inch to as much as 30 feet, but most are 1–2 feet thick (Pl. 3, fig. 1). They are generally well jointed, so that ledges break easily into sandstone blocks, which mantle steep hills. Many joints are filled with white caliche that stands out in marked contrast to the buff weathered sandstone. The sandstone layers appear uniform in thickness, and some beds can be traced a quarter of a mile across the terrain. Most are lenticular, however, and pinch and swell along the line of strike. Many beds are streaked with iron oxide which commonly works its way into massive rock from joints, so that some blocks have relatively unstained kernels. Upper weathered surfaces of these sandstone blocks are generally coated with purplish dark-brown desert varnish, but undersurfaces are buff.

Most sandstone layers display little internal structure, but some are crudely graded so that uppermost parts show only a slight diminution of grain size. Coarse clasts up to pebble size may be clustered near the base. As a rule, however, such clasts are dispersed through the lower part of thick beds and may even be present near the top. Some 2-foot beds of intraformational conglomerate exhibit grading with angular clasts of light-buff iron-stained limestone and siltstone (Williams, 1956, M.A. thesis, Univ. of California, Los Angeles, fig. 6). A few thick, massive beds contain irregular flaggy lenses of hard limy sandstone that pinch out in only 10 feet. Such structures, which are accompanied by scours and channels along the base, suggest rapid and irregular deposition. Some orange-brown sandstone layers are filled with abundant fossil fragments, especially orbitoids, and at places are almost coquinas. Many thin layers are well graded, and a few display convolute bedding, worm borings, and, rarely, scour features.

Most of the sandstone layers are medium-grained and poorly sorted, but clast size in units of the Maniobra formation ranges from clay size to blocks up to 30 feet in diameter. The clast sizes along cross-section line B-B′ (Pl. 1) were studied in detail by Kirkpatrick (1958, M.A. thesis, Univ. of California, Los Angeles). The sandstone consists of angular and subangular grains, which range considerably in size, set in a matrix of finer sand and silt. The rock also contains much calcite, stained with iron oxide, which has permeated through the matrix so that the rock is well cemented. Some relatively well-sorted sandstone beds have pore spaces filled with calcite where two or three interlocking crystals fill the void. Thin sections show that some calcite has partially replaced iron oxide, since grains of iron oxide show embayments and corrosion. The oxide is also present both as fine grains disseminated through calcite and as large particles with fairly sharp boundaries. These relations suggest that calcite cementation to a large extent followed the introduction of iron oxide, but there may have been considerable overlap in the times of their emplacement. Kirkpatrick (1958, M.A. thesis, Univ. of California at Los Angeles) found that calcite constituted more than 35 per cent in several thin sections.

Thin sections show that the clastic minerals in greatest abundance in the Maniobra sandstone are quartz, orthoclase, perthite, plagioclase, biotite, and muscovite. Many quartz grains contain strings of bubbles, and some have minute inclusions of euhedral tourmaline and zircon. Much of the quartz still exhibits straining, as shown by undulatory extinction. Fractured grains are common, and many have been separated slightly along fractures now filled by calcite cement. A few clusters of quartz grains with sutured contacts were recognized as clasts of quartzite (Kirkpatrick, 1958, M.A. thesis, Univ. of California at Los Angeles).

The feldspar minerals are relatively fresh. Although grains of plagioclase and orthoclase are to some extent sericitized and kaolinized, the perthite is generally fresh.

Flakes of biotite and muscovite are present in small amounts and are usually bent, pinched, and torn, perhaps as a result of compaction. Undistorted mica flakes are abundant in other layers, even though wedged between other grains, and may have been protected by cementation before much compaction.

Many rock types are represented as clasts in the sandstone beds. Some recognized by Kirkpatrick (1958, M.A. thesis, Univ. of California at Los Angeles), listed in the order of decreasing abundance, are metaquartzite, granite, alkali granite, quartz monzonite, granite aplite, granodiorite, gneiss, and slightly metamorphosed siltstone.

For his detailed study of rocks exposed along structure-section line B-B′ (Pl. 1). Kirkpatrick measured the percentage frequency of mineral grains. Quartz constitutes 43–80 per cent of the samples measured and averages about 68 per cent, with greater abundance in the lower

part of the section and more variability in the upper. Orthoclase increases upward from between 15 and 28 per cent to between 18 and 48 with greater variability from bed to bed. Perthite and plagioclase vary in percentage abundance; the former ranges from 1 to 14 per cent, and the latter from less than 1 per cent to about 5. Biotite and muscovite are scattered throughout the stratigraphic section but are perhaps more abundant in the upper part, where together they constitute up to 3 or 4 per cent. The sandstones may therefore be classified as arkosic with arkoses predominating over subarkoses (Pettijohn, 1957, p. 290). According to Gilbert, they are largely arkosic arenites with some arkosic wackes (Williams, Turner, and Gilbert, 1954, p. 295).

Paleontology

Introduction

The molluscan fauna of the Maniobra formation includes 30 species, subspecies, and varieties. This number is small compared to some other Eocene assemblages from Pacific Coast localities, but within the fauna are several forms diagnostic of age. Mollusks are found throughout the section in varied types of lithology (fig. 3). Although fossils are abundant, the number of identifiable species has been reduced by deep desert weathering, rock induration, and structural deformation. Fossils are found throughout the section, but most of the better preserved and identifiable mollusks are confined to two zones, one near the base of the formation, the other near the top. Foraminifera, including orbitoids as well as small calcareous forms, occur at several horizons, but the most useful fauna was collected several hundred feet stratigraphically above strata containing Lower Eocene molluscan fossils. No significant stratigraphic break was noticed within the section, and therefore deposition is assumed to be continuous.

Mollusks

The molluscan fauna from lower beds of the Maniobra formation contains several forms that are closely related to those found elsewhere in the Eocene of the Pacific Coast of North America. The beds yielding the fossils are mainly sandstone lenses within thick siltstone strata. The species regarded as particularly helpful in correlation are:

Gastropods

Chedevillia sp. *cf. C. stewarti* Clark
Clavilithes sp. *cf. C. tabulatus* (Dickerson)
Ectinochilus n. sp.
Galeodea sp. *cf. G. sutterensis* Dickerson

Two pelecypod genera, found in this assemblage, are reported for the first time in the Eocene of the Pacific Coast of North America, *Miocardia* and *Gryphaea*. These two genera are recorded from the Eocene of the Paris Basin (Cossmann and Pissarro, 1904, Pl. 16) and from the northwest coast of South America (Clark and Durham, 1946, p. 55).

The molluscan fossils from the upper beds are preserved in coarse, massive, pebbly sand-

---

PLATE 2.—CHARACTERISTIC SPECIES FROM THE EOCENE MANIOBRA FORMATION OROCOPIA MOUNTAINS, RIVERSIDE COUNTY, CALIFORNIA

Catalogue numbers are those of the Invertebrate Paleontology Collections, University of California, Los Angeles. Figures are at approximately natural size, except as otherwise stated.

FIGURES 1, 4.—*Galeodea* sp. *cf. G. sutterensis* Dickerson; lower beds, cat. no. 28988, U.C.L.A. loc. no. 3779.

FIGURES 2, 3.—*Chedevillia* sp. *cf. C. stewarti* Clark; lower beds, cat. no. 28987, U.C.L.A. loc. no. 3779.

FIGURE 5.—*Turritella andersoni* Dickerson n. var.; upper beds, cat. no. 28983, U.C.L.A. loc. no. 3780. (× 2)

FIGURES 6, 7.—*Clavilithes* sp. *cf. C. tabulatus* (Dickerson); lower beds, cat. no. 28989, U.C.L.A. loc. no. 3779.

FIGURE 8.—*Turritella buwaldana* Dickerson n. var.; lower beds, cat. no. 28985, U.C.L.A. loc. no. 3779. (× 2)

FIGURE 9.—*Turritella andersoni lawsoni* var. *secondaria* Merriam; upper beds, cat. no. 28981, U.C.L.A. loc. no. 3780. (× 2)

FIGURE 10.—*Turritella uvasana* Conrad n. var.; lower beds, cat. no. 28986, U.C.L.A. loc. no. 2779. (× 3)

FIGURE 11.—*Turritella andersoni lawsoni* var. *secondaria* Merriam; upper beds, cat. no. 28982, U.C.L.A. loc. no. 3780. (× 2)

FIGURE 12.—*Turritella andersoni lawsoni* Dickerson; upper beds, cat. no. 28984, U.C.L.A. loc. no. 3780. (× 2)

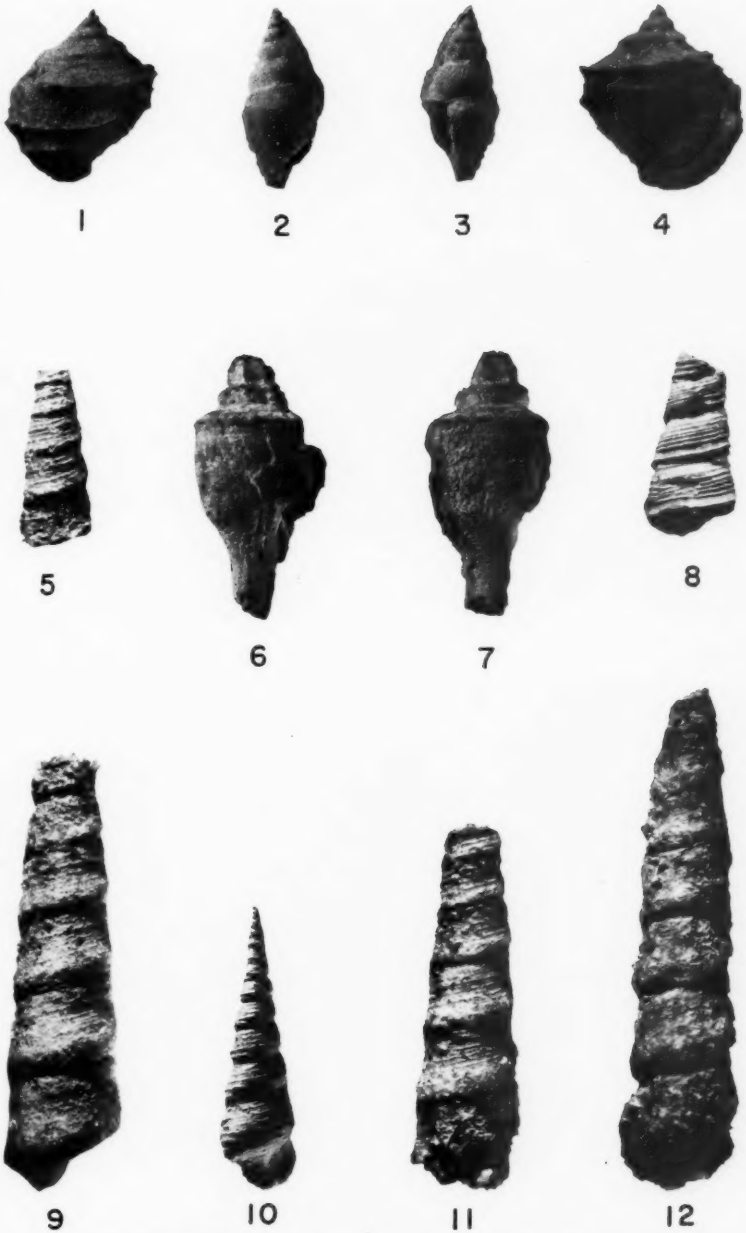

CHARACTERISTIC SPECIES FROM THE EOCENE MANIOBRA FORMATION, OROCOPIA MOUNTAINS, RIVERSIDE COUNTY, CALIFORNIA

FIGURE 1

FIGURE 2
MANIOBRA FORMATION

stone and in hard orange-brown, limy sandstone strata. This fauna differs from that in the lower beds considerably in composition. The most distinctive forms are a subspecies and a variety: *Turritella andersoni lawsoni* Dickerson and *Turritella andersoni lawsoni* var. *secondaria* Merriam. The other species determined are not so restricted in range as the *Turritella*, but they aid greatly in age determination. From the upper beds the following species have been tentatively identified:

Pelecypods

Glycymeris sp.
Barbatia sp.
Schedocardia cf. S. brewerii (Gabb)
Macrocallista sp.

Gastropods

Homalopoma sp. *cf. H. wattsi* (Dickerson)
Calyptraea sp.
Turritella andersoni lawsoni Dickerson
Turritella andersoni lawsoni var. *secondaria* Merriam
Turritella sp. *cf. T. buwaldana* Dickerson
Turritella sp. *cf. T. uvasana* Conrad
Amaurellina sp.
Ectinochilus sp. *cf. E. macilentus* (White)
Lyria sp.
Bittium sp. *cf. B. longissimum* Cooper
Keilostoma sp. *cf. K. californicum* Vokes
Cylichnina ? sp.

Foraminifera

Small Foraminifera from lower beds which occur stratigraphically above the lower molluscan horizon were collected and studied by Mr. Edwin C. Allison and examined by Profs. Robert M. Kleinpell and V. Standish Mallory. Species tentatively identified by Professor Mallory are:

Gaudryina jacksonensis coalingensis Cushman and Hanna
Clavulinoides n. sp. *Mallory*, MS.
Anomalina garzaensis Cushman and Hanna
Trifarina advena n. subsp. Mallory, MS.
Globigerina coalingensis Cushman and Hanna
Vaginulinopsis mexicanus nudicostatus Cushman and Hanna

Prof. W. Storrs Cole studied the larger Foraminifera (orbitoids) from upper beds. He reported an abundance of *Pseudophragmina* (*Proporocyclina*) *psila* (Woodring) with a few typical *Asterocyclina aster* (Woodring) and in addition a specimen belonging to the genus *Fabiana*. According to Cole certain specimens from the Maniobra formation compare favorably with *Pseudophragmina* (*Proporocyclina*) *clarki* (Cushman) from the Simi Valley, and a few have characteristics of *Pseudophragmina* (*Proporocyclina*) *perpusilla* (Vaughan) of the Tampico embayment, Mexico. These three species of *Pseudophragmina* are similar and indicate a Middle Eocene age.

Age and Correlation

The fauna from the lower beds of the Maniobra formation is more closely related to the fauna of the Capay stage than to that of the Domengine stage. This tentative conclusion is based upon closely related subspecies and varieties which have a restricted stratigraphic range within the Eocene series. Among them is *Galeodea* sp. *cf. G. sutterensis* Dickerson, which is a close relative of *Galeodea sutterensis* Dickerson, described from Capay beds at Marysville Buttes (Dickerson, 1916, p. 492). Other known occurrences of the species, all of Capay age, are from: (1) the type Capay formation in Capay Valley (Merriam and Turner, 1937, p. 94); (2) Lower zone, Arroyo Hondo formation north of Coalinga (Vokes, 1939, p. 27–29, 35); (3) Lower Llajas formation near Simi Valley (Stipp, 1943, p. 418–422); (4) the lower Umpqua formation, Oregon (Turner, 1938, p. 6–9). *Galeodea sutterensis* and its subspecies are known only from strata of early Eocene age.

The presence of *Clavilithes* sp. *cf. C. tabulatus* (Dickerson) is further evidence of Capay age. The type of *Clavilithes tabulatus* (Dickerson) was also described from Capay beds at Marysville Buttes (Dickerson, 1913, p. 283–284). The Orocopia species shows closer affinities to the type of *Clavilithes tabulatus* than to an undescribed *Clavilithes* from the upper Llajas formation, Domengine stage, of the Simi Valley.

Plate 3.—Maniobra formation

Figure 1.—Boulder bed, Maniobra formation. Granitic boulders and blocks, some larger than the jeep, lie depositionally on sandstone beds in foreground. 1300 feet west of fossil locality "F".

Figure 2.—Interbedded sandstone, grit, pebbly sandstone, and siltstone layers of the Maniobra formation; 700 feet south-southwest of fossil locality "C".

Chedevillia sp. *cf. C. stewarti* Clark from the Maniobra formation is closely related to another restricted Capay species, *Chedevillia stewarti* Clark, which occurs in the Lower Llajas formation, Simi Valley (Clark, 1942, p. 117). This gastropod is considered to be of Capay age and is as yet unknown from other localities.

This correlation of the lower beds is corroborated in part by the small Foraminifera, which indicates assignment near the Capay-Domengine boundary, Lower and Middle Eocene. This is in accord with their stratigraphic position several hundred feet above the molluscan locality placed in the Capay stage. The Foraminiferal fauna is tentatively placed within zones B-1A through B-3 (Laiming, 1943, p. 193–198) or within the Ulatisian stage (Mallory, 1953, p. 2781).

The characteristic molluscan forms from the upper beds of the Maniobra formation are *Turritella andersoni lawsoni* Dickerson and *Turritella andersoni lawsoni* var. *secondaria* Merriam. The occurrence together of these two forms suggests that the upper beds correlate with the upper Llajas formation, Domengine stage, from the Simi Valley, where they also are found together. At all other known localities, the association of subspecies *lawsoni* and variety *secondaria* has been recorded only in Domengine strata. Assignment of the upper beds to the middle Eocene is confirmed by the orbitoids.

Studies are under way to compare the stratigraphy of the Maniobra formation with other middle Eocene sections in southern California. On the basis of lithology, work done so far suggests that Eocene strata near Mt. Pinos, Transverse Ranges, show many remarkable similarities (Kirkpatrick, 1958, M.S. thesis, Univ. of California, Los Angeles). It will be some time, however, before the paleogeography of the Eocene is worked out, in view of tectonic complications involving the San Andreas, San Gabriel, and other faults of suspected large strike-slip displacement.

Origin

Rock types and fossils in the Maniobra formation indicate that the formation was deposited in a marine embayment surrounded by rugged terrain. As marine fossils are found throughout the section, these Eocene strata are probably entirely marine, with the possible exception of the lowermost few feet. At the base, weathered granite gives way upward to boulder beds with arkose and siltstone between clasts and with little if any reworking. This basal conglomerate may have been formed subaerially and then inundated as the Eocene sea advanced.

As the floor of the embayment subsided, siltstone and sandstone layers were deposited. At places thin bedding and lamination and the preservation of minor textural and structural features suggest that the region was protected from heavy wave action, because it is unlikely that the water was deep enough for the embayment floor to lie below "wave base." Siltstone and sandstone were laid down, both some distance from shore and near shore at places protected from coarse sedimentation. From time to time, masses of rubble were swept into the embayment and are now preserved as breccia lenses lying on nearly undisturbed siltstone. Much of this material slumped downslope, but some may have mixed and churned, developing incipient turbidity. Probably the coast was steep, and granitic rubble accumulated in patches along the shore after being brought down to the sea by downslope movement and minor streams. When such masses became unstable, they moved seaward by slumping and sliding.

Dispersed boulders (fig. 4) may have fallen into the Eocene sea from cliffs and stacks and into protected coves floored by silt and sand. Some rolled or slid into deeper water and caused slumps that gathered momentum and moved into water still farther from shore.

Well-bedded sandstone layers, which display graded bedding and some convolute bedding, were probably emplaced by turbidity currents. Many of these layers contain fossil fragments, including Orbitoids, which perhaps were broken up during turbulent transportation. Directional structures in the sandstone beds are rare, so that determination of the transportation direction is impossible. Many of the thick and massive sandstone beds may have been emplaced in other ways, and some were probably laid down in water so shallow that wave agitation and tidal currents could rework them.

Although the thickest and coarsest breccia units lie on the east near the base of the formation, the principal source did not necessarily lie in that direction. Breccias are also found on the southwest, to the west of cross-section line B-B′ (Pl. 1), where they also lie at and near the base of the formation. These relations suggest an east-west trough, but rugged granitic islands standing offshore might have caused the same effect.

Some of the east-west trending faults may have been active during the Eocene, for they mark boundaries between granitic basement and Eocene strata containing granitic blocks of

similar composition. As the faults moved in post-Eocene time, however, these relations can perhaps be explained as well by this later movement. Until detailed mapping combined with careful stratigraphic work reveals the displacement of these faults, it will not be possible to ascertain whether they were active during the middle Eocene or even to work out the trend of Eocene structures and of such topographic features as the coast line.

Toward the southeast, thick siltstone units of the Maniobra formation are overlapped by the basal conglomerate of younger nonmarine beds (Pl. 1). They no doubt extended farther east-southeastward before leveling by post-Eocene erosion and probably extend some distance southeastward at depth beneath the nonmarine strata. Near the eastern edge of the map area, a thin wedge of Maniobra siltstone with minor sandstone is caught in a fault zone crossing a granite hill. The facies and relations of this easternmost outcrop suggest that Eocene strata continue eastward, but reconnaissance failed to reveal other exposures.

The extent of the Maniobra beds toward the south and beneath the nonmarine strata cannot be determined from the surface geology. None of the distinctive basement rock types now exposed in the Orocopia Mountains south of the nonmarine beds and granite exposures has been recognized as a clast within the Eocene. This region was therefore not exposed to erosion during the Eocene in the same relative position to the outcrop area of the Maniobra formation. Several great faults separate the basement terrain of the high Orocopia Mountains on the south from the nonmarine beds, Eocene strata, and granitic rocks on the north. Movement on these faults, which are parts of the San Andreas system, took place during the middle and late Cenozoic and may have placed the terrain in its present position by large strike-slip displacement. Until the role of these faults, now under study, is worked out, it is not profitable to speculate further on the southward extent of the Eocene beds.

Summary

The Maniobra formation, discovered recently in the Orocopia Mountains north of the Salton Sea, contains a fauna of mollusks, orbitoids, and small Foraminifera. These marine rocks constitute about 4800 feet of interbedded sandstone, siltstone, conglomerate, and breccia, which were laid down near a rugged shore line. The fauna belong to the Capay and Domengine stages, but it is still uncertain which Eocene section elsewhere in the region is most closely related.

References Cited

Brown, J. S., 1923, The Salton Sea region, California: U. S. Geol. Survey Water-Supply Paper 497, 292 p.

Clark, Bruce L., 1942, New middle Eocene gastropods from California: Jour. Paleontology, v. 16, p. 116–119

Clark, Bruce L., and Durham, J. Wyatt, 1946, Eocene faunas from the Department of Bolivar, Columbia: Geol. Soc. America Mem. 16, 126 p.

Cossman, Maurice, and Pissaro, G., 1904–1906, Iconographic complete des coquilles fossils de L'Eocene des environs de Paris: Pelecypodes, v. 1, 45 pls., privately published

Darton, N. H., 1933, Guidebook of the Western United States: Part F. The Southern Pacific Lines, New Orleans to Los Angeles: U. S. Geol. Survey Bull. 845, 304 p.

Dibblee, T. W., Jr., 1954. Geology of the Imperial Valley region, California: Calif. Div. Mines Bull. 170, chap. 2, p. 21–28

Dickerson, Roy E., 1913, Fauna of the Eocene at Marysville Buttes, California: Univ. Calif. Dept. Geol. Sci. Bull., v. 7, p. 257–298

—— 1916, Stratigraphy and faunas of the Tejon Eocene of California: Univ. Calif. Dept. Geol. Sci. Bull., v. 9, p. 363–524

Jenkins, Olaf P., 1938, Geologic map of California: Calif. Div. Mines

Laiming, Boris, 1943, Eocene Foraminiferal correlations in California: Calif. Div. Mines Bull. 118, p. 191–198

Mallory, V. Standish, 1953, California lower Tertiary Foraminiferal sequence (Abstract): Am. Assoc. Petroleum Geologists Bull., v. 37, p. 2781

Merriam, Charles W., and Turner, F. E., 1937, The Capay middle Eocene of northern California: Univ. Calif. Dept. Geol. Sci. Bull., v. 24, p. 91–114

Miller, W. J., 1944, Geology of Palm Springs-Blythe strip, Riverside County, California: Calif. Jour. Mines and Geology, v. 40, p. 11–72

Pettijohn, F. J., 1957, Sedimentary rocks: 2d Ed., N. Y., Harper & Bros., 718 p.

Stipp, T. F., 1943, Simi oil field: Calif. Div. Mines Bull. 118, p. 417–423

Turner, F. E., 1938, Stratigraphy and Mollusca of the Eocene of western Oregon: Geol. Soc. America Special Paper 10, 130 p.

Vokes, Harold E., 1939, Molluscan faunas of the Domengine and Arroyo Hondo formation of the California Eocene: N. Y. Acad. Sci. Annals, v. 38, p. 1–246

Williams, Howel, Turner, F. J., and Gilbert, C. M., 1954, Petrography: an introduction to the study of rocks in thin section: San Francisco, W. H. Freeman & Co., 406 p.

Department of Geology, University of California, Los Angeles 24, Calif.

Manuscript Received by the Secretary of the Society, August 8, 1958

Institute of Geophysics Contribution No. 117

Appendix

Descriptions of Eocene Fossil Localities, Orocopia Mountains

(All localities shown in Plate 1)

Loc. A. Fossils occur in brown limy sandstone layers, 2–18 inches thick, interbedded in sandstone and siltstone sequence. Orange-brown hard sandstone layers are most fossiliferous. Locality is 2.87 miles S. 34° W. of Shaver Summit and 1.45 miles N. 27° W. of Hill 2650, Canyon Spring quadrangle (Corps of Eng., U.S. Army, 1944), Riverside County, California. UCLA loc. no. 3797.

Loc. B. Fossils occur in lithology similar to locality A, 2.75 miles S. 35° W. of Shaver Summit and 1.52 miles N. 23° W. of Hill 2650, Canyon Spring quadrangle (Corps of Eng., U.S. Army, 1944), Riverside County, California. UCLA loc. no. 3798.

Loc. C. Orange-brown hard limy sandstone layers, 2–18 inches thick, containing fossils, about 2.57 miles S. 32° W. of Shaver Summit and 1.52 miles N. 14° W. of Hill 2650, Canyon Spring quadrangle (Corps of Eng., U.S. Army, 1944), Riverside County, California. UCLA loc. no. 3799.

Loc. D. Massive brown conglomerate with irregular lenses of buff sandstone and minor siltstone. Fossils occur in hard brown limy sandstone clasts. Most are difficult to identify. About 3.2 miles S. 28° E. of Shaver Summit and 2.6 miles N. 72° E. of Hill 2650, Canyon Spring quadrangle Corps of Eng., U.S. Army, 1944), Riverside County, California. UCLA loc. no. 3800.

Loc. E. Fossils occur in a massive, well-indurated, coarse to pebbly, gray-brown sandstone, on the west face of a north-south trending ridge. About 4 miles S. 20° E. of Shaver Summit and about 2 miles S. 30° W. of Summit 2760, Canyon Spring quadrangle (Corps of Eng., U.S. Army, 1944), Riverside County, California. UCLA loc. no. 3780.

Loc. F. Fossiliferous grayish sandstone lenses occur within a thick siltstone unit, exposed in a small valley flanked on the northeast and southwest by granitic rocks. The fossiliferous lenses are exposed approximately 3½ miles S. 49° E. of Shaver Summit and 1 mile S. 18° W. of Summit 2760, Canyon Spring quadrangle (Corps of Eng., U.S. Army, 1944), Riverside County, California. UCLA loc. no. 3779.

Loc. G. Interbedded coarse brown sandstone, siltstone, and coarse breccia beds with giant granitic clasts up to 30 feet in diameter to east. Fossils from siltstone, 3.8 miles S. 43° E. of Shaver Summit and 3.7 miles N. 78° E. of Hill 2650, Canyon Spring quadrangle (Corps of Eng., U.S. Army, 1944), Riverside County, California. UCLA loc. no. 3801.

Loc. H. Thin brown, yellow, and white sandstone layers in buff siltstone. Fossils occur as fragments in sandstone layers, 4.92 miles S. 30° of Shaver Summit and 3.52 miles S. 80° E. of Hill 2650, Canyon Spring quadrangle (Corps of Eng., U.S. Army, 1944), Riverside County, California. UCLA loc. no. 3802.

Loc. I. Brown limy sandstone layers in yellow gypsiferous silty sandstone and siltstone. Shell debris in medium-coarse sandstone with some 2-inch clasts of granite, 4.75 miles S. 33° E. of Shaver Summit and 3.85 miles S. 81° E. of Hill 2650, Canyon Spring quadrangle (Corps of Eng., U.S. Army, 1944), Riverside County, California. UCLA loc. no. 3803.

Loc. J. Brown massive conglomerate and sedimentary breccia with clasts up to 8 feet in diameter and containing 1 per cent of brown limy sandstone cobbles with fossils. These clasts look like eroded and transported concretions. About 4.8 miles S. 38° E. of Shaver Summit and 3.95 miles S. 89° E. of Hill 2650, Canyon Spring quadrangle (Corps of Eng., U.S. Army, 1944), Riverside County, California. UCLA loc. no. 3804.

Loc. K. Brown cemented sandstone layers in buff siltstone contain fossils, associated with 6-foot gray granite exotic clast, 5.25 miles S. 37° E. of Shaver Summit and 4.18 miles S. 83° E. of Hill 2650, Canyon Spring quadrangle (Corps of Eng., U.S. Army, 1944), Riverside County, California. UCLA loc. no. 3805.

Loc. L. Fossils occur in brown sandstone layers, 5.35 miles S. 37° E. of Shaver Summit and 4.3 miles S. 82° E. of Hill 2650, Canyon Spring quadrangle (Corps of Eng., U.S. Army, 1944), Riverside County, California. UCLA loc. no. 3806.

Loc. M. Brown cemented sandstone layers in buff siltstone contain fossils, near a 6-foot gray granite exotic clast, 5.4 miles S. 39° E. of Shaver Summit and 4.4 miles S. 83° E. of Hill 2650, Canyon Spring quadrangle (Corps of Eng., U.S. Army, 1944), Riverside County, California. UCLA loc. no. 3807.

BULLETIN OF THE GEOLOGICAL SOCIETY OF AMERICA
VOL. 70, PP. 593-600, 3 FIGS. MAY 1959

CHEMICAL COMPOSITION OF ARGILLITES OF THE COBALT SERIES (PRECAMBRIAN) AND THE PROBLEM OF SODA-RICH SEDIMENTS

By F. J. Pettijohn and Harry Bastron

Abstract

Two new chemical analyses show that the varved argillites of the Precambrian Cobalt series of Ontario, Canada, contain more Na_2O than K_2O and have a Na_2O/K_2O ratio higher than most pelitic rocks but similar to that found in many graywackes. Published chemical data substantiate these observations. The Cobalt materials are also low in CaO but otherwise have a composition compatible with their presumed glacial origin.

Albitization of the detrital plagioclase feldspar seems to best account for the low lime and high soda content of these rocks. X-ray data confirm the presence of albite.

Spectrographic analyses of the argillites are also given.

CONTENTS

	Page
Introduction	593
Acknowledgment	594
The analyses	594
Discussion	596
Conclusions	598
References cited	598

ILLUSTRATIONS

Figure	Page
1. Map showing distribution of Huronian sediments and location of analyzed samples	594
2. Na_2O/K_2O content of argillites and slates	597
3. Na_2O/K_2O content of graywackes	597

TABLES

Table	Page
1. Chemical composition of Gowganda argillites	595
2. Spectrographic analyses of Gowganda argillites	595

Introduction

The average composition of the earth's crust is a subject of great importance in geology, and much effort has been expended to determine this average. Rubey (1951, p. 1115) has questioned whether the earth's crust in Precambrian time was essentially as it now is or whether the evolution of the crust was then less advanced and perhaps the average composition was more largely basaltic and hence more basic.

The problem of determining the mean chemical composition of the crust in Precambrian time is fraught with many difficulties. It occurred to us that perhaps the Precambrian glacial deposits would constitute a composite sample of the unweathered crust from a very large region and perhaps would be representative of at least the continental crust. This solution to the problem was suggested, of course, by Goldschmidt's (1954, p. 53) utilization of the glacial clays of Fennoscandia as a mean sample of continental rocks. As Goldschmidt's average closely approached the means computed by Washington and others, this method seemed adequately validated, and, therefore, it seemed reasonable to apply this method to Precambrian glacial sediments.

Accordingly, samples of the varved argillites of the Huronian Cobalt series in Ontario, Canada, were collected for chemical analyses (Fig. 1). The Gowganda formation, the glacial member of the Cobalt series, is widespread; its present areal extent is in excess of 8500 square miles. The glacial origin of these beds seems well established (Wilson, 1913, p. 140), and it is reasonable to suppose that they constitute a composite sample of a large part of the Canadian Shield as it was in Huronian times.

The results were somewhat anomalous in that these deposits proved to be unusually sodic and low in CaO. K_2O normally greatly exceeds Na_2O in argillaceous sediments; the high Na_2O content of the Cobalt beds, there-

fore, requires an explanation. The authors are uncertain of the reason for the sodic character of these deposits, but it seems desirable to publish these analyses, to comment on them, and to contribute in a small way to the discussion of the soda problem.

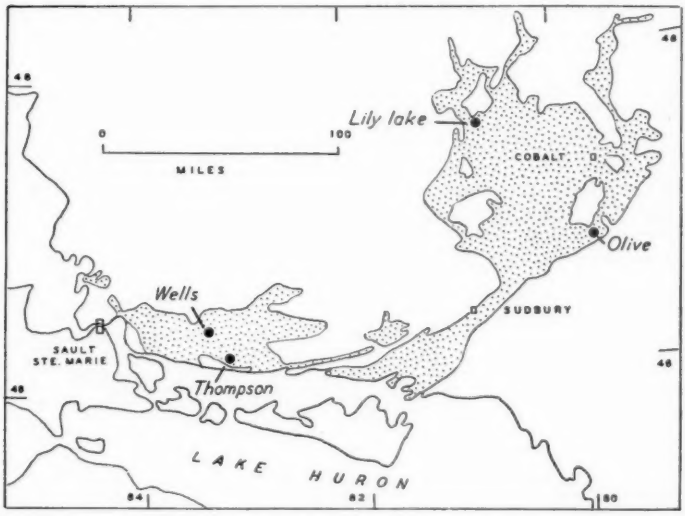

FIGURE 1.—MAP SHOWING DISTRIBUTION OF HURONIAN SEDIMENTS AND LOCATION OF ANALYZED SAMPLES (See Table 1)

ACKNOWLEDGMENT

We wish to acknowledge the interest and advice in this work by Mr. K. J. Murata of the U. S. Geological Survey.

THE ANALYSES

Two samples of the varved argillite were analyzed. One sample came from a prominent cliff on the Thessalon-Chapleau road in Wells Township, District of Algoma, Ontario. The argillite is flat lying; it is well bedded, and the laminations are rhythmic after the fashion of the varves commonly seen in the Pleistocene clays of this region. The Cobalt varves average 3–4 mm in thickness, are very regular, and are commonly marked by large ice-rafted pebbles or even cobbles sporadically scattered in the laminated argillite (Pettijohn, 1957, Pl. 23, bottom). About 20–30 annual layers were included in the analyzed sample.

A second specimen was collected some years ago on Highway No. 11 in Olive Township in the District of Nipissing in eastern Ontario. Here the argillite is also flat lying. It likewise is clearly varved and, although large rafted cobbles were not observed, it contains some larger and probably ice-rafted detrital quartz grains (Pettijohn, 1957, Pl. 24 B). The varves show micrograding and average about 1 mm in thickness. Consequently about 30–50 annual layers were included in the sample analyzed.

Search of the literature disclosed one reasonably good analysis of the matrix of the tillite phase of the Gowganda formation (Collins, 1925, p. 66).[1] The analyzed material came from Thompson Township, District of Algoma, Ontario. The tillites are massive, nonbedded rocks, with sparse cobbles and boulders, set in a fine-grained, black argillitic matrix. (*See* Pettijohn, 1957, Pl. 14, bottom, and Pl. 15 B.)

[1] One other analysis of Cobalt sediments was found. This analysis, of the argillite, does not include separate determinations of Na_2O and K_2O, and as it is rather old it is not given here. (*See* Miller, 1905, p. 42). Wilson (1913, p. 139) quotes a partial analysis of Cobalt argillite from Lily Lake in the Gowganda district. As this sample comes from a locality quite remote from those sampled by us, it constitutes a remarkable confirmation of the homogeneous nature of the Cobalt argillites and their sodic nature. It is, therefore, included in Table 1.

This material, unlike the laminated argillites, is presumably ice-deposited rather than deposited from the meltwaters in a glacial lake.

TABLE 1.—CHEMICAL COMPOSITION OF GOWGANDA ARGILLITES

Weight per cent

	A Matrix of tillite (Thompson)	B Varved argillite (Wells)	C Varved argillite (Olive)	D Argillite (Lily Lake)
SiO_2	61.98	61.68	58.82	61.54
TiO_2	0.60	0.49	0.73	....
Al_2O_3	17.20	16.48	16.46	....
Fe_2O_3	1.42	1.73	1.10	....
FeO	4.49	5.61	7.20	....
MnO	0.10	0.09	0.09	....
MgO	3.27	3.18	4.92	....
CaO	1.00	0.53	0.76	0.84
Na_2O	5.27	3.99	4.03	4.73
K_2O	2.04	2.62	1.60	2.84
H_2O+	2.70	2.95	3.73	....
H_2O-	0.10	0.08	0.11	....
CO_2	....	0.12	0.01	....
P_2O_5	....	0.20	0.17	....
SO_3	....	0.01	0.02	....
Cl	....	0.01	0.03	....
F	....	0.05	0.04	....
S	....	0.11	0.05	....
BaO	....	0.04	0.00	....
C	....	0.00	....	....
	....	99.97	99.87	....
Less O	....	.08	.06	....
Total	100.17	99.89	99.81	....

A. Matrix of boulder conglomerate, Cobalt series, section 4, Thompson Township. M. F. Conner, analyst (Collins, 1925, p. 66)

B. Varved argillite, Cobalt series, Wells Township, Lucille N. Tarrant, analyst

C. Varved argillite, Cobalt series, Olive Township, M. Balazs, analyst

D. Partial analysis of Cobalt argillite, Lily Lake (Gowganda area), District of Timiskaming, Ontario (Wilson, 1913, p. 139)

The chemical analyses of these Gowganda rocks are given in Table 1, and the spectrographic analyses of these two laminated argillites are given in Table 2. The concentrations of the minor elements, in general, conform to the abundance of the elements in the lithosphere as given by Goldschmidt (1954, p. 74).

The Cobalt materials have been averaged (Table 3, Col. A), and this average may be compared with Clarke's average shale (Col. B), Eckel's average slate (Col. C), Nanz'

TABLE 2.—SPECTROGRAPHIC ANALYSES OF GOWGANDA ARGILLITES

Weight per cent

	A (Wells)	B (Olive)
Cu	.006	.0006
Pb	.0005	.0006
Zn	.02	.01
Co	.002	.002
Ni	.004	.006
Ga	.001	.001
Cr	.02	.02
V	.009	.02
Sc	.002	.002
Y	.003	.003
Yb	.0001	.0002
La	.005	.007
Zr	.009	.01
Be	.0002	.0002
Sr	.005	.01
Ba	.03	.02
B	.002	.002

Elements looked for but not found: Ag, Au, Hg, Ru, Rh, Pd, Ce, Ir, Pt, Mo, W, Re, Ge, Sn, As, Sb, Bi, Te, Cd, Tl, In, Th, Nb, Ta, U

A. Varved argillite, Cobalt series, Wells Township, Harry Bastron, analyst

B. Varved argillite, Cobalt series, Olive Township, Harry Bastron, analyst

average Precambrian slate (Col. D), and Shaw's average pelite (Col. E). As Na_2O is distinctly high and K_2O somewhat low, the Cobalt rocks are characterized by a very high Na_2O/K_2O ratio. The content of CaO is also surprisingly low. MgO and FeO are a little higher than in the other averages cited.

It is also instructive to compare the Cobalt average with Grout's averages of the rocks of the Canadian Shield (Col. G) and Clarke and Washington's average of the igneous rocks of eastern Canada (Col. F). The Cobalt material differs most notably in its very low CaO content. It is also a little higher in MgO and Na_2O and a little lower in K_2O and in Fe_2O_3. The Cobalt samples are presumably representative of the region from whence the glacial debris came; they are therefore a sample of

pre-Huronian materials, whereas the averages of Grout and of Clarke and Washington include rocks of Huronian and later times. Perfect agreement among these averages, therefore, could not be expected.

TABLE 3.—AVERAGE CHEMICAL COMPOSITION OF PELITIC AND OTHER MATERIALS

Weight per cent

	A	B	C	D	E	F	G
SiO_2	60.83	58.10	60.64	56.30	60.76	52.76	57.76
TiO_2	0.61	0.65	0.73	0.77	0.81	2.20	1.37
Al_2O_3	16.71	15.40	17.32	17.24	16.73	16.40	16.52
Fe_2O_3	1.42	4.02	2.25	3.83	2.53	4.59	3.16
FeO	5.77	2.45	3.66	5.09	3.85	5.84	4.72
MnO	0.09	.....	.....	0.10	.....	0.17	0.08
MgO	3.79	2.44	2.60	2.54	2.49	3.27	2.75
CaO	0.76	3.11	1.54	1.00	1.74	5.30	4.07
Na_2O	4.43	1.30	1.19	1.23	1.82	4.89	3.68
K_2O	2.09	3.24	3.69	3.79	3.41	2.65	2.82
H_2O+	3.13	5.00	3.51	3.31	3.43	1.09	1.59
H_2O-	0.10		0.62	0.38		.....	0.18
CO_2	0.07	2.63	1.47	0.84	1.65	.....	1.38
P_2O_5	0.18	0.17	.....	0.14	.....	0.21	0.21
SO_3	0.02	0.64	.....	0.28	.....	.....	.....
Total	100.00	99.15	99.22	96.84	99.22	99.37	100.00

A. Average Cobalt sediment (average A, B, and C, Table 1)

B. Average shale (Clarke, 1924, p. 34)

C. Average slate (Eckel, 1904, p. 26)

D. Average Precambrian slate (Nanz, 1953, p. 58)

E. Average pelitic rock (Shaw, 1956, p. 928)

F. Average of igneous rocks of eastern Canada, 99 analyses (Clarke and Washington, 1924, p. 13)

G. Average of rocks of Canadian Shield weighted to include 70 per cent batholithic rocks, 17 per cent volcanic and small intrusive rocks, and 13 per cent sediments (Grout, 1938, p. 502)

Clearly, however, the composition of the Cobalt materials is anomalous. If it is truly a glacial flour, the low CaO content is difficult to explain; if it is a normal sediment, leached of its CaO, then the high Na_2O content is an anomaly.

DISCUSSION

It has long been observed that shales, argillites, and related materials are normally low in Na_2O and high in K_2O (Bastin, 1909, p. 463). These relationships are well seen in Figure 2 in which is shown the Na_2O/K_2O content of various slates of both Paleozoic and Precambrian age. As can be seen the Na_2O/K_2O ratio is about 0.5 or less for most argillites, and only in a few is it as high as 1.0. In marked contrast, two of the Cobalt samples have a ratio greater than 2.0. Clearly the Cobalt materials are anomalous argillites. The only common detrital sediments with comparable ratios are the graywackes[2]. In these the Na_2O/K_2O ratio is seldom less than 1.0 and commonly is much higher (Fig. 3).

Various explanations have been offered to account for the sodic nature of the graywackes. (For an extended discussion of the problem *see* Engel and Engel, 1953, p. 1086–1091.) High Na_2O content might be due to (1) soda metasomatism, (2) derivation from sodium-rich source rocks, or (3) sedimentation in a soda lake. The meager published data indicate that the sodic nature of the graywackes is for the most part related to their high content of albitic feldspar. Clearly the feldspar of the graywackes is a detrital mineral. But is its

[2] The term "graywacke" is used in the classical sense, and the analyses compiled are, with one exception, all of rocks designated graywacke by the original author.

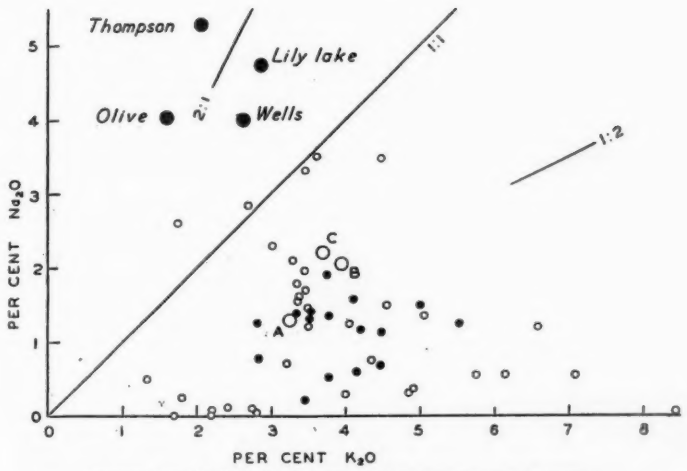

FIGURE 2.—Na_2O/K_2O CONTENT OF ARGILLITES AND SLATES

Black circles: slates (after Dale, 1914, p. 51); open circles: Precambrian argillites (after Nanz, 1953, p. 53-54). A, average shale (after Clarke, 1924, p. 34); B, average Norwegian glacial clay (after Goldschmidt, 1954, p. 53); C, composite New Zealand argillite (Reed, 1957, p. 28)

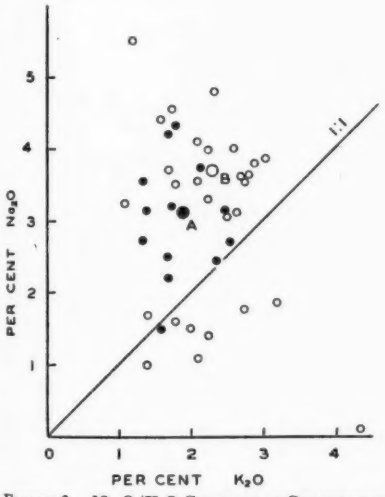

FIGURE 3.—Na_2O/K_2O CONTENT OF GRAYWACKES

Solid black circles: miscellaneous graywackes (Pettijohn, 1957, p. 306); open circles: New Zealand graywackes (Reed, 1957, p. 16). A, average graywacke (Pettijohn, 1957, p. 307); B, Composite New Zealand graywacke (Reed, 1957, p. 16)

albitic character original or is it a product of soda metasomatism? The close association of many graywackes with spilitic rocks suggests that the sodium problem is related to the origin of spilites. There is some evidence of the albitization of the feldspar *in situ* in the graywackes as they commonly contain some carbonate which is neither detrital nor a cement. This carbonate replaces both the matrix and the coarser detritus and is therefore a postdepositional product. Perhaps *in situ* albitization of the plagioclase releases lime which is deposited elsewhere in the rock as a carbonate. One is reminded of the innumerable veinlets and vugs of calcite associated with the albitized greenstones. But if the albitization of the graywackes has taken place why were the associated and interbedded slates not also albitized? Reed (1957, p. 28) has clearly shown that the argillites interbedded with graywackes in New Zealand have a normal Na_2O/K_2O ratio in contrast to the high Na_2O/K_2O ratio in the cogenetic graywackes (Figs. 2, 3). As it can be presumed that the content of detrital feldspar, like that of detrital quartz, decreases with decrease in grain size in clastic sediments, then, if the sodium content is linked to the feldspar content, Na_2O would likewise decline with decrease in grain size. And as K_2O has been shown to *increase* with decrease in grain size (Grout, 1925, p. 393) and is linked with the clay mica content, the Na_2O/K_2O ratio would be notably lower in the shales than in the associated graywackes. In general, therefore, the authors are inclined to regard the sodic content of the graywackes as an

original character inherited from the source rocks of these sediments.

But the Cobalt argillites—unlike other pelitic sediments—have a high Na_2O content. If this anomaly is related to a high content of albitic feldspar—as it seems to be[3]—then the Cobalt rocks are not normal pelitic sediments. If they are glacial, as most geologists seem to think, the Na_2O content is not so anomalous inasmuch as glacial abrasion of the average rock of the Canadian Shield (Table 3, Col. G) would yield a flour higher in Na_2O than K_2O and with a Na_2O/K_2O ratio near 1.3. The Na_2O fractionation characteristic of cogenetic graywackes and shales would not be expected. But if the Cobalt rocks are a product of the glacial mill, why are they so impoverished in CaO which is plentiful in the Shield rocks?[4]

If Grout's averages are valid, a glacial rock flour derived from the area covered by his analyses should contain 4–5 per cent CaO. The Cobalt materials average less than 1 per cent. It is difficult, therefore, to regard them as the unmodified product of a glacial mill. But, as shown by Goldich and others (for summary *see* Pettijohn, 1957, p. 499), weathering readily removes CaO, and the low CaO content could be accounted for by weathering prior to glacial erosion. But such leaching would surely remove the Na_2O, so that such a hypothesis is quite untenable.

The high Na_2O and low CaO content cannot, therefore, be related either to source rock or to leaching but must be in some manner related to one another and to a common cause. One is forced to the conclusion that soda metasomatism explains both anomalous compositional attributes. In view of the abundance of calcium-bearing feldspar in many of the presumed source rocks, the absence of such in the argillites and the presence only of albitic plagioclase requires some CaO removal and addition of Na_2O. Bastin (1935, p. 715) has observed albitization in many of the Nipissing diabases in the Cobalt area. Such albitization, however, is localized near the top of the diabase sills and in small "dikes" and is accompanied by oxidation and reddening of the rocks. Although the Nipissing diabases are widespread and coincident with the distribution of the Cobalt series, the absence of the tell-tale color change and the pervasive character of the albitization required make it difficult to attribute the process to diabase intrusion and deuteric action. There is, however, no other obvious cause.

Deposition in a soda lake might account for the sodic nature of the Cobalt varved argillites but cannot be an explanation for the sodic character of the tillites. Moreover the sodic-lake hypothesis has no other evidence to support it, and it is not compatable with the concept of glacial origin of the Cobalt beds.

Conclusions

Four analyses of Cobalt sediments disclose a very high Na_2O/K_2O ratio[5]. The Na_2O is contained in albite. As the sediments are presumed to be glacial and the presumed source rocks contain abundant CaO, the conclusion is reached that post-depositional albitization of the detrital plagioclase with loss of CaO and addition of Na_2O has taken place.

References Cited

Bastin, E. S., 1909, Chemical composition as a criterion in identifying metamorphosed sediments: Jour. Geology, v. 17, p. 445–472

[3] A half-gram sample of the argillite was treated with 25 ml 1:1 HCl and heated on a steam bath for 2 hours. A greenish solution was formed. Water was added, then 25 ml more acid. The mixture was left on the steam bath an additional 4 hours, then let stand overnight. The solution was filtered through a weighed funnel, the residue dried at 110° C and weighed. A sample of cleavlandite from Amelia, Virginia, was treated in exactly the same manner in order to be sure the acid treatment did not decompose albite completely. The sample of argillite lost 25.8 per cent in weight, while the cleavlandite lost 7.5 per cent. An X-ray powder pattern of the argillite residue made by Miss Mary E. Mrose showed the presence of only quartz and albite.

[4] There are *some* granites included in Grout's tables which do have a very high Na_2O content *and* a low CaO content. For example, a "typical pink Killarney granite" from Birch Lake, near Webbwood, Ontario, has but 0.29 per cent CaO and 6.69 per cent of Na_2O. But most of the Killarney granites and related rocks tabulated by Grout have a higher CaO content and in all except one K_2O exceeds Na_2O. As the Killarney rocks are presumed to be younger than the Cobalt, they could not be the source of Cobalt sediments.

[5] So few samples may not adequately represent the Cobalt deposits but as two are water-laid and one is ice-laid and inasmuch as the two water-laid samples come from points over 170 miles apart, their remarkable chemical similarity strongly suggests that the Cobalt glacial sediments are very homogeneous. Each water-laid sample is in a sense a composite sample in that a number of year-layers are included in the sample. More chemical data on the composition of this interesting group of sediments would be desirable. Of interest in this connection is the partial analysis cited by Wilson (1913, p. 139) from the Gowganda district.

Bastin, E. S., 1935, "Aplites" of hydrothermal origin associated with Canadian Cobalt-silver ores: Econ. Geology, v. 30, p. 715–734

Clarke, F. W., 1924, Data of geochemistry: U. S. Geol. Survey Bull. 770, 841 p.

Clarke, F. W., and Washington, H. S., 1924, The composition of the earth's crust: U. S. Geol. Survey Prof. Paper 127, 117 p.

Collins, W. H., 1925, North shore of Lake Huron: Geol. Survey Canada Mem. 143, 160 p.

Dale, T. N., 1914, Slate in the United States: U. S. Geol. Survey Bull. 586, 220 p.

Eckel, E. C., 1904, On the chemical composition of American shales and roofing slates: Jour. Geology, v. 12, p. 25–29

Engel, A. E. J., and Engel, C. G., 1953, Grenville series in the northwest Adirondack Mountains, New York: Geol. Soc. America Bull., v. 64, p. 1013–1097

Goldschmidt, V. M., 1954, Geochemistry: Oxford University Press, 730 p.

Grout, F. F., 1925, Relation of texture and composition of clays: Geol. Soc. America Bull., v. 36, p. 393–416

Grout, F. F., 1938, Petrographic and chemical data on the Canadian Shield: Jour. Geology, v. 46, p. 486–504

Miller, W. G., 1905, The cobalt-nickel arsenides and silver deposits of Temiskaming: Ontario Bur. Mines Ann. Rept., v. 14, pt. 2, p. 42

Nanz, R. H., 1953, Chemical composition of pre-Cambrian slates with notes on the geochemical evolution of lutites: Jour. Geology, v. 61, p. 51–64

Pettijohn, F. J., 1957, Sedimentary rocks (2d ed.): New York, Harper and Bros., 718 p.

Reed, J. J., 1957, Petrology of the Lower Mesozoic rocks of the Wellington district: New Zealand Geol. Survey Bull., n. ser., 57, 60 p.

Rubey, W. W., 1951, Geologic history of sea water: an attempt to state the problem: Geol. Soc. America Bull., v. 62, p. 1111–1147

Shaw, D. M., 1956, Geochemistry of pelitic rocks. Part III: Major elements and general geochemistry: Geol. Soc. America Bull., v. 67, p. 919–934

Wilson, M. E., 1913, The Cobalt series; Its character and origin: Jour. Geology, v. 21, p. 121–141

The Johns Hopkins University, Baltimore, Md.; U. S. Geological Survey, Washington, D. C.

Manuscript Received by the Secretary of the Society, October 18, 1958

Publication Authorized by the Director, U. S. Geological Survey

BULLETIN OF THE GEOLOGICAL SOCIETY OF AMERICA
VOL. 70, PP. 601-618, 11 FIGS. MAY 1959

RE-EVALUATION OF THE SALT CHRONOLOGY OF SEVERAL GREAT BASIN LAKES

BY WALLACE S. BROECKER AND ALAN F. WALTON

ABSTRACT

A re-evaluation of methods used to calculate the accumulation time for salts in the Great Basin lakes indicates that they are based on questionable assumptions and yield ages which are probably a factor of ten too small. A new approach to such calculations has been applied to Great Salt, Mono, Pyramid, and Walker lakes. The Cl^- concentration in rainfall entering the basin is used instead of the rate of Cl^- addition to these lakes as determined from chemical data on river waters. Loss of Cl^- from the surface of the lake must be taken into account, particularly when the Cl^- concentration is large. The effect of changes in climate on the rates of salt input and loss must also be considered. Radiocarbon data provide an absolute climate chronology and allow these variations to be handled quantitatively.

The study suggests that Great Salt Lake and Mono Lake have not lost a major portion of their salt by desiccation for more than 73,000 years. Pyramid Lake may also have been in existence since the end of the last interpluvial period (*i.e.*, $\sim$ 73,000 years B.P.), but Walker Lake must have desiccated during the last 10,000 years. Such histories are internally consistent and in good agreement with independent biological and geological evidence.

CONTENTS

TEXT

	Page
Introduction	602
Derivation of equations	603
Evaluation of parameters	604
Climate chronology	604
Estimates of mean depths of lakes ($\bar{h}$)	605
Estimates of linear evaporation rates (l_E)	606
Estimates of Cl^- concentration in water added to lakes (f)	608
Estimates of rate of Cl^- loss from lakes	612
Calculation of accumulation times	614
Discussion	614
Great Salt Lake	614
Mono Lake	615
Walker Lake	615
Pyramid Lake	615
Sensitivity of ages to choice of parameters	615
Comparison with previous estimates	615
Internal consistency of ages	616
Agreement of ages with other evidence	616
Conclusions	617
References cited	617

ILLUSTRATIONS

Figure	Page
1. Map of Great Basin showing locations of contemporary and fossil lakes	602
2. Lake-level chronology of Lakes Lahontan and Bonneville	604
3. Idealized-level chronology of Great Basin lakes	605
4. Relationship between the elevation of the surface of Great Salt Lake and its area, volume, and mean depth	606
5. Relationship between the elevation of the surface of Mono Lake and its area, volume, and mean depth	607
6. Relationship between the elevation of the surface of Walker Lake and its area, volume, and mean depth	608
7. Relationship between the elevation of the surface of Pyramid Lake and its area, volume, and mean depth	609
8. Theoretical Cl^- concentration as a function of k for present-day Great Salt Lake, assuming continual existence since the last interpluvial period	610
9. Theoretical Cl^- concentration as a function of k for present-day Mono Lake assuming continual existence since the last interpluvial period	611
10. Theoretical Cl^- concentration as a function of k for present-day Walker Lake assuming continual existence since the last interpluvial period	612
11. Theoretical Cl^- concentration as a function of k for present-day Pyramid Lake assuming continual existence since the last interpluvial period	613

TABLES

Table	Page
1. Cl^- concentrations in contemporary Great Basin lakes and rivers	603
2. Values selected for the parameters required for Cl^- accumulation calculations	609

Introduction

Since the early land surveys of the nineteenth century, geologists and climatologists have attempted to reconstruct the histories of pluvial lakes in the Great Basin. One problem has been to estimate the absolute time intervals between the events recorded by the deposits in the lake areas. Many workers (Pošepny, 1877; Russell, 1885, p. 224–230; Van Winkle, 1914, p. 123; Jones, 1925, p. 31; Antevs, 1938, p. 190; Eardley *et al.*, 1957, p. 1141–1149) have attempted to determine the time required for accumulation of the salt now present in these lakes. New data on both the geochemistry of the elements involved and the absolute chronology of climatic fluctuations over the past 40,000 years make a re-evaluation desirable. For this study four Great Basin lakes have been chosen, namely Great Salt Lake, Mono Lake, Walker Lake, and Pyramid Lake (Fig. 1).

Of the ions present in the lake waters, Cl^- is most suitable for such a study for the following reasons: (1) Cl^- is not incorporated to any significant extent in the lake sediments, whereas $SO_4^=$, $CO_3^=$, and K^+ are; and (2) Cl^- is derived almost entirely from the recycling of oceanic salts as opposed to release during the weathering of igneous and sedimentary rocks (Conway, 1942, p. 135; Eriksson, 1952, p. 285–289). Jones (1925, p. 29) recognized the value of limiting the salt-chronology calculations to individual ionic species. Two important factors have been neglected, however, in most of these studies. First, no quantitative account has been taken of the possibility of significant loss of Cl^- and other salts through wind entrainment, a process adequately demonstrated by the oceanic sodium, chlorine, and sulfate in rain

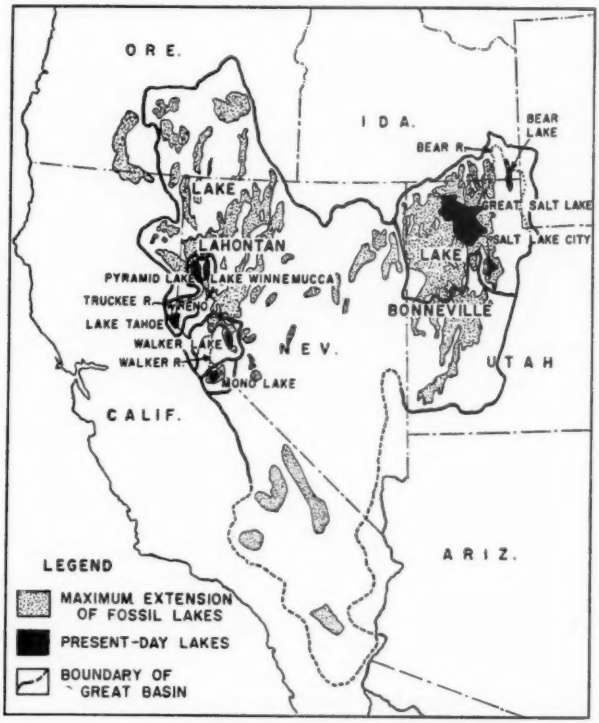

FIGURE 1.—MAP OF GREAT BASIN SHOWING LOCATIONS OF CONTEMPORARY AND FOSSIL LAKES

The outlines of the hydrographic basins of present-day Great Salt, Mono, Walker, and Pyramid lakes are shown.

water (Eriksson, 1952, p. 294). Second, the Cl^- concentration in present-day river water probably does not provide a reliable estimate of the normal rate of salt accumulation in the lakes. Eardley *et al.* (1957) recognized these problems but did not evaluate them quantitatively.

This paper attempts to re-evaluate the time required for accumulation of the salt present in each of the four lakes. This will provide an estimate of the date of the last complete desiccation of each lake. Since climatic variations were similar for the four lakes, the results should be consistent. One problem is the large differences in their respective salinities. As shown in Table 1, Great Salt Lake has a chlorinity about 10 times higher than that in Mono Lake, which in turn has a chlorinity about 10 times higher than that of either Pyramid Lake or Walker Lake.

Derivation of Equations

If the volume of the lake remains nearly constant, only two factors influence its Cl^- concentration: (1) rate of influx of Cl^- from river water, and (2) rate of loss of Cl^- by entrainment in the wind. The rate of change of Cl^- in the lake with time can be expressed as

$$\frac{dC}{dt} = \frac{fI - G}{A_L \bar{h}}$$

where C = Cl^- concentration in lake water, t = time, f = Cl^- concentration in river water supplying the lake, I = rate of addition of river water to the lake, G = rate of Cl^- loss through wind entrainment, A_L = area of lake, and $\bar{h}$ = mean depth of lake. For this problem direct addition of rain water may be considered negligible in comparison with the water supplied by rivers. Volume changes of the lake must be considered separately. The following substitutions can be made before integration:

(a) During periods when no major fluctuations of lake level occur

$$I = A_L l_E$$

where l_E is the linear evaporation rate.

(b) To a first approximation G may be considered proportional to C and A_L, *i.e.*,

$$G = kCA_L$$

where k is a constant.[1]

[1] k has the dimensions of length/time. It may be considered to be the linear rate of water loss through wind entrainment.

Table 1.—Cl^- Concentrations in Contemporary Great Basin Lakes and Rivers

Locations*	Cl^- Concentration† (1870–1910) (ppm)	Cl^- Concentration† (1940–1957) (ppm)
Great Salt Lake System		
Bear River		
Evanston	4.9 (1)††	7.5 (1)****
Woodruff	.....	29.6 (1)****
Preston	.....	56.2 (1)****
Corinne	.....	375 (1)****
Great Salt Lake**	24,500 (1)††	187,000 (2)****
Mono Lake System		
Mono Lake**	11,610 (1)††	14,000 (1)****
Walker Lake System		
Walker River		
Wellington	.....	6.4 (1)****
Mason	13.1 (1)††	.....
Schurz	.....	24.2 (1)****
Walker Lake**	584 (1)††	1460 (1)****
Pyramid Lake System		
Lake Tahoe	2.3 (1)††	1.9 (17)†††
Truckee River		
Truckee	.....	1.5 (15)†††
Reno	.....	4.7 (1)****
Derby	9.1 (10)***	.....
Wadsworth	.....	16.6 (1)****
Nixon	.....	55.2 (1)****
Pyramid Lake**	1430 (1)††	1685 (1)****

* Stations for each system are arranged according to distance from the river source

† Increase in Cl^- concentration is the result of decreases in volume of the respective lakes

** Numbers in parentheses indicate the number of analyses on which the averages are based

†† Analyses quoted by Russell (1885)

*** Analyses given by Clarke (1924)

††† Analyses given in U. S. Geol. Survey Water-Supply Papers 1200 (1955, p. 201) and 1253 (1957, p. 225)

**** Analyses performed by the authors

Making these substitutions and integrating between the limits $t = 0$ and $t = t$ with the value of C at $t = 0$ being C_0, one obtains the following:

$$C = \frac{fl_E}{k}\left(1 - e^{-kt/\bar{h}}\right) + C_0\, e^{-kt/\bar{h}}.$$

The factor $\frac{k}{\bar{h}}$ represents a rate constant for attainment of equilibrium. The half-equilibrium time, $t_{\frac{1}{2}}$, may be expressed as, $\frac{0.693\bar{h}}{k}$, and the equation may be conveniently rewritten as:

$$C = \frac{fl_E}{k}\left(-1e^{-0.693t/t_{\frac{1}{2}}}\right) + C_0\, e^{-0.693t/t_{\frac{1}{2}}}.$$

Two extreme cases may be considered:

(1) If $t \gg t_{\frac{1}{2}}$, then the lake has reached

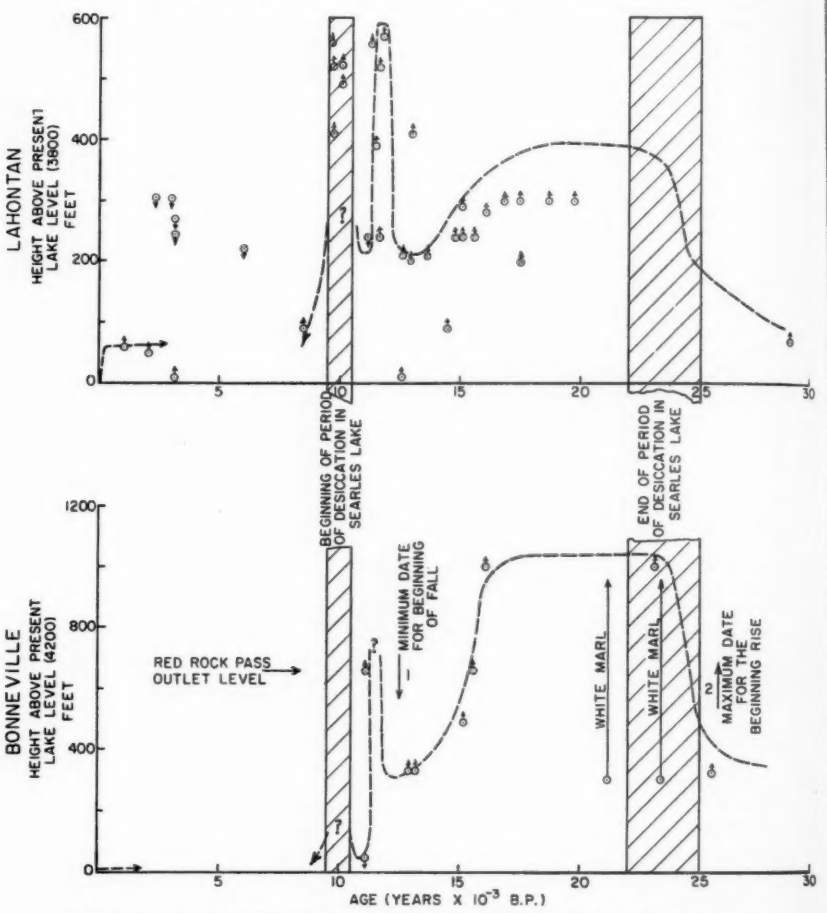

FIGURE 2.—LAKE-LEVEL CHRONOLOGY OF LAKES LAHONTAN AND BONNEVILLE

Points with upward-directed arrows represent samples deposited from the lake, and points with downward-pointed arrows represent samples from terrestrial deposits. Ruled areas represent periods of initial rise and desiccation of the waters in Searles Lake. Arrows 1 and 2 represent the ages obtained on material taken immediately above and below the organic-rich layer in the Great Salt Lake core. Curves originally published by Broecker and Orr (1958). The Searles Lake data are from Libby (1954, p. 739) on samples submitted by Flint and Gale.

equilibrium and has a constant Cl^- concentration given by

$$C = \frac{f l_E}{k}$$

(2) If $t \ll t_{\frac{1}{2}}$, and if $C_0 = 0$, then

$$C = \frac{f l_E t}{h}$$

EVALUATION OF PARAMETERS

Climate Chronology

The parameters h, l_E, f, and k must be estimated for each lake. Because of the great climatic changes which occurred during the Pleistocene, the values of these parameters cannot be assumed to have remained constant with time. Since any variations must be taken into account, the chronology of the major

climatic fluctuations in the Great Basin must be estimated independently.

Using radiocarbon dates, Broecker and Orr (1958) have constructed a chronology of the climatic fluctuations over the past 30,000 years in the Lake Lahontan and Lake Bonneville areas. Their lake-level versus time curves are shown in Figure 2. It is assumed that the fluctuations of Mono Lake followed a similar pattern.

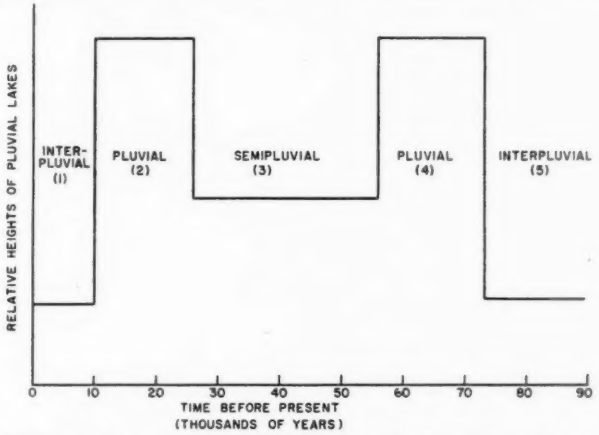

FIGURE 3.—IDEALIZED-LEVEL CHRONOLOGY FOR GREAT BASIN LAKES

For this study the lake history can be divided into the following five distinct periods, each of which can be characterized by a nearly uniform climate.

(1) 0–10,000 years B.P.; interpluvial conditions (similar to those at present)

(2) 10,000–26,000 years B.P.; pluvial conditions (high lake levels)

(3) 26,000–56,000 years B.P.; semipluvial conditions (intermediate lake levels)

(4) 56,000–73,000 years B.P.; pluvial conditions (high lake levels)

(5) 73,000–150,000 years B.P.; interpluvial conditions (low lake levels, similar to those at the present time)

The boundaries at 10,000 years and at 26,000 years are defined by the data shown in Figure 2. Evidence given by Flint and Rubin (1955, p. 657), Emiliani (1955, p. 569), Broecker and Orr (1958, p. 1021), and Broecker *et al.*, (1958, p. 510) indicates that intermediate conditions prevailed during period (3). No direct evidence for the time of the beginning of this period has been obtained in the Great Basin, but ocean cores indicate it began about 56,000 years B.P. (Broecker *et al.*, 1958, p. 513). Evidence from numerous regions including the Great Basin suggests that this period of intermediate climate was preceded by a pluvial period with a climate similar to that during period (2). Estimates by Broecker *et al.*, (1958, p. 513) place the beginning of this period about 73,000 years before the present. These estimates are in good agreement with those given by Emiliani (1955). Extrapolation of data from ocean cores suggests that the beginning of period (5) was 150,000 years B.P. (Broecker *et al.*, 1958, p. 515). An idealized picture of Great Basin climate is shown schematically in Figure 3.

This chronology is not acceptable to some geologists who have studied the lake deposits in the Great Basin. These workers consider the radiocarbon ages to be too low. However the accumulation times are not strongly dependent on the choice of the chronology. The conclusions of this study would not be greatly altered even if the chronology given here is found to be incorrect.

Although the values of the parameters will differ from one period to the next, it will be assumed that they remained constant within a given period. Since some fluctuations certainly did occur within a given period, the values chosen represent the average for that time interval.

Estimates of Mean Depths of Lakes ($\bar{h}$)

Since the value of $\bar{h}$ is directly related to the elevation of the lake surface, data such as

those given by Broecker and Orr (1958) relating elevation and time allow $\bar{h}$ to be estimated for each lake during each climate period. The precise relationship between $\bar{h}$ and elevation for each lake can be obtained from topographic maps of the areas involved. Plots of area, volume, and the resulting values of $\bar{h}$ as a function of elevation are given for each lake in Figures 4, 5, 6, and 7. The problem becomes one of selecting the proper lake levels for each period. The level of each lake during periods (1) and (5) has been placed at the level recorded in 1890. The Broecker and Orr curves (Fig. 2) show that for Lake Lahontan and Lake Bonneville the pluvial-period levels averaged about two-thirds of their maximum increase in level. This estimate will be applied to period (4) as well as period (2). For period (3) a level equivalent to one-quarter of the maximum increase has been selected. Similar changes in level are attributed to Mono Lake, for which only the maximum elevation is known. The elevations selected and the resulting values of $\bar{h}$ are listed in Table 2.

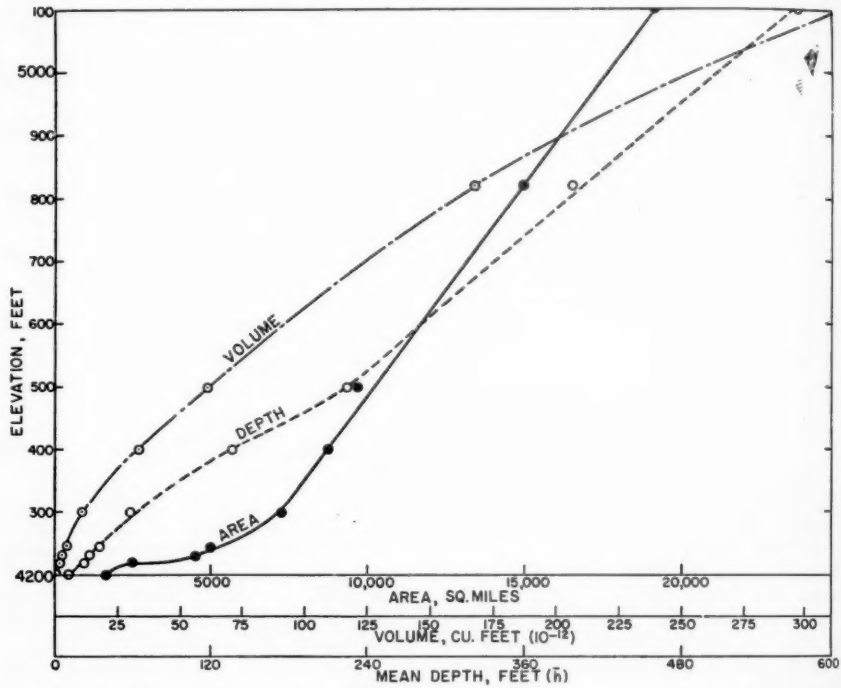

FIGURE 4.—RELATIONSHIP BETWEEN THE ELEVATION OF THE SURFACE OF GREAT SALT LAKE AND ITS AREA, VOLUME, AND MEAN DEPTH

Data taken from curves published by Eardley *et al.* (1957, p. 1145).

Estimates of Linear Evaporation Rates (l_E)

Water-balance studies provide reliable estimates of the present linear evaporation rates for Great Salt Lake (E. L. Peck, 1955, unpub. M. A. thesis, Univ. of Utah) and Pyramid Lake (Hardman and Venstrom, 1941, p. 82). The rates for Walker Lake and Mono Lake have been estimated from available evaporation-rate maps (Meyer, 1942, p. 56; Horton, 1943, p. 750). The results are given in Table 2. The relatively low value for Great Salt Lake is related to its high salinity rather than to a great difference in climate.

The evaporation rates probably decreased during periods of high water levels, but the

changes are difficult to estimate. The rise in lake level resulted from some unknown combination of increased rainfall and decreased evaporation. Evaporation losses occur in two ways; (1) loss from the lake surface, and (2) loss from soils of the hydrographic basin. The magnitude of the second process can be expressed by a parameter, ϕ, the fraction of rainfall entering the basin which runs off into the lakes. Studies by Thornthwaite and Mather (1955) show that ϕ is strongly influenced by such factors as vegetation cover and the distribution of rainfall and temperature within each year.

With present knowledge it is impossible to evaluate the relative effects of (1) rainfall in hydrographic basins; (2) evaporation from lake surfaces; and (3) evaporation from soils on the size of the lakes.

It will be assumed arbitrarily therefore that one-third of the lake expansion for any period was caused by an increase in the amount of rain input to the basin and the other two-thirds by a decrease in the net loss of water by evaporation. It is assumed further that the decrease in loss rate arises from an equal-percentage decrease in the evaporation rate over the lake and over the soils in the hydrographic basin. With these assumptions the values for the parameters l_E, l_R, and ϕ (where l_R is the average annual rainfall over the hydrographic basin) can be evaluated for pluvial and semipluvial periods, using the following relationship:

$$\underset{input}{l_R A_B} = \underset{loss}{l_E A_L} + (1 - \phi) l_R (A_B - A_L).$$

To carry out this calculation the contempo-

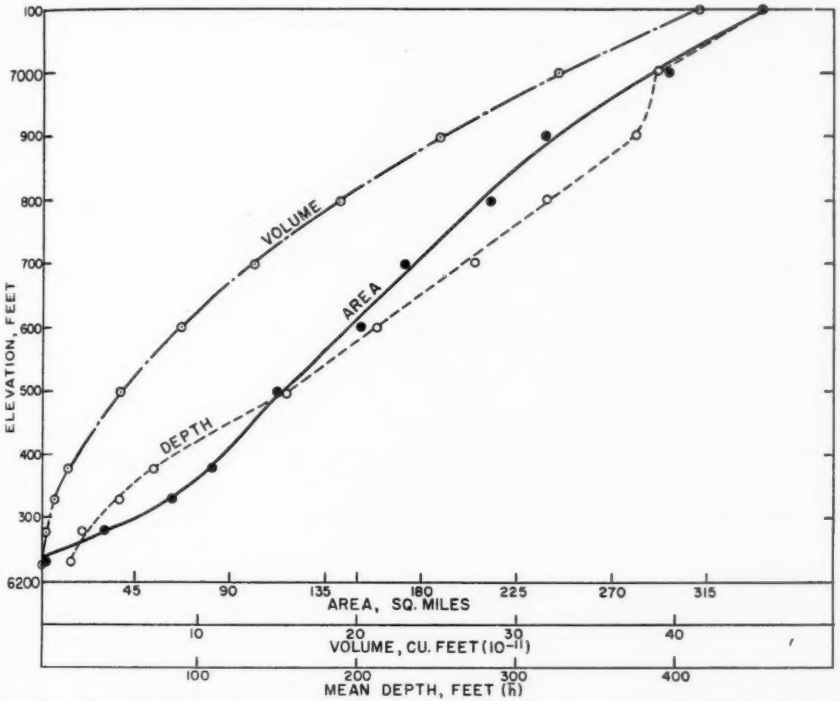

FIGURE 5.—RELATIONSHIP BETWEEN THE ELEVATION OF THE SURFACE OF MONO LAKE AND ITS AREA, VOLUME, AND MEAN DEPTH

Data obtained from topographic maps of the Mono Lake area and from a subsurface map of Mono Lake published by Russell (1889, Pl. XIX).

rary values of l_E, l_R, A_L, and A_B (area of basin) must be known. The current ϕ value is then fixed. Estimates of l_E and A_L were given heretofore. Rainfall data given by the U. S. Department of Agriculture (1936) allow l_R to be computed for each basin. The areas of the basins are obtained directly from the maps published by Russell (1885, Pl. XLVI, 1889, Pl. XVII) and Gilbert (1890, Pl. XII). The results are summarized in Table 2.

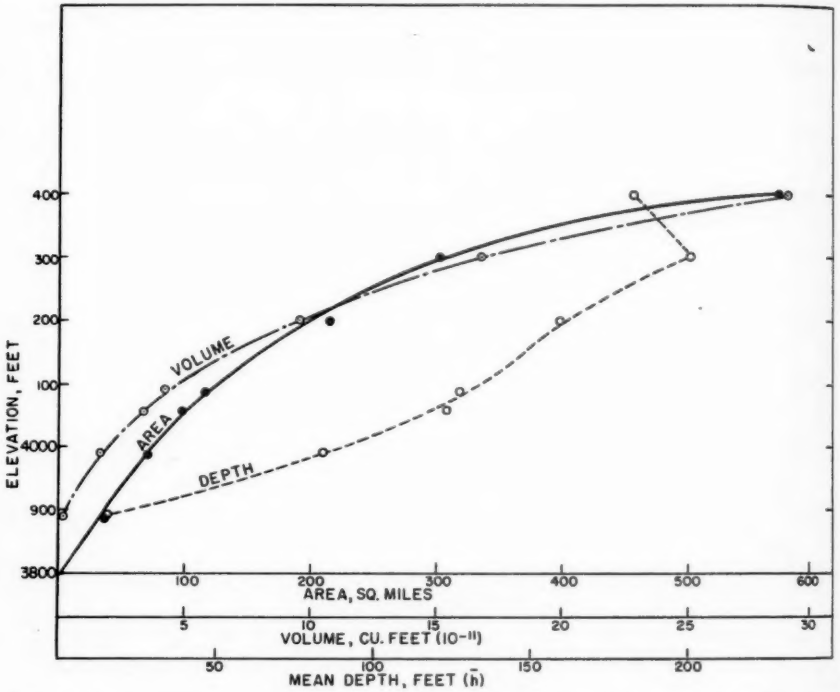

FIGURE 6.—RELATIONSHIP BETWEEN THE ELEVATION OF THE SURFACE OF WALKER LAKE AND ITS AREA, VOLUME, AND MEAN DEPTH

Data obtained from topographic maps of the Walker Lake area and from a subsurface map of Walker Lake published by Russell (1885, Pl. XV).

The effect of the high salinity of Great Salt Lake on its present size is taken into account in the calculation. Pyramid Lake is known to have merged with lakes in other basins during the high-water periods, but it is not possible to calculate the net effect on the system, because topographic maps for the other basins are not available. It is assumed that there was no net transfer of salt from one basin to the next. The calculation is carried out as if the lake was confined to its own basin. As pointed out by Ernst Antevs (personal communication), this will lead to an underestimate of the accumulation time, since salt certainly was lost through overflow into the Black Rock and Smoke Creek deserts.

Estimates of Cl^- Concentration in Water Added to Lakes (f)

Estimates of f must also be made for each climatic period. Data for the present concentrations in the Bear River (supplying Great Salt Lake) and in the Truckee River (Pyramid Lake) are shown in Table 1. The large downstream increases in concentration are anomalous. Since Cl^- is nearly absent in both igneous and sedimentary rocks, its presence in rivers is due primarily to recycling of oceanic salts (Conway, 1942, p. 135). Although evapo-

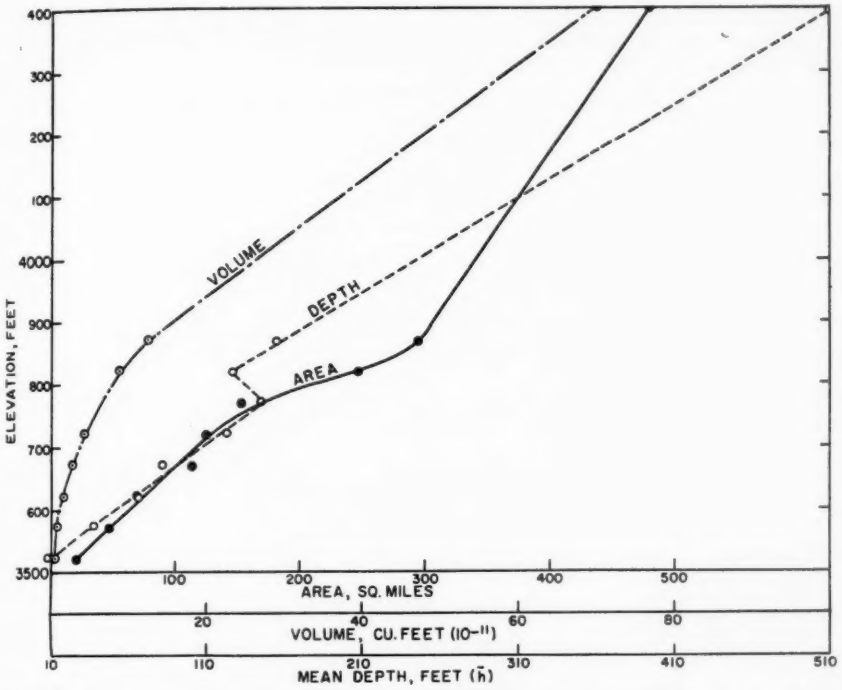

FIGURE 7.—RELATIONSHIP BETWEEN THE ELEVATION OF THE SURFACE OF PYRAMID LAKE AND ITS AREA, VOLUME, AND MEAN DEPTH

Data obtained from maps published by Russell (1885, Pl. XLVI and Pl. IX).

TABLE 2.—VALUES SELECTED FOR THE PARAMETERS REQUIRED FOR Cl^- ACCUMULATION CALCULATIONS

Climate period	$E_{aver.}$ Feet above sea level	$E_{max.}$ Feet above sea level	A_B Square miles	A_L Square miles	V_L Cubic feet × 10^{-11}	$\bar{h}$ Feet	l_E feet per year	l_B feet per year	ϕ	f' ppm	f ppm
Great Salt Lake											
Interpluvial	4200	..	21,200	1650	0.6	12	3.4	1.25	.15	.25	1.2
Pluvial	4820	5130	50,000	15,000	167	400	3.6	2.7	.27	.25	0.6
Semipluvial	4430	..	50,000	9000	40	170	3.9	2.0	.21	.25	0.7
Mono Lake											
Interpluvial	6410	..	615	90	2.4	95	4.0	1.4	.32	.25	0.6
Pluvial	6830	7050	615	220	21.0	340	3.6	2.1	.39	.25	0.4
Semipluvial	6570	..	615	135	12.0	200	3.7	1.6	.37	.25	0.5
Walker Lake											
Interpluvial	4080	..	3700	110	4.1	125	5.0	0.75	.17	.25	1.3
Pluvial	4300	4400	3700	300	16.7	200	4.5	1.2	.24	.25	0.8
Semipluvial	4160	..	3700	175	7.0	150	4.9	0.9	.19	.25	1.0
Pyramid Lake											
Interpluvial	3870	..	2750	295	12.7	155	4.4	1.15	.34	.25	0.6
Pluvial	4225	4400	(2750)	420	51.5	400	4.1	1.3	.39	.25	0.5
Semipluvial	4000	..	(2750)	340	27.2	240	4.25	1.2	.36	.25	0.55

ration will certainly result in increases in Cl^- concentration, it does not account for increases of the magnitude observed. Grazing, cultivation, and irrigation programs have undoubtedly greatly accelerated the gradual migration of fallout Cl^- from the soils of the basin into the surface drainage systems. Since no existing chemical data predate these activities in either of these areas, direct measurements of Cl^- concentrations in lower sections of the rivers merely set a maximum limit for the interpluvial rate of salt accumulation.

The use of river-water data is also complicated by the possibility of recycling of the lake Cl^- within the basin. The extremely high value for the Bear River at Corinne may reflect such a process.

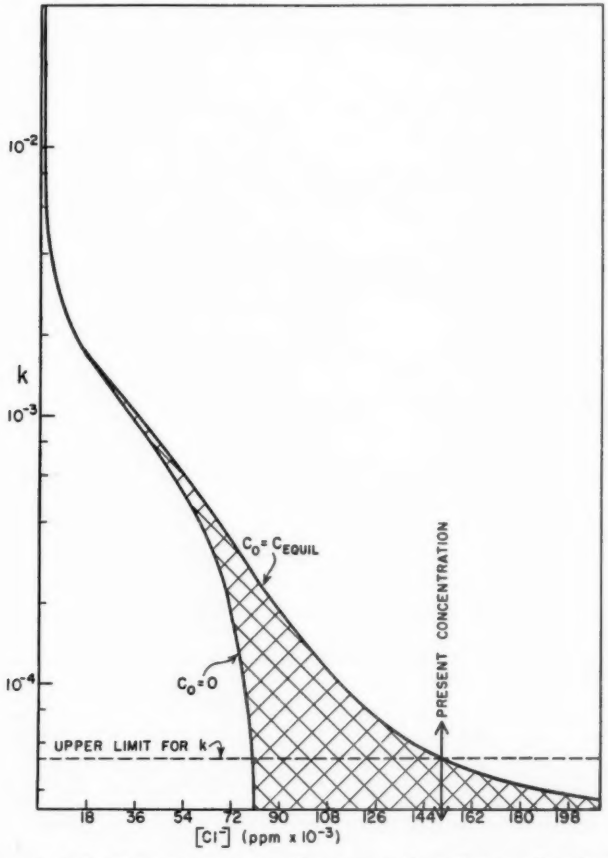

FIGURE 8.—THEORETICAL Cl^- CONCENTRATION AS A FUNCTION OF k FOR PRESENT-DAY GREAT SALT LAKE ASSUMING CONTINUAL EXISTENCE SINCE THE LAST INTERPLUVIAL PERIOD

C_o is the Cl^- concentration at the end of the last interpluvial period. The crosshatched area defines the possible range of present-day concentrations if no postpluvial desiccation has occurred.

Because of these difficulties an indirect approach must be used. The total amount of Cl^- entering a given hydrographic basin may be estimated from the total annual rainfall in the basin and the average Cl^- concentration in the rain. Junge and Gustafson (1957, p. 168) conclude that 80 per cent of recycled Cl^- is carried to earth by rain in humid areas, but Junge (personal communication) feels that in an arid area the figure may be less than 50 per cent. Erik Eriksson (personal communication)

estimates that 50 per cent of the total Cl^- may return in rainfall, and the remainder may return as dry fallout. It is unlikely that all the

where f, A_B, A_L, l_R, and l_E are as previously defined, and f' is the average Cl^- concentration of the rainfall entering the basin.

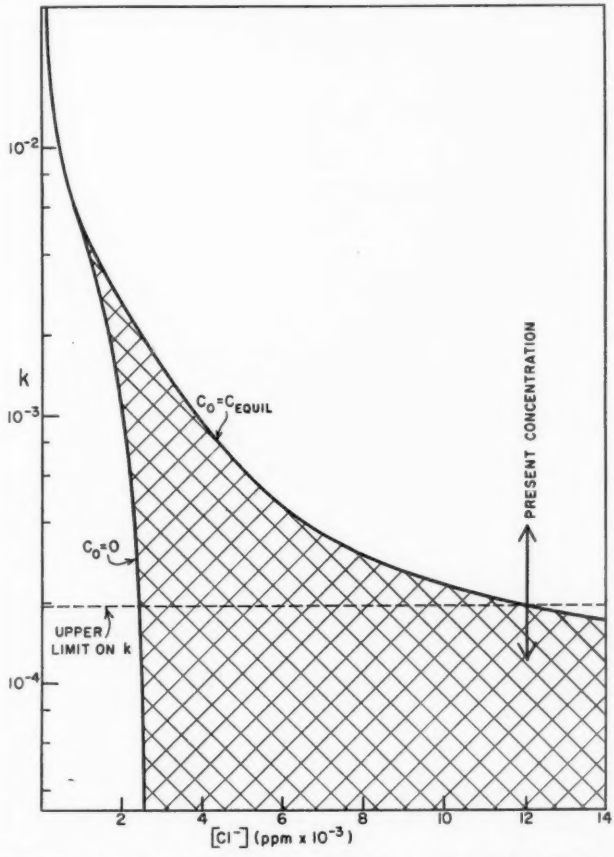

FIGURE 9.—THEORETICAL Cl^- CONCENTRATION AS A FUNCTION OF k FOR PRESENT-DAY MONO LAKE ASSUMING CONTINUAL EXISTENCE SINCE THE LAST INTERPLUVIAL PERIOD

C_o is the Cl^- concentration at the end of the last interpluvial period. The crosshatched area defines the possible range of present-day concentrations if no postpluvial desiccation has occurred.

Cl^- entering the basin will be washed into the lakes. In the absence of better data on both the amount of dry fallout and the fraction of total Cl^- washed into the lakes, it will be assumed that the loss of Cl^- through inefficient runoff is compensated by the dry fallout entering the basin. In this case the Cl^- concentration in the water entering the lake, f, can be estimated as follows:

$$f = \frac{A_B l_R f'}{A_L l_E}$$

Isochlor maps prepared by Junge and Gustafson (1957, p. 165) provide estimates of f'. Although data are limited, 0.25 ± 0.10 ppm seems to be a reasonable estimate for the concentration during the winter season when the majority of rainfall occurs. Since at present f' is relatively constant over the interior of the continent (Junge and Gustafson, 1957) and since the oceanic Cl^- concentration remains nearly constant, there is no reason to believe that f' should undergo large variations with

climate. The resulting values of f are given in Table 2. Mountain streams such as the Upper Truckee which should be far less affected by assumed negligible. Such additions would result in a lowering of the time estimates present in this paper.

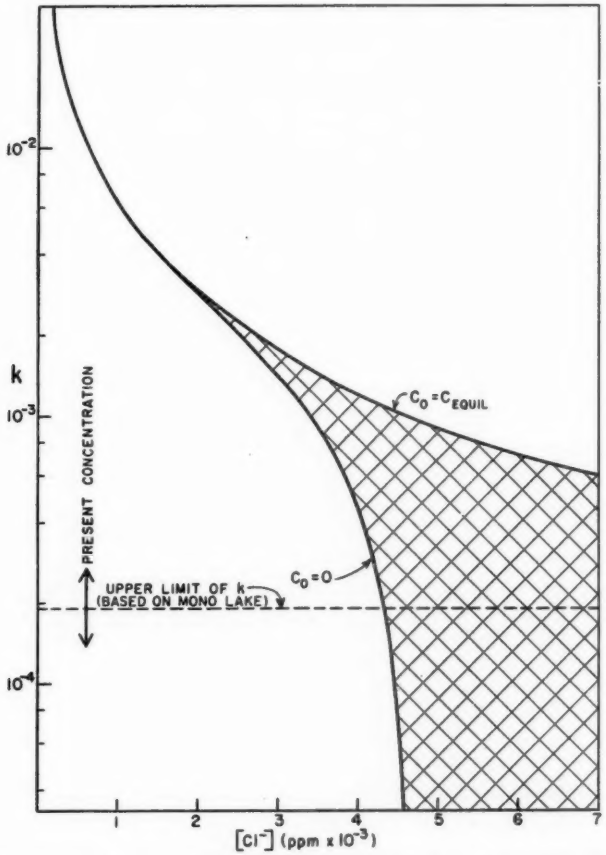

FIGURE 10.—THEORETICAL Cl^- CONCENTRATIONS AS A FUNCTION OF k FOR PRESENT-DAY WALKER LAKE ASSUMING CONTINUAL EXISTENCE SINCE THE LAST INTERPLUVIAL PERIOD

C_o is the Cl^- concentration at the end of the last interpluvial. The crosshatched area defines the possible range of present-day concentrations if no postpluvial desiccation has occurred.

man's agricultural activities have Cl^- concentrations only slightly higher than the computed f values. The Chewaucan River, in a nearly uninhabited region of Oregon, has an average concentration of about 0.5 ppm (Van Winkle, 1914, p. 122) which is in agreement with the estimates based on rainfall data.

It should be noted that contributions of Cl^- from other sources such as local volcanism and recycling of old salt deposits have been

Estimates of Rate of Cl^- Loss from Lakes

The constant k, which relates the rate of salt loss from the surface of a given lake to its salt concentration and area, is the most difficult parameter to evaluate. As shown by Woodcock (1953, p. 364), the quantity of salt entrained is strongly dependent on the wind force over the water. Conway (1942, p. 136) and Eriksson (1955, p. 244) have demonstrated that the concentration of salt in rain decreases

rapidly inland from the coast. Junge and Gustafson (1957) conclude that this decrease is due to vertical mixing of salt entrained over the ocean rather than fallout. The order of magnitude of k for the oceans may be estimated from data on the Cl^- concentration in rain, the area of the ocean, and the mean world rainfall rate. The observed Cl^- concentrations range from about 12 ppm for average oceanic rains to 0.25 ppm for average interior-continental rainfall (based on data given by Junge and Gustafson, 1957). The corresponding range in k is 2.0×10^{-3} to 4.5×10^{-5} feet per year.

The Cl^- concentrations in saline lakes such as Mono Lake and Great Salt Lake allow an upper limit to be placed on k. As previously stated, the values of f and k determine the equilibrium Cl^- concentration in any lake. For example, if k were that given by oceanic rains (2.0×10^{-3} feet per year), the Cl^- concentration in Great Salt Lake would be approximately 2000 ppm at equilibrium. This equilibrium would be approached with a half life of about 3000 years. The present Cl^- concentration of 150,000 ppm is not consistent with such a large value of k. A more refined

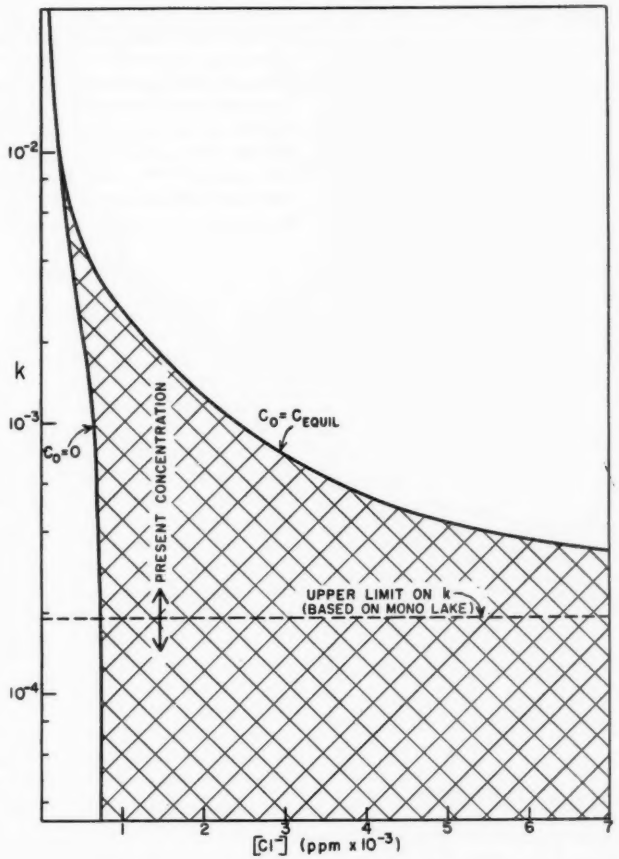

FIGURE 11.—THEORETICAL Cl^- CONCENTRATIONS AS A FUNCTION OF k FOR PRESENT-DAY PYRAMID LAKE ASSUMING CONTINUAL EXISTENCE SINCE THE LAST INTERPLUVIAL PERIOD

C_0 is the Cl^- concentration at the end of the last interpluvial period. The crosshatched area defines the possible range of present-day concentrations if no postpluvial desiccation has occurred.

upper limit of k may be obtained as follows: Assuming the Cl^- concentration in the lake had achieved equilibrium at the end of the last interpluvial period, the Cl^- concentration in the present-day lakes is predicted as a function of k. These computed values may then be compared with the observed concentration. The calculations are carried out using the equations derived and the values of the parameters listed in Table 2. The results are shown in Figures 8 and 9. Since the assumption of equilibrium at the end of the last interglacial period gives a maximum present-day Cl^- concentration, the point at which the $C_0 = C_{equil.}$ curve crosses the observed concentration gives an upper limit for k. The limit placed on k for Great Salt Lake is 5.5×10^{-5} feet per year. The fact that salt has been lost from the lake through overflow to the Snake River system (Gilbert, 1890, p. 171) and through deposition on the salt flats (Eardley *et al.*, 1957, p. 1143) would reduce k even more. A similar limit for Mono Lake is 2.0×10^{-4} feet per year. Both these limits fall within the range estimated for the ocean. Since the Great Salt Lake value may be abnormally low because of the barrier introduced by the Wasatch fault scarp on the eastern side of the basin, the Mono Lake limit will be used when Pyramid and Walter lakes are considered. Since all four lakes were quite dilute during the pluvial and semipluvial periods, the rate of Cl^- loss must have been negligible with respect to the input rate. The loss term involving k need not be considered for these periods.

Calculation of Accumulation Times

An attempt will be made herein to determine whether the lakes have desiccated during the last 10,000 years, or whether they have existed continuously since the last interpluvial period. Conditions were such that during the period from 73,000 to 10,000 years ago desiccation was highly improbable.

The present Cl^- concentrations in the lakes will be compared with those predicted if the lakes had existed continuously since the last interpluvial period. If the predicted value exceeds the observed value by a large factor, the lake must have desiccated during the last 10,000 years. Also the salt deposited cannot have been redissolved by the present lakes.

The calculations are made for two cases:

$$C = 0 \text{ at } t = 73{,}000 \text{ years B.P.}$$

$$C = C_{equil.} = \frac{f}{k} \text{ at } t = 73{,}000 \text{ years B.P.}$$

The actual concentration at the end of the last interpluvial period was probably between these limits. Because of the uncertainty in the rate of loss of Cl^- from the surface of the lakes, calculations are made for various values of k. The results are shown in Figures 8, 9, 10, and 11. If the lakes have existed since the last interpluvial period, for a given value of k, the present Cl^- concentration should fall between the limits defined by the curves marked $C = C_0$ and $C = C_{equil.}$.

Discussion

Great Salt Lake

From Figure 8 it is clear that the present concentration in the lake is possible only if k is less than 5.5×10^{-5} feet per year. The high salt concentration cannot be accounted for by accumulation during a portion or even all of postpluvial time; it must represent therefore an accumulation period of at least 73,000 years.[2] The required accumulation period would be even greater if the salt lost during the overflow of the lake or if that deposited on the salt flats were included. The possibility that desiccation did occur and was followed by solution of the deposited salts cannot be excluded. If this did occur, then the absence of remnant salt deposits in the sediments underlying Great Salt Lake (Eardley *et al.*, 1957, p. 1170) would necessitate complete solution. Existence of thick halite deposits overlain by lacustrine muds in the Searles Lake basin

[2] Feth (1959) points out that springs in the Great Salt Lake basin may be contributing significant quantities of salt to the lake. If it can be demonstrated (1) that the rate at which Cl^- is currently being added by this process is sufficiently large, (2) that the addition rate has probably been continuous over long periods of time, and (3) that the Cl^- added is "old" (therefore added to the basin more than 73,000 years ago) rather than recycled "recent" lake Cl^-, then the age calculations for Great Salt Lake presented in this paper are not valid. The absence of evidence for such large salt springs in the other basins, however, suggests that they are related to the very high salt concentration in the present lake and hence contain "recent" salt. Also, the quantity of "old" salt added by this mechanism must be at least comparable in magnitude to that added by fallout in order to balance the safety factor in the present calculation (therefore the "recent" salt lost to the sediments below the lake, lost by deposition on the salt flats, and lost by overflow through Red Rock Pass).

(Flint, personal communication), however, renders such a sequence of events unlikely.

Mono Lake

As in Great Salt Lake, the magnitude of the Cl^- concentration in Mono Lake is consistent with an accumulation period of more than 73,000 years.[3] Desiccation near the end of the last interpluvial period may also be excluded since the present amount of salt greatly exceeds that which could have accumulated in a period of 73,000 years (see $C_0 = 0$ curve, Fig. 9).

Walker Lake

The Cl^- concentration in Walker Lake is much too small to be consistent with a 73,000-year accumulation time and a k value less than 2.0×10^{-4} feet per year. Only if k were nearly 100 times larger than that for Mono or Great Salt Lakes would the present Cl^- concentration be possible. Since there is no reason to expect such a large variation in k from lake to lake, Walter Lake must have desiccated during postpluvial times, and the majority of its salt must remain buried in the sediments beneath the lake. Calculations based on the data in Table 2 show that the present salt concentration represents an accumulation period of about 11,000 years.

Pyramid Lake

The Cl^- concentration in Pyramid Lake is consistent with a 73,000-year accumulation period only if its concentration at the end of the last interpluvial period was far below equilibrium. Since for Mono Lake, which has similar parameters, an equilibrium value for the end of the last interpluvial period is most reasonable, some explanation must be given for the present low Cl^- concentration in Pyramid Lake. The following possibilities exist: (1) postpluvial desiccation followed by partial solution of the deposited salt; (2) complete desiccation near the end of the last interpluvial period; (3) continuous accumulation accompanied by loss of salt to other basins by overflow during pluvial and semipluvial periods; and (4) Huntington's (1925, p. 198) idea that Pyramid Lake was freshened by deposition of salt in the Winnemucca Basin. This process is possible because Lake Winnemucca receives most of its water from the overflow of Pyramid Lake. This supply would be terminated during low-water periods resulting in the desiccation of Lake Winnemucca. From volume data it can be estimated that 15 per cent of the salt in Pyramid Lake would be removed during each such desiccation; thus the process would have to be repeated at regular intervals to be effective in removing salt. The last natural desiccation of Lake Winnemucca is believed to have occurred about 120 years ago (Hardman and Venstrom, 1941, p. 74). The salt data alone cannot be used to distinguish between the four possibilities.

Sensitivity of Ages to Choice of Parameters

In order to demonstrate that the accumulation times are not greatly sensitive to the numerous assumptions made in taking climatic conditions into account, the time estimates given may be compared with those obtained using the simplest model. In this case the ages are computed by dividing the total amount of Cl^- in the present-day lakes by the rate of Cl^- addition to the basin. The following accumulation times are obtained: Great Salt Lake 62,000 years, Mono Lake 460,000 years, Walker Lake 11,000 years, Pyramid Lake 82,000 years. These ages would lead to the same conclusions as those based on the more complex model.

Comparison With Previous Estimates

The age estimates are considerably larger than those given previously. Russell (1885, p. 226) estimated that the salt in Walker Lake was accumulated in less than 500 years; Eardley *et al.*, (1957, p. 1147) estimated that

[3] Feth (1959, Table 2) gives the Na^+/Cl^- ratios in the lakes under discussion. He infers that the deviation in the magnitude of this ratio from unity is an indication of one or more sources of Cl^- other than bedded halite or the oceans. Although the chemistry of Mono Lake is admittedly complex, to suggest from the Na^+/Cl^- ratio alone (2.53) that the lake has received only a small proportion of its Cl^- from the ocean can be demonstrated to be incorrect. It is certainly possible to assume that Na^+ has been derived from both the ocean and solution of sedimentary and/or igneous rocks whereas the Cl^- is largely from the ocean. Indeed as Conway (1942) has already pointed out more than half of the Na^+ in igneous streams is derived from the weathering of silicate minerals. The proportion of "oceanic" to "rock" Na^+ could vary from area to area thus leading to considerable variations in the Na^+/Cl^- ratios in lake waters. Feth's conclusion that since the Na^+/Cl^- varies in the lakes under discussion, another source of Cl^- other than the ocean *must* be assumed is therefore not tenable.

the present rivers could supply an amount of salt equivalent to that in Great Salt Lake and the adjacent salt flats in 5300 years; and Jones (1925, p. 31) concluded that the Cl^- in Pyramid Lake could have accumulated in less than 4000 years. These estimates are based on the assumption that the contemporary compositions of the rivers supplying the lakes provide an adequate estimate of the average rate of salt addition. Whereas Jones (1925, p. 29) restricted his calculations to a single ionic species (Cl^-), Russell used the total salt, neglecting the fact that the chemical composition of the salts in the rivers supplying the lake is different from that of the accumulated salts. Only Eardley and his co-workers recognized the importance of gain and loss of salt by wind transport.

Internal Consistency of Ages

It is important to consider whether the estimates given in this paper are internally consistent. The main problem is to explain the low age for Walker Lake. One possible explanation is that it desiccated in postpluvial times. Evaporation-rate maps (Meyer, 1942, p. 56; Horton, 1943, p. 750) show that Walker Lake lies at the edge of a region of intense aridity. A small northward shift of the present climate pattern would have a much larger effect on Walker Lake than on the other lakes. Also, as shown in Figures 5, 6, and 7, the topography of the present lake floors is such that a much smaller change in climate would be required to reduce Walker Lake to a playa than would be required for either Mono or Pyramid lakes. Great Salt Lake does not fit this pattern, however, since its salt concentration and topography make it more susceptible to desiccation than Walker Lake. Perhaps Great Salt Lake also desiccated and redissolved its salt, whereas the Walker Lake salt deposits were covered with clay, making solution impossible. Russell (1885) has suggested that the narrow, deep profile of Walker Lake would permit such burial, whereas the broad, flat structure of the Great Salt Lake basin would greatly impede complete coverage by river sediment.

As pointed out to the authors by both Antevs and Orr (personal communications), another possible explanation has been given by Jones (1925, p. 46), who suggested that Walker Lake did not exist before Lake Lahontan reached its highest level. Jones postulated that the Walker River was at one time a tributary of the Carson River and flowed northward through an old stream channel which is still evident in Mason Valley and Churchill Canyon. When Lake Lahontan achieved its highest level, it flooded Churchill Canyon and flowed over the topographic barrier, separating Mason Valley from the Walker Lake basin. The gorge cut by the lake during this overflow later became the channel for the present Walker River. If the salt added to the Walker Lake basin during the overflow of Lake Lahontan may be considered negligible, then the time required to accumulate the present amount of salt in the lake should provide an estimate of the date of the highest lake level. It is interesting to note that the Cl^- accumulation age of approximately 11,000 years agrees well with the C^{14} estimate of 11,700 years (*see* Broecker and Orr, 1958, p. 1023).

There is a serious objection to the latter theory however. Russell (1885, pl. XLVI) concluded that Walker Lake achieved the maximum Lake Lahontan level. If this is true, then Walker Lake would have been filled with water of the same salinity as that in the rest of Lake Lahontan. It can then be shown that the amount of Cl^- in Walker Lake immediately after the overflow would have been greater than that present in the lake today.

A possible alternative originally suggested by Antevs (1936) is that the Walker River flowed into the Carson River during a portion of postpluvial times, allowing Walker Lake to desiccate. In this case no extreme climatic conditions would have to be postulated.

It is interesting, however, to estimate the magnitude of the climate change necessary to desiccate Walker Lake. Reduction of Walker Lake to a playa would require a decrease in area of at least a factor of five. Since at its maximum the lake had an area no more than five times its present area, the change in climate necessary to produce desiccation is thus comparable to the change in going from pluvial to interpluvial conditions.

Agreement of Ages with Other Evidence

Biological evidence supports the contrast between the histories of Pyramid and Walker lakes. Two endemnic species, a sucker (*Chasmistes cujus*) and a trout (*Salmo smaragdus*), found in Pyramid Lake attest to its continuous history (Hutchinson, 1937, p. 54).

If the lake had desiccated, these species would have become extinct, as it is generally concluded that they could not live in the Truckee River. On the other hand, no such species have been found in Walker Lake. The biological evidence supports some combination of explanations (2), (3), and (4) given for the low Cl^- concentration in Pyramid Lake and excludes (1), a postpluvial desiccation.

Considerable geological evidence points to a period of warmer and drier climate during postpluvial times. In addition to indirect evidence such as high postpluvial sea levels (Fairbridge, 1958) and "warm" pollen sequences (Zumberge and Potzger, 1956), direct evidence from the Great Basin itself has been presented by Antevs (1955). He cites accumulation of caliche, wind erosion and arroyo cutting, disappearance of permanent ice from the mountains, and breaks in guano accumulation in cave deposits as evidence for greater aridity. Moore (1956, p. 752) suggests that the change from aragonite to calcite deposition in parts of the Great Basin points to warmer climates in the past. Thus the suggested desiccation of Walker Lake in postpluvial times because of climate conditions or diversion of the Walker River is not inconsistent with independent geological evidence.

Conclusions

The following conclusions can be drawn from the present study.

(1) Cl^- ion concentrations provide the most reliable basis for salt chronologies.

(2) Estimates of Cl^- accumulation rates calculated from the present Cl^- concentrations in river waters are maximal. Computations based on rainfall data provide more reliable results.

(3) In salt-balance calculations, loss of salt from the surface of the lake must be considered. This has been shown to be important only when the lakes possess relatively high Cl^- concentrations.

(4) In salt-accumulation time calculations, major climatic variations must be considered.

(5) Provided that the major source of Cl^- is recently recycled oceanic Cl^- it has been shown that Great Salt Lake and Mono Lake have accumulation times dating back to at least the end of the last interpluvial period. There is a strong suggestion that the same is true for Pyramid Lake, but Walker Lake must have desiccated in postpluvial times.

(6) The salt accumulation ages are consistent with each other and also with independent geological and biological evidence.

(7) The desiccation of Walker Lake suggests either a substantially more arid climate than that of today in the Great Basin at some time during the past 10,000 years or a postglacial diversion of the Walker River into the Carson River drainage system.

References Cited

Antevs, Ernst, 1938, Postpluvial climatic variations in the southwest: Am. Meteorol. Soc. Bull., v. 19, p. 190–193

—— 1955, Geologic, climatic dating in the west: Am. Antiquity, v. 20, p. 317–335

Broecker, W. S., and Orr, P. C., 1958, Radiocarbon chronology of Lake Lahontan and Lake Bonneville: Geol. Soc. America Bull., v. 69, p. 1009–1032

Broecker, W. S., Turekian, K. K., and Heezen, B. C., 1958, The relation of deep sea sedimentation rates to variations in climate: Am. Jour. Sci., v. 256, p. 503–517

Clarke, F. W., 1924, The data of geochemistry: 5th edition, U. S. Geol. Survey Bull. 770, 841 p.

Conway, E. J., 1942, Mean geochemical data in relation to oceanic evolution: Royal Irish Acad. Proc., v. 48, p. 119–151

Eardley, A. J., Gvosdetsky, Vasyl, and Marsell, R. E., 1957, Hydrology of Lake Bonneville and sediments and soils of its basin: Geol. Soc. America Bull., v. 68, p. 1141–1202

Emiliani, Cesare, 1955, Pleistocene temperatures: Jour. Geology, v. 63, p. 538–578

Eriksson, Erik, 1952, Composition of atmospheric precipitation: Tellus, v. 4, no. 4, p. 280–303

—— 1955, Airborne salts and the chemical composition of river waters: Tellus, v. 7, p. 243–250

Fairbridge, Rhodes W., 1958, Dating the latest movements of the Quaternary sea level: New York Acad. Sci. Proc., series 2, v. 20, p. 471–482

Feth, J. H., 1959, Re-evaluation of the salt chronology of several Great Basin lakes; A discussion: Geol. Soc. America Bull., v. 70, p. 637–640

Flint, R. F., and Rubin, Meyer, 1955, Radiocarbon dates of pre-Mankato events in eastern and central North America: Science, v. 121, p. 649–658

Gilbert, G. K., 1890, Lake Bonneville: U. S. Geol. Survey Monograph 1, 375 p.

Hardman, George, and Venstrom, Cruz, 1941, A 100-year record of Truckee River runoff estimated from changes in levels and volumes of Pyramid and Winnemucca lakes: Am. Geophys. Union Trans., v. 22, p. 72–90

Horton, Robert E., 1943, Evaporation maps of the United States: Am. Geophys. Union Trans., v. 24, p. 743–753

Huntington, E., 1925, Tree growth and climatic interpretations: Carnegie Inst. Wash. Pub. 352, p. 155–204

Hutchinson, C. Evelyn, 1937, A contribution to the limnology of arid regions, primarily founded on observations made in the Lahontan Basin: Conn. Acad. Arts Sci. Trans., v. 33, p. 47–132

Jones, J. C., 1925, Geologic history of Lake Lahontan: Carnegie Inst. Wash. Pub. 352, p. 3–50

Junge, C. E., and Gustafson, P. E., 1957, On the distribution of sea salt over the United States and its removal by precipitation: Tellus, v. 9, p. 164–173

Libby, W. F., 1954, Chicago radiocarbon dates, V: Science, v. 120, p. 732–742

Meyer, Adolph F., 1942, Evaporation from lakes and reservoirs: St. Paul, Minn. Res. Comm., 110 p.

Moore, George W., 1956, Aragonite speliothems as indicators of paleotemperature: Am. Jour. Sci., v. 254, p. 746–753

Pošepny, F., 1877, Zur Genesis der Salzablagerungen, besonders jener im nordamerikanischen Westen: Sitzunsber. Kais. Akad. D. Wissensch. Wien., v. 76, Abt. 1, p. 179–212

Russell, I. C., 1885, Geological history of Lake Lahontan: U. S. Geol. Survey Monograph, v. 11, 287 p.

—— 1889, Quaternary history of Mono Valley, California: U. S. Geological Survey 8th Ann. Rept., p. 261–394

Thornthwaite, C. W., and Mather, J. R., 1955, The water balance: Climatology, v. 8, Drexel Inst. Tech., 63 p.

U. S. Department of Agriculture, 1936, Atlas of American Agriculture: Washington, U. S. Govt. Printing Office

U. S. Geological Survey, 1955, Quality of surface waters of the United States, 1951, Parts 9–14, Colorado River basin to Pacific slope basins in Oregon and lower Columbia River basin: Water-Supply Paper 1200, 285 p.

—— 1957, Quality of surface waters of the United States, 1952, Parts 9–14, Colorado River basin to Pacific slope basins in Oregon and lower Columbia River basin: Water-Supply Paper 1253, 344 p.

Van Winkle, Walton, 1914, Quality of the surface waters of Oregon: U. S. Geol. Survey Water-Supply Paper 363

Woodcock, A. H., 1953, Salt nuclei in marine air as a function of altitude and wind force: Jour. Meteorology, v. 10, p. 362–371

Zumberge, James H., and Potzger, John E., 1956, Late Wisconsin chronology of the Lake Michigan basin correlated with pollen studies: Geol. Soc. America Bull., v. 67, p. 271–288

LAMONT GEOLOGICAL OBSERVATORY, COLUMBIA UNIVERSITY, PALISADES, NEW YORK;
NATIONAL PHYSICAL LABORATORY, TEDDINGTON, MIDDLESEX, ENGLAND

LAMONT GEOLOGICAL OBSERVATORY CONTRIBUTION NO. 336

MANUSCRIPT RECEIVED BY THE SECRETARY OF THE SOCIETY, JUNE 7, 1958

BULLETIN OF THE GEOLOGICAL SOCIETY OF AMERICA
VOL. 70, PP. 619-636, 3 FIGS., 1 PL. MAY 1959

GEOLOGY OF THE BUFFALO MOUNTAIN-CHEROKEE MOUNTAIN AREA, NORTHEASTERN TENNESSEE

BY RICHARD J. ORDWAY

ABSTRACT

The Buffalo Mountain-Cherokee Mountain area in northeastern Tennessee includes about 45 square miles and is located along the southeast border of the Appalachian Valley and Ridge geomorphic province. The mountainous part of the area is underlain almost entirely by the Buffalo Mountain thrust sheet, which has been separated by two minor thrust faults into three imbricate thrust blocks.

Cambrian and Precambrian (?) rocks in the Buffalo Mountain thrust sheet consist of the Unicoi, Hampton, and Erwin formations (Chilhowee group) and the Shady dolomite. Younger, Cambrian-Ordovician rocks beneath the thrust sheet include the Honaker limestone, Nolichucky shale, Knox dolomite, and Athens shale.

During or following the thrusting, all the rocks in the area were folded into a synclinorium trending northeast-southwest. Some folding apparently preceded the thrusting. Several "shear faults" mapped by Keith in this area do not appear to exist. An interesting feature of the structure is the number of slices that have been broken off and dragged along the thrust surfaces. Slices of younger rocks have been found between older rocks, and slices of older rocks between younger. Cleavage and a low-rank metamorphism are present. Deformation probably occurred in late Paleozoic time during the Appalachian orogeny.

CONTENTS

TEXT

	Page
Introduction	620
Location, size, and topographic features of the area	620
Previous work	621
Present work	621
Acknowledgments	621
Summary of the regional geology	621
Rock formations	621
Regional structure	622
Age of the deformation	623
Description of formations	623
Chilhowee group	623
Introduction	623
Unicoi formation	624
Hampton formation	625
Erwin formation	625
Age and stratigraphic relationships	626
Shady dolomite	626
Honaker limestone	627
Nolichucky shale	627
Knox dolomite	627
Athens shale	627
Geologic structure	628
General statement	628
Thrust blocks	628
Cherokee block	628
Intermediate block	628
Pinnacle block	629
Attitude of the major thrust faults	630
Faults and related structures	630
Canah Hollow minor thrust fault	630
Ashhopper Hollow faults	630
Large Unicoi mass west of Erwin	630
Other fault slices	631
Normal fault at Millstone Creek	631
Tear fault west of Canah Hollow	631
Minor thrust fault at Sinking Creek	632
Drag folds	632
Deformation along the thrust surfaces	632
Warm Cove	632
Cleavage and metamorphism	633
Mechanics of the thrust faulting	633
Terminology	633
Origin of the Buffalo Mountain thrust fault	634
Root zone	634
Minimum net slip and breadth	635
Order of thrusting	635
References cited	635

ILLUSTRATIONS

Figure	Page
1. Index map of northeastern Tennessee	620
2. Stratigraphic section of part of the Chilhowee group along Sinking Creek (north of Horse Cove)	625
3. Diagrams demonstrating that strata in thrust plate were folded before the initiation of the Buffalo Mountain thrust fault	634

Plate	Facing page
1. Geologic map and structure sections of the Buffalo Mountain-Cherokee Mountain area, Tennessee	619

TABLES

Table	Page
1. Generalized section of geologic formations in northeastern Tennessee	622
2. Terminology of Lower Cambrian Chilhowee group	624

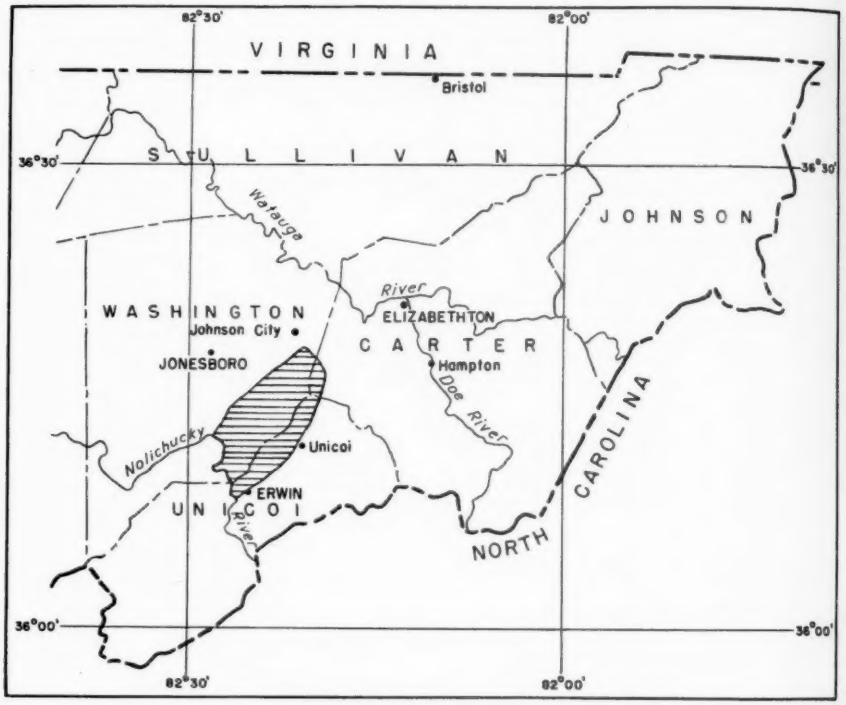

FIGURE 1.—INDEX MAP OF NORTHEASTERN TENNESSEE
(Shaded section is the Buffalo Mountain-Cherokee Mountain area.)

INTRODUCTION

Location, Size, and Topographic Features of the Area

The Buffalo Mountain-Cherokee Mountain area is located in Unicoi, Washington, and Carter counties in northeastern Tennessee along the southeast border of the Appalachian Valley and Ridge geomorphic province (Fig. 1). The main range of the Appalachian Mountains (Blue Ridge) lies a short distance to the southeast. The study area is south of Johnson City and north of Erwin. It is about 10 miles long, 3–5 miles wide, and includes approximately 45 square miles. The Nolichucky River forms a convenient southwestern boundary. Included in this area are Cherokee Mountain, Buffalo Mountain, and a smaller mountainous section west of the south end of Buffalo Mountain. The entire mountainous part of the area, about 30 square miles, is part of the Cherokee National Forest.

Buffalo High Point, a little more than 3520 feet in altitude, is the highest point in the area. The lowest point, 1500 feet, is along the Nolichucky River in the southwest corner of the area. Drainage is southwest into the Nolichucky River, which here flows northwest. The mountainous areas have a thick cover of vegetation, and the courses of most of the creeks support a dense growth of rhododendron.

In the Buffalo Mountain-Cherokee Mountain area, bedrock differences are reflected in the topography. The mountainous area is bordered on the west, north, and east by a lowland underlain by dolomite, limestone, and shale. This mountainous area consists mainly of sedimentary clastic rocks—pebble conglomerate, graywacke, sandstone, quartzite, siltstone, and shale—which have been thrust upon the younger rocks of the Valley and Ridge province. The sedimentary clastic rocks in the thrust sheet crop out southwest of the Nolichucky River beyond the arbitrary southwest limit of this area.

Resistant quartzite beds form the crests of mountains and ridges, and some of them make dip slopes and flatironlike spurs. Some creeks in the mountains follow faults, some follow belts of weaker rocks, and others cut across the strike of weaker and stronger rocks alike. The more resistant beds make small waterfalls in the creeks. Outcrops are well exposed in many creeks. The more resistant quartzite beds make small cliffs and are well exposed on the mountain slopes along their strike. The weaker rocks which make up the greater part of the formations, however, show few outcrops on the mountain sides between the creeks. Numerous road cuts in the area, such as those along Sinking Creek north of Horse Cove, expose the rocks. Briar, Ramsey, and Harris creeks have the best exposures of the Unicoi formation.

As the area has not been glaciated, float rock is useful in mapping, particularly on ridge crests where the float is nearly in place.

Previous Work

Many published reports cover different aspects of the geology of northeastern Tennessee and of the southern Appalachians; some of these are concerned with the Buffalo Mountain-Cherokee Mountain area. Safford (1869) made a comprehensive report on the geography, geology, and mineral resources of Tennessee. Keith (1907) was first to show that the rocks in the Buffalo Mountain-Cherokee Mountain area are part of a great thrust sheet. Keith's descriptions and diagrams of the thrust faults in this area have become classic.

King *et al.* (1944), in studying the manganese prospects at Horse Cove, Warm Cove, and Canah Hollow, made stratigraphic sections and described the geology and structure of northeastern Tennessee; this material has proved to be of great assistance.

A paper by Stose and Stose (1944), including a small-scale map of the Buffalo Mountain-Cherokee Mountain area, is important with respect to the southwest part of the area. Billings (1954, p. 192), Butts *et al.* (1933), Eardley (1951, p. 92), and Rodgers (1953, p. 142) refer to this area or include geologic maps of it.

Present Work

The writer spent about 4½ months in field work in the Buffalo Mountain-Cherokee Mountain area between June and December of 1947. As the structure of the younger rocks underlying the lowland around the mountainous area is uniform, and as a study of these rocks was beyond the scope of this report, most of the field work was concentrated on the sedimentary clastic rocks in the thrust sheet that makes up the mountainous part of the area.

The Buffalo Mountain-Cherokee Mountain area is covered by parts of four adjoining, 7½-minute topographic maps on a scale of 1:24,000, with contour intervals of 20 or 40 feet. These are the Jonesboro, Johnson City, Unicoi, and Erwin quadrangles, covering respectively the northwest, northeast, southeast, and southwest parts of the area. These maps, published by the Tennessee Valley Authority and the U. S. Geological Survey, served as excellent bases for the geologic mapping. An aneroid barometer was used in locating positions in the field.

Acknowledgments

The writer appreciates the co-operation of members of the Tennessee Division of Geology, particularly of Mr. H. B. Burwell, State Geologist in 1947 and Mr. Herman W. Ferguson, Assistant State Geologist in 1947.

Prof. Chester R. Longwell and John Rodgers of Yale University, Dr. Philip B. King of the U. S. Geological Survey, and Herman W. Ferguson visited the writer in the field and were of great assistance in working out field techniques, checking stratigraphic units, and interpreting geologic structures. In addition, they have made many valuable suggestions concerning the manuscript. Their help is gratefully acknowledged.

Miss Jean Lowry worked in an adjoining area and discussed with the writer the problems common to both areas. In addition, Miss Lowry has been kind enough to study and describe 13 thin sections of specimens from the Buffalo Mountain-Cherokee Mountain area.

This report has been written in partial fulfillment of the requirements for the degree of Doctor of Philosophy at Yale University.

Summary of the Regional Geology

Rock Formations

The Buffalo Mountain-Cherokee Mountain area in northeastern Tennessee is underlain by Precambrian(?), Cambrian, and Ordovician sedimentary rocks. Table 1 (after King *et al.*, 1944, p. 9) is a generalized section of geologic formations in northeastern Tennessee.

TABLE 1.—GENERALIZED SECTION OF GEOLOGIC FORMATIONS IN NORTHEASTERN TENNESSEE
(From King *et al.*, 1944, p. 9)

Age	Formation		Character	Thickness (in feet)
Lower Ordovician	Athens shale		Gray to black shale, calcareous below, sandy above	1000–5000
	Knox dolomite		Gray to blue-gray limestone and dolomite, in part cherty; argillaceous seams in lower part	4000
Upper Cambrian	Nolichucky shale		Green calcareous and dolomitic shale, and shaly dolomite	100
	Honaker dolomite		Gray to blue-gray dolomite and limestone, with many silty and shaly laminae	2000
Middle Cambrian	Rome formation		Red shale and siltstone, some green shale, and some dolomite; residual clay contains some manganese deposits	1200–1800
	Shady dolomite		Blue-gray dolomite, white dolomite, ribboned dolomite and limestone; residual clay contains many manganese deposits.	900–1200
Lower Cambrian	Chilhowee group	Erwin formation	White vitreous quartzite, in part containing *Scolithus*, greenish sandy shale and siltstone, some beds of purple ferruginous quartzite	1200–1500
		Hampton formation	Dark-greenish argillaceous shale, sandy shale, and siltstone; some beds of arkosic quartzite, in part containing *Scolithus*	1200–1500
		Unicoi formation	Coarse-grained arkosic quartzite, conglomerate, arkosic sandy shale and siltstone; some beds of amygdaloidal basalt.	2000–5000
	Unconformity			

Regional Structure

In the southern Appalachians the Valley and Ridge geomorphic province corresponds closely to the folded and thrust-faulted structural division of the Appalachian Mountains. Most of this northeast-southwest elongated zone is underlain by limestone, dolomite, and shale, which have been deformed by folds and faults trending northeast. Southeast dips are the rule. Some metamorphism occurred in the southeast part of this division, and the degree of metamorphism increases to the southeast into the main range of the Appalachian Mountains (Blue Ridge).

The mountainous areas along the southeast border of the Valley and Ridge province generally consist of clastic rocks that have been thrust upon younger Cambrian and Ordovician carbonate rocks and shales. At certain places erosion has cut entirely through these thrust sheets, exposing the limestone, dolomite, and shale under them. These exposed areas of younger rocks surrounded by older rocks (windows) are important structural features in northeastern Tennessee.

King *et al.* (1944, p. 11–12) describe the general geology of northeastern Tennessee as follows:

"... [northeastern Tennessee] is characterized by overthrust faults of great linear extent, by many transverse faults, and by subordinate folds. These features contrast with the numerous folds and discontinuous faults of that part of the Appalachian Valley immediately to the northwest.

"... overthrusting has moved thrust sheets composed of great masses of rock for many miles northwestward over other masses of rock. During or shortly after the thrusting, the thrust sheets were folded broadly into a synclinorium to the northwest and an anticlinorium to the southeast...

"Although the deformation of the rocks within the belt has been profound, it has caused comparatively little metamorphism. Schistose structure is absent, and cleavage in the shale and flowage in the limestone and dolomite are uncommon. In general only the incompetent rocks are crumpled and contorted...

"The Bald Mountain thrust sheet, the highest of the series, rode forward on the Bald Mountain overthrust. In the southwest part of the area it forms a partly detached outlier in the synclinorium... [this includes the Buffalo Mountain-Cherokee Mountain area]... The nature of the Bald Mountain thrust sheet was first recognized by Keith..."

Nearly all the rocks in the mountainous section of the Buffalo Mountain-Cherokee Mountain area are part of a single thrust sheet, here named the Buffalo Mountain thrust sheet. It has been subdivided in the Buffalo Mountain-Cherokee Mountain area by two minor thrust faults into three imbricate thrust blocks, called here the Cherokee, Intermediate, and Pinnacle blocks (Pl. 1). These thrust blocks are composed of rocks belonging to the Unicoi, Hampton, and Erwin formations and the Shady dolomite. The Cherokee block forms the northwest part of the mountainous area and is generally a homocline with northeast strikes and southeast dips. The intermediate block includes the southwest parts of Cherokee and Buffalo mountains and the mountainous area between. Its structure is also mainly homoclinal with northeast strikes and southeast dips. The Pinnacle block forms the southeast border of the mountainous area and structurally is a spoon-shaped syncline which trends northeast. The Cherokee block dips beneath both the Intermediate and Pinnacle blocks, and the Intermediate block dips under the Pinnacle block.

Evidence for the existence of thrust faults in the Buffalo Mountain-Cherokee Mountain area consists almost solely in the recognition that older rocks rest upon younger rocks. Most rocks above and below the thrust faults are nearly parallel, although there are some significant divergences.

Age of the Deformation

Ordovician rocks are the youngest affected by the folding and faulting in the Buffalo Mountain-Cherokee Mountain area, but Mississippian formations are involved elsewhere in northeastern Tennessee. This deformation probably occurred during the Appalachian orogeny in the late Paleozoic, but evidence must come from other areas. Butts (1940, p. 504) stated: "At no place from central Pennsylvania to Alabama has a single example of a strong, angular unconformity been seen [in the Paleozoic formations]."

Thus a single orogenic episode may be indicated. The youngest rocks known to be affected are those of the slightly folded Dunkard series in Pennsylvania, which are Permian. However, these strata occur far west of the severely deformed belt in which the youngest beds involved are Middle Pennsylvanian.

Spieker (1956, p. 1775–1780) discussed the diastrophism associated with the Appalachian Mountains in the light of recent discoveries made in Utah relative to the Laramide orogeny. Field work has shown that about 17 episodes of normal faulting, thrusting, and folding occurred in Utah, beginning in the late Jurassic and extending at least through the mid-Cenozoic. According to Spieker, a hypothesis of continuous orogeny fits the available facts as well as the concept of episodic movements. In the light of the great length and diversity demonstrated for the Laramide orogeny, Spieker questioned the assumption that the major folding occurred throughout the Appalachian belt at the same time. The possibility exists that folding and faulting which occurred earlier in the Paleozoic in the Appalachian belt may have been more severe than that which took place after the middle part of the Pennsylvanian period but before the late Triassic.

The Buffalo Mountain-Cherokee Mountain area furnishes little significant evidence in the solution of these problems.

Description of Formations

Chilhowee Group

Introduction.—The Chilhowee group consists of the oldest rocks in the Buffalo Mountain-Cherokee Mountain area. This group is divided into three main units—the Unicoi, Hampton, and Erwin formations— following King *et al.* (1944, p. 28). Other formation names were used previously for these rocks by Keith

(1907). Table 2 (after King *et al.*, 1944) shows this terminology. No correlation was intended between the names in the different columns.

"Unicoi formation", "Hampton shale", and "Erwin quartzite" were generalized rock-unit names used by Keith (1907) in northeastern Tennessee. Hampton and Erwin are towns in or near the Buffalo Mountain-Cherokee Mountain area, and Unicoi is a county in northeastern Tennessee. According to Keith the Unicoi formation consists for the most part of arkose and conglomerate, with some amygdaloidal basalt; the Hampton formation is made up primarily of shaly rocks, and the Erwin mainly of quartzite.

TABLE 2.—TERMINOLOGY OF LOWER CAMBRIAN CHILHOWEE GROUP
(From King *et al.*, 1944, p. 27)

Safford (1869)	Keith (1904; 1905; 1907)	Keith (1903; 1907)	Butts (1940)		King *et al.* (1944)	
	Hesse quartzite					
	Murray slate	Erwin quartzite		Erwin quartzite	Basal clastic group	Erwin formation
Chilhowee sandstone	Nebo quartzite		Chilhowee group			
	Nichols slate	Hampton shale		Hampton shale		Hampton formation
	Cochran conglomerate				(subsequently changed to	
Ocoee conglomerate and slates	Hiwassee slate	Unicoi formation		Unicoi formation	Chilhowee group)	Unicoi formation
	Snowbird formation					

These terms are inadequate to describe accurately the lithology of the Chilhowee group in the Buffalo Mountain-Cherokee Mountain area. Each unit includes sedimentary clastic rocks ranging in grain size from shale to pebble conglomerate, but the coarser clastic rocks are most common in the Unicoi formation. The amount of feldspar decreases upward in the group.

Unicoi formation.—The Unicoi formation is characterized by thin to thick beds of feldspathic sandstone (called arkose by some previous workers), quartzite, and pebble conglomerate, with included basalt, amygdaloidal basalt, and graywacke. Siltstone, and silty, sandy shale are common, however, and beds of vitreous white, gray, and greenish quartzite are present.

The base of the basalt zone, 2500–3000 feet below the top of the Unicoi formation on Buffalo Mountain, subdivides the formation into lower and upper members. The basalt is a fine-grained dull-greenish rock which weathers to red and brown material. Some of the basalt layers are amygdaloidal. They occur in bodies up to 150 feet thick. Briar Creek exposes one basalt layer; Ramsey Creek has two; Ashhopper Hollow (with well-exposed outcrops along the road) shows three; Canah Gap exposes five sheets separated by sedimentary strata; and the road cut just northeast of the mouth of Whaley Brook shows two layers. Elsewhere along the western slope of Buffalo Mountain only one basalt layer was found. Basalt outcrops were not found at each creek along the strike, and outcrops on the mountain slopes are scarce. Therefore, it was not possible to trace the basalt sheets continuously in the field. Probably the basalt occurs in discontinuous, lenticular bodies at nearly the same stratigraphic position; along the strike, in some creeks no basalt sheet is exposed, and in others one to five sheets are exposed.

These basalt sheets probably originated as lava flows and not as sills. Evidence for this origin follows: (1) in some of the outcrops, the top of the basalt body is amygdaloidal, the base is slightly amygdaloidal, and the central portions are nonamygdaloidal; (2) in other outcrops, several amygdaloidal zones occur, indicating several different flow units; (3) there is an indication of vague pillow structure at the base of one of the basalt sheets along the road

northeast of Whaley Brook; (4) chilled zones are lacking along both contacts, and none of the wall rock shows signs of alteration; (5) no apophyses were found extending into the wall rock.

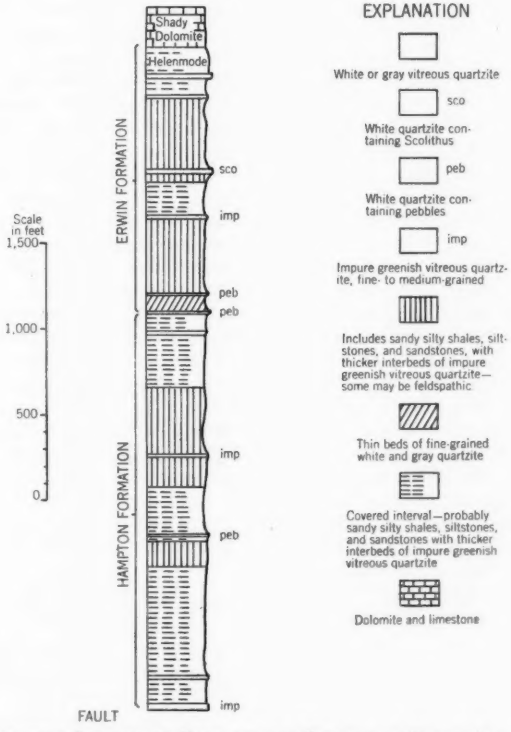

FIGURE 2.—STRATIGRAPHIC SECTION OF PART OF THE CHILHOWEE GROUP ALONG SINKING CREEK (NORTH OF HORSE COVE)

Amygdules consist of quartz, calcite, and chlorite. The chlorite occurs in irregularly shaped patches and in ribbonlike strips half an inch by 2–3 inches. Perhaps these chlorite ribbons represent original chlorite amygdules which were smeared out during the deformation.

Hampton formation.—The Hampton formation (Fig. 2) consists of thin beds of sandy and silty shale, siltstone, and sandstone, with some feldspathic quartzite and fine pebble-conglomerate beds near the base and beds of vitreous white quartzite and medium-grained impure greenish quartzite throughout the formation.

Erwin formation.—The Erwin formation is characterized by medium to thick beds of vitreous white quartzite, but the greater part of the formation consists of sandy shale, silty shale, siltstone, sandstone, and impure greenish vitreous quartzite.

The Helenmode member at the top of the Erwin formation is about 150 feet thick (estimated) at Sinking Creek. Most of this member seems to consist of thin-bedded fine-grained clastic rocks—sandy shale, siltstone, sandstone, and fine-grained quartzite. Considerable detrital mica is present in some beds. These rocks appear somewhat darker than the average rock in the Chilhowee group.

Two small areas underlain by the Helenmode member occur in structural basins on different ridges at altitudes of approximately 2440 feet in the southwest synclinal part of the Cherokee block. No outcrops were seen, but pieces of dark coarse sandstone, containing well-rounded quartz grains cemented with iron and man-

ganese, occur as float above the upper quartzite zone near the top of the Erwin formation. This resistant cliff-making quartzite zone was traced on each ridge around the circumferences of the basins. Three small pits have been dug in search of manganese in these two basins. Red soil is present in each basin, and quartz dolocasts and manganese pellets have been reported (King *et al.*, 1944, p. 271). These may indicate a small mass of residuum representing the Shady dolomite in the center of each basin, but the writer did not see any dolocasts, and the evidence is considered insufficient to warrant mapping of Shady dolomite in these basins.

Age and stratigraphic relationships.—The same rock types occur in all three units, so that it is difficult to assign outcrops to the proper formation in the field. The coarse-grained feldspathic quartzite, pebble conglomerate, and basalt of the Unicoi formation, and the white quartzite beds near the top of the Erwin formation, however, are easily distinguished. Therefore, rock types as observed in the outcrops, rather than formational units were mapped in the field. Boundaries between formations were selected at either the bottom or the top of resistant, mappable quartzites which could be traced over considerable distances in the field. These units conform as nearly as possible to equivalent units described elsewhere in northeastern Tennessee (King *et al.*, 1944), but the formation boundaries may not be located at exactly the same horizons in the stratigraphic section in each block.

The Chilhowee group in the Buffalo Mountain-Cherokee Mountain area appears to have a total thickness of about 8000 feet, and the base of the Unicoi formation is not exposed. This total is apportioned approximately among the different units as follows:

Thickness in Feet	
1550–1550	Erwin formation
2700–3000	Hampton formation
2500–3000	Unicoi formation above the base of the basalt zone
1000–1000	Unicoi formation below the base of the basalt zone
7750–8550	Total thickness estimated for the Chilhowee group

The Chilhowee group comprises an apparently conformable sequence of sedimentary clastic rocks which lie conformably beneath the Lower Cambrian Shady dolomite. The worm tube, *Scolithus*, is the only fossil that has been found within the group in this area. According to Butts (1940, p. 40) the Erwin formation has yielded very few fossils, including species of *Olenellus*, *Hyolithes*, and *Obolella*, which are Early Cambrian. Therefore, evidence for the Early Cambrian age of the Chilhowee group consists of Lower Cambrian fossils in the Erwin formation and the overlying Shady dolomite. Because the sequence as a whole is conformable, the Hampton and Unicoi formations were also assigned to the Lower Cambrian until recently. The lower part of the Chilhowee group, however, may be Precambrian (Snyder, 1947, p. 146–152). According to King *et al.* (1958, p. 964), the U. S. Geological Survey now restricts beds classed as Cambrian to those for which paleontological data are available. The Chilhowee group as a whole is classed as Cambrian and Precambrian (?).

The formation names used by Keith (1907)—Snowbird, Hiwassee, Cochran, Nichols, Nebo, Murray, and Hesse—are based on localities many miles southwest of this area. Correlation between the units in these areas and in the Buffalo Mountain-Cherokee Mountain area is uncertain. Therefore, it seems best to use local names in this area.

Shady Dolomite

In Stony Creek Valley, 20 miles northeast of Unicoi village, the Shady dolomite is about 1150 feet thick and has been subdivided into the lower white, lower blue, ribboned, middle blue, upper white, and upper blue units (King *et al.*, 1944, p. 18–19).

In the Buffalo Mountain-Cherokee Mountain area, two places are underlain by Shady dolomite—Horse Cove and Canah Hollow. No outcrops of Shady dolomite were seen in Horse Cove, which is 2 miles north of Buffalo High Point, but the surface of the cove is covered by a red soil containing jasperoid and quartz dolocasts, which are indicative of the Shady dolomite. The Horse Cove manganese prospect is situated at an altitude of about 2540 feet on a bench at the northwest end of the cove. Five trenches made by the Metals Reserve Company in 1943 exposed barren waddy clay and brown residual clay beneath the surface soil (King *et al.*, 1944, p. 270). Some manganese nodules were found, but not enough to warrant further work. The Shady dolomite in Horse Cove occurs in the Cherokee thrust block stratigraphically above the Helenmode member of the southeast-dipping Erwin formation. The southeast border

of the cove is formed by rocks of the Unicoi formation. These are in the Pinnacle thrust block.

The Shady dolomite is well exposed in Canah Hollow, and the upper four units have been recognized. The rocks are considered to be part of the Intermediate block. They dip beneath the Pinnacle block and are folded into the same northwest-plunging syncline as the adjoining rocks of the Pinnacle block.

On the ridge east of Canah Hollow, the Shady dolomite has been cut by a minor thrust fault in such a way that a part of the sequence has been repeated. The thrust fault is followed by a small slice of rocks belonging to the Unicoi formation.

Folding of the Shady dolomite in Canah Hollow has made accurate calculations of thicknesses difficult, but about 750 feet seems to be exposed. The middle and upper blue units consist of light-blue-gray to dark-blue-gray dolomite, in thin to thick beds, with some thin beds of silty well-laminated dolomite. Lenses and nodules of light-gray-black chalcedonic chert were found in the upper blue unit.

Some grayish and light-bluish dolomites occur in the upper white unit, which is predominately white laminated or massive dolomite. The ribboned dolomite unit consists of medium-grained dark-blue-gray dolomite with bands, blebs, and small lenses of white and pink coarsely crystalline dolomite. Some silty well-laminated blue-gray dolomite and some limestone occur in the ribboned unit.

The Rome formation, which in many places overlies the Shady dolomite, does not crop out in the Buffalo Mountain-Cherokee Mountain area.

Honaker Limestone

The Honaker limestone crops out along the east margin of the Buffalo Mountain-Cherokee Mountain area. Throughout much of this belt, the beds are vertical or overturned and dip steeply southeast. Much of the formation consists of dark-blue limestone with numerous distinct tan-brown silty laminae, which show on weathered surfaces. Fresh surfaces show massive blue limestone with only faint laminae.

Nolichucky Shale

In the Buffalo Mountain-Cherokee Mountain area the Nolichucky shale appears to be less than 100 feet thick and to form an outcrop paralleling the northwest margin of the belt of Honaker limestone. Throughout most of this belt the Nolichucky shale seems to be overturned and to dip steeply southeast. It separates the Honaker limestone below from the Knox dolomite above. The few outcrops expose weathered and fractured brownish shale. No limestone was seen. Cleavage, bedding, and joints break the shale into small chips. No fossils were found.

Knox Dolomite

The Knox dolomite forms a broad belt of outcrop in the Buffalo Mountain-Cherokee Mountain area, but the formation was not studied in detail. Typically the rocks are dark-blue dolomite and limestone, both massive and thin-bedded, with numerous tan-brown silty laminae, but some lighter-blue and buff limestone, and dolomite occur. Calcite veinlets are present in places. Grayish-black chert nodules and masses are abundant at certain horizons. Weathered surfaces are light gray to pale blue.

Lenses, beds, and irregular small masses of well-rounded quartz grains are present in certain parts of the Knox dolomite. Sedimentary breccias and conglomerates of limestone fragments in a limestone matrix form beds about a foot thick.

Elsewhere in eastern Tennessee the Lenoir or Mosheim limestones of early Middle Ordovician age intervene between the Knox dolomite and Athens shale. However, if these limestones are present in the Buffalo Mountain-Cherokee Mountain area, they were not distinguished from the upper Knox.

Athens Shale

The Athens shale crops out in two places in the area, just northwest of the Buffalo Mountain thrust fault on the northwest side of Cherokee Mountain. A third possible outcrop is at the head of Hootowl Hollow between Round Knob and White Rock, where a considerable amount of shaly float occurs above the highest Knox outcrops and below the lowest outcrop of quartzite in the Unicoi formation; as no outcrops were found, the formation was not mapped here. Small weathered chips of Athens shale are difficult to distinguish from small weathered pieces of the finer-grained rocks of the Chilhowee group.

In this area the Athens is bluish-black and black thin-bedded shale, which is crumpled in places and appears to have considerable chlorite. Cleavage is well developed. No fossils were found.

Geologic Structure

General Statement

The mountainous part of the Buffalo Mountain-Cherokee Mountain area is underlain almost entirely by the Buffalo Mountain thrust sheet, which has been separated by two minor thrust faults into three imbricate thrust blocks—the Cherokee, Intermediate, and Pinnacle blocks. The older rocks in the Buffalo Mountain thrust sheet have been thrust to the northwest relative to the younger rocks exposed in the lowland around the mountains. The Buffalo Mountain thrust sheet is composed of rocks belonging to the Unicoi, Hampton, and Erwin formations, and the Shady dolomite. The rocks beneath the thrust sheet include the Honaker limestone, Nolichucky shale, Knox dolomite, and the Athens shale. Strata above and below the thrust faults are commonly almost parallel. The thrust sheet and the underlying rocks were folded together, either during or shortly after the thrusting, into a synclinorium involving the whole area. The axis of this synclinorium trends northeast.

In this report the fault that forms the outer boundary of the mountainous area is called the Buffalo Mountain thrust fault. It extends from the Nolichucky River northeastward along the northwest slope of Cherokee Mountain to Round Knob and White Rock and thence southwestward along the southeast slope of Buffalo Mountain to the Nolichucky River. According to this interpretation the major thrust fault extends under each of the three thrust blocks in the area, but major movement may also have occurred along the thrust fault separating the Cherokee and Pinnacle blocks.

Thrust Blocks

Cherokee block.—The Cherokee block extends northeastward from Cherokee Knob to White Rock and Round Knob. Synclines occur at each end of the block, but in most of it the rocks form a homocline that strikes northeast and dips moderately southeast beneath the Pinnacle and Intermediate blocks. The Shady dolomite in Horse Cove is the youngest rock formation in the Cherokee block.

Intermediate block.—The Intermediate block extends southward from the vicinity of Cherokee Knob to the Nolichucky River and beyond. The main structure within the block is homoclinal with a northeast strike and gentle to moderate southeast dip, but the north end of the block forms a syncline and rests upon the crumpled, folded southwest end of the Cherokee block. The Shady dolomite in Canah Hollow is the youngest formation in this thrust block. Rocks in the Intermediate block dip under those in the Pinnacle block.

The divergence of strikes and dips in adjacent portions of the Pinnacle and Intermediate blocks has been interpreted as a thrust fault by Keith (1907) and as an unconformity by Stose and Stose (1944). As the contact between the two blocks is not exposed, the interpretation must rest mainly on identification of the units in the Intermediate block. These were interpreted as part of the Chilhowee Group by Keith but as part of a late Precambrian series (Ocoee) by Stose and Stose. Evidence available to the writer supports Keith's interpretation.

Rocks in the Intermediate block appear to form a conformable sequence. Lithologically they correspond closely to the Unicoi, Hampton, and Erwin formations and the Shady dolomite as exposed in the Cherokee and Pinnacle blocks and as described elsewhere in northeastern Tennessee. Above the fault along the northwest edge of the Intermediate block are coarse-grained clastic rocks with layers of feldspathic pebble conglomerate. At the top of this sequence is a ridge-making thick-bedded vitreous white quartzite about 40 feet thick, which is feldspathic at its base. This white quartzite is well exposed at the Nolichucky River and for 2½ miles along its strike to the northeast, where it forms big outcrops along ridge crests and at Dry Creek. This sequence closely resembles the upper part of the Unicoi formation. Above it is about 3000 feet of thin-bedded fine-grained sedimentary clastic rocks, which seem typical of the Hampton formation. Above this to the southeast, the Erwin formation is represented by approximately 1550 feet of beds, with a vitreous white quartzite at its base, purplish ferruginous quartzite in the lower part, two ridge-making thick-bedded vitreous white quartzites in the upper part, and typical Helenmode sandstone float at the top. The Shady dolomite in Canah Hollow overlies the Erwin formation. An erosional remnant of the overlying Pinnacle block occurs between the Erwin formation and Shady dolomite in a small syncline just west of Canah Hollow. It is not known whether the Canah Gap area is underlain by rocks belonging to this erosional remnant of the Pinnacle block (Pl. 1) or by the Shady dolomite.

According to Stose and Stose (1944, p. 404):

"These Ocoee rocks differ from Lower Cambrian rocks in the following particulars: the basal beds

are black quartzite and black slate, while the basal Lower Cambrian is composed of crumbly coarse-grained arkose and thin layers of soft argillite. They lack the basalt flows which are characteristic of the Lower Cambrian Unicoi formation . . . Because the white quartzites at the top are not well-bedded, are lenticular, and relatively thin, and are separated by beds of arkose and argillite, they do not form long continuous ridges, which is the characteristic topographic expression of the thick well-bedded quartzites of the Lower Cambrian."

Dark quartzites with glassy black quartz grains have been seen in the Chilhowee group in the Pinnacle block. Therefore, the few dark quartzites in the Intermediate block cannot be used as evidence that these rocks belong to the Ocoee series. As only the upper part of the Unicoi formation is exposed in the Intermediate block, the basalt flows could not be present. Graphitic slate occurs along the Nolichucky River near the thrust fault at Stony Point and seems to be limited to the vicinity of this fault.

The white quartzite at the top of the Unicoi formation and the upper white quartzites in the Erwin formation just west of Canah Hollow make prominent outcrops and form continuous ridges until they are cut off by faults.

Dolomite crops out about 3100 feet north of Organ Gap at an altitude of about 2300 feet in a creek that flows westward into Deacon Creek. This mass of dolomite is strong supporting evidence that a thrust fault, not an unconformity, separates the Intermediate and Pinnacle blocks. The mass is interpreted as a fault slice caught along this thrust fault.

Pinnacle block.—The Pinnacle thrust block forms a spoon-shaped syncline elongated northeast-southwest. Only the Unicoi and Hampton formations are represented.

Keith stated (1907, p. 8):

"In the overthrust quartzite mass of Buffalo Mountain the synclinal fold is complicated by numerous shear faults along which the strata have been piled up like gigantic shingles . . . These did not at their roots cause offsets in the main fault outlining the quartzites, although they probably did in their upper portions. Both the main fault and the shear faults are marked by strong curves and have plainly been deformed and folded since their production."

Keith shows four of these "shear faults" in the Pinnacle thrust block as defined in this report. The writer believes that these faults are not present. The quartzite at the top of the Unicoi formation was walked out in the field nearly all the way around the spoon-shaped syncline of the Pinnacle block. It can be traced continuously except in two areas: (1) few outcrops occur about one-third of a mile northwest of Buffalo High Point on one of the headwater branches of Briar Creek; (2) east and southeast of Buffalo High Point this quartzite is not exposed. Lack of outcrops here may result from a facies change along the strike by which this resistant white quartzite changes to less resistant feldspathic quartzite.

As the quartzite at the top of the Unicoi formation can be traced continuously around each end of the Pinnacle block syncline, and as it forms nearly continuous outcrops in between, at least three of Keith's four "shear faults" are eliminated, and strong doubt is cast upon the existence of the fourth. Keith apparently assumed a certain number of resistant quartzites in the Unicoi formation, and wherever more than this number were found in the field, they were interpreted as repetitions by faulting.

Keith mapped several faults cutting and repeating the amygdaloid (basalt) zone. He stated (1907, p. 5) that the amygdaloid was a contemporaneous lava deposited as a sheet upon the conglomerate that constitutes the lower part of the Unicoi formation. Presumably, Keith's faults were intended to explain the presence of more than one basalt flow in certain localities. Field work by the writer shows that the number of basalt flows in the basalt zone ranges from none to five. The facts are better explained by assuming that both basalt flows and quartzites may be lenticular bodies; the number of bodies may differ from place to place.

At three places in the Pinnacle block—at each end of the syncline and part way along the western slope—a thick-bedded ridge-making vitreous white quartzite, feldspathic at its base, crops out continuously for as much as a mile along the strike and then disappears. This lies about 550 feet below the quartzite at the top of the Unicoi formation. Three possible hypotheses explain this disappearance.

(1) One of Keith's "shear faults" is present and has left these remnants of a once-continuous quartzite.

(2) A disconformity may be present, and erosion may have removed part of a once-continuous quartzite. This is supported by the presence of pebble conglomerate float in Sinking Creek at one locality where the thick white quartzite disappears. The largest pebbles in the conglomerate have diameters of about 1 inch. This is a coarser-grained sedimentary rock than any found elsewhere in this part of the area and might represent deposits formed by the

agent which caused erosion of the quartzite. However, no disconformity has been recorded in this part of the Chilhowee group in northeastern Tennessee.

(3) The quartzite layer may occur in lenticular bodies and may not have originally formed a continuous layer. Each of these explanations seems inadequate.

Attitude of the Major Thrust Faults

Along the northwest slope of Cherokee Mountain, rocks of the Chilhowee group above the Buffalo Mountain thrust fault dip approximately 10°–20° more steeply southeastward than the Knox dolomite beneath the fault. Probably some folding occurred before the thrusting, and the thrust cut diagonally across a fold.

At the north end of the area at Round Knob, the Buffalo Mountain thrust fault dips about 35° south. Along the east slope of Buffalo Mountain, this fault dips gently west. To the southwest, however, this westward dip gradually steepens and becomes nearly vertical, and probably the fault is overturned. For much of this distance the younger rocks beneath the Buffalo Mountain thrust sheet (Knox dolomite, Nolichucky shale, and Honaker limestone) are overturned and dip steeply southeast.

The thrust fault separating the Intermediate and Pinnacle blocks dips east at a gentle to moderate angle. Along Straight Creek, Horse Cove, and Basil Hollow, the fault separating the Cherokee and Pinnacle blocks dips 20°–50° southeast.

Faults and Related Structures

Canah Hollow minor thrust fault.—On the ridge east of Canah Hollow some of the Shady dolomite has been repeated by a minor thrust fault cut off at each end by larger thrust faults. The Shady dolomite at Canah Hollow is part of the Intermediate block, but structurally it forms the southwest end of the spoon-shaped syncline of the Pinnacle block. Northward and up the hill from the intersection at Canah Hollow of the power line and the John Sevier Highway, the following sequence of rock units is found: upper white unit of the Shady dolomite, upper blue unit, the thrust fault, and then successively upward the ribboned, middle blue, upper white, and upper blue units of the Shady dolomite.

A small slice of rocks belonging to the Unicoi formation occurs at an altitude of about 2280 feet on the crest of the ridge east of Canah Hollow. This slice is along the fault that repeats parts of the Shady dolomite. It is about 400 feet long and as much as 40 feet thick. It includes coarse-grained feldspathic quartzite and finer-grained clastic rocks that show considerable jointing and fracturing. Thus a small mass of older rocks has been dragged along a fault and left so that younger rocks now occur above and below it.

This feature is difficult to explain structurally; possibly the strata were broadly arched and then a thrust fault developed across this arch at a low angle; or an anticline might have formed, become overturned, and then been broken and developed into the thrust fault. As the upper block moved forward relative to the underlying block, a small slice of older rocks in the core of the arch could have been dragged along this fault and left in a position which would allow any combination of younger rocks above and below it.

Ashhopper Hollow faults.—At Ashhopper Hollow a large slice of rocks in the Unicoi formation has apparently been dragged along between two minor thrust faults. These thrusts are cut off to the southeast by the Buffalo Mountain thrust fault, and to the north they intersect and die out. Movement along these faults was probably not great. The irregularities in the strikes and dips of these rocks are explained best by faults. The zone containing the basalt sheets apparently has been repeated—one outcrop of the zone is located at Canah Hollow and the other at Ashhopper Hollow. As the dips here are consistently to the northeast, the basalt zone seems to have been repeated, and thrust faulting appears to fit the available facts best.

Another interpretation might assume a nearly recumbent anticline with all the rocks in Ashhopper Hollow in the lower limb and overturned to the west. This is improbable, as there is no evidence of overturning, and as the strikes and dips do not support it.

Large Unicoi mass west of Erwin.—In the south corner of the Buffalo Mountain-Cherokee Mountain area, a large mass of rocks belonging to the Unicoi formation crops out southeast of Garland Cemetery and the John Sevier Highway, southwest of Canah School, and west of Erwin. These rocks strike northeast and, with one local exception, dip steeply northwest beneath the Shady dolomite of Canah Hollow. It is not known whether these rocks belong to the upper or lower member of the Unicoi formation.

They lie between the Shady dolomite of Canah Hollow and the Honaker limestone in Greasy Cove outside the Buffalo Mountain thrust sheet. Two interpretations of the structure of this mass of Unicoi rocks seem possible. According to the first, this mass of Unicoi rocks may be part of the Pinnacle block and belong in the lower member of the Unicoi formation. In this interpretation, the main Buffalo Mountain thrust fault forms the east boundary of the block. The imbricate thrust fault separating the Intermediate and Pinnacle blocks forms the west boundary of the mass, dips southeast beneath the mass, and intersects the Buffalo Mountain thrust fault. Thus the structure is similar to that of the mass of rocks belonging to the lower member of the Unicoi formation west of Canah Hollow (Pl. 1), and both masses of this lower member of the Unicoi formation are underlain by the same thrust fault. Structure section *D-D'* (Pl. 1, interpretation 1) shows this hypothesis. The second possible interpretation considers this mass of Unicoi rocks as a large slice caught between the Buffalo Mountain thrust fault and the Intermediate block. Structure section *D-D'* (Pl. 1, interpretation 2) shows this hypothesis. Older rocks in the slice have been dragged along the fault and now have younger rocks above and below them.

The first interpretation—that this mass of Unicoi rocks is part of the Pinnacle block—is mechanically more simple, perhaps, than the second interpretation of a large slice, but the writer believes that the facts fit the second interpretation better. Outside the map area south of Garland Cemetery and the Nolichucky River, the faults extending southward along the east and west sides of Canah Hollow intersect. The sharp angle of intersection does not suggest the looping of a single fault around the margins of a thrust plate that has been folded and partially dissected by erosion. If this mass of Unicoi rocks were part of the Pinnacle block, in order to pass beneath this mass, the underlying thrust fault would have had to be warped an implausible amount between the south end of the Pinnacle block proper and the north end of the mass in question.

Other fault slices.—Beneath the Pinnacle block are a number of small masses of limestone and dolomite that have been dragged along the fault and now occur as slices of younger rocks with older rocks above and below. Eight of these slices have been found, five between Haynes Knob and Horse Cove, one just north and one just south of Briar Creek, and one about half a mile north of Organ Gap. The two slices near Briar Creek are the largest and are dark blue and buff limestone, with subordinate dolomite. All eight slices are mapped as unknown limestone or dolomite. As the Pinnacle block rode forward (relatively) over the Honaker limestone and Knox dolomite, in addition to the Shady dolomite in the Cherokee and Intermediate blocks, small bodies of any of these units could have been broken off and dragged along beneath the thrust sheet. The slice half a mile north of Organ Gap occurs between the Intermediate and Pinnacle blocks; the other seven slices occur between the Cherokee and Pinnacle blocks.

Slices of older rocks occur between younger rocks, and slices of younger rocks occur between older ones. Probably other slices are present along the thrust faults in the area, but it would be almost impossible to recognize them in the field unless rocks other than the Chilhowee group were involved, or unless the slices were sufficiently large to be structurally evident.

Normal fault at Millstone Creek.—The white quartzite at the top of the Unicoi formation in the Intermediate block has been offset by a minor fault at the Nolichucky River near the mouth of Millstone Creek. The structure is interpreted as a steeply dipping normal fault striking N. 20°–30° E. with the western side downthrown. Slickensides indicate that the latest movement along the fault conforms to this interpretation. The white quartzite is well exposed on both sides of the fault, and the outcrop is offset (Pl. 1).

Tear fault west of Canah Hollow.—In the Intermediate block west of Canah Hollow, two ridge-making vitreous white quartzites occur stratigraphically beneath the Helenmode member of the Erwin formation and are terminated abruptly to the southwest about half a mile north-northeast of Stony Point. These two quartzites make conspicuous outcrops along their strikes to the southwest and then disappear abruptly. Dips change southward from 50° to the southeast to 90° near their southwest ends, where the quartzites show considerable jointing and fracturing. Apparently these two quartzites have been cut off at their southwest ends by a vertical tear fault that strikes about north. Rocks on the east side of the fault have been shoved northward relative to the rocks on the west side. Apparently the contact between the Hampton and Erwin formations is also offset along this fault. East of the fault, rocks strike northeast and are vertical; west of

the fault, strikes are north-northwest, and dips are 25°–30° east.

Another possible interpretation is that these two quartzites lens out along their strikes to the southwest. It seems unlikely, however, that both quartzites would lens out abruptly at the same place. The tear-fault interpretation is supported by the changes in strikes and dips on each side of the fault, although there are local exceptions, and by the pronounced fracturing of the quartzite near the fault.

No evidence has been found to indicate whether or not this tear fault affects the lower member of the Unicoi formation in the synclinal remnant of the Pinnacle thrust sheet west of Canah Hollow. On Plate 1 the tear fault does not cut this body of rocks.

Minor thrust fault at Sinking Creek.—Southward from the Lone Oak Church at Sinking Creek, the following sequence is found: Knox dolomite, Athens shale, Knox dolomite, and finally, the Hampton formation in the Cherokee block. These rocks strike about N. 50°–60° E. and dip 30°–50° southeast, except the rocks in the Hampton formation, which dip about 80° southeast at the fault. Therefore, the mass of Knox dolomite above the Athens shale seems to have reached its present location by faulting. On Plate 1 a small thrust fault forms the southeast boundary of the Athens shale. This fault dies out in the Knox dolomite to the northeast and is cut off or overridden by the Cherokee block to the southwest. Although this fault was not observed in the field in the Knox dolomite northeast of the last outcrop of the Athens shale northeast of Sinking Creek, the dolomite at this locality is folded and somewhat brecciated.

Drag folds.—Small drag folds in the Buffalo Mountain-Cherokee Mountain area indicate a relative movement of the upper block to the northwest. Drag folds have been found in rocks just beneath the faults under both the Intermediate and Pinnacle blocks. Similar drag folds have been found in rocks in the Intermediate and Pinnacle blocks.

Deformation along the thrust surfaces.—The imbricate thrust fault between the Intermediate and Pinnacle blocks is exposed at two places at an altitude of about 2280 feet on the east side of Canah Hollow near its head. Deformation of the rocks above and below this fault is surprisingly small. The thrust fault strikes N. 20°–25° E. and dips 25°–45° southeast. Some brecciation and recrystallization has occurred along the thrust surface, silica has been added to the Shady dolomite beneath the fault, and a calcareous cement has been added to the quartzite in the Unicoi formation above the fault. A zone of pulverized rock 2–6 inches thick occurs along the fault.

According to Miss Jean Lowry, a thin section of Shady dolomite from a foot below this imbricate thrust fault at Canah Hollow consists of dolomite in a fine-grained ground mass and coarser-grained calcite in veins (80 per cent); quartz in veinlets and as scattered angular grains, badly strained (20 per cent); and traces of hematite (specularite ?), pyrite, and zircon. Finely brecciated areas are present, and younger calcite veins cut and offset the quartz veins and cut across the brecciated areas.

The rock seems to show the following history. The dolomite was badly shattered; the cracks were filled with quartz; more deformation granulated the quartz veinlets and brecciated parts of them and the surrounding dolomite; hydrothermal solutions then deposited pyrite, hematite, and quartz in that order; later deformation opened more cracks which were filled by calcite. Thus three pulses of deformation seem to be recorded in this rock. Perhaps the first two pulses were movements along the thrust fault, and the third pulse the folding that followed the thrusting.

At other places in the Buffalo Mountain-Cherokee Mountain area, outcrops within a few feet of the thrust faults show little deformation either above or below the faults. It is difficult to realize that a major thrust fault separates these rocks, which appear to be conformable.

The thrust faults probably originated far beneath the surface, since rocks in the Unicoi formation have been thrust over the Athens shale, and this involves a stratigraphic throw of 3–4 miles. It is difficult to reconcile the surprisingly small amount of deformation along the fault surfaces with the enormous stresses that must be involved in movement at this depth, but it is not known how much rock was eroded from the area of the thrust plate before or during thrusting. The entire stratigraphic section, up to and including the Athens shale, may not have been moved in the plate. But if the thrust fault were near the surface, it would seem logical to expect much more fracturing and brecciation than is present either in the thrust plate or in the rocks beneath the thrust sheet.

Warm Cove.—Warm Cove is about 5 miles north of Erwin (east of Cherokee Knob in the vicinity of Buchanan School) and has been mapped by Keith (1907) and by King *et al.* (1944) as a window in the Buffalo Mountain

thrust sheet underlain by Knox dolomite. Warm Cove was mapped by Stose and Stose (1944) as a part of the thrust sheet and as underlain by Shady dolomite.

Warm Cove is a triangular area bounded on the northwest by the Cherokee block, on the east by the Pinnacle block, and on the southwest by the Intermediate block. Limestone and dolomite outcrops are well developed along the east and southwest margins of the cove. Most of the outcrops consist of fine-grained dark-blue limestone, some of which is banded, with subordinate amounts of buff limestone and dolomite. These rocks resemble the Knox dolomite on the northwest side of Cherokee Mountain.

Along the southwest border of the cove, these calcareous rocks strike northwest and dip southwest underneath the Intermediate block; on the east side of the cove, they strike north-northeast and dip to the east under the Pinnacle block. This structure shows a doming of the rocks in the cove.

At the southwest corner of Warm Cove just south of Cherokee Knob, erosion has cut through the overlying Intermediate block and exposed the calcareous rocks beneath, so that there is a continuous outcrop from the limestone and dolomite in the cove to the Knox dolomite west of the cove. This proves that Warm Cove is a window (almost complete), underlain by the Knox dolomite.

Cleavage and Metamorphism

Cleavage is present in the rocks of the southeast part of the Buffalo Mountain-Cherokee Mountain area. None was seen in the Cherokee block. In the Pinnacle block, cleavage is present in a belt that includes the southeast slope, crest, and upper part of the northwest slope of Buffalo Mountain and extends northeastward from the Nolichucky River to an irregular boundary a mile or more northeast of Buffalo High Point. Cleavage occurs also in the south part of the Intermediate block west of Canah Hollow.

The cleavage increases in prominence to the southeast but not uniformly. Cleavage is not present in all the strata within the belt. It tends to occur only in the thinner-bedded finer-grained darker strata, but it is not present everywhere even in these beds. Commonly in the coarser-grained beds, a joint set will correspond in strike and dip to the cleavage in the finer-grained strata.

Where the cleavage is best developed, it consists of closely spaced nearly parallel surfaces about an eighth of an inch or more apart. These appear to be closely spaced joints and might be called fracture cleavage.

Cleavage commonly strikes about northeast and dips 25°–70° southeast, most of the dips ranging from 40°–60°. Cleavage occurs in both the Intermediate and Pinnacle blocks and in both limbs of the spoon-shaped syncline in the Pinnacle block. As the cleavage has a consistent northeast strike and southeast dip, it probably originated from application of the same set of forces and was formed after the thrusting and folding as one of the last results of the deformation.

In a thin section from an outcrop about 4400 feet west-southwest of Laughran Chapel on the southeast slope of Buffalo Mountain, bedding and cleavage are nearly perpendicular. According to Miss Lowry, sericite is oriented parallel to and along the cleavage surfaces, primarily in the finer-grained laminae. All the sericite shows this orientation, but sericite makes up only a small percentage of the mineral content in the rock. Chlorite is oriented parallel to the bedding planes.

A low-rank metamorphism is present in the Buffalo Mountain-Cherokee Mountain area. In the belt that shows cleavage in the southeast part of the area, some of the shale has been metamorphosed to slate. Most of the quartzite is metaquartzite, as individual grains show sutured contacts.

Thin sections of quartzite, graywacke, and sandstone from the Chilhowee group in each of the three thrust blocks were examined by Miss Lowry, and all show that the original cement (normally argillaceous) has been replaced by sericite and chlorite.

Mechanics of the Thrust Faulting

Terminology.—The Buffalo Mountain thrust fault has been called a "shear thrust", a "folded initial shear thrust", and an "overthrust". "Shear" has been used in the popular sense of rupture caused by shearing stresses, but as nearly all faults probably result from shearing stresses, it is not considered correct to call any one kind of fault a shear fault. The term "overthrust" implies that the hanging wall was the active element. Determination of the active fault block or the actual amounts of movement of each block is difficult on any fault and probably impossible on the Buffalo Mountain fault. The term "thrust fault" is used here for a low-angle large-scale reverse fault.

Origin of the Buffalo Mountain thrust fault.—Keith (1907, p. 8) stated that

> "... at no point is there indication of association of the fault [Buffalo Mountain thrust fault] with an anticline, but its plane was due to a shear passing at a low angle through the formations in succession."

plate. Toward the northwest the Buffalo Mountain thrust fault moves upward in the stratigraphic section in rocks beneath the thrust plate, so that younger rocks are encountered successively toward the northwest. Probably these strata were about horizontal at the time of thrusting.

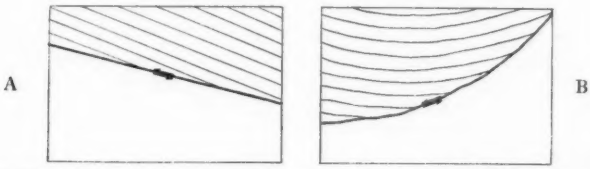

FIGURE 3.—DIAGRAMS DEMONSTRATING THAT STRATA IN THE THRUST PLATE WERE FOLDED BEFORE THE INITIATION OF THE BUFFALO MOUNTAIN THRUST FAULT

A shows strata before folding of thrust surface; *B* shows strata after folding of thrust surface.

The writer believes that the Buffalo Mountain thrust fault developed across folded or tilted strata, as shown by the manner in which the strata above and below the fault surface are beveled.

Structure section *B-B'* (Pl. 1) shows that the strata in the thrust plate have been beveled in such a manner that the thrust surface cuts downward through the stratigraphic section toward the northwest—successively older rocks are encountered along the base of the thrust plate as the thrust surface is followed northwest. Structure sections *C-C'*, *D-D'*, and *E-E'* (Pl. 1) also show this type of beveling.

Along the Buffalo Mountain thrust fault the upper block was thrust relatively northwest. The root zone for the thrust sheet is toward the southeast. The initial dip of the thrust surface was probably at a gentle southeast angle. The northwest dip of this fault surface along the southeast slope of Buffalo Mountain is due to later folding.

Figure 3*A* illustrates a possible explanation of the occurrence of successively older rocks toward the northwest along the base of the Buffalo Mountain thrust plate. The sedimentary rocks are assumed to have dipped at a moderate angle to the southeast before the faulting. The thrust surface developed across these tilted strata with a more gentle dip to the southeast, so that the thrust surface cut across successively older rocks toward the northwest. Figure 3*B* shows the configuration of the thrust surface after folding.

The structure sections show that the strata beneath the thrust plate were beveled at an angle different from that within the thrust

The Buffalo Mountain thrust fault may have originated by compression along a northwest-southeast axis, which developed an arch in the Lower Cambrian formations southeast of the present position of the thrust plate. With continued compression this arch overturned to the northwest, and a thrust fault developed from this fold as resistance to bending increased. The thrust sheet then rode relatively northwestward, cutting across nearly horizontal strata that now lie beneath it. Frictional resistance to movement increased with growth of the plate, and the plate failed and was imbricated. As regional compression continued, the thrust blocks were folded into a synclinorium as now seen in Buffalo and Cherokee mountains.

Root zone.—The root zone of the Buffalo Mountain thrust sheet is southeast of the present location. Faults, folds, and cleavage all strike generally northeast-southwest. Presumably this deformation was caused by compression acting along a northwest-southeast axis, although the compression could have been the indirect result of a couple oriented at an angle to this axis of compression. Therefore, the root zone must be either northwest or southeast of the present location. Drag folds suggest a relative movement of the thrust sheet northwest over the underlying younger rocks. The root zone for the thrust sheet must be southeast of the present location, because this is the only area in which rocks of equal or older age crop out and from which these rocks could have been translated. The increase to the southeast in the prominence of cleavage argues for increased deformation to the southeast and thus for a root zone in that direction.

Minimum net slip and breadth.—Only a minimum figure can be given for the net slip along the Buffalo Mountain thrust fault. According to Keith (1907, p. 9): "With due allowance for the subsequent folding and faulting of the plane, it is probable that the original displacement on the shear plane along that line was at least 20 miles."

Billings (1954, p. 192) has stated: "Although the net slip along the overthrust in the vicinity of Buffalo Mountain, Tennessee, is approximately 6 miles, the minimum breadth is 12 miles, and this figure has been erroneously stated to be the net slip."

The minimum breadth of the Buffalo Mountain thrust plate is estimated by the writer to be 11–12 miles. Depending upon the assumptions made concerning the structure, the minimum net slip along the Buffalo Mountain thrust fault is estimated at 5–12 miles. Rocks above and below the fault cannot be matched in a breadth of 5–12 miles, probably more. The figures given will be increased considerably by allowances for the later folding of the thrust surfaces. The estimates given are based on the geologic maps and structure sections by Keith (1907) and King *et al.* (1944).

Order of thrusting.—The Cherokee block dips beneath the Intermediate and Pinnacle blocks and is crumpled at its southwest end, where the Intermediate block rests upon it. The Intermediate block dips beneath the Pinnacle block. Nevertheless, this arrangement of blocks does not give evidence concerning the order of the thrusting.

Imbrication along minor thrusts could have taken place before, during, or after major thrusting, but probably did not develop until an advanced stage in the major thrusting, when frictional resistance to the thrusting had been increased greatly. The Buffalo Mountain thrust sheet thus rode forward on the Buffalo Mountain thrust fault until it arrived close to its present location, after which the two minor thrust faults developed and divided the thrust sheet into the three imbricate blocks.

References Cited

Billings, M. P., 1954, Structural geology: 2d ed., N. Y., Prentice-Hall, Inc., 514 p.

Butts, Charles, 1940, Geology of the Appalachian Valley in Virginia, Part I, Geologic text and illustrations: Va. Geol. Survey Bull. 52

Butts, Charles, Stose, G. W., and Jonas, Anna I., 1933, Southern Appalachian region: 16th Internat. Geol. Congr. Guidebook 3

Eardley, A. J., 1951, Structural geology of North America: N. Y., Harper and Brothers, 624 p.

Keith, Arthur, 1903, Description of the Cranberry quadrangle (N. C.-Tenn.): U. S. Geol. Survey, Geol. Atlas, Cranberry folio (no. 90), 9 p.

—— 1904, Description of the Asheville quadrangle (N. C.-Tenn.): U. S. Geol. Survey, Geol. Atlas, Asheville folio (no. 116), 10 p.

—— 1905, Description of the Grenneville quadrangle (Tenn.-N. C.): U. S. Geol. Survey, Geol. Atlas, Grenneville folio (no. 118), 8 p.

—— 1907, Description of the Roan Mountain quadrangle (Tenn.-N. C.): U. S. Geol. Survey, Geol. Atlas, Roan Mountain folio (no. 151), 11 p.

King, P. B., Ferguson, H. W., Craig, L. C., and Rodgers, John, 1944, Geology and manganese deposits of northeastern Tennessee: Tenn. Div. Geology Bull. 52, 275 p.

King, P. B., Hadley, J. B., Neuman, R. B., and Hamilton, Warren, 1958, Stratigraphy of Ocoee series, Great Smoky Mountains, Tennessee and North Carolina: Geol. Soc. America Bull., v. 69, p. 947–966

Rodgers, John, 1953, Geologic map of east Tennessee with explanatory text: Tenn. Div. of Geology Bull. 58, pt. II, 168 p.

Safford, J. M., 1869, Geology of Tennessee: Nashville, 550 p.

Snyder, F. G., 1947, The problem of the Lipalian interval: Jour. Geology, v. 55, p. 146–152

Spieker, E. M., 1956, Mountain-building chronology: Am. Assoc. Petroleum Geologists Bull., p. 1769–1815

Stose, G. W., and Stose, A. J., 1944, The Chilhowee group and Ocoee series of the southern Appalachians, Parts 1 and 2: Am. Jour. Sci., v. 242, p. 367–390 and 401–416

State Teacher's College, New Paltz, N. Y.

Manuscript Received by the Secretary of the Society, June 18, 1957

Short Notes

BULLETIN OF THE GEOLOGICAL SOCIETY OF AMERICA
VOL. 70, PP. 637-640 MAY 1959

RE-EVALUATION OF THE SALT CHRONOLOGY OF SEVERAL GREAT BASIN LAKES: A DISCUSSION

BY J. H. FETH

Broecker and Walton (1959) have presented their analysis of probable ages of Great Salt Lake, Mono Lake, Pyramid Lake, and Walker Lake, concluding that the first two have existed continuously for 73,000 years, that Pyramid Lake may have been in existence since the end of the last interpluvial, but that Walker Lake must have desiccated during the last 10,000 years. Estimates are based on increments of Cl^- entering each lake basin from rainfall. Exception is taken to earlier estimates based on Cl^- increments from river waters and the like.

Broecker and Walton have clearly attempted to circumscribe the variables as they recognized them in the assumptions and the calculations upon which their conclusions have been based. This discussion stems from the present writer's belief that Broecker and Walton did not recognize important geologic considerations and increments from ground-water sources that throw serious doubt on the validity of their conclusions as to the ages of Great Salt Lake and Mono Lake at least.

Premise 2 of Broecker and Walton (1959) states that "... Cl^- is derived almost entirely from the recycling of oceanic salts, ..." and Broecker (personal communication) informs the writer that the sense of the statement intends recycling in an essentially continuous process without implying storage of salt through any significantly long period of time—as would be the case in the event of deposition as halite and subsequent leaching of bedded-salt deposits. This is confirmed by the statement that "...it will be assumed that the loss of Cl^- through inefficient runoff is compensated by the dry fallout entering the basin."

A corollary premise is that "... contribution of Cl^- from other sources such as local volcanism and erosion of old salt deposits has been assumed negligible."

In other words, it is assumed by Broecker and Walton that all the Cl^- introduced into the waters of the four lakes with which they deal, with exceptions insignificant to their calculations, is derived from rain washing airborne oceanic salt from the atmosphere.

With reference to Great Salt and Mono Lakes, at least, the assumption appears to the present writer to be untenable.

Table 1 shows increments of chloride to the Great Salt Lake basin from three springs and from the Sevier River. Discharge of the springs was measured (two cases) or estimated (one case) by the writer, and chemical information is from unpublished analyses in files of the Geological Survey. The calculation for the Sevier River is based on data published (U. S. Geol. Survey, 1957) for the water year 1951–1952. The Sevier River does not presently flow to Great Salt Lake, but its drainage area was tributary to pluvial Lake Bonneville during the Provo and Bonneville stages (Gilbert, 1890, p. 13); hence, for a long time the river basin contributed salt to Lake Bonneville.

Table 1 merely suggests a reasonable order of magnitude of chloride increments from sources that "have been considered negligible" by Broecker and Walton. The source of chloride in the waters of the three springs cited has not been determined; it may be hypothecated, though, that it is wholly or in part from saline waters or bedded salt deposited with sand, silt, and clay in pre-Lake Bonneville water bodies that are believed to have occupied the Great Salt Lake basin before Lake Bonneville time. This circumstance, if it prevails, does not vitiate the data cited, as Broecker and Walton have specified contemporaniety of Cl^- supply, and pre-Lake Bonneville time in the sense here used is prior to the 73,000-year period under consideration. Bedded halite has been penetrated in exploratory drilling done for engineering works in the northwestern part of

the basin and may occur elsewhere at depths not yet reached in drilling.

The chloride in the Sevier River originates directly or indirectly from bedded halite in the Arapien shale of Jurassic age which is shown

TABLE 1.—INCREMENTS OF CHLORIDE TO GREAT SALT LAKE BASIN

Source of water	Discharge cfs	Cl^- ppm	Tons Cl^- per acre-foot	Tons Cl^- per year	Tons Cl^- in 73,000 years
Hooper Hot Springs	0.04	5200	7	200	15×10^6
Utah Hot Springs	2.0	12,500	17	25,000	1800×10^6
El Monte Spring	.25*	580	0.8	140	10×10^6
Sevier River at Lyndyll	179	365	0.5	65,000	4800×10^6
					6625×10^6

* Estimated.

by Spieker (1949, Pl. 1) to crop out in some tens of square miles in the Sevier, Juab, and San Pete valleys.

The Sevier River, clearly, did not flow at maximum Provo and Bonneville stages of Lake Bonneville, although it probably did during rising and waning stages of the lake. It is pertinent, therefore, to examine what may happen in areas of exposed rock salt overlain by ponded water. Lake Mead provides a convenient analogy.

Evaporites of Tertiary age (Longwell, 1936) underlie part of the Lake Mead basin, although the area of exposed halite amounted (Gould, 1954, p. VIII-304) to only about 22 acres. Gould continues with an estimate that in the period 1935 to 1948, about 900 acre-feet of rock salt was dissolved from the reservoir floor. Assuming 2.1 as the density of halite, that volume of salt represents more than 2.5×10^6 tons of halite dissolved in a 13-year period, or nearly 0.2×10^6 tons of halite per year. These calculations find general confirmation in a statement (Howard, 1954, p. VII-185) that a total increase of about 20×10^6 tons of dissolved solids occurred in Lake Mead during the same period of time, and that the portion of the increase represented by "increased concentrations of sodium and chloride [may be] attributed largely to dissolving of halite." The rate of solution of salt probably diminishes with time as part of the outcrop is silted over, but complete cessation of solution is unlikely as the very process itself, where outcrops occur on sloping surfaces, would tend to renew exposures. Numerical comparison with tonnages potentially picked up by water of Lake Bonneville overlying outcrops of halite in the Sevier River basin is not warranted by these data. But the probability that increase in salinity was appreciable seems to be implicit in the record of Lake Mead.

Another comparison of some interest may be made by use of data from the table. Assuming that the three springs during the period of 73,000 years stated as the age of Great Salt Lake since the last interpluvial had discharges and concentrations of Cl^- comparable with those cited, they would, in that time span, have contributed about 1800×10^6 tons of chloride. Using data from Broecker and Walton (1959, table 2, values for "Interpluvial" stages), the volume of water in Great Salt Lake is about 1.38×10^6 acre-feet, and (Table 1) the Cl^- concentration is 187,000 parts per million (ppm), or 255 tons per acre-foot. Thus there is in the order of 350×10^6 tons of chloride in waters of Great Salt Lake today, or a bit more than one-fifth of the load of chloride calculated from the data given. There are obvious objections to such calculations, and they are not advanced with any thought that they represent conditions that actually existed. The figures are intended merely to show that reliance on rainfall as the sole source of Cl^- entering the basin is analogous to eating only the white meat of the turkey and throwing the rest of the bird away.

Inasmuch as the Great Salt Lake basin receives ground water from many sources other than those cited in the table (Peck, 1954), for which neither volumes discharged nor salinities of the waters are well known, it must be that actual tonnages of chloride delivered to Great Salt Lake today are very large. The writer feels that, however large the fluctuations over Pleistocene time, the contributions of chloride from sources "considered negligible" by Broecker and Walton are so great as to make the time values calculated by those authors for the salt increment (rainfall alone) to the basin unreasonably large.

With respect to Mono Lake, the writer can state qualitatively that there are ground-water increments to the present lake from reported springs peripheral to the lake. From numerous vents covered by waters of the lake but readily detected by the boils caused on the present water surface, discharges of large volume occur

on the bed of the lake. The latter have not, to the writer's knowledge, ever been measured as to discharge or sampled for chemical analysis.

The water of Mono Lake falls within the group of alkaline-lake waters characterized by Clarke (1924, p. 179) as representative of volcanic regions. And the lake, of course, lies (Russell, 1889) surrounded by volcanic rocks—rhyolitic to the south, and basaltic toward the north. Such data as are available demonstrate that the water of Mono Lake is complex in chemical character and probably in origin and suggest that assigning origin of the chloride fraction to rainfall alone is an oversimplification of the facts.

Table 2 shows the ratio Na:Cl, in equivalents per million or equivalents per liter, for a number of bodies of water of interest in the present discussion.

It may be assumed that oceanic-salt nuclei carry sodium and chloride in essentially the same proportions in which the elements occur in sea water—that is, near a ratio of unity. If all significant Cl^- increment is air-borne, and if Na^+ follows Cl^-, then according to the ratios shown Great Salt Lake most closely approximates the sea-water relationship between sodium and chloride, Walker Lake follows, Pyramid Lake diverges somewhat farther, and Mono Lake diverges by a factor of nearly 3. It has been shown in this discussion that there is an abundant source of NaCl in the Great Salt Lake basin, the presence of which might contribute to the similarity of the ratio Na:Cl in Great Salt Lake to that found in sea water. The diverging ratios in waters of the other three lakes imply increments of sodium from sources other than bedded halite or the ocean. The position required by Broecker and Walton's premise, namely, that all other constituents of the lake waters may be derived from a variety of sources but chloride comes largely from the sea, seems unrealistic.

The remaining data suggest that Walker Lake may most nearly depend upon oceanic salt for the chloride content of its water, that Pyramid Lake is perhaps a blend of oceanic salt with salt from other sources, and that Mono Lake has received but a small proportion of its sodium and chloride from air-borne sea salts. These conclusions are of course at variance with the fundamental premise used by Broecker and Walton.

Broecker and Walton discuss "... great climatic changes which have occurred during the Pleistocene" and show that parameters used in their later calculations must take into account those climatic variations; their Table 2 accordingly shows their interpretations of variations of several parameters in interpluvial, pluvial, and semipluvial stages. Yet

TABLE 2.—RATIOS OF SODIUM TO CHLORIDE

Source of water	Ratio $\frac{Na}{Cl}$	Source of data
1. Pacific Ocean	0.86	Unpublished analysis, U. S. Geol. Survey
2. Great Salt Lake	0.92	Calculated from Clarke (1924, p. 157)
3. Mono Lake	2.53	Calculated from Clarke (1924, p. 162)
4. Pyramid Lake	1.38	Calculated from Clarke (1924, p. 160)
5. Walker Lake	1.16	Calculated from Clarke (1924, p. 160)
6. Spring, E. shore of Mono Lake	4.15	Waring (1915, p. 145)
7. Spring, N. shore of Mono Lake	5.44	Waring (1915, p. 145)
8. Spring, W. shore of Mono Lake	7.76	Unpublished analysis, U. S. Geol. Survey

those authors assume that the concentration of chloride in rainfall (their factor *f'*, Table 2) remained constant throughout all climatic changes envisioned.

The concentration of chloride in rainfall represents a resolution of variables that must include at least the following: (1) distance from the ocean; (2) direction, intensity, and duration of prevailing winds; (3) removal of salts from the air by precipitation in areas reached by the clouds before they impinge on the area for which data are required; and (4) the turbulence, wind intensities and directions, and relative humidity prevailing in ocean areas where salt nuclei are formed and become air-borne. These variables are integral parts of "climate," and if Broecker and Walton assume large changes in Pleistocene climates it appears that they should have allowed for fluctuations in the chloride concentration in rainfall along with fluctuations in other climatic variables.

In summary, the present writer feels that Broecker and Walton have contributed interesting concepts—notably, removal of salt from inland basins by wind entrainment—to an attempt to derive a salt chronology for the lakes with which they dealt. It appears, however, that they made no allowance for geologic and ground-water increments of chloride that, in Great Salt Lake especially, are overwhelmingly important; they seemingly disregarded

the geologic environment and the complex nature of Mono Lake; and they made no provision for variation in Cl^- concentration with recognized climatic fluctuations during Pleistocene time. For these reasons, the present writer cannot accept the ages calculated by Broecker and Walton as reliable even within reasonable limits.

References Cited

Broecker, W. S., and Walton, Alan, 1959, A re-evaluation of the salt chronology of several Great Basin lakes: Geol. Soc. America Bull., v. 70, p. 601–618

Clarke, F. W., 1924, The data of geochemistry: 5th ed., U. S. Geol. Survey Bull. 770, 841 p.

Gilbert, G. K., 1890, Lake Bonneville: U. S. Geol. Survey Mon. 1, 375 p.

Gould, H. R., 1954, Sedimentology, *in* Smith, W. O., Vetter, C. P., Cummings, G. B., and Others, Lake Mead comprehensive survey of 1948–49: U. S. Dept. Interior, U. S. Dept. Navy, and others (Boulder City, Nev.), 3 v., p. VIII-211–323

Howard, C. S., 1954, Chemical limnology, *in* Smith, W. O., Vetter, C. P., Cummings, G. B., and others, Lake Mead comprehensive survey of 1948–49: U. S. Dept. Interior, U. S. Dept. Navy, and others (Boulder City, Nev.), 3 v., p. VII-173–186

Longwell, C. R., 1936, Geology of the Boulder Reservoir floor: Geol. Soc. America Bull., v. 47, p. 1393–1476

Peck, E. L., 1954, Hydrometeorological study of Great Salt Lake: Univ. Utah Eng. Expt. Sta. Bull. 63, 57 p.

Russell, I. C., 1889, Quaternary history of Mono Valley, California: U. S. Geol. Survey 8th Ann. Rept., pt. 1, p. 261–394

Spieker, E. M., 1949, The transition between the Colorado Plateaus and the Great Basin in central Utah: Utah Geol. Soc. Guidebook to the Geology of Utah, no. 4, 106 p.

U. S. Geological Survey, 1957, Quality of the surface waters of the United States, Parts 9–14: U. S. Geol. Survey Water-Supply Paper 1253 (S. K. Love, director of compilation), 344 p.

Waring, G. A., 1915, Springs of California: U. S. Geol. Survey Water-Supply Paper 338, 410 p.

U. S. Geological Survey, Menlo Park, California

Manuscript Received by the Secretary of the Society, November 18, 1958

Publication Authorized by the Director, U. S. Geological Survey

BULLETIN OF THE GEOLOGICAL SOCIETY OF AMERICA
VOL. 70, PP. 641–644, 2 FIGS. MAY 1959

ROCK COMPASS: A NEW AID FOR COLLECTING ORIENTED SPECIMENS

BY D. E. T. BIDGOOD AND W. B. HARLAND

Oriented rock specimens are required in several types of investigation, and particularly in petrofabric and paleomagnetic studies. They have generally been collected by using compass and clinometer to measure the strike and dip of a surface on the specimen, which has already been detached, replaced, and marked. This method has the advantage of using the equipment normally carried by a field geologist. However it has the following disadvantages.

(1) Accuracy is limited by the flatness of surfaces available. Where only irregular surfaces are exposed it is possible to mark a horizontal line around the specimen together with an orientation arrow on top. These practical difficulties lead either to undue restriction of samples to those with suitable surfaces, or to accumulation of errors which may easily exceed 5°.

(2) Orientation in azimuth depends on the magnetic field near the rock. In general this may not differ much from the local declination, but this should not be assumed; moreover the local declination may not be known.

(3) It takes an appreciable time to read the compass which may add to other inconveniences—*e.g.*, the removal of tools from near the compass. This is more troublesome in high latitudes with weak magnetic fields.

(4) There are practical difficulties in marking rocks indelibly—*e.g.*, on wet or friable surfaces.

(5) The reorientation of the specimen in the laboratory requiring the simultaneous use of clinometer and level may be tedious.

When faced with the need for collecting some hundreds of oriented samples in Greenland for measurement of rock magnetism the authors devised the "rock compass" described here. It has proved efficient in a variety of circumstances and is being adopted by other workers.

The design is essentially a three- (or four-) axis universal stage or theodolite on a rigid tripod and has the following features:

(1) There is a base plate with three equal legs at the corners of an isosceles triangle. Their length is such as to allow the plate to fit over a typical convex surface, and the feet are blunt-pointed to fit into three localizing cavities drilled in the rock with a tungsten carbide hand drill. The locating holes are positioned by tapping each leg of a rigid triple-pointed steel locating punch of identical plan. This gives a firm unambiguous indelible mount.

(2) Three axes of rotation (A1, A2, A3) with scales marked in degrees are as follows:

A3 (axis perpendicular to the base plate) gives the angle between the direction through two marked legs and a horizontal direction. This may be called the *strike scale*, and the horizontal direction (strike) is the A2 axis.

A2 (mounted on and parallel to the base plate) is the axis about which the level plate with T bubbles is rotated to a level position. This is the *dip scale*, and to avoid ambiguity the quadrant should be specified.

A1 (perpendicular to the level plate) allows rotation in a horizontal plane (the *azimuth scale*) and mounts a vertical direction plate for direct measurement of azimuth or for sighting. This direction plate carries a further rotating sighting arm which can be elevated and depressed (the *elevation scale*). This movement is necessary when sighting up or down, but the reading on the scale need not be recorded unless as part of the procedure to survey the position of the sample. The direction plate may also carry a trough compass for direct reading of magnetic azimuth.

(3) The direction plate may be used in a number of ways. The azimuth scale may be read with the trough compass needle at zero. Alternatively or additionally the sighting device may be used to record the azimuth of any distinctive features, or it may be used to sight to an ancillary instrument on a tripod when the direction of the rock-compass azimuth may be related directly to a ray from a prismatic compass or theodolite. Sighting from awkward positions is aided by a Brunton mirror or by a rotating prism attached to the sighting arm.

The following routine was found to be most generally efficient for two collectors. At a selected site four to six blocks were chosen

within sight of a single station; they were loosened, replaced, punched, drilled with three holes, and numbered. During this time the held compass needle was thereby eliminat with a distinct gain in precision. The ex locations as well as the stratigraphic positio

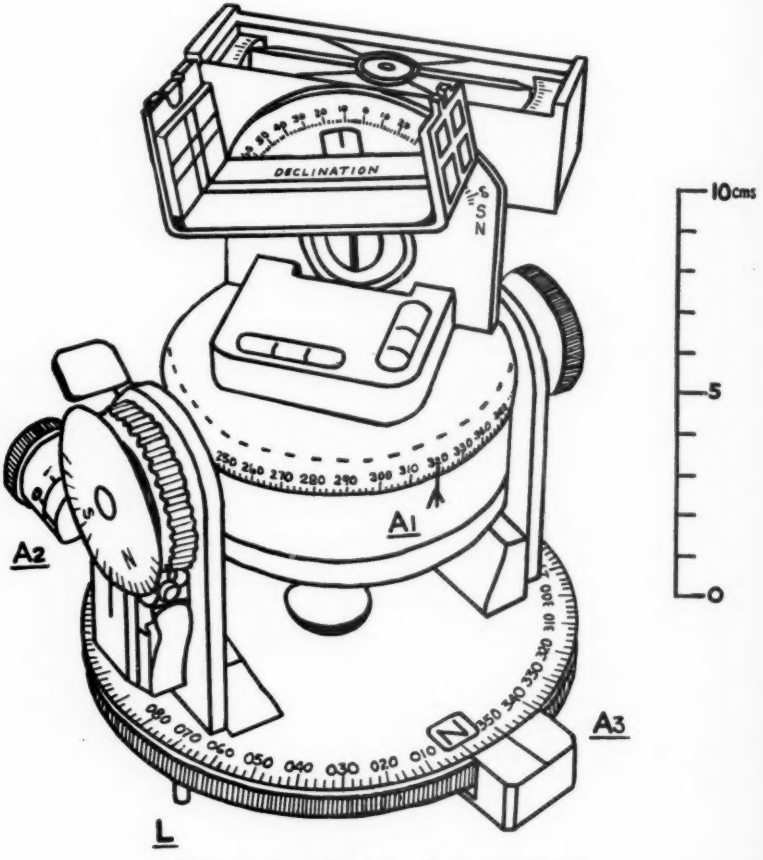

FIGURE 1.—ROCK COMPASS AS DESCRIBED IN TEXT

A1, A2, and A3 mark respectively the azimuth scale, the dip scale, and the strike scale. One of the legs is visible at L.

tripod was set up and compass bearings were taken to known points to resect the position and find the declination (a small director or theodolite was used where greater precision was necessary). Then in quick succession the rock compass was placed in position on each sample, oriented and sighted on the tripod, and the return sight was noted along with the three readings (A1, A2, A3) called out from the rock compass. Delay due to instability of a hand-

of the samples could be found by marking the tripod position and measuring the distances and elevations from each specimen.

The usual field kit comprised the rock compass, three-point locating punch, single sharp punch, small enclosed hand drill, and a number of tungsten carbide 4-mm bits, small brush for clearing surface to replace specimen, plaster and/or paint for numbering specimen, heavy and trimming hammers, and chisel. Possibly,

in addition, a Brunton compass, light tripod, and prismatic compass or light director (theodolite) and tape are useful.

of which quadrant the dip reading occupied. If the specimen is to be reoriented with the dip removed then A2 is also set at zero.

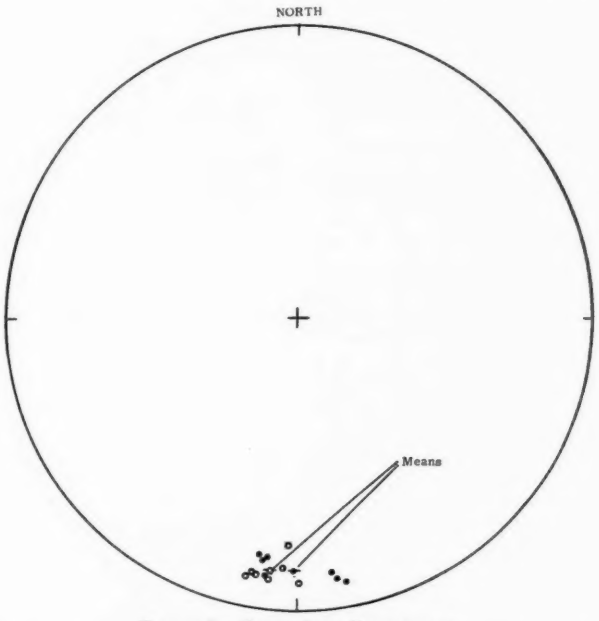

FIGURE 2.—EQUAL-AREA STEREOGRAM

Upper hemisphere shows poles of remanent magnetization of 14 samples of Exeter trap rocks, Devon. Open circles by rock compass, solid circles by compass clinometer.

For paleomagnetic purposes the true dip of sediments may be the critical requirement. Where good bedding surfaces or other foliation are obtainable these are measured with the rock compass: the feet of the tripod in the locating holes, if drilled to a depth of about 2 mm, define a plane which is nearly parallel to the required surface. In such cases the dip is read directly from the dip scale, and the strike from the azimuth. Even when dips are obtained while collecting with the rock compass they should be supplemented by determinations using other means.

In the laboratory the rock compass is set in the locating holes with A2 and A3 at the original readings and A1 at zero, and the specimen with instrument is rotated on a piece of plasticine until the bubbles are both centered. The specimen is then dipping as in the field, and the direction of dip is derived directly from the strike scale together with the record

The rock compass (Fig. 1) was adapted from a standard Astro-compass available on the war-surplus market. The authors will be glad to supply notes on the simple conversion of this instrument and the scale conventions used.

Having used a variety of methods the authors are clear as to the superiority, for systematic collecting, of the system outlined above. However, they are indebted to Mr. J. C. Belshé of the Department of Geodesy and Geophysics, Cambridge, for the following statistical comparison of results obtained by the prototype rock compass (since improved) and the compass clinometer method.

Seven samples were taken by each method from a quarry near Ide, Devon, in the Hatherleigh series of the Exeter trap rocks. The results for the measurement of remanent magnetization in these samples is summarized. Here k is an estimate of the precision, and a the radius

of confidence at the 5-degree level following the theory of dispersion set forth by Fisher (1953).

	k	a	Mean direction		N
			D	I	
Rock compass	171	4.6°	S5.8°W	−14.8°	7
Compass-clinometer	71	7.2°	S0.5°W	−15.6°	7

A plot of the data is shown in Figure 2.

Finally, the authors wish to thank Dr. Lauge Koch, Leader of the Danish East Greenland Expedition 1957; the collecting on this expedition stimulated the authors to design this instrument.

Reference Cited

Fisher, Sir R. A., 1953, Dispersion on a sphere: Royal Soc. London Proc. A, v. 217, p. 295

SEDGWICK MUSEUM, CAMBRIDGE, ENGLAND
MANUSCRIPT RECEIVED BY THE SECRETARY OF THE SOCIETY, AUGUST 11, 1958

BULLETIN OF THE GEOLOGICAL SOCIETY OF AMERICA
VOL. 70, PP. 645-650, 1 FIG., 1 PL. MAY 1959

UPPER ORDOVICIAN (?) AND UPPER SILURIAN FORMATIONS OF THE NORTHERN KLAMATH MOUNTAINS, CALIFORNIA

BY FRANCIS G. WELLS, GEORGE W. WALKER, AND CHARLES W. MERRIAM

Introduction

Upper Ordovician(?) phyllite and Upper Silurian sedimentary rocks are brought to the surface in broad northeasterly trending folds between Shasta and Scott Valleys, Siskiyou County, California. These rocks are here named the Duzel formation and the Gazelle formation respectively.

Duzel Formation

Pale gray-green phyllitic graywackes form the characteristic and predominant country rock in most of the area between two valleys south of Yreka. They crop out throughout the drainage basin of Moffett Creek (Pl. 1). As the name Moffett is pre-empted, the writers propose the name Duzel formation for the phyllitic sequence, after Duzel Creek, a tributary of Moffet Creek, which is just east of Duzel Rock, a conspicuous mass of white marble that caps the highest peak in the area.

Exposures of the graywacke are poor; outcrops rarely project more than 1 foot above stream beds. Elsewhere it slabs off into screes of thin crinkled plates most of which are less than an inch thick. Even road cuts do not afford good structure sections. The crumpled structure is a most distinctive feature. The dark gray green of the original wacke is masked in float fragments by the pale-green chloritic sheen of partings along which the rock disintegrates.

The phyllitic graywacke is thinly layered and fissile. In general, it is layered at 1- to 2-mm intervals, although occasional beds up to 3 inches occur, and some a foot to 18 inches thick crop out at stratigraphic intervals of 1 to several hundred feet. Such beds are hard in contrast to the fragile thin layers.

The rock is a wacke, mostly of well-sorted grains. The predominant grain sizes range from silt to granules. Fine-grained layers predominate. Stringers of quartz, most of which are less than 1 inch thick, both parallel and crosscut the layers; locally within small overturned folds they form knots.

Except for the presence of chlorite and sericite the rock is petrographically closely similar to graywackes of the younger Gazelle formation.

Limestone and associated chert beds occur within the phyllite. Many are less than 2 feet thick, but others up to 200 feet in outcrop width are conspicuous in Horseshoe Gulch and to the northeast along the ridge. The largest is more than a mile long and several hundred feet thick. Although most of these beds are massive, some are thinly bedded.

Chert, in part originally sedimentary as shown by Radiolaria, in part developed by replacement of limestone lentils, is associated with the limestone.

Interstratification of the limestone beds with phyllitic graywackes is exhibited in Horseshoe Gulch, a mile to the south in Trail Gulch, and along the ridge to the northeast.

Bold outcrops of marble resting on phyllite form the conspicuous knobs, Duzel Rock and Facey Rock. No traces of fossils have been found in them. At their base and top are thin layers of greenstone crumpled, slickensided, sheared, and commingled with the marble and rendering the greenstone schistose in places, thus indicating movement between the marble and the underlying phyllite. These features are likewise found in the marble bodies that overlie the Gazelle beds and cap Robbers Rock, Mallethead, and Bonnet Rock. Possibly these marble bodies are not in depositional contact with either the underlying Duzel or underlying Gazelle formations. They may be remnants of the younger Devonian rocks that are exposed along the south side of the valley of the East Fork of Scott River and were thrust over both formations.

Attitudes of beds indicate that the Duzel is involved in a northward-plunging synclinorium, the east limb of which has been thrust over beds of the younger Gazelle formation. In the southern part of the area the syncline has been cut off by a steeply dipping northward-trending fault which has dropped beds of the Duzel formation against peridotite and quartz-mica schist. Farther north the basal contact of the Duzel formation may also be a fault, but the nature of the contact is uncertain because of

the lack of outcrops and the reconnaissance nature of the mapping.

The phyllite of the Duzel formation has been folded into isoclinal folds with an amplitude of a few millimeters, commonly partially overturned. Drag folds are common. Their orientation confirms the interpretation of the major structure as given above.

Because the Duzel and Gazelle formations are in fault contact throughout the area, it is not known whether there is an angular discordance between the two formations. However, the more intense folding and metamorphism of the rocks of the Duzel formation suggest that the two formations are discordant.

As the top of the Duzel formation is not exposed in the area and as the base is uncertain, the total thickness has not been determined. Below Duzel Rock 1250 feet of crinkled phyllite and phyllitic graywacke is exposed in the valley of Duzel Creek, but the structure of the formation indicates that its total thickness must be many times this figure.

A large and distinct coral and brachiopod fauna has been collected from the limestones in Horseshoe Gulch. Although these collections have not been completely worked up they contain two genera, *Catemipora* sp. and *Grewingkia* sp., characteristic of the Fish Haven dolomite of the Great Basin and generally regarded as uppermost Ordovician. Hence, the Duzel formation is the oldest fossil-bearing formation in the Klamath Mountains.

Gazelle Formation

The name Gazelle formation is here given to a sequence of clastic rocks with included limestone reefs that crops out in the valley of the East Fork of Scott River, across the Gazelle Mountain, and throughout the northern part of the valley of Willow Creek, an area of about 60 square miles. These sedimentary rocks are in fault contact with the older Duzel formation on the north, south, and west sides. On the east side the Gazelle formation is locally overlain by Devonian sedimentary and volcanic rocks and has been intruded by diorite and a great body of peridotite that makes up most of the Scott Mountains. The base of the formation is not exposed. Some of the most extensive exposures of the formation are found on the flanks of Gazelle Mountain from which this sedimentary sequence takes its name.

The formation consists essentially of hard, fine-grained, siliceous graywacke, dark-gray to black siltstone and mudstone, and siliceous and feldspathic grit. It also contains appreciable quantities of chert conglomerate, limestone, and limestone conglomerate, and is overlain by volcanic flow, agglomerates, and pyroclastic rocks.

Five members have been distinguished in the area studied, but in most places in continuous exposures one or more of these is lacking or poorly developed, and all vary markedly in thickness. The total thickness of the Gazelle formation exceeds 2400 feet.

Outcrops are poor. The columnar section given in Figure 1 is a composite of four sections measured: (A) up the Callaghan-Gazelle road from South Fork Creek, sec. 19, to the Summit, sec. 34, T. 41 N., R. 6 W.; (B) from Willow Creek SE/4, sec. 23, to the crest northeast of Mallethead Rock, sec. 14, T. 42 N., R. 7 W.; (C) from floor of Lime Gulch to top of Bonnet Rock, sec. 6, T. 42 N., R. 6 W.; and (D) from Meadow Valley, sec. 5, T. 42 N., R. 7 W., to Robbers Rock (5781), sec. 32, T. 41 N., R. 8 W.

Black siliceous siltstone, the lowest member exposed, floors the valleys of Lime Gulch, Willow Creek, the East Fork of Scott River above the confluence of Noyes Creek, and Meadow Creek and Noyes Valley below an altitude of 3400 feet. Broad folding and faulting bring it as high as 4200 feet in places. Chert beds, limestone lentils, and thin discontinuous chert conglomerate breccia beds are taken as the top of this unit. The bottom is not exposed; 600 feet is probably a fair average figure for its thickness. Fossils were found in the limestone at locality H (Pl. 1).

The best exposures are in a series of road cuts as much as 10 feet high, extending for 1½ miles along the south side of the Gazelle-Callaghan road. Here dense, dark-gray, siliceous siltstone breaks into units up to 3 inches thick, some of which show color layering of 1–2 mm. Generally the grains are indistinguishable, although in some layers they grade from clay through silt to visible sand grains, and a few beds of fine breccia with fragments about 5 mm. in diameter were noted. These beds, all less than 1 inch in thickness, are flat lying except where compressed into small folds. In Noyes Valley, the basal member of the formation consists of dark-red siltstone and porcellaneous siltstone. These rocks commonly retain their color when weathered but may bleach to a light gray. Nodules and pyrite cubes are notably absent. A search for graptolites was unsuccessful.

Under the microscope much of the black siltstone is amorphous or too fine-grained for resolution. Determinable grains are mostly angular quartz, some feldspar, and chalcedonic fragments.

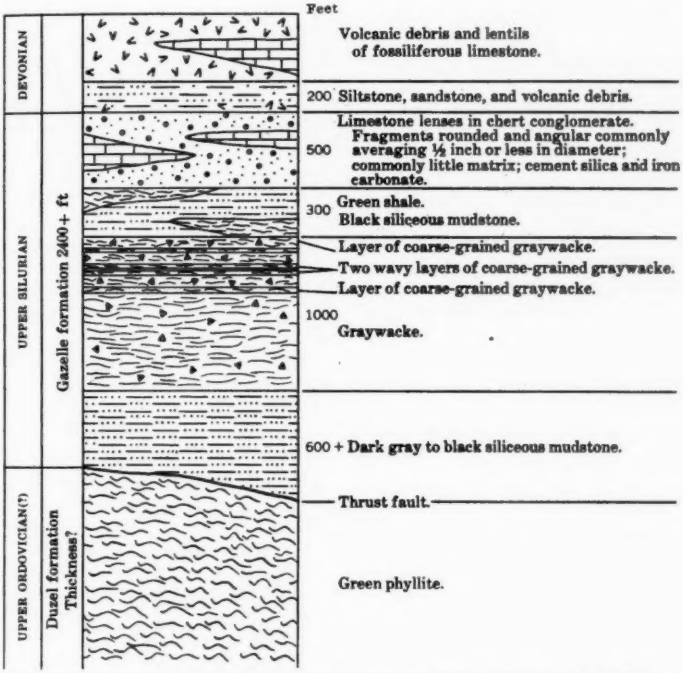

FIGURE 1.—COMPOSITE COLUMNAR SECTION OF THE GAZELLE FORMATION

Graywacke, roughly 1000 feet thick, overlies the black siltstone. It is best exposed along the Gazelle-Callaghan road from Nigger Bend to the saddle on top of Gazelle Mountain. Everywhere the rock is weathered to a characteristic khaki color, sharply contrasting with the black siltstone and probably indicating a more heterogeneous composition. The fresh rock is presumably dark gray to greenish gray.

Characteristically, the graywacke member is rhythmically layered in units mostly less than 1 inch thick. Toward the top of the member many hard resistant beds range up to 40 feet in thickness. They crop out conspicuously. The highest thick, resistant bed usually caps the graywacke member.

The siliceous graywacke is composed of poorly sorted, angular grains of quartz, feldspar, chert, fine-grained sedimentary rocks, flow rocks, and minor amounts of calcium carbonate. Grain size averages less than 0.02 mm. Some layers near the top of the member are grits of angular quartz, feldspar, and rock fragments with virtually no interstitial "paste".

The grain size averages about 0.6 mm. A sample from the top of Gazelle Mountain analyzed 83.53 per cent SiO_2. Generally the mineral grains are only slightly altered and recrystallized, although in some areas deformation and alteration have produced minor quantities of saussurite, calcite, sericite, muscovite, and biotite. Some strata contain abundant disseminated dark-gray to black opaque grains, partly of iron oxides, but chiefly, perhaps, of carbonized vegetal material. Some strata also contain numerous small rhomb-shaped holes which are iron-stained on edges. Both shape and iron staining suggest former siderite fillings.

Tuffaceous olive-green shale, about 200 feet thick, stratigraphically overlies the graywacke member. Good and fairly continuous exposures occur about 2000 feet south of Robbers Rock, but throughout most of the area the

thickness and distribution of this member is highly erratic. Near Robbers Rock the shale lies conformably between thinly laminated dark-gray siltstone and dark siliceous graywacke below and chert conglomerate above. Bedding is seldom evident in the shale, although locally one-eighth-inch to one-quarter-inch layering was noted. The shale weathers to small irregular green flakes. Where this member is absent, the underlying siltstone or graywacke grades upward into highly siliceous grit or into fine chert conglomerate.

Coarse siliceous clastic rocks and limestone, averaging 400 feet in thickness, but ranging from 200 to 600 feet, overlie the green shales. Apparent discordance of the bedding of this member on the strata beneath, frequently noted in the field, is due to faulting between the incompetent underlying shale and the competent siliceous rocks consequent on their mutual folding.

The member consists largely of highly siliceous, well-cemented clastic rocks but contain appreciable quantities of nearly pure limestone and limestone conglomerate. The siliceous clastic unit is continuous although variable in character throughout the area; the included carbonate lenses are discontinuous.

The highly siliceous rocks are predominantly chert conglomerate composed almost entirely of rounded, subangular, and angular pebbles of chert, quartzite, quartz, and fine-grained siliceous sediments. A few pebbles of dacitic or andesitic larva and sparse crystal fragments of feldspar were also identified. Sparse cement is mainly silica but locally iron carbonate. The rocks are light gray mottled by dark-gray rock fragments. A yellowish-brown iron stain is characteristic of weathered surfaces wherever the cement is iron carbonate. Pebble size averages a quarter of an inch or less; in some outcrops cobbles and boulders up to 8 inches in diameter have been found. Some layers, made up of angular chips of chert, quartz, and feldspar an eighth of an inch across, are properly termed siliceous grit. In most outcrops, the conglomerate and the grit contain virtually no matrix. Where some matrix does occur it consists of a mozaic of nearly equidimensional quartz and feldspar crystals.

The limestone strata, which are noticeably discontinuous, occur in some places near the base, elsewhere in the middle or at the top of the siliceous member. Locally the limestone itself includes small lenses of chert conglomerate. The thickness of the limestone also varies; in Lime Gulch it is more than 200 feet thick, constituting a substantial part of the entire member. Throughout the area the average thickness is probably about 70 feet.

The limestone is commonly thick-bedded and massive, although in one or two localities it is thinly plated near, and parallel to, its base. Plating is probably due in part to shearing, but it may also be related to bedding. The rock is characteristically a fine-grained, even-textured blue-gray or yellow-gray rock that weathers to irregular light-gray surfaces. Weathered surfaces are extremely rough wherever silica has replaced irregular carbonate seams and fossil remains. At several localities, mostly at or near its base, the limestone includes a carbonate-cemented limestone conglomerate. Where truly basal, the conglomerate contains admixed siliceous rock fragments and mineral grains.

The lenticular nature of the limestone, involving variation in thickness over short distances, the presence of conglomerates in the limestone and in the siliceous rocks above and below, and the presence, locally, of abundant coralline remains indicate that the limestone lenses probably represent Paleozoic bioherms.

On the south side of the valley of the East Fork of Scott River the beds of the Gazelle formation are overlain by 200 feet of siltstone, sandstone, and tuff, in turn overlain by lavas and agglomerate with thin interbeds of tuff and lentils of fossiliferous Devonian limestone. These sedimentary and volcanic rocks are not included in the Gazelle formation and until more thoroughly studied will not be given formational rank.

On a broad scale the Gazelle formation is relatively undeformed, with low dips outlining a broad anticline. The black siliceous mudstone, although usually horizontal, is full of small overturned folds, and in places the strata are buckled and faulted upward.

Corals and brachiopods occur in the limestone lenses at four localities. Collections were made from the coarse siliceous clastic rocks, the massive limestone, the nodular limestone, and the argillaceous shales just below the massive limestone. The coral *Heliolites* and the brachiopod *Atrypella* are present in all, thus clearly demonstrating the Late Silurian age of the Gazelle formation. The largest population has been found in the shale and nodular limestone at the conical hill in

sec. 6, T. 42 N., R. 6 W., where Merriam identified the following species:

Corals:
Cystiphyllum sp.
Cyathophyllid sp.
Heliolites sp.
Brachiopods:
Gypidula sp. cf. *G. galeata* (Dalman) Kozlowski 1929
Atrypella sp. cf. *A. enuis* Kirk and Amsden
Atrypa sp. (small form)
Alaskospira dunbari Kirk and Amsden?
Stricklandia sp. (large, heavy-ribbed)
Trilobites:
Encrinurus sp.

U. S. Geological Survey, Washington, D. C.; U. S. Geological Survey, Denver, Colo.; U. S. Geological Survey, Menlo Park, Calif.

Manuscript Received by the Secretary of the Society, November 26, 1958
Publication Authorized by the Director, U. S. Geological Survey

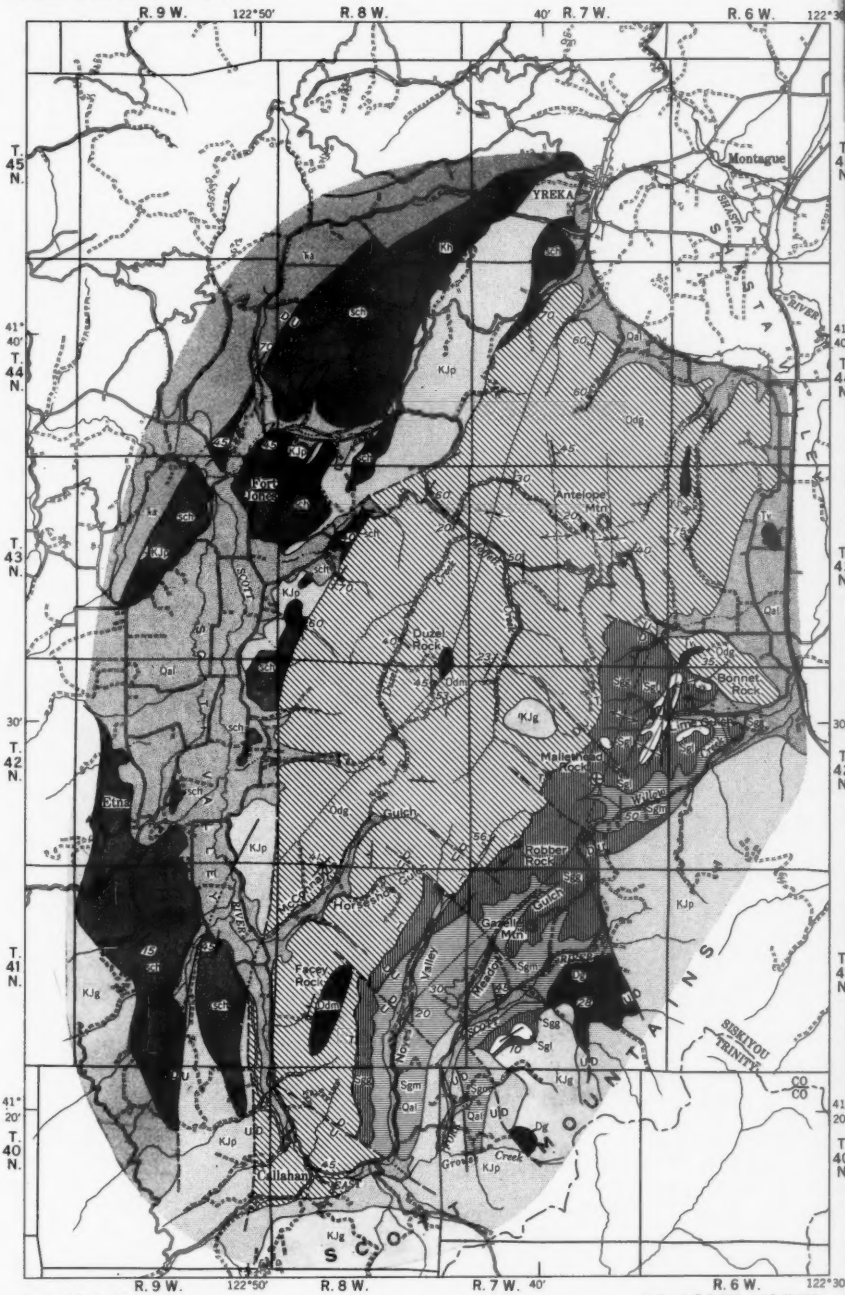

RECONNAISSANCE GEOLOGIC MAP OF THE AREA BETWEEN SHASTA AND SCOTT VALLEYS, EASTERN SISKIYOU COUNTY, CALIFORNIA

1958

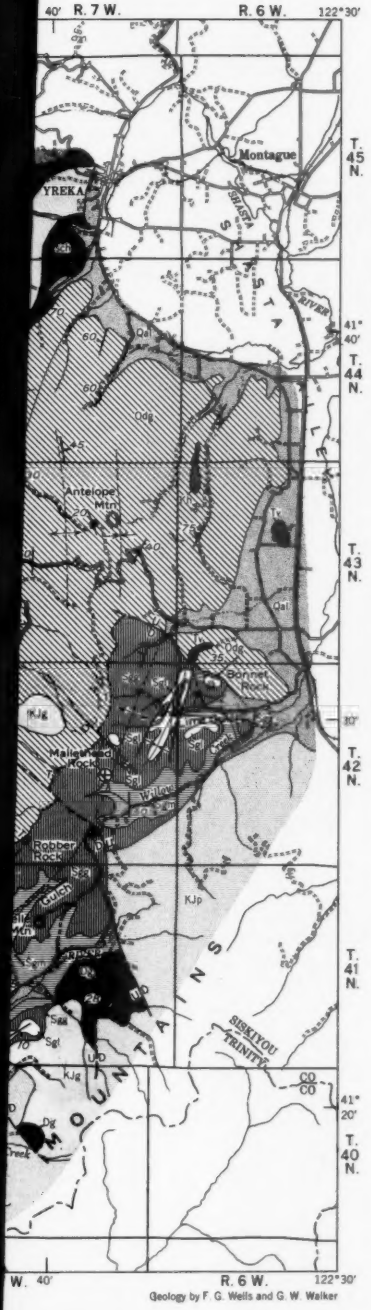

Geology by F. G. Wells and G. W. Walker

EXPLANATION

Qal — Alluvium

Tv — Basaltic flows

UNCONFORMITY

Upper Cretaceous

Kh — Hornbrook formation

UNCONFORMITY

Upper Jurassic and Lower Cretaceous

KJg — Granitoid intrusive rocks

KJp — Peridotite largely serpentinized

Upper(?) Triassic

ka — Applegate group

Altered lava flows, flow breccia, and pyroclastic mostly of basic composition. Also tuffaceous chert, and limestone

UNCONFORMITY

Dg — Greenstone

Includes thin limestone lentils

Upper Silurian

Sgl / Sgm — Gazelle formation

Graywacke, chert, limestone, and limestone breccia limestone, Sgl; black siliceous mudstone, Sgm

UNCONFORMITY ?

Upper Ordovician(?)

Odm / Odg — Duzel formation

Graywacke metamorphosed to pale gray-green phy Odg; marble, Odm

UNCONFORMITY

sch — Siliceous muscovite schist

Contact

Fault

Dashed where inferred, dotted where concealed U, upthrown side, D, downthrown side

Thrust fault

T, upper plate; dashed where inferred

Anticline showing trace of axial plane

Dashed where approximately located

Syncline showing trace of axial plane

Dashed where approximately located

30 — Strike and dip of bedding

Horizontal bedding

Strike and dip of foliation

TRUE NORTH
MAGNETIC NORTH
APPROXIMATE DECLINATION 1956

REA BETWEEN SHASTA AND COUNTY, CALIFORNIA

5 6 Miles

Wells *et al.*, Pl. 1

ATION

- ium — QUATERNARY
- flows — TERTIARY
- RMITY
- formation — CRETACEOUS
- RMITY
- usive rocks — JURASSIC AND CRETACEOUS
- serpentinized
- e group — TRIASSIC
  cia, and pyroclastic rocks, n. Also tuffaceous rocks,
- RMITY
- tone — DEVONIAN
  estone lentils
- Sgl
- rmation — SILURIAN
  nd limestone breccia, Sgs,
  ceous mudstone, Sgm
- RMITY ?
- Odm
- mation — ORDOVICIAN
  pale gray-green phyllite,
  e, Odm
- RMITY
- PRE-UPPER ORDOVICIAN(?)
- ovite schist

ct

t
otted where concealed;
downthrown side

ault
d where inferred

ace of axial plane
cimately located

ce of axial plane
imately located

of bedding

edding

of foliation

ION 1956

BULLETIN OF THE GEOLOGICAL SOCIETY OF AMERICA
VOL. 70, PP. 651–654 MAY 1959

PRELIMINARY STUDY OF STOCHASTIC TERMS USED IN GEOLOGY

BY BAHNGRELL W. BROWN

In a paper read before the Rocky Mountain Section of The Geological Society of America (Brown, 1958) I emphasized the probabilistic nature of geology. This has always been tacitly understood among geologists, and we find occasional direct reference to probable hypotheses (Chamberlin, 1897, p. 837–838) or evaluation and "balance of probabilities" (Spieker, 1946, p. 146). Teichert (1958, p. 106) makes specific reference to "the very high mathematical improbability" of an event in historical geology. Quantitative probability treatment of this sort represents, in my opinion, a distinct advance in our science.

It is apparent when scanning the geologic literature that its language carries frequent reference to such stochastic expressions as "probably," "likely," "overwhelming evidence," "little doubt," "equally possible," etc. It may also be noted, if the study is critical, that there is little consistency in the probability meaning one might read into these terms. Very often the meaning is completely in question. For the doubtful cases the reader does not know whether or not it was the author's wish to leave a rather wide fringe of uncertainty concerning his ideas. These observations should raise the question whether or not an agreed-upon and clear-cut stochastic symbolic language would be of benefit to geology.

I have examined sufficient examples in our literature to be convinced that this is a very real problem in geological communication and not just semantics.

There are many concepts in geology and many observations about which there must always be some degree of doubt. Geology is by its very nature a stochastic science. Greater use of quantitative meaning in probability terms can hasten our efforts to make a more quantitative science of geology. Ideally speaking, we might quantitatively evaluate the formal degree of likelihood for every expression that would indicate some degree of doubt. Also, somewhere between this ideal and present usage, there should be a practical and reasonable solution.

There is disagreement among mathematicians in the matter of definition of likelihood and of equally likely, but there is no argument concerning the quantitative expression of equal likelihood once defined. The concept "equally likely" is an *a priori* intuitive idea according to Fry (1928, p. 1–6). With this we may or may not agree, but would surely agree that the value 50 per cent or 0.5 could express the intuition adequately. There are two principal schools of mathematics, calling themselves "insufficient reasonists" and "cogent reasonists" (Fry, 1928, p. 6), which define "equally likely" in different ways. The insufficient reasonist says two events are equally likely if there is no reason to think them otherwise. The cogent reasonist says they are equally likely only if there is a cogent reason for thinking so. Both schools express equal probability in the same fashion: p equals .5, and on this point we, also, can be agreed.

De Morgan (Nagel, 1955, p. 386) defined probability as "the state of mind with respect to an assertion, a coming event, or any other matter on which absolute knowledge does not exist." (GEOLOGY?). The calculus of probability is the precise statement of this state of mind.

Unfortunately—and this is probably where most of our difficulty lies—there are two probability languages, a *popular* and a *mathematic*. Some of the mathematic language was derived from the ever-popular gaming tables, more precisely defined. In the word *probable* itself there is a multiplicity of meaning. Mathematicians cannot agree on the meaning. If we are to be precise in our geological application of this word or of any other term denoting or connoting probability, we should first agree on the meaning of *probability*.

Likelihood seems to be the essence of probability. Degree of likelihood can be expressed numerically. By mathematical convention, equal likelihood carries a value of 50 per cent (expressed as p equals .5). Impossibility is 0 per cent (p equals 0), and absolute certainty is 100 per cent (p equals 1). Any degree or range of likelihood can be expressed quantitatively. It may not be practical to be at all times quantitative in geologic statements. For that reason we should qualitatively define the more commonly used stochastic expressions.

I am rather in agreement with Carnap (1953, p. 132) in finding it necessary to distinguish between a "statistical probability," which defines the state of a real system—physical, biological, etc.—and an "inductive probability," which is a framework in which we may analyze concepts and statements of science and which does not necessarily express the state of the real system, but does express *the state of our judgment concerning the reality of a system.*

It is not the purpose here to review probability as it pertains to stochastic systems defining a geologic real-state; these matters will be considered in a later paper. There has been little opportunity for geologists to exercise "statistical probability" outside the fields of sedimentation and petrofabrics. On the other hand, we do frequently encounter inductive probability in areas in which geologic statements and evaluations of statements are normally made. Since words rather than mathematical symbols are commonly employed in those areas, and since there has been little effort to assign precise stochastic meaning to the words, a sharpened usage for probability terms seems desirable.

Numerous examples from the geological literature were studied for their utilization of probability terms. Table 1 sums the results of this study and illustrates current usage for the more common stochastic terms. The principal observation has been that many of the judgments or opinions are stated without a clear-cut pronouncement of the magnitude or range of the author's own belief in the statement. An author may understandably and justifiably be reluctant to state a statistical probability in geology without adequate statistical support, but the utter lack of supporting evidence should be no concern of *inductive* probability. It does not alter an opinion or the probability of the opinion to learn that the route to the opinion was poor and the supporting reasoning invalid. The route to an inductive probability judgment may even be entirely intuitive (and it seems to me there should be ample room in geologic work for intuitive reasoning).

TABLE 1.—COMMONLY USED STOCHASTIC TERMS

Term and synonym	Usual probability	Other meaning
Likely, probable, little doubt	above .5; high	indefinite range
Unlikely, improbable, doubtful	below .5; low	indefinite range
Possibly, may be, perhaps	indefinite	low probability
May be, could be that	indefinite	can be permissive
Probably, likely, much evidence that	above .5; indefinite	indefinite range
Improbably, unlikely	below .5; low	close to zero
Equally possible, equally likely, just as reasonably	exactly or near .5	indefinite
Invariably, undoubtedly	exactly or near 1.0	always
Impossibly, never	exactly 0	low probability
If . . . then, all terms relative to formal proof	at or near 1	conditional p
Most likely, little doubt, most probably, overwhelmingly	near 1; high	indefinite range

Whatever the route taken to reach a stated opinion, whether by *a priori* reasoning or by formal argumentation from sufficient cause, the reader deserves to get a clear statement of the probability of the author's belief and, whenever practicable, an equally clear statement of the route to the judgment.

As a "state of mind" p *equals 0* and p *equals 1* can hardly be recommended, since they reflect an improbable achievement. If a repetitious event has happened m times successfully and has failed zero times, then the probability $P = (1 \text{ plus } 1/m)\ (1 \text{ plus } 2/m)^{-1}$. Quantity P is unity only for an infinite m. For this reason we must think of unity and zero as the limits of probability and not as probabilities.

On the basis of this study I would like to suggest fixed probability limits for a few of the more commonly used stochastic terms. Probability terms other than these should either be avoided or be clearly defined.

The stochastic terms selected to convey probability meaning are as follows:

Impossibly: *Lim* p approaches 0

Improbably: p is less than .5

Equally likely: p approximates .5
Probably: p is greater than .5
Undoubtedly: *Lim* p approaches 1
Possibly: Indeterminate probability ranging from 1 to 0

The writer is indebted to W. C. Krumbein for helpful criticism.

References Cited

Brown, B. W., 1958, Stochastic geology (Abstract): Geol. Soc. America Bull., v. 69, p. 1724
Carnap, R., 1953, What is probability: Sci. Am., v. 189, September, p. 128–138
Chamberlin, T. C., 1897, The method of multiple working hypotheses: Jour. Geology, v. 5, p. 837–848
Fry, T. C., 1928, Probability and its engineering uses: New York, D. Van Nostrand, 476 p.
Nagel, E., 1955, Principles of the theory of probability: International Encyclopedia of Unified Science, Univ. of Chicago Press, p. 343–422
Spieker, E. M., 1946, Late Mesozoic and early Cenozoic history of central Utah: U. S. Geol. Survey Prof. Paper 205-D, p. 117–161
Teichert, C., 1958, Some biostratigraphical concepts: Geol. Soc. America Bull., v. 69, p. 99–120

Mississippi Southern College, Hattiesburg, Miss.

Manuscript Received by the Secretary of the Society, October 30, 1958

BULLETIN OF THE GEOLOGICAL SOCIETY OF AMERICA
VOL. 70, PP. 655-660, 1 FIG. MAY 1959

EXPERIMENTAL STUDY OF CHROMATOGRAPHIC-TYPE ACCUMULATION OF ORGANIC COMPOUNDS IN SEDIMENTS: AN INTRODUCTORY STATEMENT

BY BARTHOLOMEW NAGY AND JOHN P. WOURMS, JR.

Organic compounds may be concentrated in layers of sedimentary rocks by basically chromatographic-type processes. The same mechanisms may also lead to the separation of mixtures of organic compounds and to the concentration of the fractions in rock strata[1]. The chromatographic processes are the result of fluid flow through beds containing fine-grained mineral particles.

Chromatographic separation and concentration of organic compounds with mineral particles, such as clay minerals, is a common practice in organic chemistry and biochemistry. For example, Binkley (1955) reports the use of clay-mineral-packed columns for the chromatography of carbohydrates. Nikkilä and Oker-Blom (1952) used montmorillonite clay for the selective adsorption of lipid-containing materials in a study of lipoproteins, and Lindau and Rhodius (1935) studied the adsorption of albumin on quartz powder. The successful separation and concentration of several organic compounds in the laboratory on columns packed with the common sedimentary-rock minerals suggests that similar chromatographic processes might have taken place in nature, in the sediments and in sedimentary rocks.

Trask (1938) pointed out that the organic-matter content of marine sediments, following deposition in the sedimentary basins, is diversified and usually low, compared to the amount of minerals present. The newly deposited sediments have high porosities, but the overburden pressure of subsequent arrivals causes compression, reduction of the pore volumes, and displacement of a part of the sea water originally filling the pores. The displaced fluid, including traces of organic compounds, is forced to migrate through overlying or adjoining layers of clay-mineral and quartz-bearing sediments. This, in effect, is a chromatographic system.

The fact that water does move in newly deposited sediments has been shown by, among others, Kidwell and Hunt (1957). Drilling-test holes in the deltaic sediments of the Orinoco River in Venezuela supplied evidence for intrastratal fluid flow and have shown a related pressure-gradient distribution in sediments indicated to be less than 10,000 years old by C^{14} dating. Compaction of newly deposited sediments is not, however, the only cause for fluid flow. Mounting pressures in the sinking geosyncline, various tectonic disturbances, etc., can all cause the pore-filling fluids to move.

The causes of the chromatographic effect in sediments are ion exchange, adsorption, and partition chromatography. Since quartz and the clay minerals, the major components of detrital sediments, all possess ion-exchange capacities of varying magnitudes, the ionic components of the migrating fluids cannot pass unaffected. Clay minerals are noted for their high ion-exchange capacity, and consequently beds abundant in clay are expected to accumulate more organic ions than are beds composed mainly of quartz. The adsorption chromatographic experiment with the carbohydrate, cellobiose, described below, and the partition chromatographic experiments of Roper, Doscher, and Kobayashi (1958) with light hydrocarbon constituent gases in "columns" of sedimentary rocks indicate the diversity of sedimentary chromatographic mechanisms.

The chromatographic experiments were designed to answer these two questions: Can chromatographic processes function in sediments and sedimentary rocks under simulated *geological conditions*? If they can, what are some of the physical laws that control such processes? The work is based on the assumption that it is possible to set up in the laboratory representative, or at least approximative, model experiments of this particular geological phenomenon.

Ion-exchange chromatography was studied with various size fractions of (Ottawa) quartz sand and illite (Fithian, Illinois, API Clay Mineral Standard No. 35). Both the quartz and the clay samples contained particles of uniform

[1] Binkley (1955, p. 55) defines column chromatography, a process which is believed to be similar to the sedimentary chromatographic effect, as "*the separation, by selective adsorption, of a mixture of substances into zones or bands, on a column of powdered materials, after the passage of proper solvents*".

size, obtained by repeated fractionations and decantations. The columns were eluted with sea water, collected at the shore in Long Island Sound at New Rochelle, New York, and filtered through only Whatman No. 2 filter paper. The chlorinity of the sea-water sample was 14,100 ppm, indicating dilution by surface waters (average sea-water chlorinity is 18,980 ppm). The organic ions used in the ion-exchange experiments were the two triphenylmethane dyes, known by their commercial names, crystal violet and rosaniline.

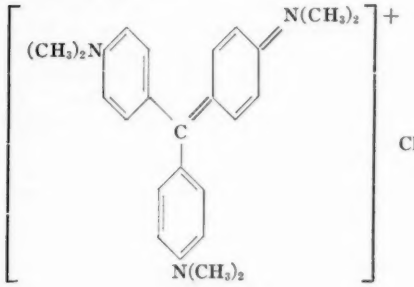

Crystal violet

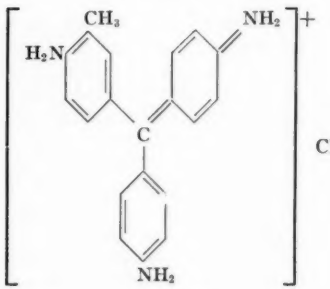

Rosaniline

The two dyes are structurally similar. Triphenylmethane dyes are resonance hybrids in which the major contributing structures carry the cationic charge on one of the nitrogen atoms or on the methane carbon atom. They were chosen because their ions are strongly adsorbed on clays and sand from aqueous solutions and because they have distinctive colors even at low concentrations, permitting the visual observation of the movement of the bands. Working with dilute solutions promised a more precise definition of the laws of sedimentary chromatographic processes; it does not reveal, however, the maximum to which sediments can concentrate organic matter. Since this property of sediments is believed to be particularly affected by local variations in the geological environment, it was not investigated in this introductory study.

The elution experiments were preceded by a study of ion-distribution equilibria between the stationary and mobile phases, in order to define some of the causes of the sedimentary chromatographic effect and in order to facilitate the construction of the columns. The equilibrium-distribution coefficients, K_d, and the chromatographic separation factors[2], α, between quartz, illite, sea water, and the triphenylmethane ions were determined by the method of Tompkins and Mayer (1947). The sand and clay were first shaken overnight with sea water, the supernatant liquid was poured off, the samples were washed with alcohol, and then the samples were shaken again with known volumes of 0.80×10^{-5} N and 0.88×10^{-5} N solutions of crystal violet and rosaniline in sea water, respectively. The shaking was performed at room temperature and in darkness; the containers were surrounded by a light-proof shield. Changes in the supernatant liquid concentrations were colorimetrically determined.

The distribution coefficient, K_d, may be used to calculate separation efficiency; it can also be related to the classical, chromatographic "plate theory", according to the derivation of Mayer and Tompkins (1947). Its application is limited to columns of uniform K_d. The equilibrium-distribution coefficient is also a measure of the relative amounts of ions taken up by the mineral matter; the data in Table 1 show that the triphenylmethane ion adsorption ability of the solids increases with decreasing particle size. A measure of the chromatographic separation possible between the two ions is α, the separation factor. The results show that a separation of the mixtures of crystal violet and rosaniline ions is possible, but that α does not seem to be affected by the particle size. These results predict that, when a mixture of the two ions in sea water is passed through layers of sand and clay, each ion will be concentrated into moving bands of maximum concentrations traveling at different speeds, and each will be subject to adsorption and trapping when they reach layers of clay.

Ion-exchange columns were prepared consisting of layers of quartz sand and sand coated

[2] $\alpha = \dfrac{K_d \text{ crystal violet}}{K_d \text{ rosaniline}}$

with a thin (0.001 mm) film of illite. The clay-coated sand was prepared by evaporating to dryness a water suspension of the 0.5 μ illite fraction in the presence of the sand. This was done to provide a clay-bearing layer permeable at the differential pressures used to flow sea water through the columns and also to simulate the microscopic observation that clay minerals often coat and grow into the sand grains of sandstones. The columns were formed as follows: On top was layer B, 2.6–2.8 cm thick, consisting of the 0.15-mm size sand fraction, below which was the illite-coated layer, C, 0.6–0.7 cm thick, and prepared of the same sand fraction; layer D, on the bottom, was 9.2–10.4 cm thick and prepared of the 0.15-mm sand fraction. The diameter of the columns was 2.2 cm. After the columns were packed, filtered sea water was passed through them.

A sample of the 0.03-mm sand fraction was dyed with a 1:1 mixture of crystal violet and rosaniline and washed with water. The dyed-quartz slurry was poured over layer B and was designated as layer A; after compaction it formed layers 2.5–2.8 cm thick in the columns. Layer A was prepared to simulate, among others, a possibility that fine-grained mineral particles adsorb various organic ions from the decaying organic matter in the soils; they carry these ions with them to the basins of sedimentation, following the erosion of the soils, and release them when they are eluted with sea water migrating through the compacting sediments. After the dyed-quartz slurry was in place sea water was passed through the columns at pressure differentials ranging between 0.3 and 3.1 psi. Following elution the columns were extruded, the layers were separated, and the organic ions were removed from sand and clay by shaking the fractions with a 0.3 N NaOH solution in 95 per cent alcohol, following the suggestion of Prof. D. J. Hennessy (Personal communication). After adjustment to neutral pH the dye concentrations were colorimetrically determined.

In the design of the elution experiment an attempt was made to simulate the environment of detrital sediments, newly deposited close to shore in marine basins and not yet deeply buried. The mineral and fluid composition of the system, the layered structure, the low differential pressures, the temperature not exceeding room temperatures, and the high porosities (approximately 50 per cent) are analogous. It should be pointed out that the hydrodynamics of the laboratory systems is simpler than that of natural accumulations.

TABLE 1.—EQUILIBRIUM DISTRIBUTION COEFFICIENTS AND CHROMATOGRAPHIC SEPARATION FACTORS OF TWO TRIPHENYLMETHANE IONS ON QUARTZ SAND AND ILLITE

Grade name Wentworth scale	Mineral	Median particle size (mm.)	K_d Crystal violet	K_d Rosaniline	α
coarse sand	quartz	0.9	1.53	0.73	2.1
medium sand	quartz	0.3	18.04	6.39	2.8
fine sand	quartz	0.15	10.31	4.04	2.6
medium silt	quartz	0.03	20.90	8.04	2.6
fine clay size	illite	0.0005	~12,278	~4,656	2.6

The results are plotted in Figure 1. Elution with sea water resulted in the partial displacement of the triphenylmethane ions from layer A and led to their concentration in the clay-coated sand layer, C. The concentration in layer C reached a value which was 110 per cent higher than the initial concentration in A. The maximum concentration in the uncoated layer B, which was located between C and A, was 50 per cent less than the initial concentration in A. In the uncoated layer D, below the clay trap, the concentration did not reach a value higher than 9 per cent of A. The results indicate that even small amounts of clay present in layers of sand can lead to a significant concentration of organic ions; it appears that much higher concentrations may well be attained with more clay. Separation of the two dyes was observed; rosaniline moved before crystal violet. After only 38.5 ml sea water was passed through the columns, 14 times more rosaniline was present in the clay-coated layers. At the maximum dye concentration in C, that is when 821 ml sea water had passed through the columns, the original 1:1 mass ratio of the two ions was re-established.

If the migration of sea water stops at an early

stage an effective separation of the dye mixture has been achieved in the clay-trap layer. The migration of these organic, ionic solutions through layers of sand and clay is characterized by the gradual build-up and then the decrease of concentrations; the clay-bearing layers contain significantly higher accumulations of organic compounds, and all layers exhibit a preferential accumulation of ions sometime during the cycle.

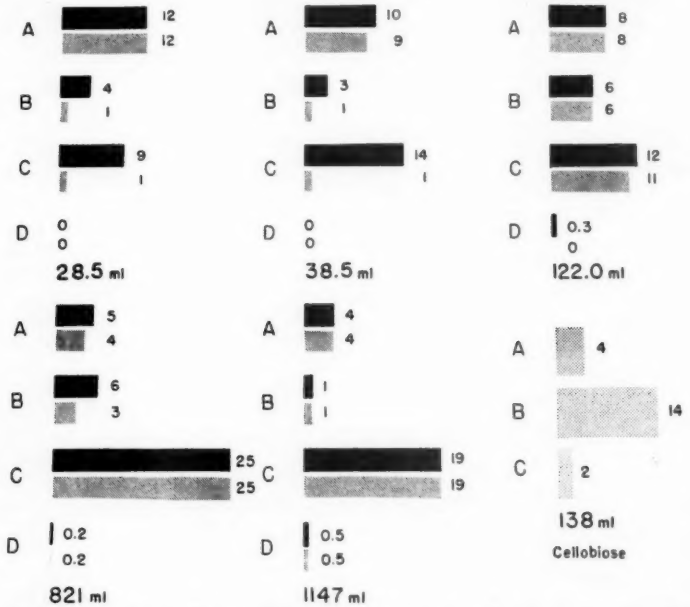

FIGURE 1.—CONCENTRATION OF TRIPHENYLMETHANE CATIONS AND CELLOBIOSE IN THE QUARTZ SAND AND ILLITE-COATED QUARTZ SAND LAYERS OF THE CHROMATOGRAPHIC COLUMNS

Solid bars represent rosaniline, and the ruled bars represent crystal violet. Numbers at the right of the bars are in mg (organic ions)/kg (minerals) units. The letters A, B, C, D represent the layers referred to in the text. The ml values define the volume of sea water that has passed through the column. Direction of flow is from A to D. Note that, because of their difference in mass, changes in concentrations of only fractional mg/kg units in one of the thick layers can effect significant concentration changes in the thin but adsorptive illite-coated layer.

Triphenylmethane dyes, of course, do not occur in nature; therefore they are of somewhat limited usefulness in organic geochemistry experiments. The chromatographic laws which govern their movement probably apply, however, to the ion-exchange chromatography of a number of naturally occurring metabolic decomposition products in soils and sediments. For example, proteins, peptides, and amino acids are ions carrying a net charge, positive in acid and negative in alkaline solutions, at pH values far from their isoelectric points. Amino acids may occur in sedimentary matter. Possibly amino acids can be separated from other types of organic compounds by basically chromatographic processes. Adsorption and partition chromatography seems to be involved in the separation and concentration of certain other types of organic compounds, such as carbohydrates and hydrocarbons.

Adsorption chromatography experiments were performed with quartz sand, illite, and cellobiose, in order to show that this process can also take place with sedimentary rock minerals and to illustrate this phenomenon with a naturally occurring organic compound. Frontal analysis type experiments with the carbohydrate, cellobiose, a water-soluble metabolic decomposition product of cellulose, resulted in the concentration of cellobiose in the

clay-coated sand layers. Cellobiose is a disaccharide sugar (4-O-(β-D-glucopyranosyl)-D-glucopyranose):

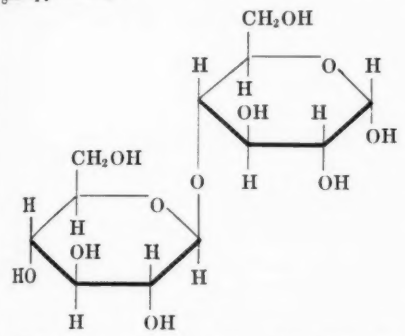

Cellobiose units, joined together, form the polymeric chains of the wood, bacterial and animal cellulose molecules. Wood-destroying molds of the "brown-rot" type secrete enzyme systems which degrade cellulose through hydrolysis into cellobiose and then into glucose, leaving the lignin content mainly unaffected; this was first shown by Pringsheim (1912).

$$\text{Cellulose} \xrightarrow{\text{cellulase}} \text{Cellobiose} \xrightarrow{\text{cellobiase}} \text{Glucose}$$

The decay of wood by the wood-rotting fungi is, of course, of wide occurrence in nature and adds cellobiose and other hydrolisate sugars to soils and sediments.

Chromatographic columns were packed with layers of quartz sand and illite-coated sand. On top was a 3.5-cm thick layer, A, of the 0.15-mm particle size fraction sand; layer B, 0.45 cm thick and containing the same size fraction, was coated with a thin film of the 0.5 μ illite fraction. Finally there was a bottom sand layer, C, of the same size fraction; this layer was 9.0 cm thick. Dilute solutions of cellobiose in water (2×10^{-5} M) were passed through the columns.

After completion of the runs the columns were extruded, the cellobiose separated from clay and sand, and its concentration colorimetrically determined by the method of Dische and Popper (1926), using sulfuric acid and a 1 per cent solution of indole in ethyl alcohol to develop the mahogany-brown color. The results for one column are illustrated in Figure 1. The concentration of cellobiose in the clay-bearing layer was 3.5 times higher than in the uncoated sand above and 7 times higher than in the layer below. The experiments suggest that cellobiose and other carbohydrates can accumulate principally through the adsorption chromatographic process in clay-containing sediments. This experiment was designed to simulate nonmarine environments.

Both the ion-exchange and the adsorption-chromatography experiments show that small amounts of organic compounds can be subjected to chromatographic processes when they are migrating through sedimentary mineral matter. This of course is a laboratory experiment awaiting substantiation by field analyses. The geologist who has seen oil-well cores, however, cannot but wonder how fluids could have migrated through the intimate shale and sandstone interlamination without being affected by chromatographic separation and accumulation processes. It appears that chromatography is a step in the preferential accumulation of organic compounds in sedimentary rocks.

References Cited

Binkley, W. W., 1955, Column chromatography of sugars and their derivatives: Adv. Carbohydrate Chem., v. 10, p. 55–94

Dische, Z., and Popper, H., 1926, Über eine neue kolorimetrische Mikrobestimmungsmethode der Kohlehydrate in Organen und Körpersäften: Biochem. Zeitschrift. Bd. 175, pp. 371–411

Kidwell, A. L., and Hunt, J. M., 1957, Migration of oil in recent sediments at Pedernales, Venezuela: Paper presented before the 42nd Annual Meeting of the Am. Assoc. Petroleum Geologists

Lindau, G., and Rhodius, R., 1935, Die physikalisch-chemische Analyse adsorbierter Eiweissmoleküle in der Grenzfläche festflüssig: Zeit. physikal. Chemie, Abh. A, Bd., 172, p. 321–347

Mayer, S. W. and Tompkins, E. R., 1947, Ion exchange as a separation method. IV. A theoretical analysis of the column separation process: Jour. Am. Chem. Soc., 69, 2866–2874

Nikkilä, E., and Oker-Blom, N., 1952, Adsorption of serum lipids by montmorillonite: Science, v. 116, p. 586–686

Pringsheim, H., 1912, Über den fermentativen Abbau der Cellulose: Zeit. physiol. Chemie, v. 78, p. 266–291

Roper, W. A., Doscher, T., and Kobayashi, R., 1958, Evidence of chromatographic effect during flow of gases through oilfield cores: Jour. Petroleum Technology, v. 10, p. 61–63

Tompkins, E. R., and Mayer, S. W., 1947, Ion exchange as a separation method. III. Equilibrium studies of the reactions of rare earth complexes with synthetic ion exchange resins: Jour. Am. Chem. Soc., v. 69, p. 2859–2865

Trask, P. D., 1938, Petroleum source beds: Science of Petroleum, v. 1, p. 42–45, Oxford Univ. Press

FORDHAM UNIVERSITY, NEW YORK 58, N. Y.

MANUSCRIPT RECEIVED BY THE SECRETARY OF THE SOCIETY, AUGUST 12, 1958

BULLETIN OF THE GEOLOGICAL SOCIETY OF AMERICA
VOL. 70, PP. 661-664, 1 PL. MAY 1959

FROTH VEINS, FORMED BY IMMISCIBLE HYDROTHERMAL FLUIDS, IN MERCURY DEPOSITS, CALIFORNIA

BY EDGAR H. BAILEY

Immiscibility of two fluid phases has been postulated as a mechanism to explain the fractionation of magmas and the separation of sulfides from silicate melts, yet very few rocks or ores displaying textures supporting liquid-immiscibility hypotheses have been described (Moyd, 1942; Shaub, 1942). Ingerson (1955, p. 370–371) summarizes experimentally investigated systems that involve liquid immiscibility and may be of possible geologic application, and he concludes, "The present writer is not convinced that true liquid immiscibility has been demonstrated beyond doubt in any hydrothermal system." The froth veins described here seem clearly to have been deposited from hydrothermal solutions containing a hydrous fluid and immiscible droplets of oil. Although they represent a special case and are little more than geologic curiosities of restricted occurrence, they provide good examples of textures that result from crystallization in a two-fluid phase system.

These veins occur as an integral part of the ore deposits in several quicksilver mines in California, although as far as I am aware they have been described, briefly, only by Yates (1946, p. 248). Similar material also has been described by Renouard (1955, p. 2163–2165) as occurring in gash veins in petroliferous sediments in Lebanon.

Typical froth veins are composed of close-packed spherical shells of quartz, chalcedonic quartz, or opal enclosing droplets of oil, but some contain spheres that are empty or only partly filled with a solid hydrocarbon. The spaces between the shells are commonly filled with the same mineral that forms the shells, and as a result the veins superficially appear to be composed of silica containing numerous round holes. In some veins, however, the interspaces between the oil-filled spheres are voids. The spheres in any one vein range widely in size with small spheres nestled among larger ones, but generally the largest are less than 1 mm in diameter. The resulting veins closely resemble a solidified froth, hence the term "froth vein." Because of their texture, the presence of oil in the spheres but not in the interspaces, and their geologic occurrence, the froth veins are believed to result from initial deposition of silica on interfaces between hydrous vein fluids and immiscible droplets of oil. This was followed in many places by continuing deposition of silica between the spherical silica shells.

Opal froth veins that look much like "honeycomb" candy are abundant in the Abbott quicksilver mine, Lake County, California, in or near the ore bodies, which in this deposit are confined to opalized serpentine. The veins are clearly later than most of the cinnabar ore, but locally they contain a little cinnabar and pyrite. They consist largely of isotropic opal with numerous spherical holes ranging in size from 0.005 mm to several millimeters (Pl. 1, fig. 1). Although the holes range widely in size they are so closely packed that the walls between adjacent holes at the points of closest approach consist of thin partitions, which indicate the veins originally consisted of closely packed, thin-shelled spheres. Because of the abundance of oil-filled openings, many of the vein rocks have a specific gravity of only 1.5 or less. Despite the close packing none of the holes are distorted or flattened by mutual interference, as they would be in a gas–liquid froth. This feature, which is in contrast to an undeformed highly vesicular pumice, also indicates the veins resulted from an accumulation of thin opal shells formed about oil droplets; subsequently most of the interspaces have been filled by similar opal. Many of the shells contain a thin oil, and in some there is also a gas bubble. Others are hollow; still others are filled with opal or contain small crystals of a carbonate or a solid green hydrocarbon resembling curtisite (Wright and Allen, 1930). The difference in kind and degree of filling indicates that some of the opal shells were sufficiently porous to permit either outward leakage of the lighter oil fractions or inward leakage of hydrothermal solutions. That there was leakage is also indicated by rarer occurrences of a second spherical shell of opal attached to the inside wall of a larger spherical cavity, as in a froth vein from the Jumbo mine, Sonoma County, California (Pl. 1, fig. 2).

Because of the close association of the froth

veins with the ore at the Abbott mine, and the occurrence of vapor bubbles in the entrapped oil, W. W. Virgin of the U. S. Geological Survey attempted to determine their temperature of deposition by heating fragments under a microscope and observing the temperature at which the bubble disappeared. Although this test was made on material in which most of the spheres still contained oil droplets it was unsuccessful because of leakage. Virgin states (Written communication, 1957):

"The sample was crushed and small fragments were tested with the Richter heating stage. The oily nature of the rock presented observational difficulties in the heating cell of the stage and no results could be obtained. Small fragments were also used with the Kofler micro hot stage where observational difficulties could be minimized. The temperature of the stage was raised to 200°C. at a rate of 2°–3° per minute. As the temperature was increased, some vapor bubbles decreased in size, some increased in size, and some disappeared. The variable results apparently were due to the fact that the enclosure of the oil droplets in many cases was not complete. It would seem that the permeability of the rock allowed the transfer of oil and vapor as it was heated. The heating stage method of determining the temperature of disappearance of the vapor phase cannot be justified in this case. Another observation tending to bear this out is the variable size of vapor bubbles in oil droplets of the same size. Since there is a definite relation between the degree of filling of liquid inclusions and the temperature at which they became filled with a homogeneous phase, consistent results could not be expected."

A somewhat more successful attempt to determine a maximum for the temperature of deposition was made by gradually heating oil extracted from the veins and observing the temperature at which a distillate first came off. W. W. Virgin, who also conducted these tests, reports that the first observable distillate was obtained at approximately 145°C. Without more detailed knowledge of the depth of deposition of the froth veins, and the changes they may have undergone since deposition, this temperature cannot be regarded as the true temperature of deposition. Although it is a fairly reasonable maximum temperature for the veins in this environment, the studies of White and others (1956, p. 57) suggest that 145°C. is close to the upper limit for deposition of opal.

Somewhat different froth veins are common in the ore bodies of the famous New Almaden quicksilver mine, Santa Clara County, California, and in several of the smaller mines in the district. The veins are spatially related to the quicksilver ore, but they are younger than nearly all the cinnabar. Locally they contain scattered grains and patches of cinnabar, but these all seem to be fragments of pre-existing material rather than a direct crystallization from the vein fluids.

The New Almaden froth veins differ from those of the Abbott mine in being composed of quartz, rather than opal, and in containing a much heavier oil. Superficially they appear to consist of fine-grained white quartz containing spherical droplets of oil, which has been converted to a solid black tar where exposed to air, as in long-open workings or on dumps. The spherical holes range in size from less than 0.05 mm to more than 5 mm, and all sizes exist together. Locally the veins consist of spherical shells of quartz with spaces between. In these places the shells are nowhere filled with the hydrocarbon.

In thin section (Pl. 1, fig. 3), the shells of quartz consist of a double layer with crystals that have grown each way from a narrow zone where the quartz is much finer-grained and highly sutured. The cross section of the narrow

PLATE 1.—PHOTOMICROGRAPHS OF FROTH VEINS

FIGURE 1.—Photomicrograph of thin section of opal froth vein from the Abbott quicksilver mine Lake County, California, taken with plane light. To prepare thin section oil originally present has been removed by solution from all cavities except those completely contained within the thin slice.

FIGURE 2.—Photograph of broken surface of froth vein from Jumbo mine, Sonoma County, California, showing small silica shells within larger shells that have accumulated to form the vein.

FIGURE 3.—Photomicrograph of thin section of quartz froth vein from New Almaden mine, Santa Clara County, California, taken with crossed nicols. Note the double character of the quartz shells and the hollow openings between some of them. The shells were originally filled with oil that was removed to make section suitable for photography.

FIGURE 4.—Photograph of spheres deposited on surface of botryoidal quartz. Darkest spheres are shells filled with oil, lighter ones are hollow, and white ones are solid quartz. Cinnabar occurs in some of the spherical shells.

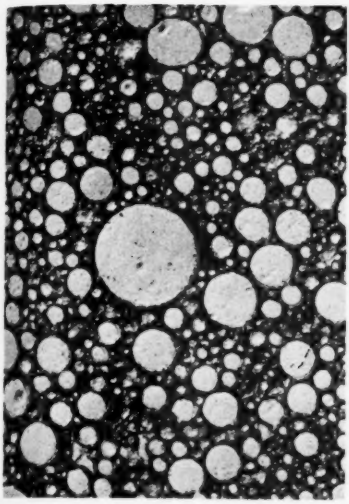

FIGURE 1

FIGURE 2

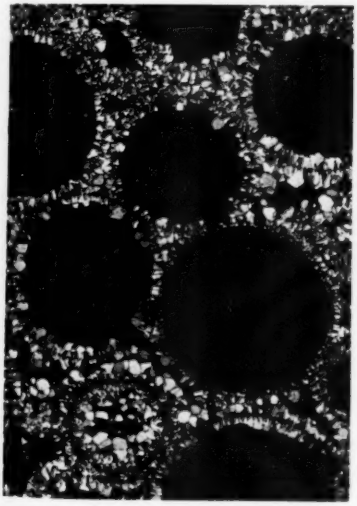

FIGURE 3

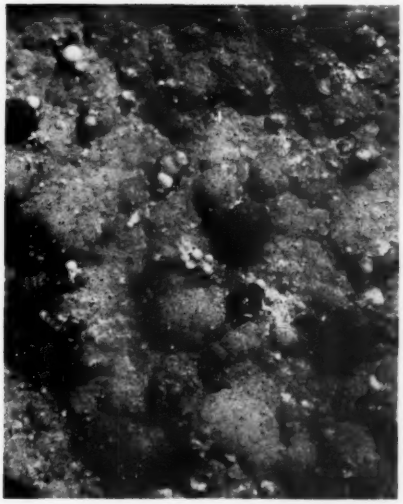

FIGURE 4

PHOTOMICROGRAPHS OF FROTH VEINS

zone is in all cases essentially an undistorted circle, and it is interpreted as marking the original interface between the hydrous fluid and the oil droplet along which the quartz was first deposited. Where two quartz spheres join, the inferred interfaces are generally close together and locally seem to coalesce. The spaces between the double-walled spheres are either voids or are filled with quartz or dolomite. The centers commonly contain hydrocarbons, but in some places they are filled with quartz or dolomite, indicating leakage after the formation of the quartz shell.

Froth veins similar to those at New Almaden have been found at the Jumbo quicksilver mine in Sonoma County, California, in silicified and carbonatized serpentine (Bailey, 1946, p. 229). They differ in that the silica that forms the spherical shells contains cinnabar apparently deposited directly from the hydrous fluid containing droplets of oil.

In the San Quentin Pit at the Manhattan mine in Napa County, California (Averitt, 1945, p. 82–84), froth veins occur in silicified tuffs or opalite. The veins consist of chalcedonic and coarser quartz and contain numerous spherical openings. Some of the openings are filled with a brown solid hydrocarbon, but many contain only a thin film of hydrocarbon coating minute crystals of quartz, and a few contain needles of aragonite. Later veins of pink chalcedonic quartz cut the froth veins, and near the pink veins some of the holes in the froth veins are filled with similar pink quartz.

Veins of similar origin, though different in appearance, partly fill cracks in opalized serpentine near the Cinnabar King mine in Sonoma County, California (Bailey, 1946, p. 229–230). They differ from the froth veins because precipitated minerals occur as coatings rather than as complete fillings of an open fracture (Pl. 1, fig. 4). The vein coating consists of an early layer of chalcedonic quartz, a thin layer of carbonate, and a surface layer of somewhat botryoidal chalcedonic quartz. Perched on the surface of the latter are small spheres of radially oriented quartz crystals; many of the spheres contain a droplet of thin oil. Some or all of the spheres consist of two layers; in these the crystals of the inner layer point inward, and those of the outer layer point outward. The spheres also contain considerable cinnabar concentrated along, though not confined to, the zone between the two layers of quartz. This is believed to provide clear evidence that the cinnabar-depositing fluid was also the fluid containing the droplets of oil, and most of the cinnabar crystallized early along the interface between the immiscible liquids.

In summary, the froth veins have textures most easily explained as resulting from initial deposition of silica at interfaces separating a hydrous vein fluid and immiscible droplets of oil, followed by close packing of the silica shells and further deposition of silica between them. Locally cinnabar was deposited as a part of the original silica shell, indicating that the immiscible fluids also were ore fluids.

References Cited

Averitt, Paul, 1945, Quicksilver deposits of the Knoxville district, Napa, Yolo, and Lake counties, California: Calif. Jour. Mines and Geology, v. 41, p. 65–89

Bailey, E. H., 1946, Quicksilver deposits of the western Mayacmas district, Sonoma County, California: Calif. Jour. Mines and Geology, v. 42, p. 199–230

Ingerson, Earl, 1955, Methods and problems of geologic thermometry: Econ. Geology, Fiftieth Anniversary Volume, pt. 1, p. 341–410

Moyd, Louis, 1942, Evidence of sulfide-silicate immiscibility at Gap nickel mine, Pennsylvania: Am. Mineralogist, v. 27, p. 389–393

Renouard, Georges, 1955, Oil prospects of Lebanon: Am. Assoc. Petroleum Geologists Bull., v. 39, p. 2125–2169

Shaub, B. M., 1942, An unusual asymmetrically banded fissure vein: Am. Mineralogist, v. 27, p. 507–516

White, D. E., Brannock, W. W., and Murata, K. J., 1956, Silica in hot-spring waters: Geochim. et Cosmochim. Acta, v. 10, p. 27–59

Wright, F. E., and Allen, E. T., 1930, Curtisite, a new organic mineral from Skaggs Springs, Sonoma County, California: Am. Mineralogist, v. 15, p. 169–173

Yates, R. G., 1946, Quicksilver deposits of eastern Mayacmas district, Lake and Napa counties, California: Calif. Jour. Mines and Geology, v. 42, p. 231–286

U. S. Geological Survey, Menlo Park, Calif.

Manuscript Received by the Secretary of the Society, November 14, 1958

Publication Authorized by the Director U. S. Geological Survey

BULLETIN OF THE GEOLOGICAL SOCIETY OF AMERICA
VOL. 70, PP. 665–666 MAY 1959

TERMINOLOGY OF POST-VALDERS TIME: A DISCUSSION

BY J. TERASMAE

William S. Cooper (1958) is to be commended for his article on the terminology of post-Valders time. It is important that the numerous names proposed for subdivisions of post-Wisconsin time should be critically reviewed as new evidence accumulates and an appropriate terminology established. This revision should be a careful re-assessment of the existing terminology, and current terms in general use should not be discarded lightly. The writer does not object to the proposed terms, and he finds the terminology as proposed by Cooper very useful for a general understanding of the thermal fluctuations during this time.

The writer is convinced that Cooper did not attempt to establish an elaborate terminology for the post-Valders time but rather a provisional, fundamental subdivision of that episode based on temperature changes as a dominating factor. Once a fundamental terminology for the post-Valders time is generally accepted further elaboration becomes possible and necessary. In that regard the writer believes that a general terminology based on temperature changes only is not sufficient for a detailed subdivision of post-Wisconsin time necessary for stratigraphic and chronologic studies. Other factors, both climatological and ecological, should also be given due attention. The biological nature of the evidence, when plant and animal fossils are used, perhaps indirectly, for subdividing the post-Wisconsin time, demands consideration of all factors which influence the life and environment of these organisms.

It seems somewhat unwarranted to the writer, furthermore, that fixed lower and upper limits have been accepted for the *provisional time units*. Perhaps they might be better referred to as thermal units. Recent studies by Deevey and Flint (1957) and by Livingstone and Livingstone (1958) have shown that episodes such as the Anathermal are not time parallel in a south–north direction and hence can be limited in time in a local sense only. For example, it is self-evident from the table presented by Deevey and Flint (1957) that the late-glacial episode in Connecticut began earlier than that in Maine. By a similar reasoning, based on palynological studies by the writer (in press), Potzger (1953), Potzger and Courtemanche (1954; 1956a; 1956b), and Livingstone and Livingstone (1958), the late-glacial episode is even younger in Canada.

An event such as the Cochrane readvance (Hughes, 1956) should be given due attention, and the end of the Anathermal episode should not be set at 9500 years B.P., when probably most of northern Quebec and Ontario were still covered by glacier ice, and important readvances of ice must have occurred. The final decision on this matter, however, must await more extensive field work.

The writer wishes to draw attention to the fact that information on Wisconsin and post-Wisconsin events in Canada is rapidly accumulating (Prest, 1957) and will certainly contribute to the establishment of a suitable terminology for those times. In the writer's opinion more studies should be made before a final, generally acceptable terminology to cover post-Wisconsin time can be proposed. It is equally important in this connection to distinguish clearly between time-stratigraphic, climate-stratigraphic, and rock-stratigraphic units.

References Cited

Cooper, Wm. S., 1958, Terminology of post-Valders time: Geol. Soc. America Bull., v. 69, p. 941–945

Deevey, E. S., and Flint, R. F., 1957, Postglacial hypsithermal interval: Science, v. 125, p. 182, 184

Hughes, O. L., 1956, Surficial geology of Smooth Rock Cochrane district, Ontario: Geol. Survey Canada Paper 55-41

Livingstone, D. A., and Livingstone, B. G. R., 1958, Late-glacial and postglacial vegetation from Gillis Lake in Richmond County, Cape Breton Island, Nova Scotia: Am. Jour. Sci. v. 256, p. 341–359

Potzger, J. E., 1953, Nineteen bogs from Southern Quebec: Can. Jour. Botany, v. 31, p. 283–401

Potzger, J. E., and Courtemanche, A., 1954, Bog and lake studies on the Laurentian Shield in Mont Tremblant Park, Quebec: Can. Jour. Bot., v. 32, No. 5, p. 549–560

——, 1956a, A series of bogs across Quebec from the St. Lawrence valley to James Bay: Can. Jour. Botany, v. 34, p. 473–500

——, 1956b, Pollen study in the Gatineau Valley, Quebec: Butler Univ. Bot. Studies, v. 13, p. 12–23

Prest, V. K., 1957, Pleistocene geology and surficial deposits, Chapter VIII (p. 443–495) in Geology and economic minerals of Canada, 4th ed.: Geol. Survey Canada Econ. Geology Ser. no. 1

Terasmae, J., in press, Contributions to Canadian palynology II. Part I, A palynological study of post-glacial deposits in the St. Lawrence Lowlands: Geol. Survey Canada Bull.

GEOLOGICAL SURVEY OF CANADA, OTTAWA, ONTARIO, CANADA

MANUSCRIPT RECEIVED BY THE SECRETARY OF THE SOCIETY, OCTOBER 18, 1958

PUBLISHED WITH PERMISSION OF THE DIRECTOR, GEOLOGICAL SURVEY OF CANADA, OTTAWA, ONTARIO, CANADA

TERMINOLOGY OF POST-VALDERS TIME—A REPLY

BY WILLIAM S. COOPER

My reply to Doctor Terasmae's comments on my Short Note may be given very briefly. My objective in writing the paper was a strictly limited one; it dealt with terminology alone and made no attempt to improve on current concepts of late-Pleistocene history. My proposal was adjusted to what seems clearly to be the current view—that temperature has been the dominating factor. It is admittedly an oversimplification, but justifiable in the present state of our knowledge. I would point out, further, that the time limits of my units were adjusted to those set by Deevey and Flint and by Flint. (*See* explanatory note to Table 1 of my paper.) Deevey and Flint set arbitrary limits to their Hypsithermal even though they provide for lack of time parallelism in the stratigraphic sequences of the northeastern United States.

BULLETIN OF THE GEOLOGICAL SOCIETY OF AMERICA
VOL. 70, PP. 667-668, 2 FIGS. MAY 1959

TENSIONAL CONCEPT OF RIFTING

BY ROBERT R. WHEELER

A study of geological and geophysical data bearing upon the structure and stratigraphic sequence within the Dead Sea rift valley, primarily to evaluate its possibilities for oil accumulation, leads to a review of geological theories of rifting. The favored mechanisms considered to account for the formation of rift valleys are that the principal stress has been one of tension accompanied by gravitational downdropping of the central narrow fault block; or, that the primary stress has been one of compression with reverse faulting that has *forced* the central block downward. The tensional and compressive explanations of rifting were briefly reviewed by Jeffreys (1952) who explained that Bullard's studies of gravity in East Africa showed that the rift valleys were systematically negative isostatic anomalies and that the floor, being lighter than normal, should have caused the rift blocks to rise. Even the slightest rise of the valley floor would open the faults so that upward movement would be unresisted. Consequently, Bullard favored an earlier theory that the faults were reversed and that the rift blocks should be considered forced downward under compression. Jeffreys further noted the major geological objection that faults of this type ordinarily branch off, in which case subsidiary faulting bordering the graben should show thrusting; in no case had this been demonstrated. Jeffreys then speculated that neither tension at the surface nor compression was needed to explain rifting, that perhaps in the deeper crustal zone of no strain tension would exist, accompanied by fracturing, so that the outer parts would be pulled downward, thus simulating normal faulting without requiring horizontal tension at the surface. This admittedly tentative idea seems quite incompatible with the buoyancy aspects of equal-density crustal segments at depths involving isostatic compensation.

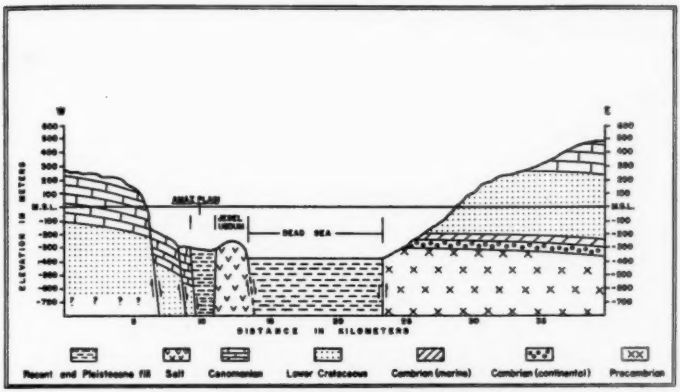

FIGURE 1.—DIAGRAMMATIC CROSS SECTION
Southern end of the Dead Sea Graben. By P. Grader, Geological Survey of Israel

A review of the general geological and geophysical evidence bearing on the rift problem reveals that the striking feature of these geological anomalies consists of the extreme length of the fault system; the length is measured in hundreds of miles, and the width, as in the case of the Dead Sea graben, probably averages no more than 10 miles. Another significant aspect of the Dead Sea graben is that the Trans-Jordanian (eastern) border is structurally much higher than the western margin, and, moreover, the western margin shows downwarping as well as subsidiary normal faulting stepping down into the valley. In other words, the numerous, large, plunging anticlinal arches appear to be dragged into the graben.

Although a well drilled recently along the western margin of the Dead Sea graben at Jebel Usdom penetrated nearly 9000 feet of rock salt, indicating a post-Cretaceous evaporite fill of great thickness, it is still unknown how much marine Tertiary sediments may have filled the rift valley. By analogy to the Suez graben, one might suspect that there has been a downward movement of the graben axis of 10,000–15,000 feet, primarily during Tertiary time. The asymmetrical relation (Fig. 1) of the Trans-Jordan block, structurally higher by more than 1000 feet than the Judean or western block, suggests that the graben axis may be a narrow shear system separating an upthrown block to the east and a downthrown block to the west. By this reasoning, one might suspect that the eastern and western border faulting converge at depth into a single fault plane and that the graben axis is merely an adjustment zone separating two major blocks pulled apart by tension and differentially elevated.

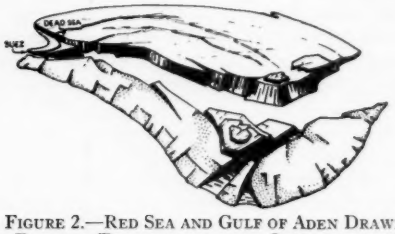

FIGURE 2.—RED SEA AND GULF OF ADEN DRAWN AS FAULTED TRENCHES IN THE CENTER OF THE UPLIFTED AND BROKEN NUBIAN-ARABIAN SHIELD AND ITS BASALT COVER

View from southwest. Left foreground: Egypt and Abyssinia; right foreground: Somaliland; background: Arabian peninsula. (Redrawn after Hans Cloos, 1953, Pl. II)

All the geological evidence in the region of the African-Middle East rift valleys favors a tensional mechanism, including the fact that the subsidiary border faulting is typically normal (nowhere thrust), and the areal pattern is commonly one of zig-zag rectilinear fracturing (contrasted with the generally arcuate pattern of thrust faulting). The regional distribution of this rifting, located centrally within a broadly domed Nubian-Arabian shield, strongly suggests tension (Fig. 2).

Only the negative gravity anomalies are interpreted as opposed to a tensional mechanism. One then must re-evaluate the geophysical assumption—which is fundamentally the concept of isostatic compensation. If the central blocks do not extend to depths in which such buoyancy relations occur, the isostatic concept would be inapplicable. In the [illegible] a region it seems likely that the border faults converge at a depth of a few miles into a single shear far above the depth at which isostatic readjustment is assumed to operate. The axial block could be explained as a downdropped wedge-shaped segment between two tensionally separated border faults converging into a single shear at (from a crustal viewpoint) shallow depths.

Primarily, the object is to suggest that the negative anomalies may not demonstrate buoyancy relations. The tensional aspects, on the other hand, may be more recent adjustments to pre-Tertiary compression and possibly large-scale horizontal displacements.

The writer thanks P. Grader of the Israel Geological Survey for the cross section and for criticizing the manuscript.

References Cited

Jeffreys, Sir Harold, 1952, The Earth: 3d ed. Cambridge, Cambridge Univ. Press, 392 p.

Cloos, Hans, 1953, Conversation with The Earth, pt. II: New York, Alfred A. Knopf.

PYRAMID OIL & GAS CORP., MEADOWS BLDG., DALLAS 6, TEXAS

MANUSCRIPT RECEIVED BY THE SECRETARY OF THE SOCIETY, SEPTEMBER 2, 1958

LEGEND

CENOZOIC

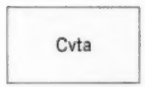

Vitric tuff and alluvium

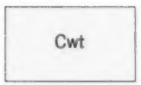

Welded tuff

Silicified tuff

Silicified wood locality

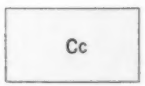

Conglomerate

41°10′

Altered quartz porphyry

Quartz monzonite

Quartz monzonite porphyry

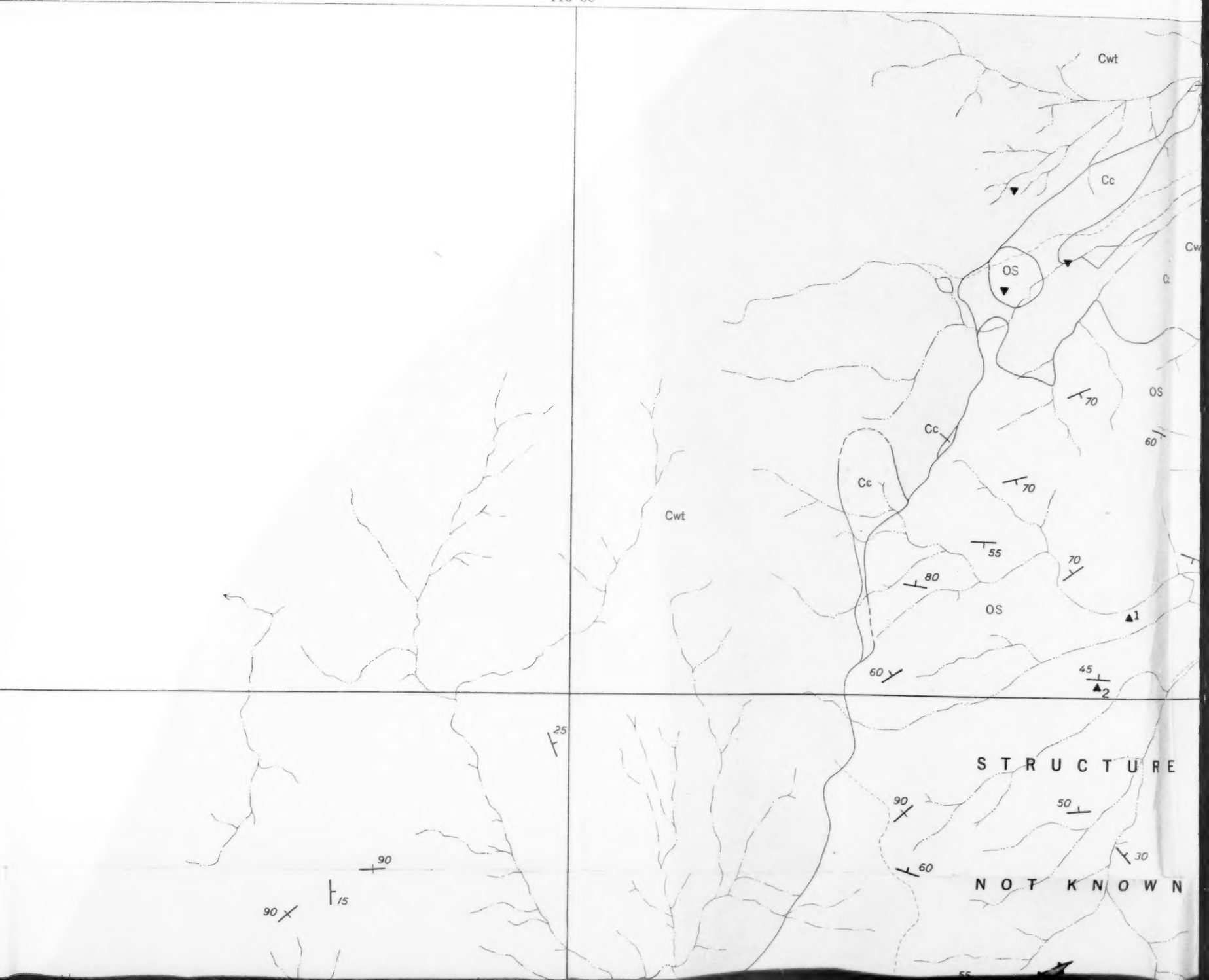
116°00'
Cwt
Cc
OS
Cc
Cwt
Cc
OS
70
60
70
55
80
70
OS
1
60
45
2
25
90
15
90
90
60
STRUCTURE
50
30
NOT KNOWN

116° 00′
OS
Cc
Cc
Cwt
70
55
80
OS
60
25
90
15
90
90
60
STRU
NOT

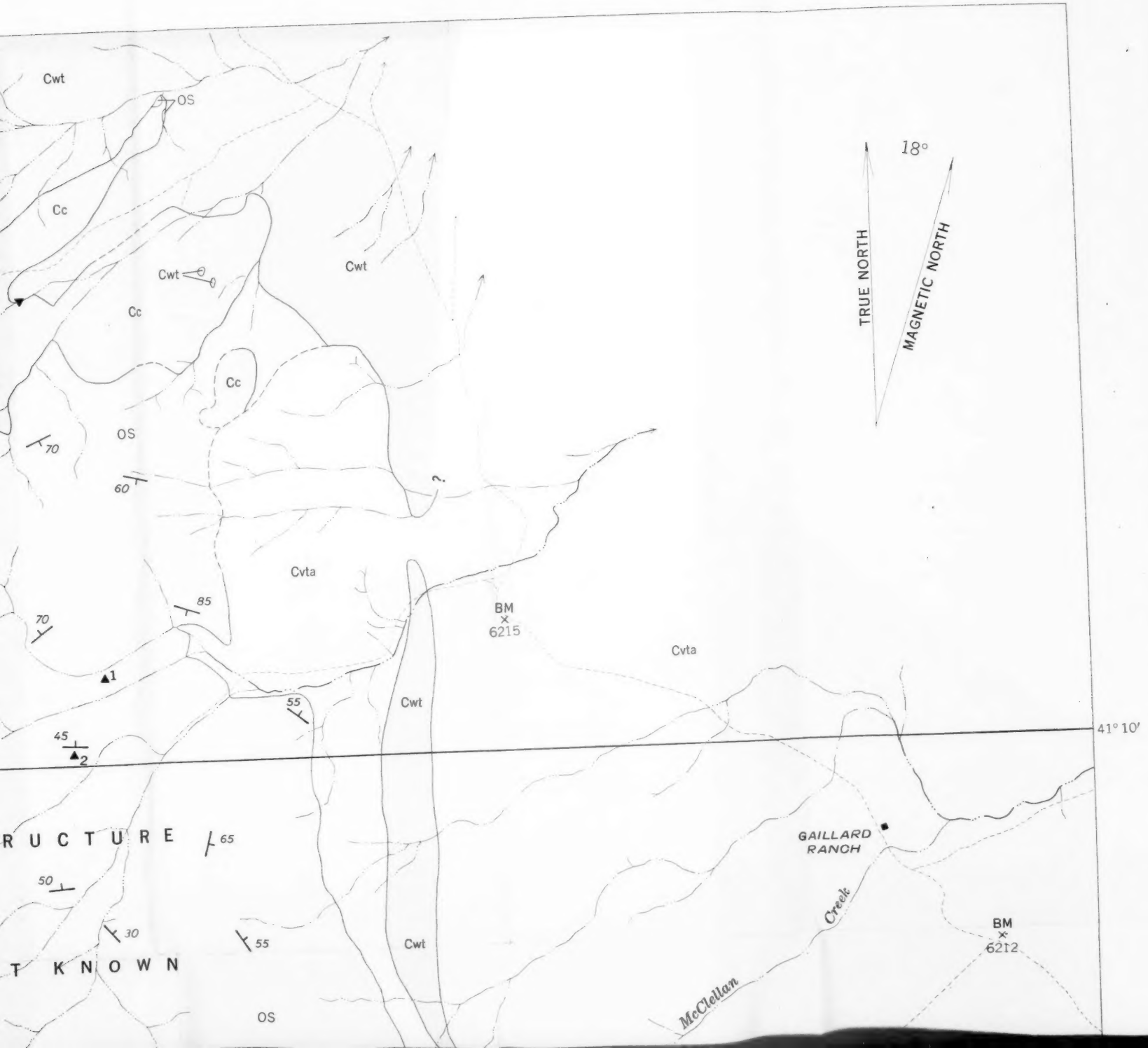
Cwt
OS
Cc
Cwt
Cwt
Cc
Cc
OS
70
60
?
Cvta
70
85
BM
×
6215
Cvta
▲1
55
Cwt
45
▲2
41° 10′
R U C T U R E
65
50
30
55
Cwt
T K N O W N
OS
GAILLARD
RANCH
Creek
McClellan
BM
×
6212
18°
TRUE NORTH
MAGNETIC NORTH

41° 10′

Conglomerate

Altered quartz porphyry

Quartz monzonite

Quartz monzonite porphyry

Altered diorite

Biotite-quartz latite

PALEOZOIC

EASTERN FACIES

DEVONIAN

COAL CREEK SEQUENCE

UPPER PLATE

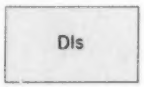

Limestone and shale

LOWER PLATE

Fractured limestone

● Fossil locality

Calcareous siltstone and limestone

DEVONIAN?

McCLELLAN CREEK SEQUENCE

Limestone

WESTERN FACIES

ORDOVICIAN-SILURIAN

Chert and shale

Brecciated chert and shale

△ Silurian graptolite locality

▲ Ordovician graptolite locality

ORDOVICIAN

BASCO FORMATION

Upper chert member

Shale member

▲ Middle Ordovician graptolite

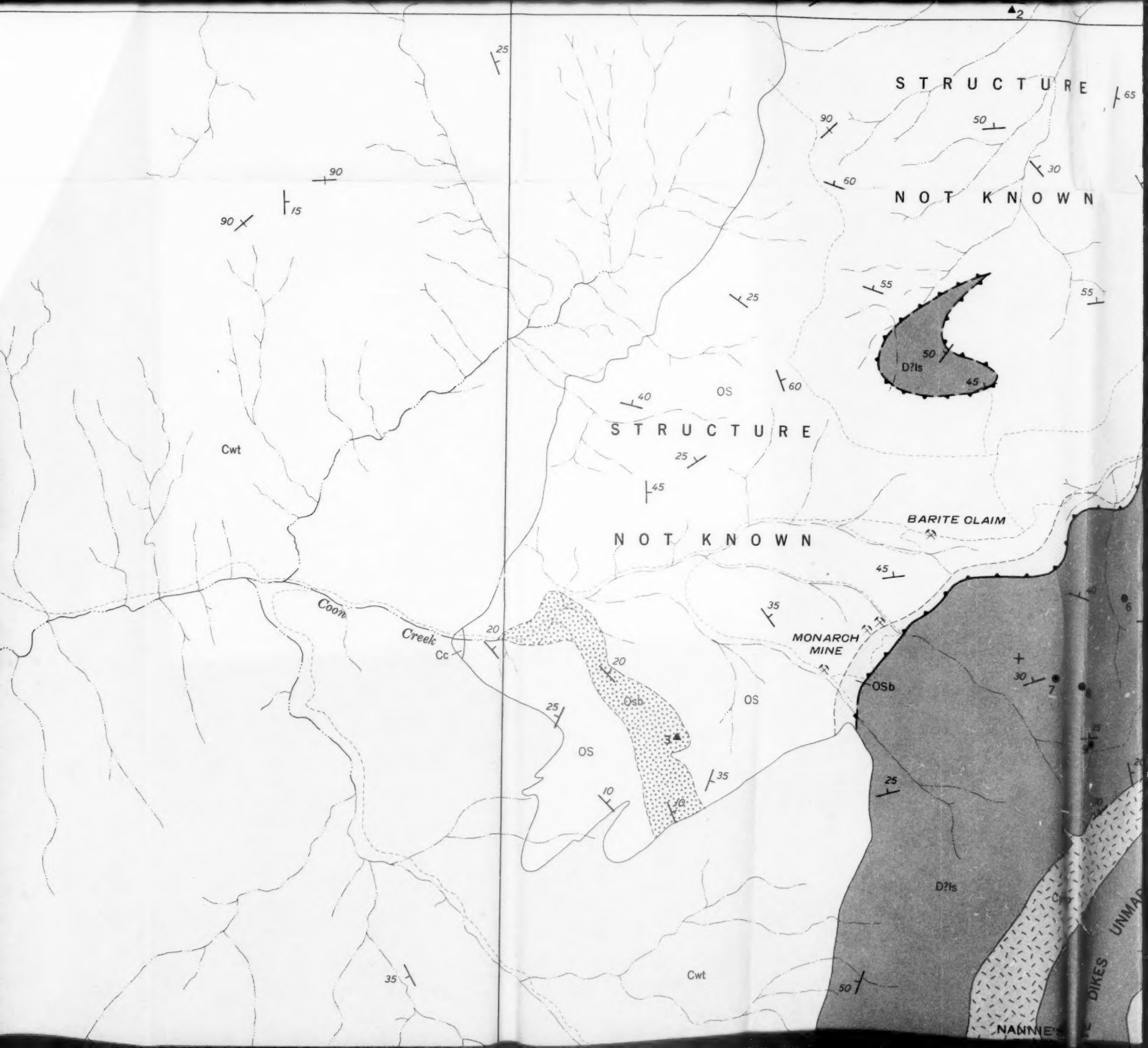
STRUCTURE
NOT KNOWN
STRUCTURE
NOT KNOWN
BARITE CLAIM
MONARCH MINE
Coon Creek
Cc
Cwt
OS
Osb
D?ls
DIKES
NANNIE'S

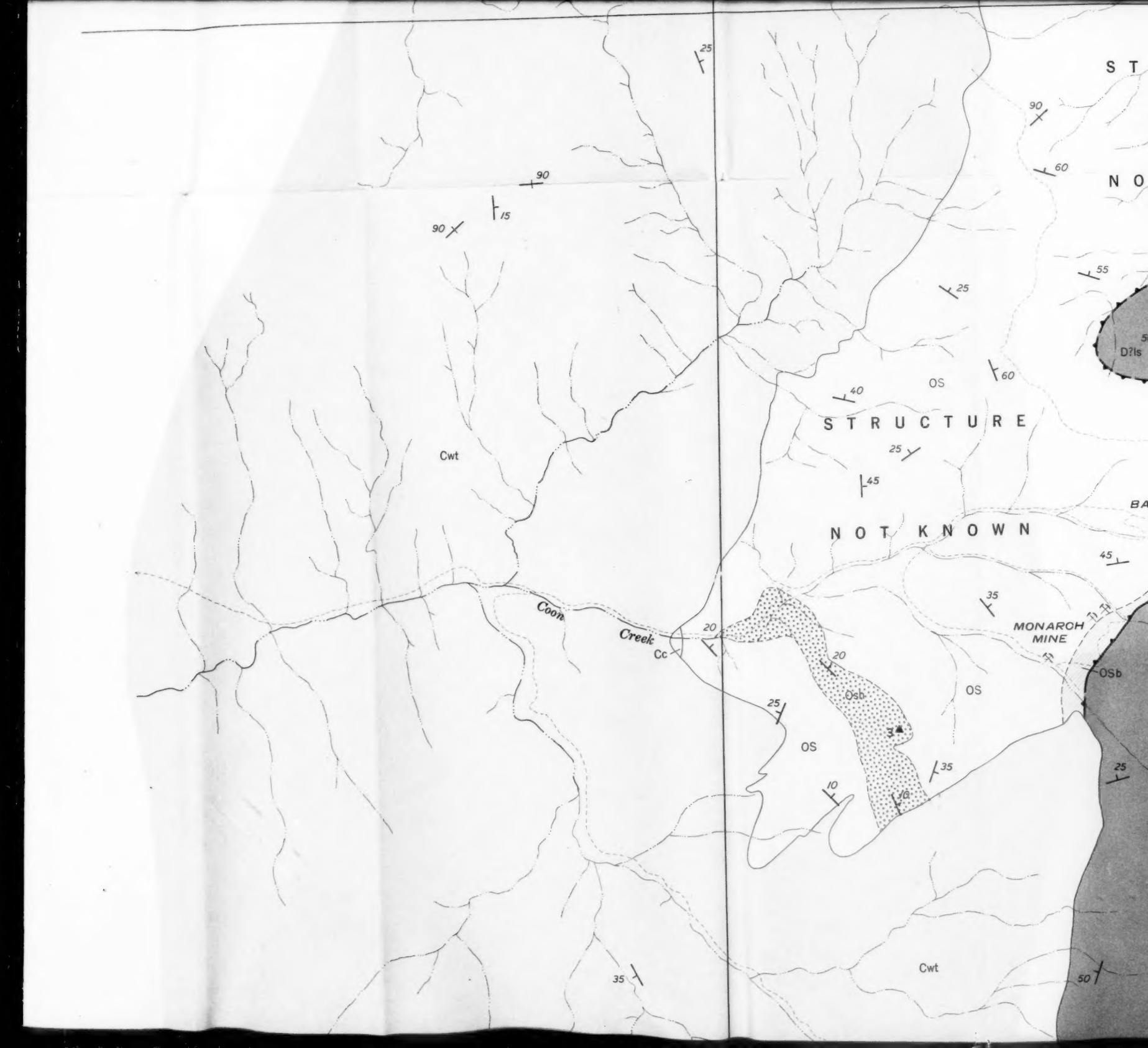
Cwt
Coon Creek
Cc
OS
STRUCTURE
NOT KNOWN
MONARCH MINE
Osb
OSb
Cwt
D?ls

TRUCTURE
65
50
30
55
NOT KNOWN
Cwt
GAILLARD RANCH
Creek
McClellan
BM
6212
OS
55
40
50
D?ls
45
OSb
80
40
30
30
BARITE CLAIM
4
5
D?ls
Cvta
40
6
35
30
7
8
25
9
20
70
70
Cmp
LONE WOLF MINE
D?ls
D?ls
UNMAPPED
DIKES
Cl
Cl
NANNIE'S PEAK
Cd

Calcareous siltstone and limestone

DEVONIAN?

McCLELLAN CREEK SEQUENCE

D?ls

Limestone

● Fossil locality

\+ Silicified limestone

Ouch

Upper chert member

Osh

Shale member

▲ Middle Ordovician graptolite locality

Olch

Lower chert member

Ocs

Op

Calcareous siltstone member, Ocs; sandstone bed, Oss; altered peridotite lens, Op

▲ Lower Ordovician graptolite locality

Contact, dashed where inferred

U / D

Normal fault, dashed where inferred
U, *upthrown side;* D, *downthrown side*

Fault, showing relative movement; dashed where inferred

Major thrust fault, dashed where inferred

Minor thrust fault, dashed where inferred

Syncline

41° 05′

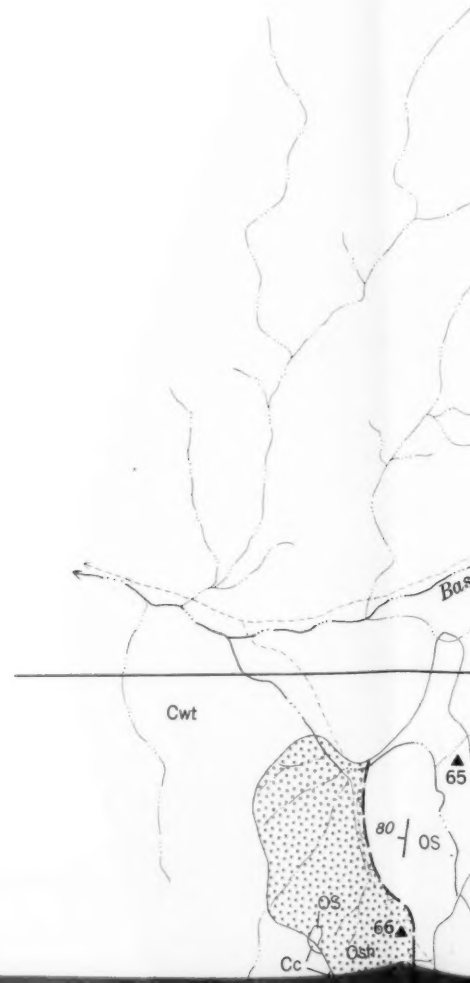

NANNIE'S PEAK BM x 8780
RIP VAN WINKLE MINE
LONE MOUNTAIN MINE
BIOTITE - HORNBLENDE
DIKES
Basco Creek
STRUCTURE
A
B
Cwt
Cc
OS
Ocs
Olch
Osh
Oss
Op
Ouch
Cmp
D?ls
Dfls
Dcsls
Dls
OSb
Cl
Cd

RIP VAN WINKLE MINE
LONE MOUNTAIN MINE
A
B
Basco Creek
STRUCTURE
STRUCTURE
Cwt
Cc
OS
Ocs
Olch
Op
Oss
Osh
Ouch
OSb
D?ls
Dfls
Dcsls
Dls
Cmp
Is

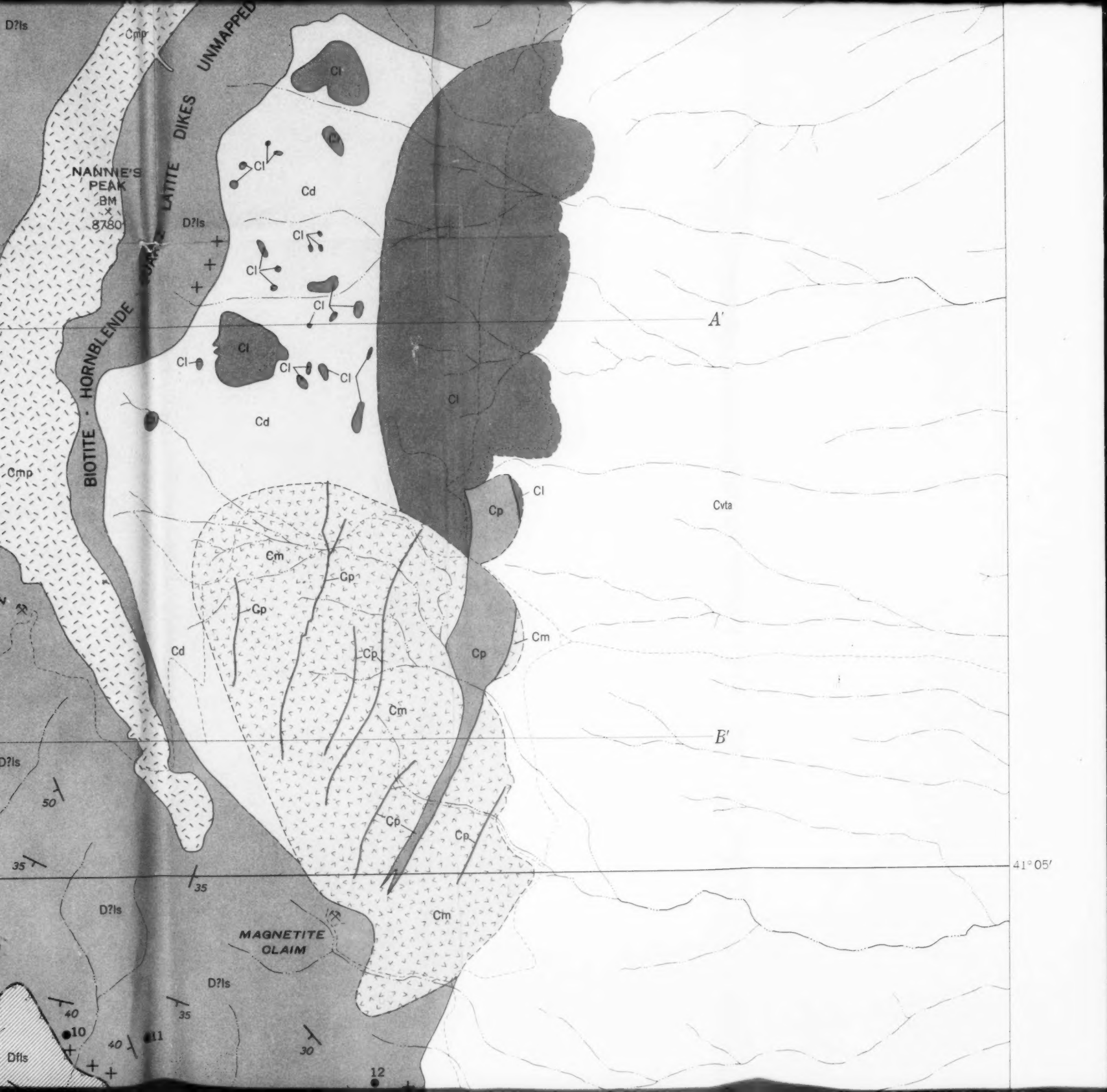
D?ls
Cmp
UNMAPPED
LATITE DIKES
NANNIE'S PEAK
BM
8780
Cl
Cd
Cp
BIOTITE - HORNBLENDE
A'
Cvta
Cm
B'
41°05'
MAGNETITE CLAIM
Dfls
50
40
35
30
10
11
12

41° 05′

Major thrust fault, dashed where inferred

Minor thrust fault, dashed where inferred

Syncline

Drainage

Unimproved road

35

Strike and dip of beds

90

Strike of vertical beds

30

Strike and dip of overturned beds

60

Generalized strike and dip of crumpled beds

BM
×
8780
Permanent bench mark

Mine or claim

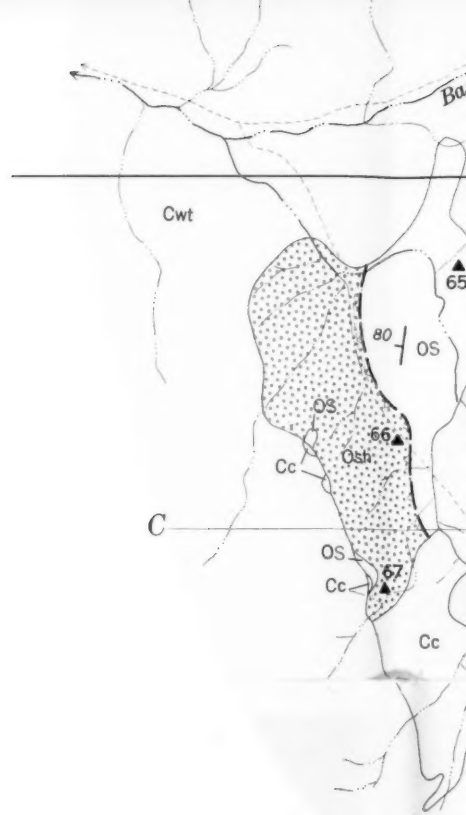

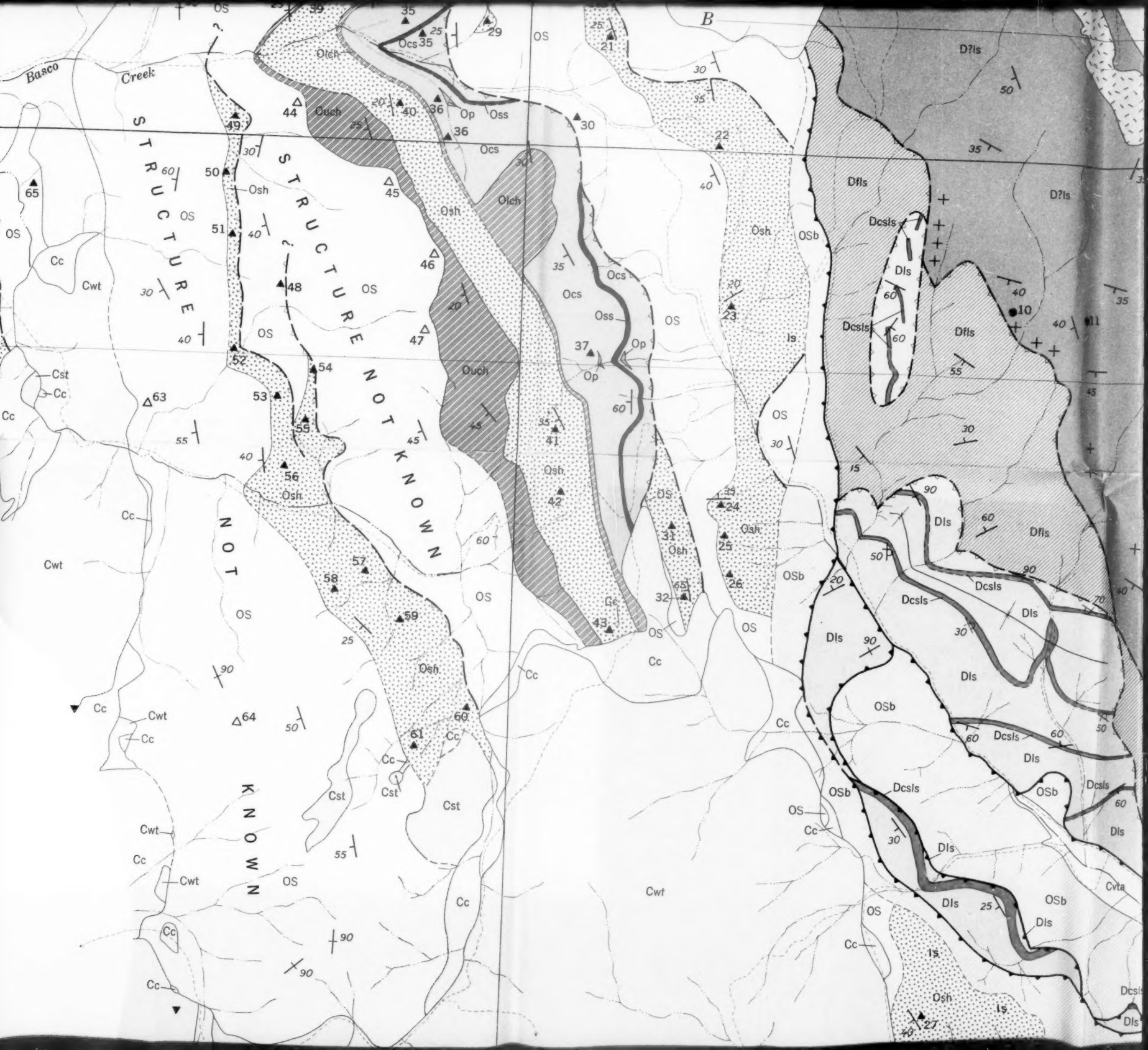
B
Basco Creek
STRUCTURE ?
STRUCTURE NOT KNOWN
Olch
Ouch
Ocs
Oss
Op
Osh
OSb
Dls
Dfls
D?ls
Dcsls
Is
OS
Cc
Cwt
Cst
Cvta

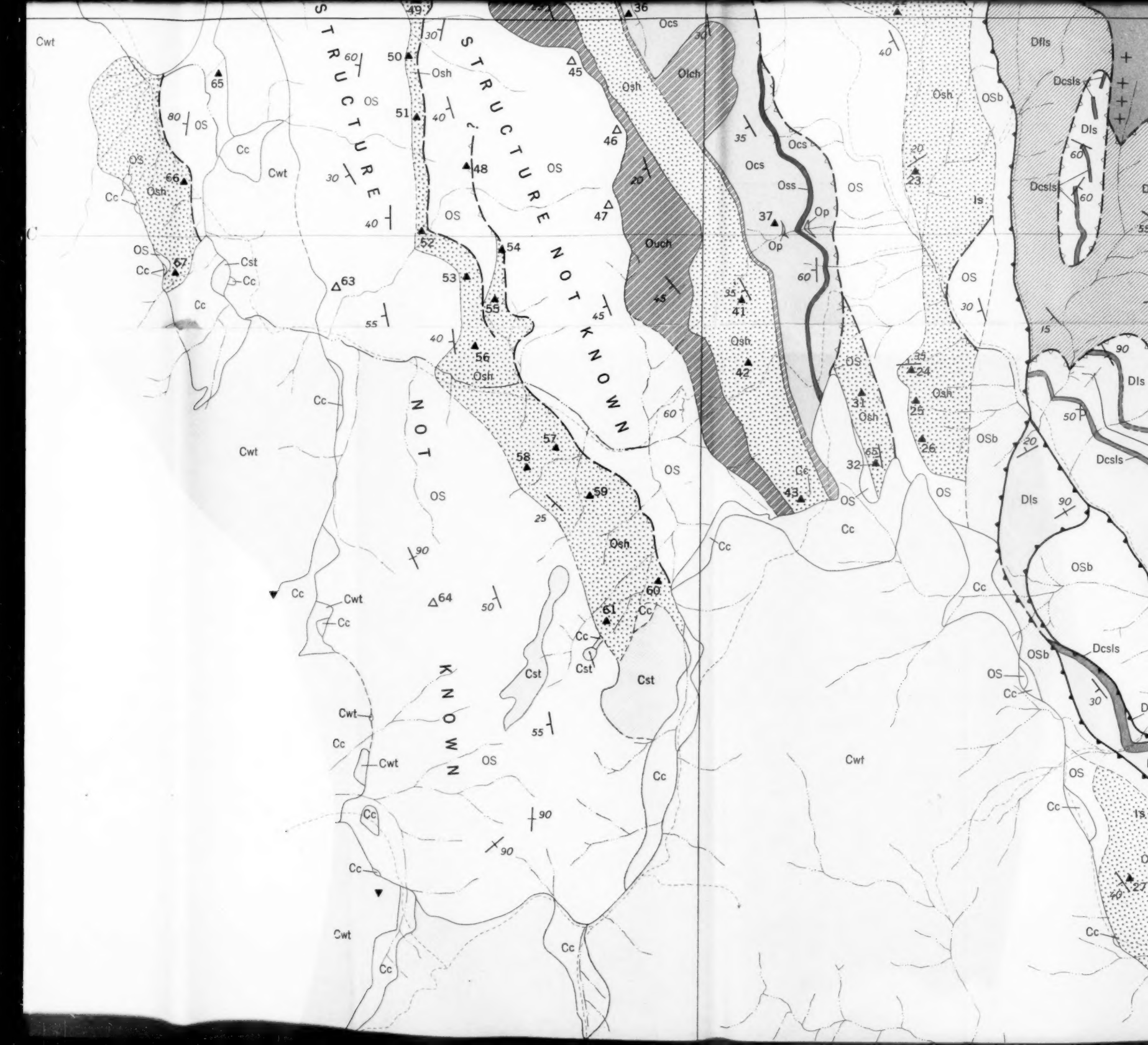
STRUCTURE NOT KNOWN
STRUCTURE ?
Cwt
Cc
OS
Osh
Cst
Ouch
Och
Ocs
Oss
Op
Is
OSb
Dls
Dfls
Dcsls

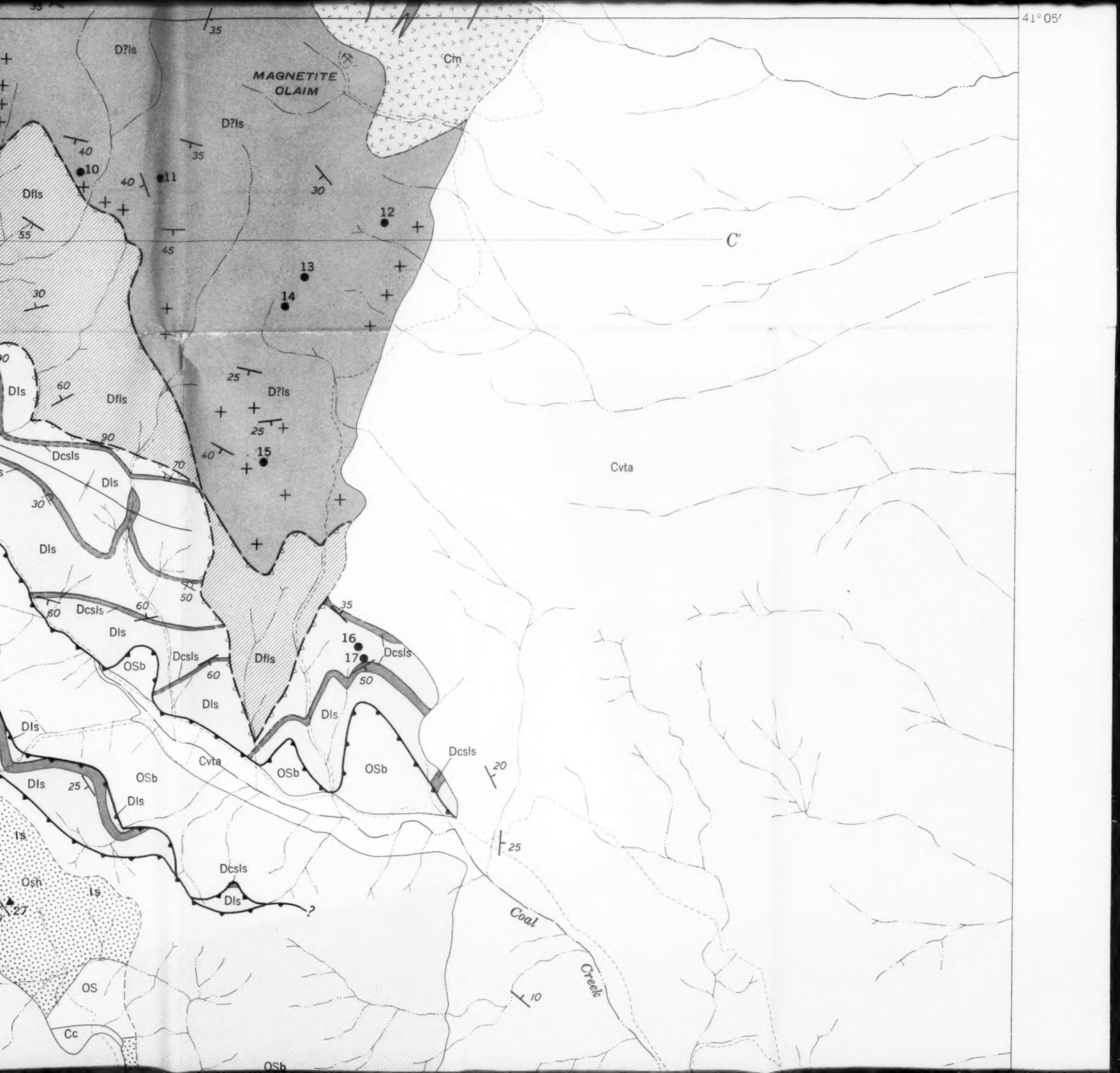
41° 05′
MAGNETITE
OLAIM
D?ls
Cm
Dfls
Dls
Dcsls
Cvta
OSb
Is
Osh
OS
Cc
C
C′
10
11
12
13
14
15
16
17
27
Coal
Creek

Strike and dip of beds

Strike of vertical beds

Strike and dip of overturned beds

Generalized strike and dip
of crumpled beds

BM
×
8780
Permanent bench mark

Mine or claim

NOT KNOWN
NOT KNOWN
Cwt
Cc
OS
Osh
Cst
Dls
Dcsls
Dfls
OSb
Is
56
57
58
59
60
61
64
42
43
24
25
26
27
31
32
35
40
50
55
60
65
70
90
20
30
25
116°00'

NOT KNOWN
NOT KNOWN
Cwt
Cc
OS
Osh
Cst
Dls
Dcsls
OSb
56
57
58
59
60
61
42
43
24
25
26
27
31
32
Δ64
40
50
55
60
65
90
20
30
116° 00′

Dls
Dfls
D?ls
Dcsls
Cvta
OSb
Osh
Is
OS
Cc
Cwt
15
16
17
Coal
Creek
25
60
90
70
40
30
50
35
20
10
27
?

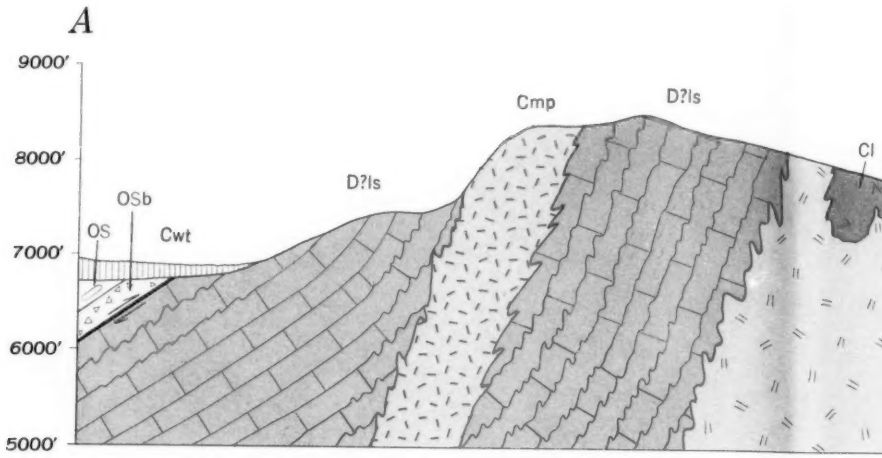

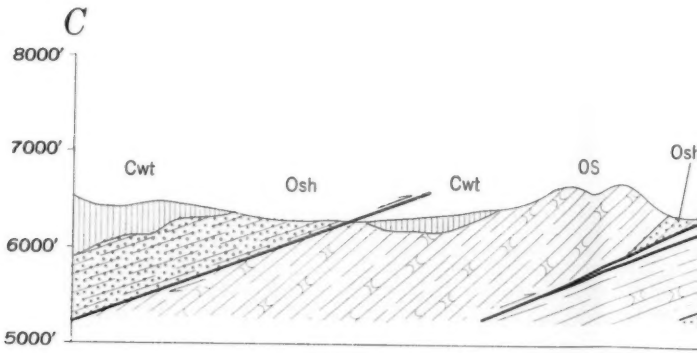

GEOLOGIC MAP A

116° 00′

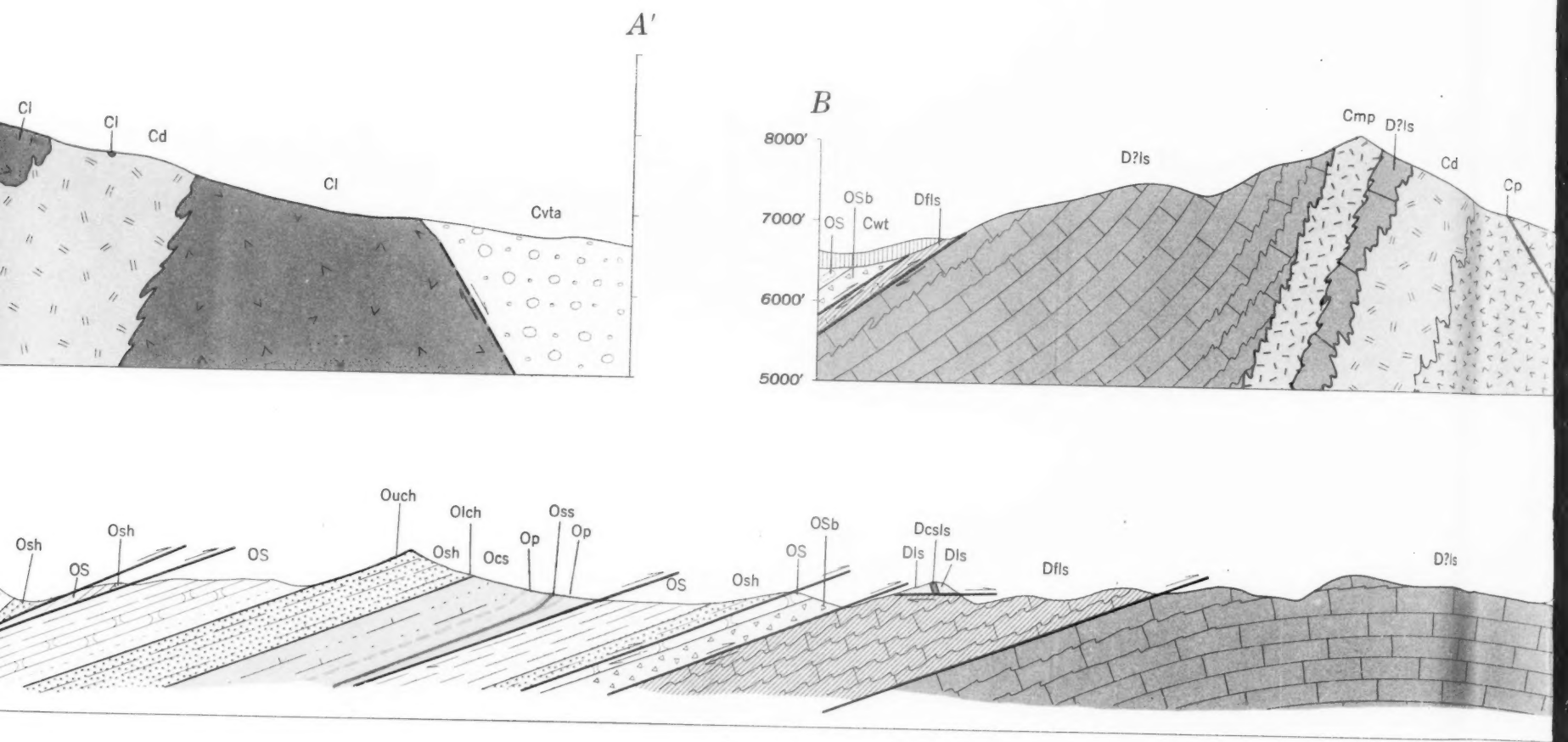

AND SECTIONS OF LONE MOUNTAIN, ELKO COUNTY

1 0 1 2 Miles

116° 00′

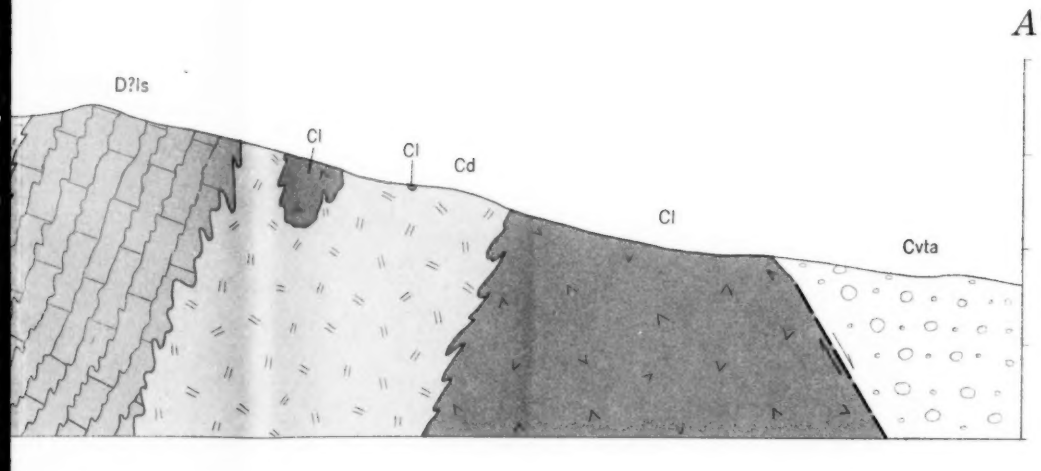

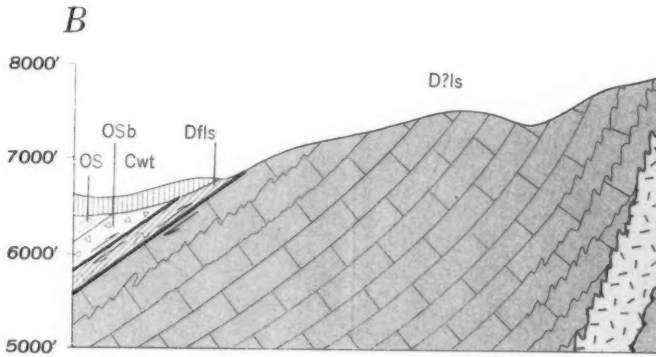

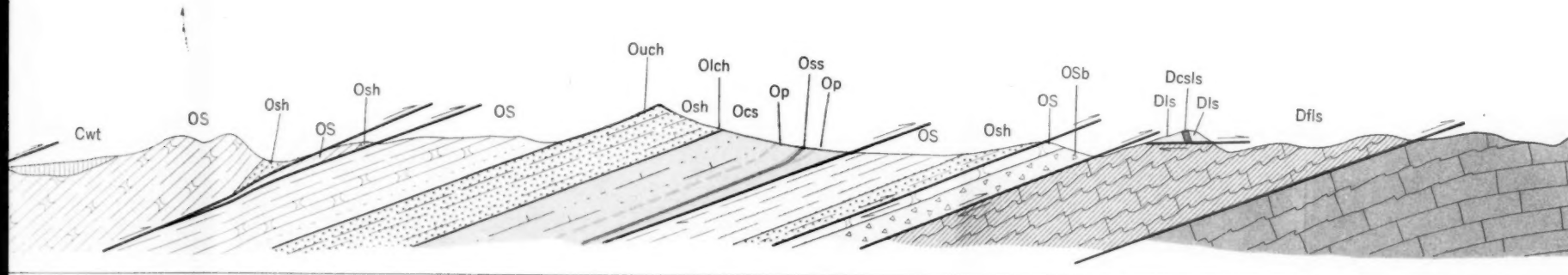

GIC MAP AND SECTIONS OF LONE MOUNTAIN, ELKO

1 0 1 2

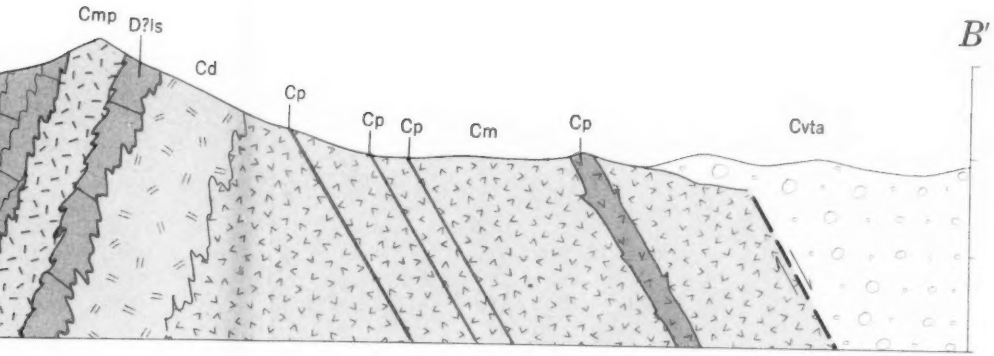

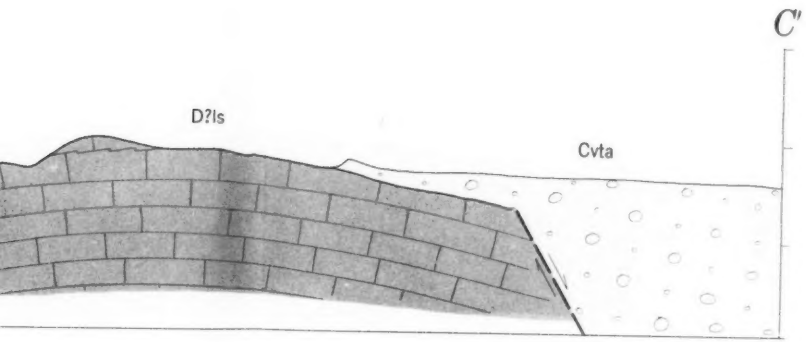

KO COUNTY, NEVADA

2 Miles

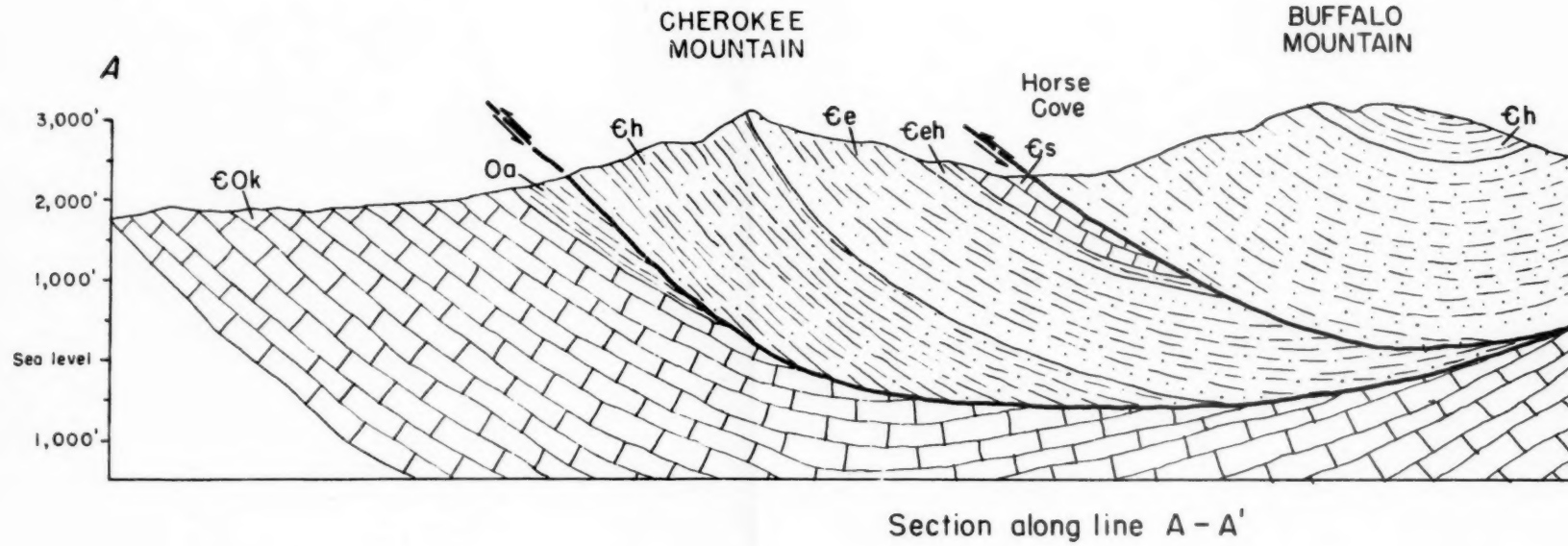

Section along line A – A'

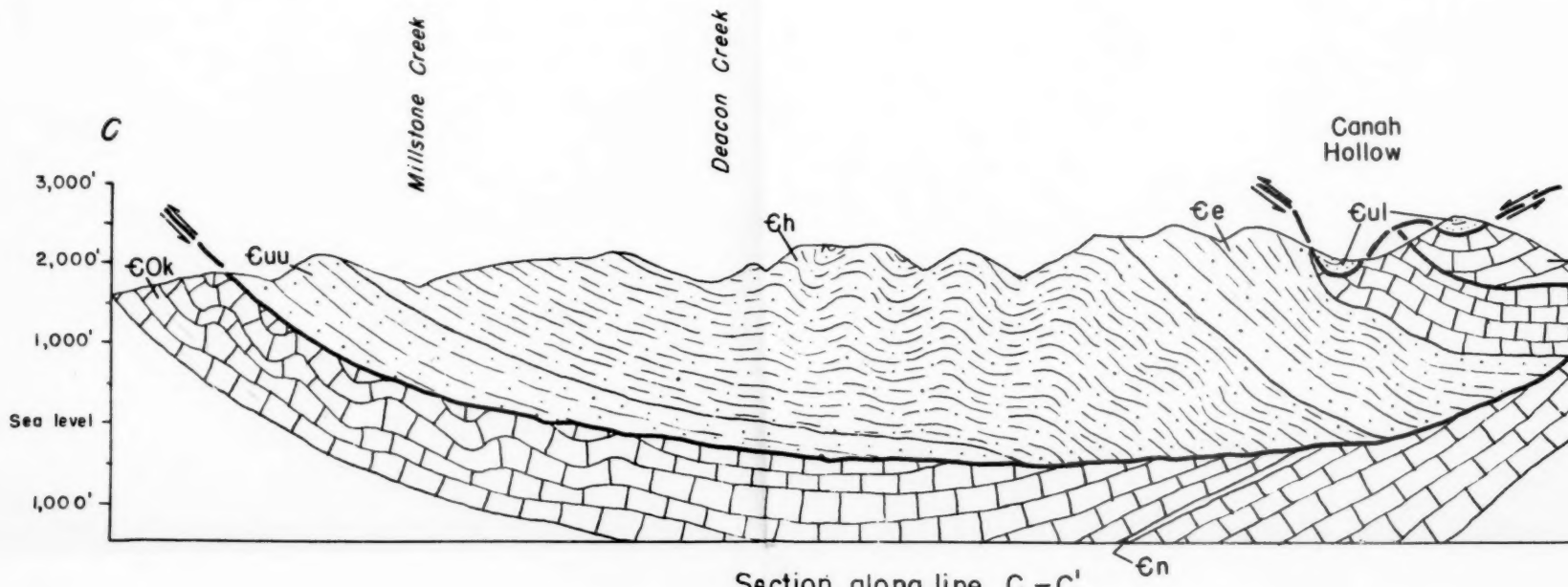

Section along line C – C'

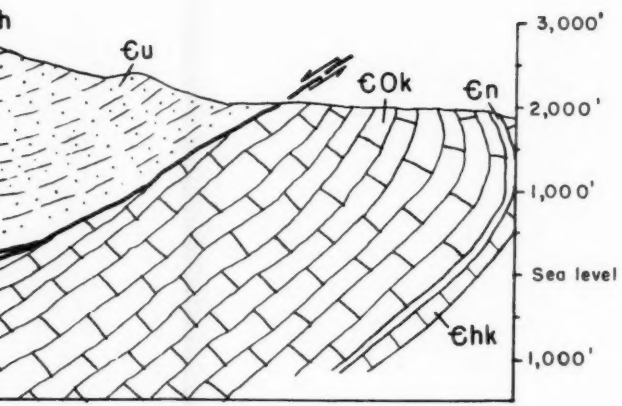
A'
h
€u
€Ok
€n
3,000'
2,000'
1,000'
Sea level
€hk
1,000'

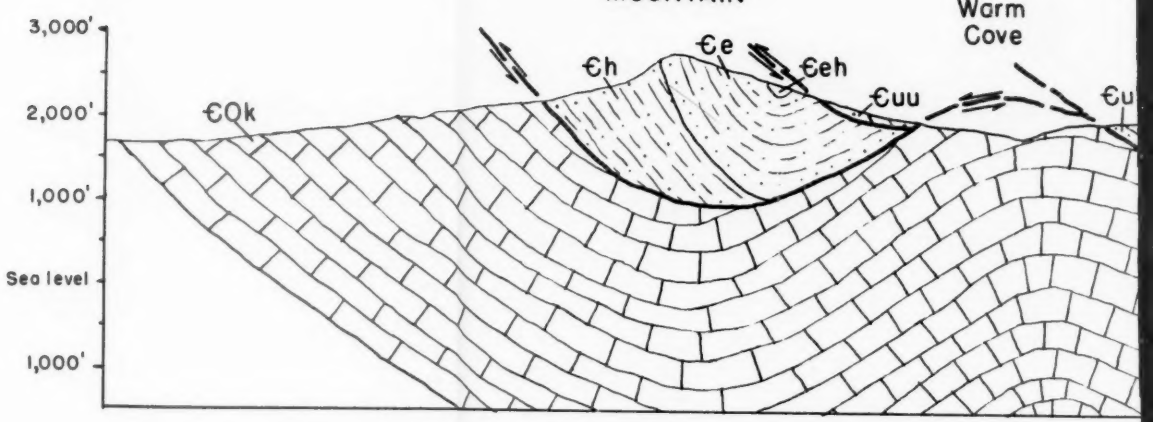
B
CHEROKEE
MOUNTAIN
Warm
Cove
3,000'
2,000'
1,000'
Sea level
1,000'
€Ok
€h
€e
€eh
€uu
€u

Section

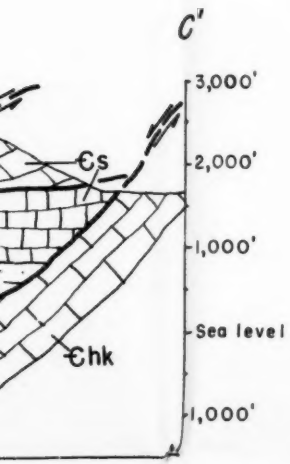
C'
3,000'
2,000'
1,000'
Sea level
1,000'
€s
€hk

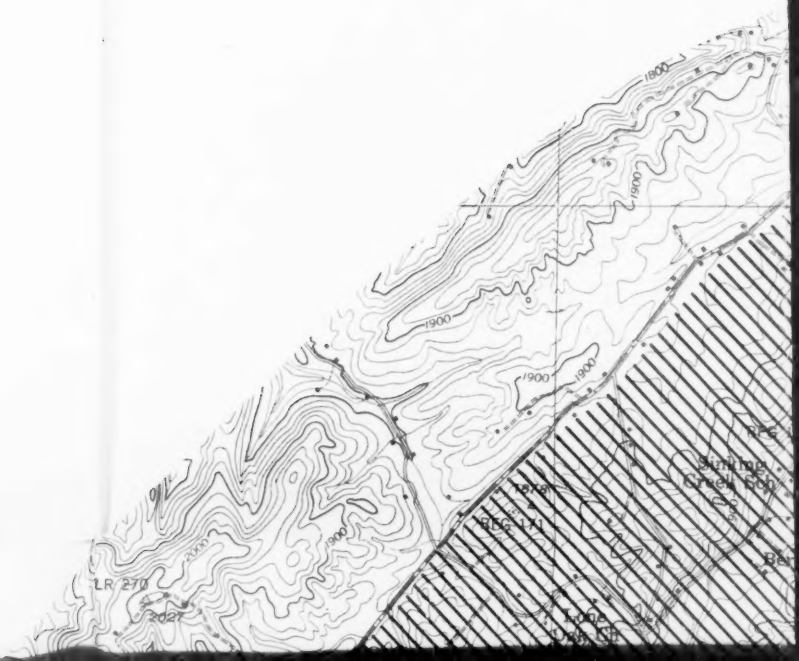
1800
1900
2000
2021
LR 270

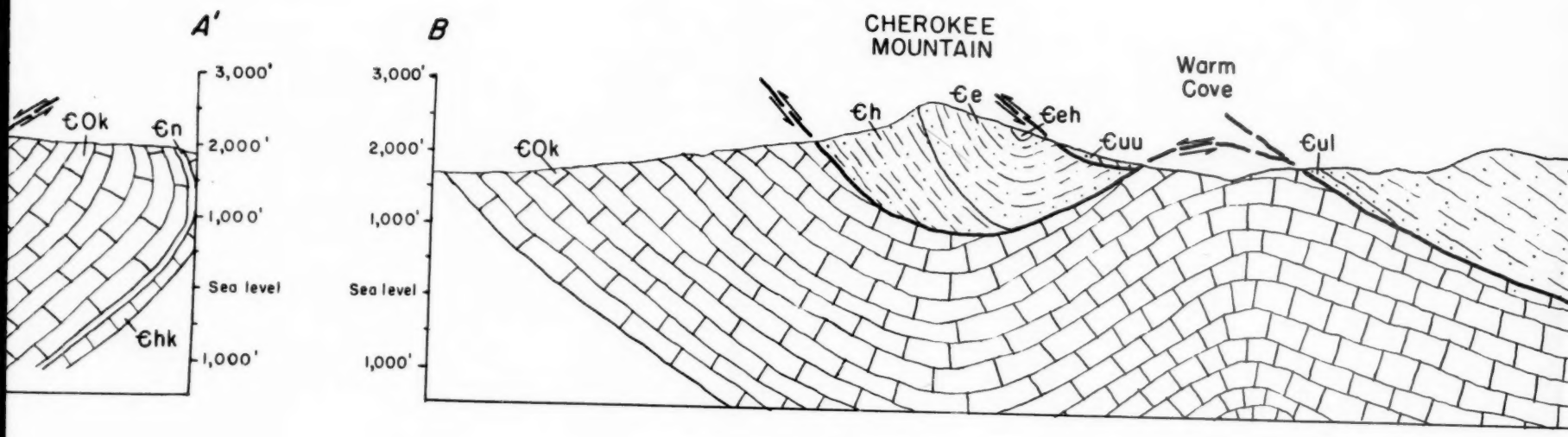

Section along line B – B'

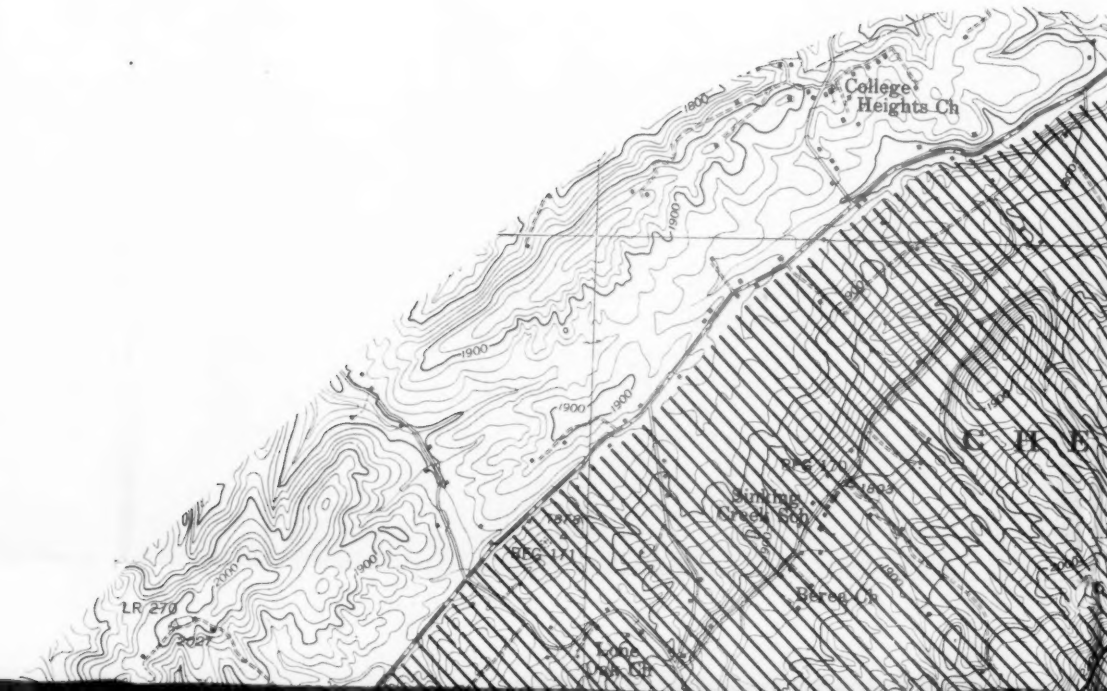

BUFFALO MOUNTAIN

B'

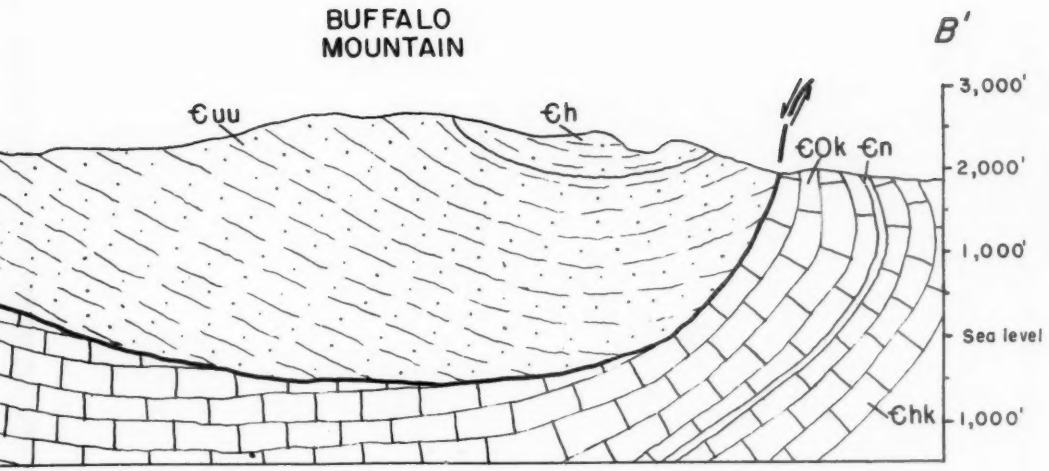

B'

40

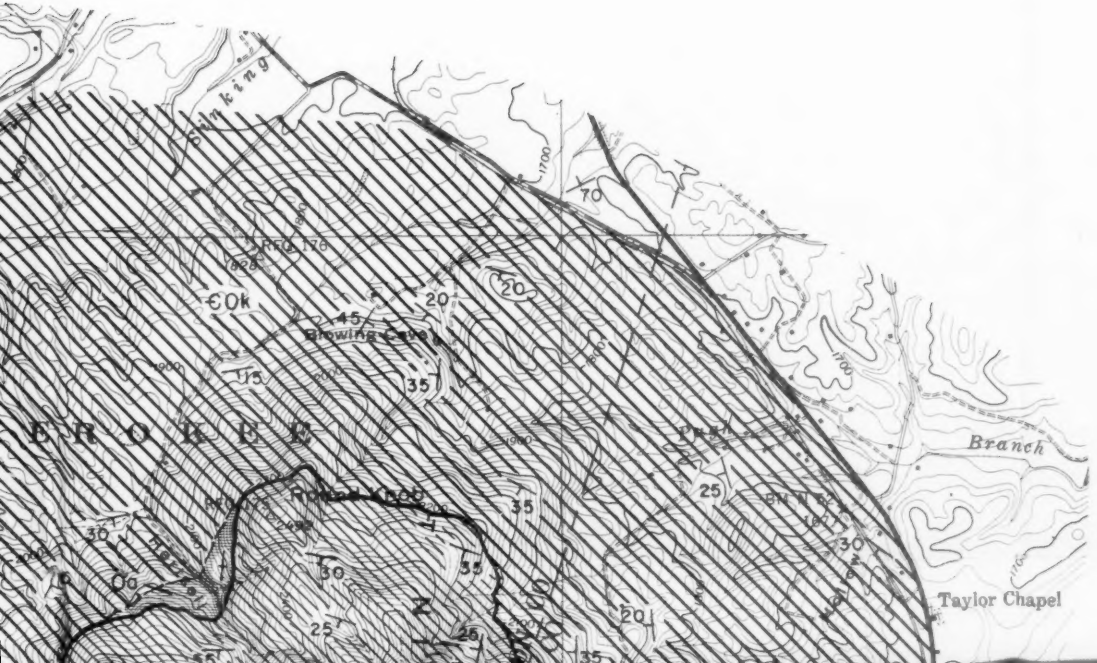

EXPLANATION

MIDDLE AND LOWER ORDOVICIAN

Oa — *Athens shale*

UPPER AND MIDDLE CAMBRIAN

COk — *Knox dolomite*

Cn — *Nolichucky shale*

Chk — *Honaker limestone*

LOWER CAMBRIAN

Cs — *Shady dolomite*

Ceh — *Helenmode member of Erwin formation*

Ce — *Erwin formation (includes Helenmode in some sections)*

Ch — *Hampton formation*

Cu — *Unicoi formation (undivided)*

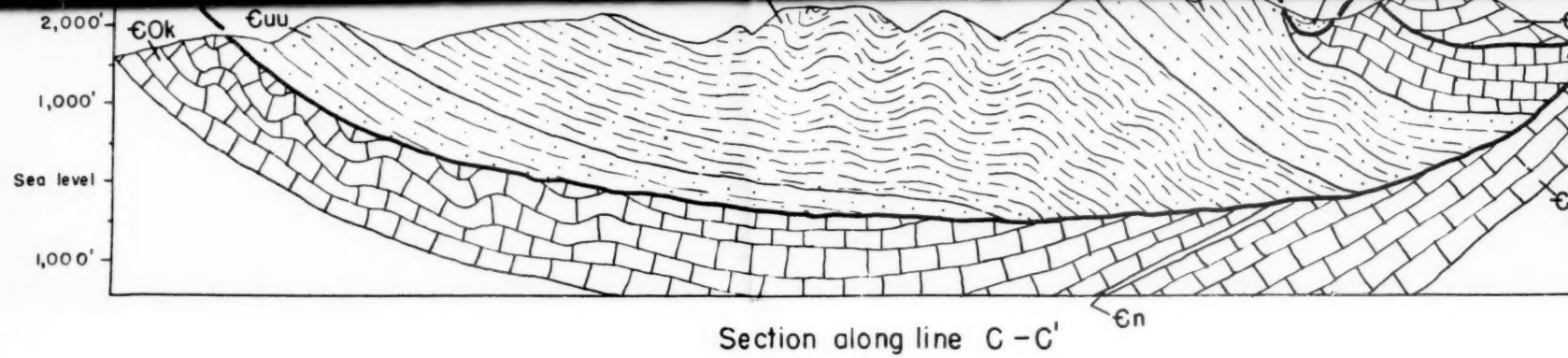

Section along line C – C'

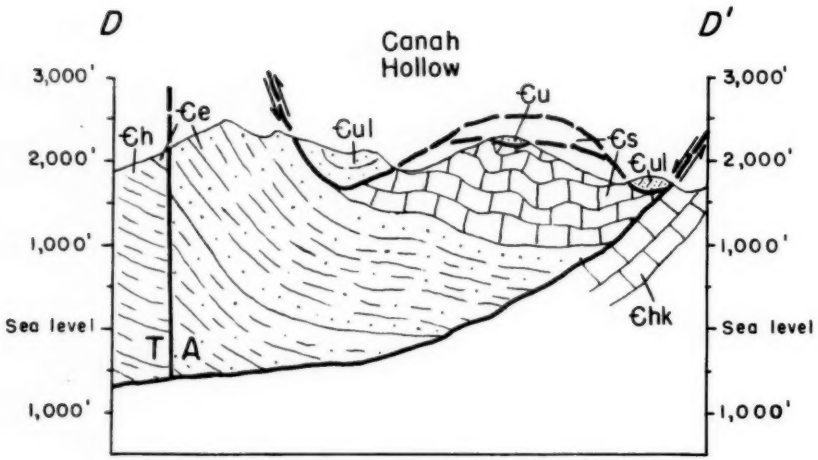

Section along line D – D'

Interpretation 1

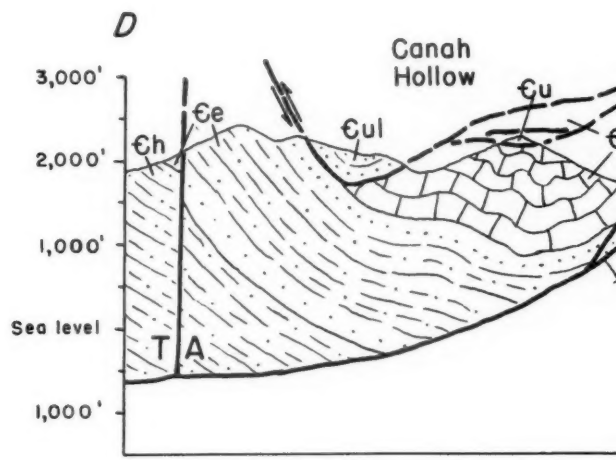

Section along line D – D'

Interpretation 2

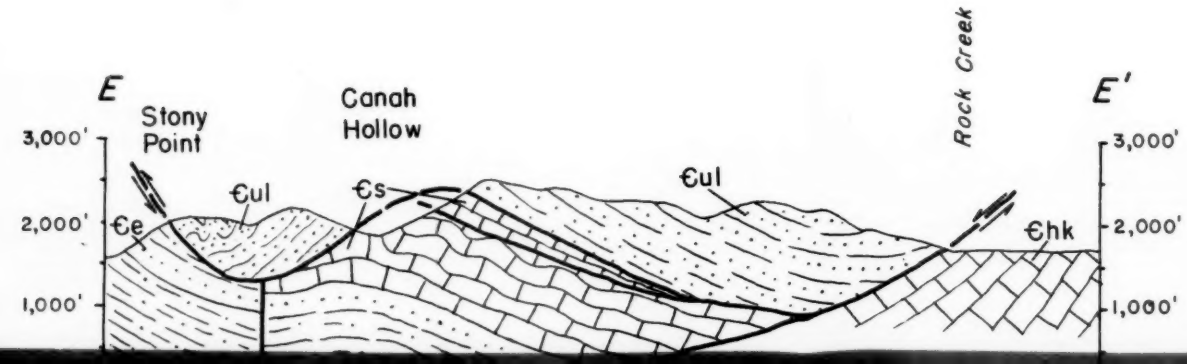

Cs
2,000'
1,000'
Sea level
Chk
1,000'

D'
3,000'
Cs
Cu
2,000'
1,000'
Chk
Sea level
1,000'

D'

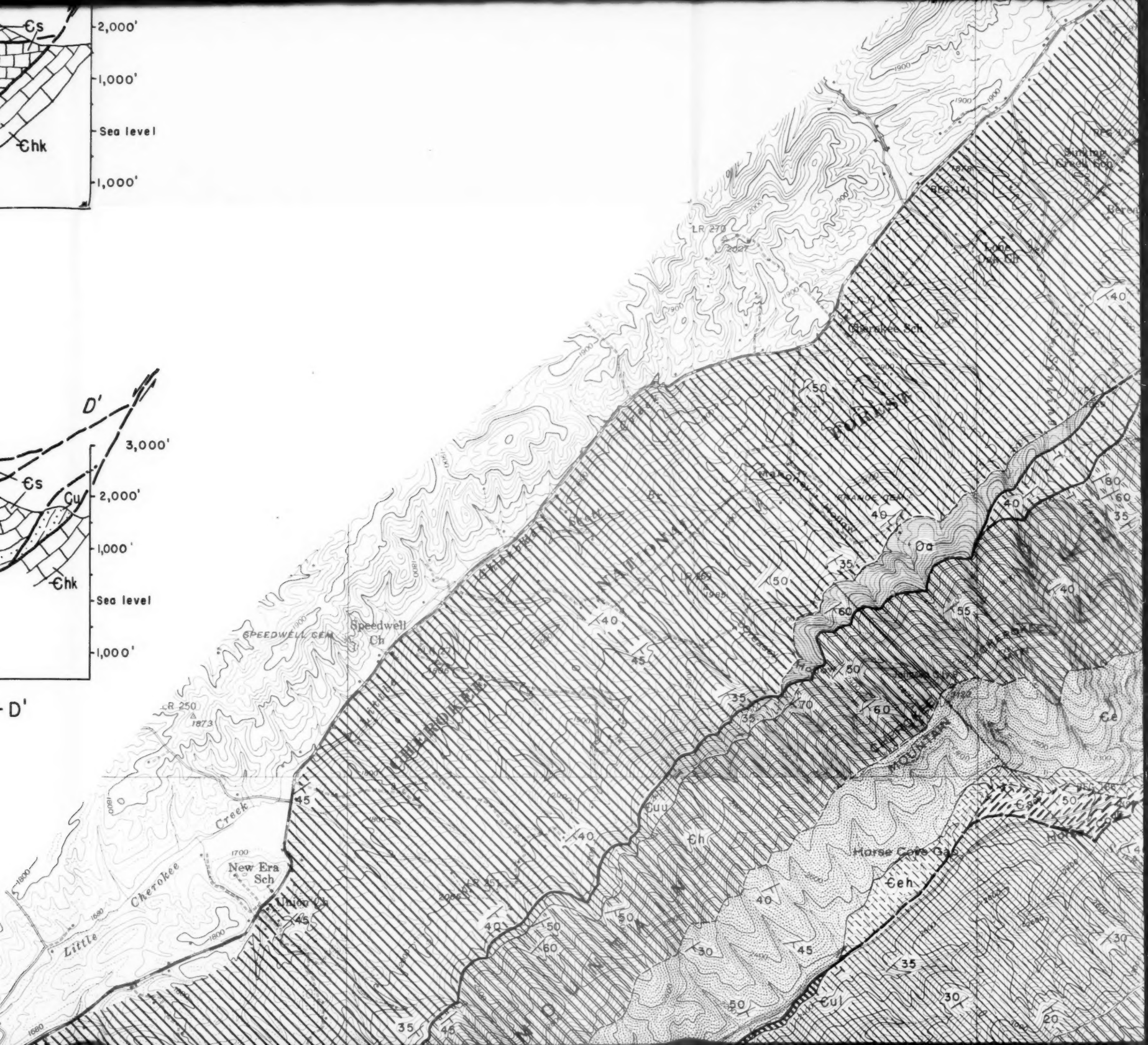
Speedwell Ch
New Era Sch
Union Ch
Little Cherokee Creek
Cherokee Sch
Horse Cove Gap
Ou
Cuu
Ch
Cul
Ceh
Ce
Oa
Cherokee National Forest

Speedwell Cem
Speedwell Ch
Speedwell Church Rd
Cherokee Sch
Berea Ch
Sinking Creek Sch
Long Oak Ch
Mason Town Branch
Grange Cem
Oa
Oau
Eh
Horse Cove Gap
Eeh
Ee
New Era Sch
Union Ch
Creek
Forest
Mountain
Ridge
Trail
Br
Run
Creek
LR 270
LR 69
SR 1973
SR 1971
SR 1972
SR 1974
SR 1975
SR 1976
SR 1977
SR 1978
SR 1979
SR 1980
SR 1981
SR 1982
SR 1983
SR 1984
SR 1985
SR 1986
SR 1987
SR 1988
SR 1989
SR 1990
SR 1991
SR 1992
SR 1993
SR

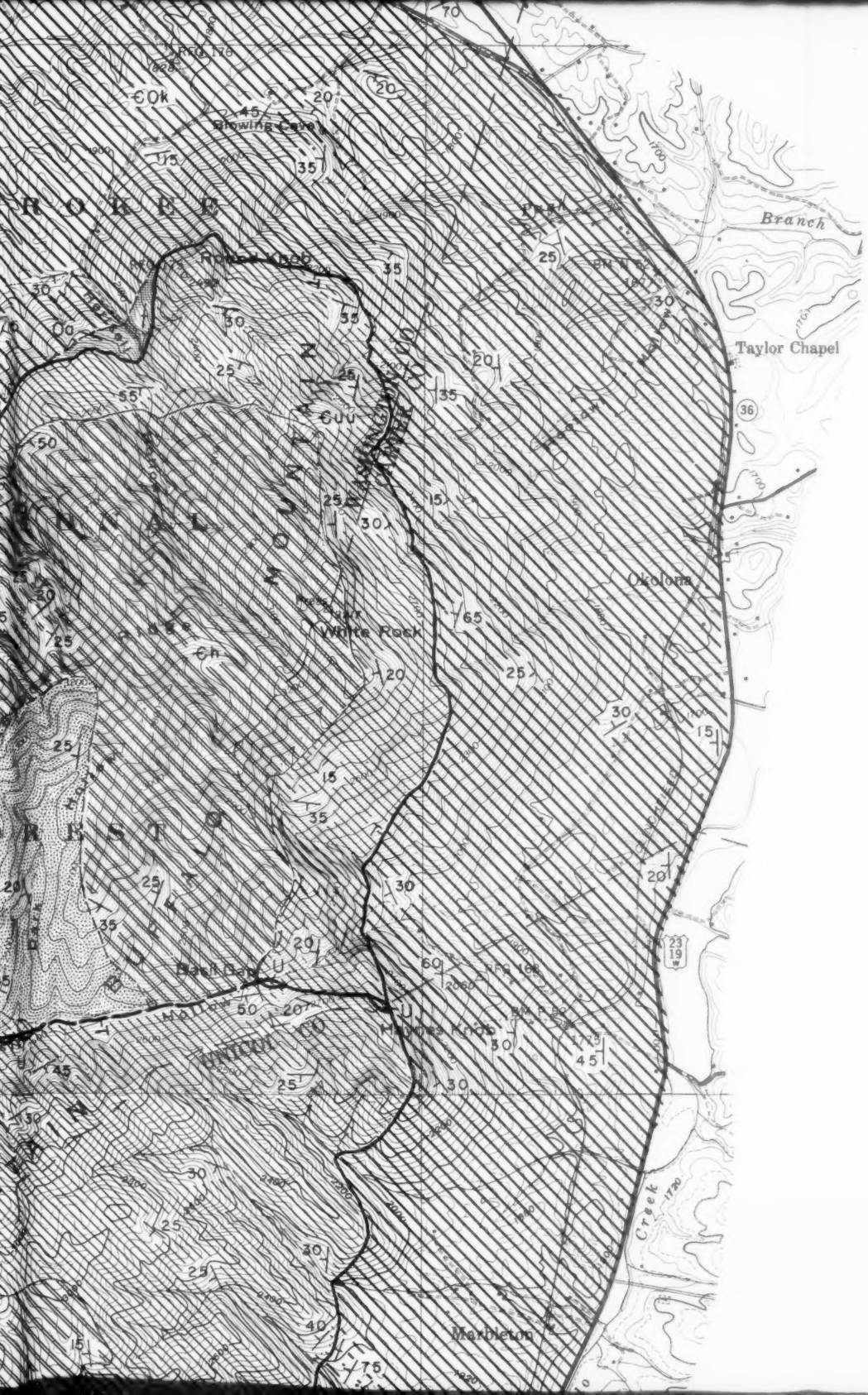

LOWER CAMBRIAN

formation

Ce

Erwin formation (includes Helenmode in some sections)

Ch

Hampton formation

Cu

Unicoi formation (undivided)

Cuu

Upper member of the Unicoi formation

Cul

Lower member of the Unicoi formation

U

Limestone and dolomite of unknown age

60

Strike and dip of inclined strata

Horizontal strata

Strike of vertical strata

85

Strike and dip of overturned strata

60

Strike and dip of cleavage

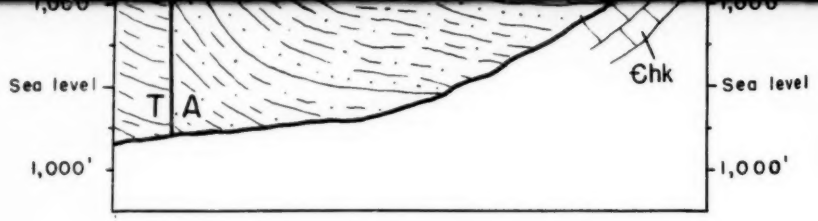

Section along line D – D'

Interpretation 1

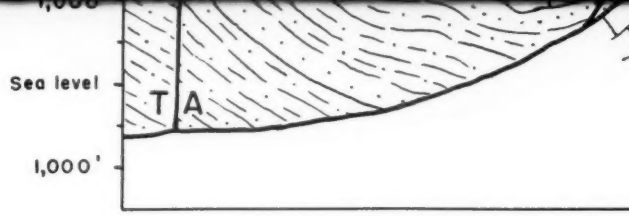

Section along line D – D'

Interpretation 2

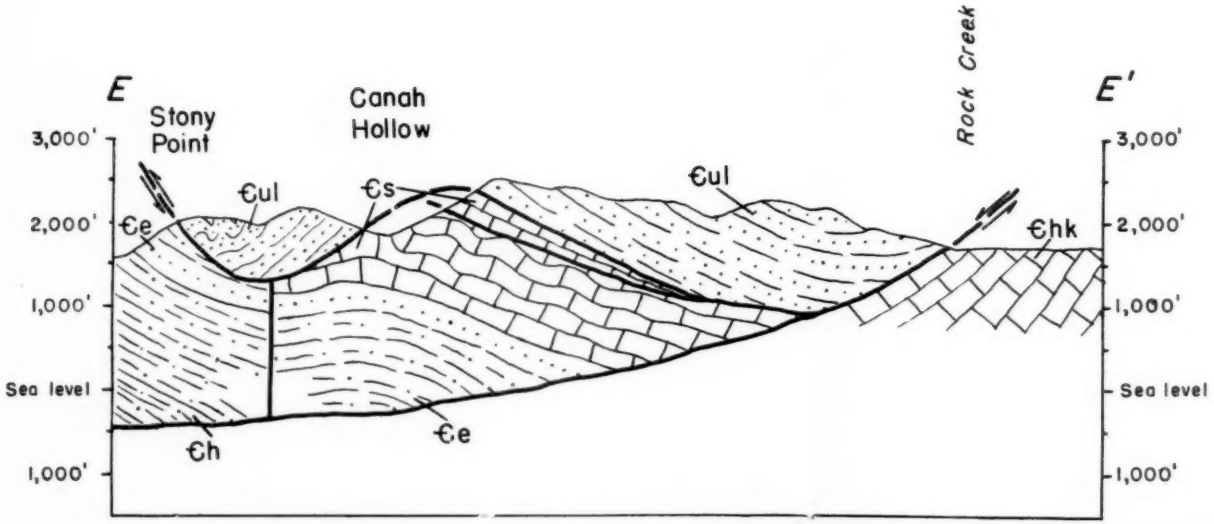

Section along line E – E'

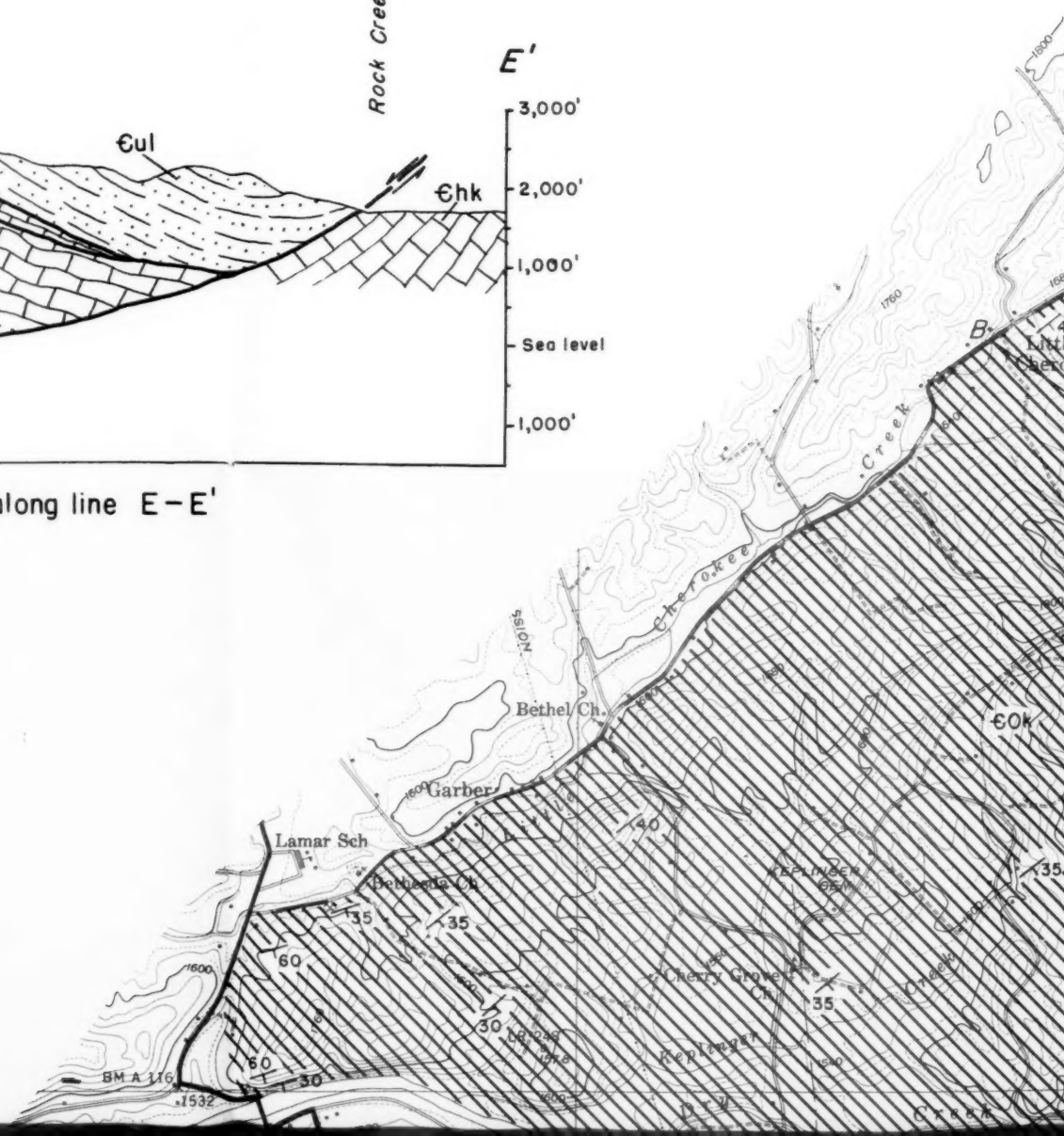

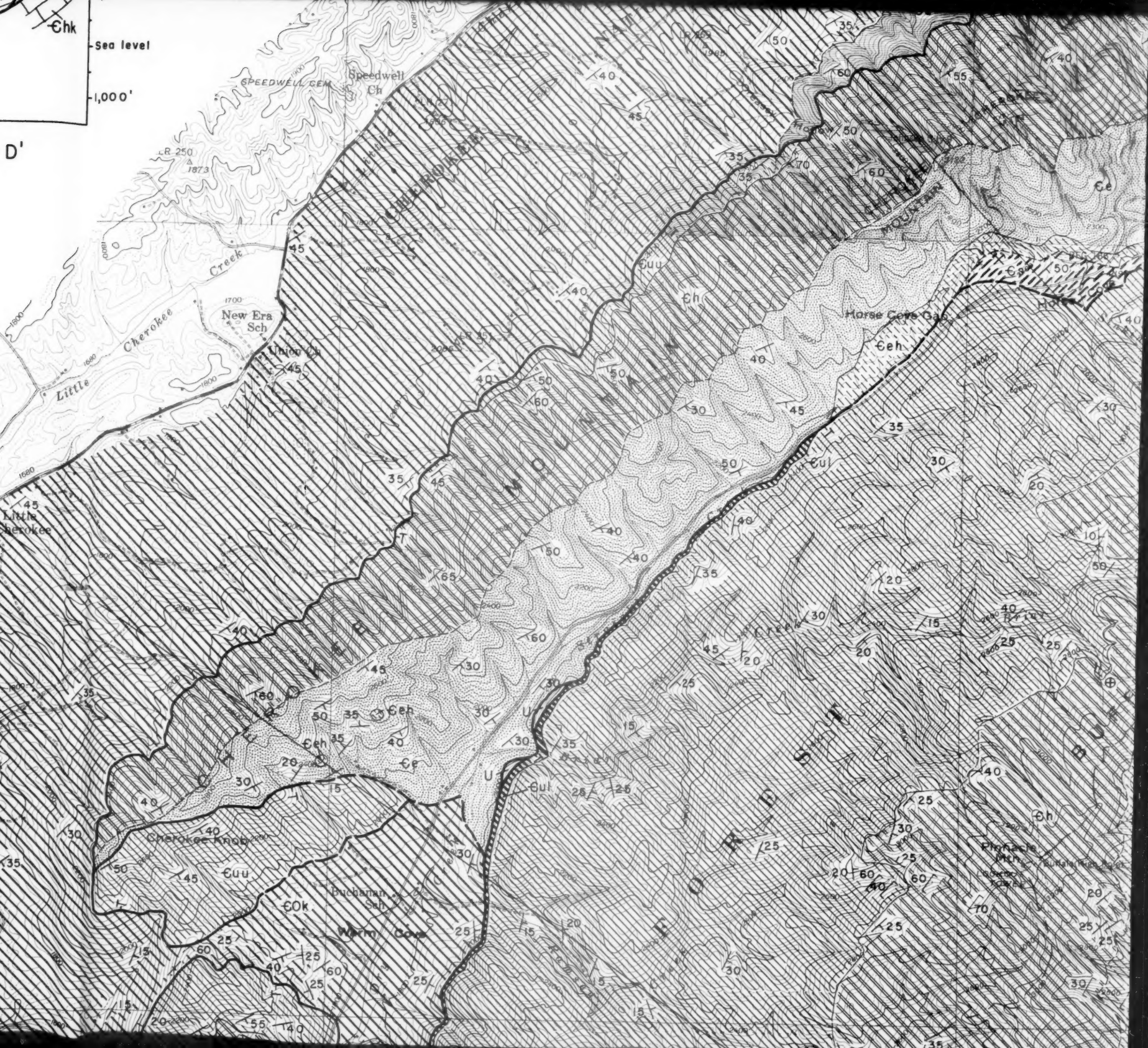
Ehk
Sea level
1,000'
D'
Speedwell Ch
Speedwell Cem
Creek
New Era Sch
Union Ch
Little Cherokee
Little Cherokee
Cherokee Knob
Buchanan Sch
Worm Gap
Horse Cove Gap
Pinnacle Mtn
Eeh
Eul
Euu
Eh
Ee
Ek

Speedwell Ch
SPEEDWELL CEM
Creek
New Era Sch
Union Ch
CHEROKEE NATIONAL FOREST
Cuu
Ch
Horse Cove Gap
Ceh
Cul
Ce
Cherokee Knob
Cuu
buchanan Sch
Warm Cove
Pinnacle Mtn
Ch
Ceh
Ce
Cul
Cuu
COk
U
Ceh
Ce
Cul
U
Ceh
Ceh
Ce
U
Cul
Ceh
Ceh
Ceh

60

Strike and dip of inclined strata

Horizontal strata

Strike of vertical strata

85

Strike and dip of overturned strata

60

Strike and dip of cleavage

Geologic boundaries

Dashed where location is indefinite

T

Thrust fault

Dashed where location is indefinite;
T, ***top side of thrust plate.***

D

Normal fault

Dashed where location is indefinite;
D, ***down thrown side.***

Tear fault

Dashed where location is indefinite;
arrows show relative displacement

Garber
Lamar Sch
Bethesda Ch
Cherry Grove Ch
BM A 116
1532
TAYLOR BRIDGE
NOLICHUCKY
RIVER
BM Z 115
1531
Dedrick Island
HIGHWAY
SEVIER
107
JOHN
BM LHT 803
1533
N 181
1511
Kansas City
BM LHT 802
1538
81
MOUNTAIN
Ember
2654
Embreeville
GAGING STATION
BM 1527
N 179
1545
Chimney Rock
The Horseshoe
BM LHT 799

Cherokee Knob
Buchanan Sch
Warm Cove
Dry Creek
Leach Gap
Pinnacle Mtn
Jones Chapel
Dry Creek Sch
Orgee Gap
Fishery
CLINCHFIELD
Dry
Indian
Walker
Walden
Cuu
Cuk
Cul
Culi
Ch
Ce
Cn
T
D
U
CLINCH MOUNTAIN
WASHINGTON
CO
CO

Pinnacle Mtn
Leach Gap
Swingle Cem
Unico
Jones Chapel
North
Glinchfield
Peterson Cem
Dry Creek Sch
Dry
Fishery
Orgon Gap
Washington
Unicoi
Eastern Continental Divide
N

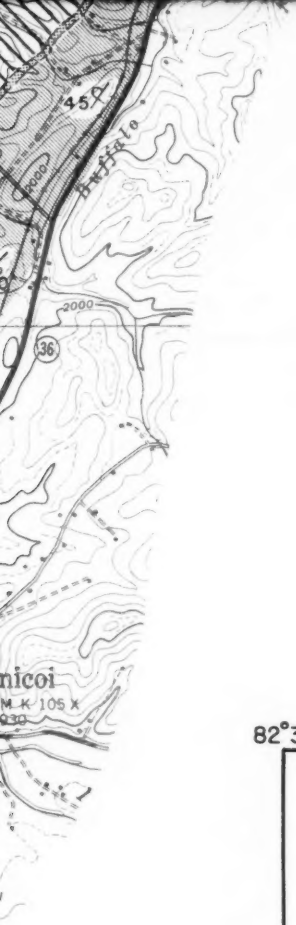

Dashed where location is indefinite;
D, *down thrown side.*

Tear fault

Dashed where location is indefinite; arrows show relative displacement

Note: On sections only.

Horizontal movement in tear fault; A, *away from observer;* T, *toward observer. Arrows on thrust faults show relative displacement.*

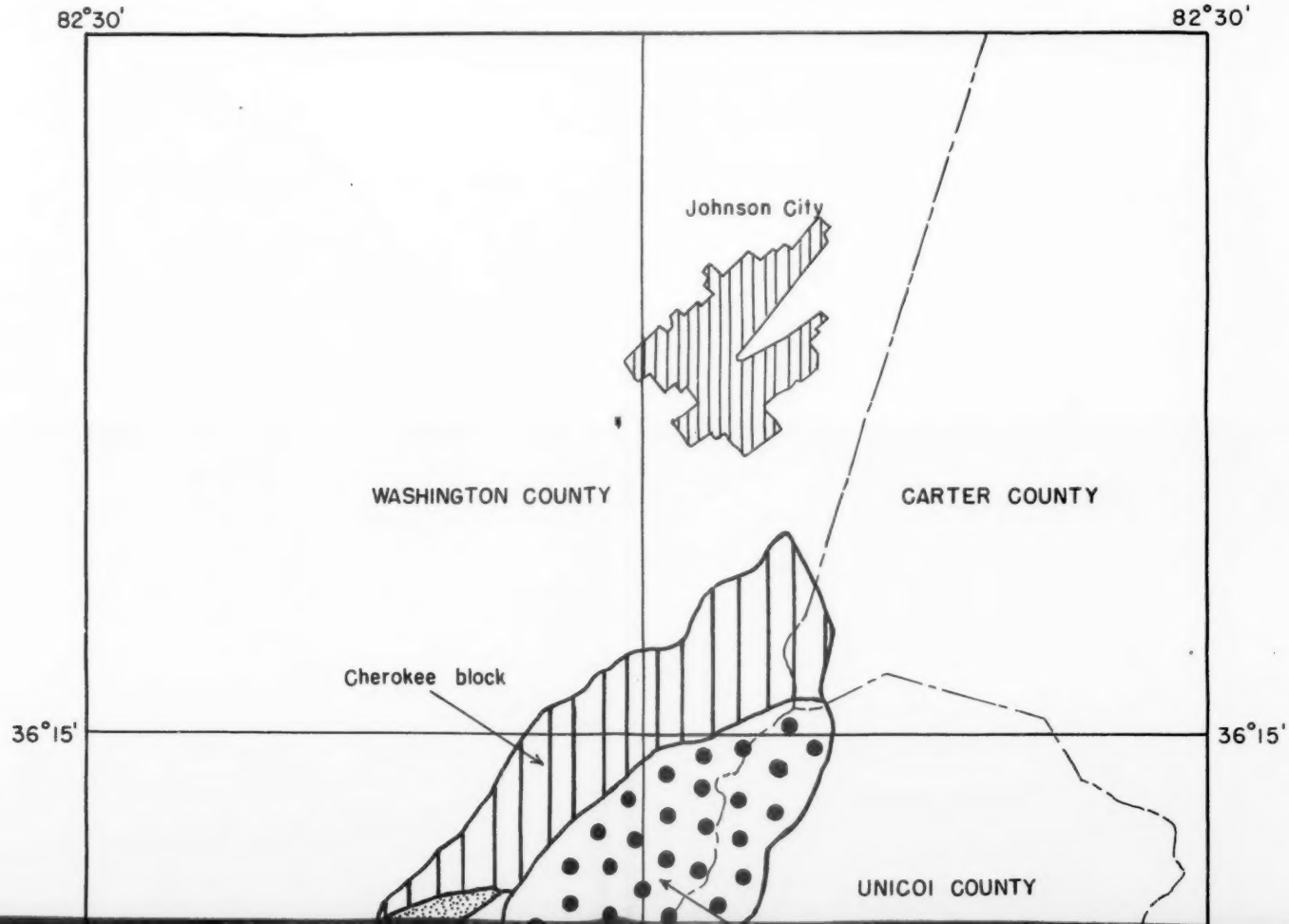

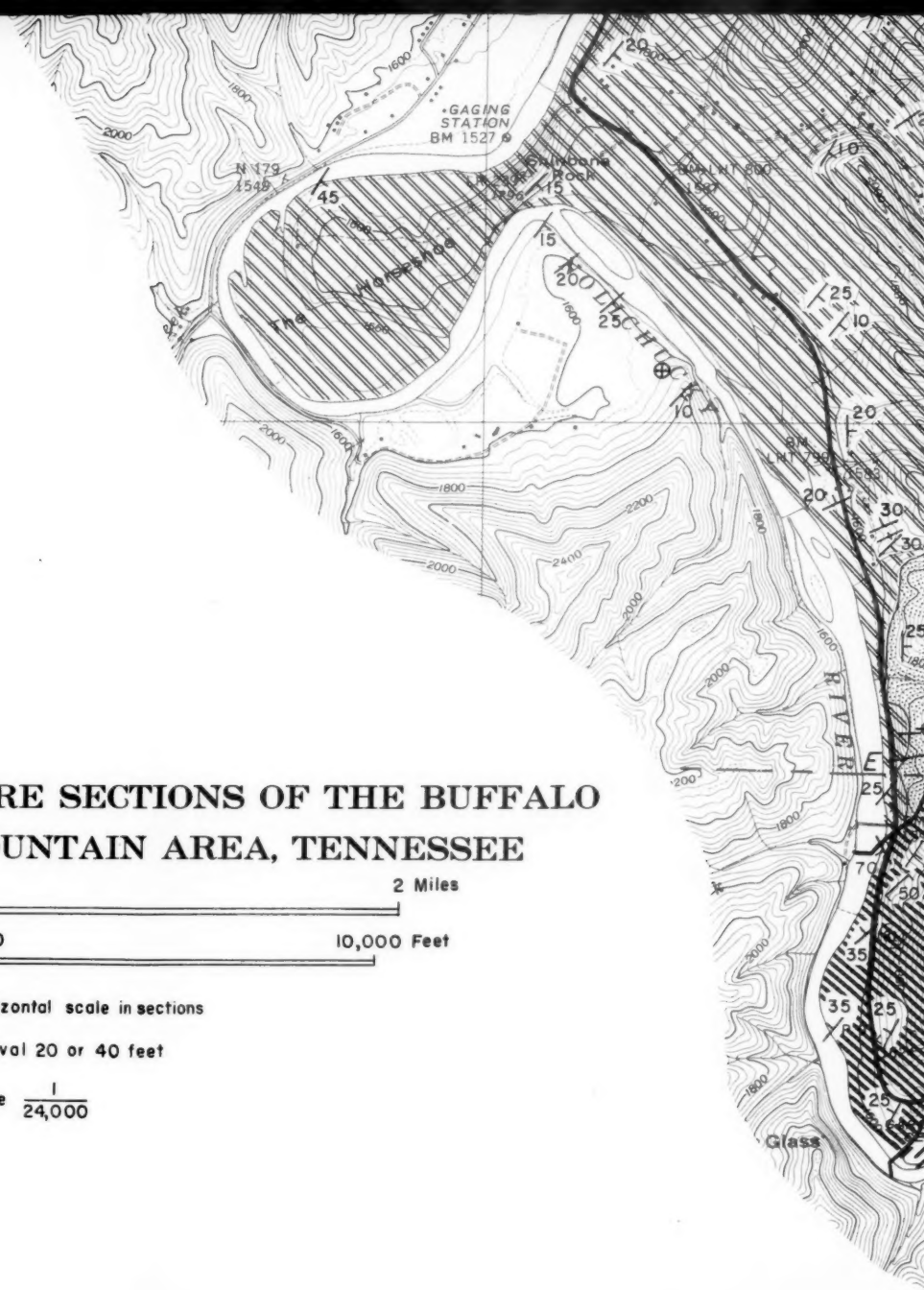

GEOLOGIC MAP AND STRUCTURE SECTIONS OF THE BUFFALO MOUNTAIN-CHEROKEE MOUNTAIN AREA, TENNESSEE

0 1/2 1 2 Miles

0 5,000 10,000 Feet

Vertical scale=Horizontal scale in sections

Contour interval 20 or 40 feet

Scale $\frac{1}{24,000}$

Fishery
Rock Creek
Rock Creek Sch
Hulan Hollow
ERWIN
(BM X 52)
(1675)
Bend
Island
Capah Gap
Capah Sch
Organ Gap
JOBS CEM
EVERGREEN CEM
FISH HATCHERY
BM T 52
1759
BM V 52
1721
BM V 52
1735
BM LHT 796
1658
LR 213
1719
Erwin 1
Indian
Rock
Creek
Elephant Back
CLINCHFIELD
Cul
Cuu
Cuh
Cus
Cu
Ch
Chk
Ce
COk

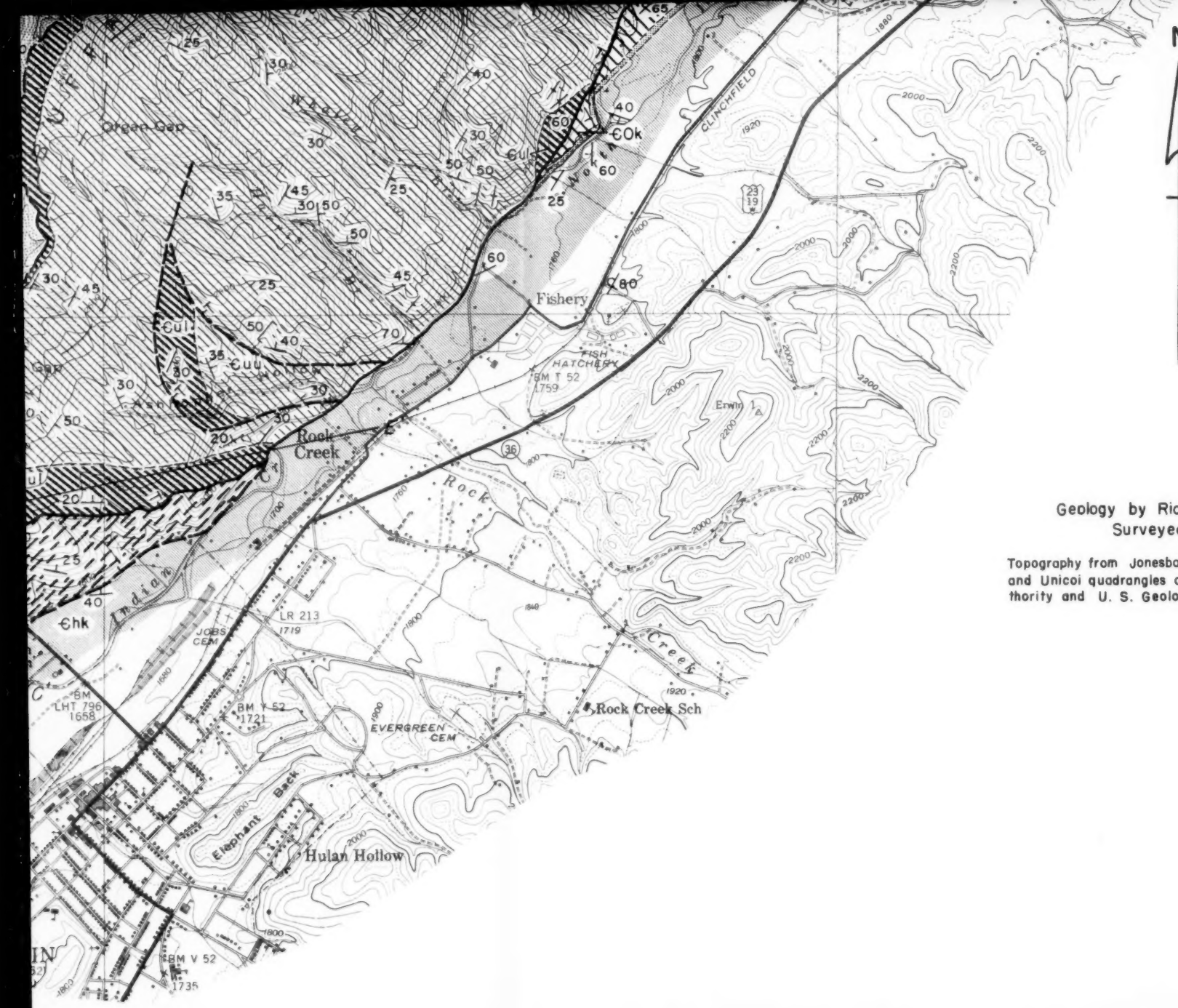

Geology by Richard J. Ordway
Surveyed in 1947

Topography from Jonesboro, Johnson City, Erwin and Unicoi quadrangles of Tennessee Valley Authority and U. S. Geological Survey.

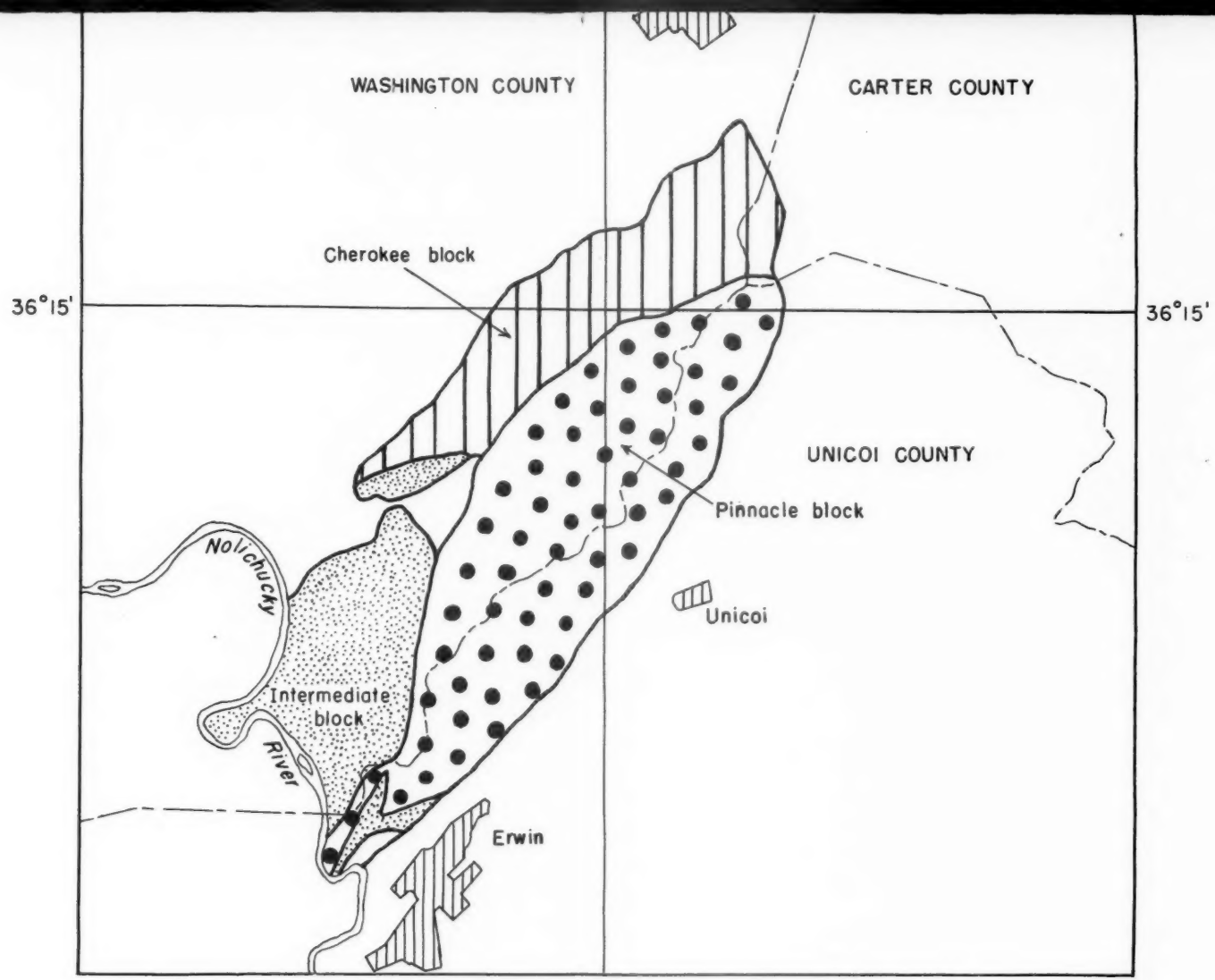

Map of Buffalo Mountain–Cherokee Mountain Area Showing the Three Thrust Blocks

0 2 4 Miles

Scale $\frac{1}{125,000}$